Factors Affecting Stress Assisted Corrosion Cracking of Carbon Steel under Industrial Boiler Conditions

A Dissertation
Presented to
The Academic Faculty

by

Dong Yang

In Partial Fulfillment
Of the Requirements for the Degree
Doctor of Philosophy in the
School of Mechanical Engineering

Georgia Institute of Technology
Atlanta, GA
August, 2008

Factors Affecting Stress Assisted Corrosion Cracking of Carbon Steel under Industrial Boiler Conditions

Approved by:

Dr. Preet M. Singh

Advisor
School of Materials Science and Engineering
Georgia Institute of Technology

Dr. Richard W. Neu

Co-Advisor
School of Mechanical Engineering
Georgia Institute of Technology

Dr. W. Steven Johnson

Committee Member
School of Mechanical Engineering
Georgia Institute of Technology

Dr. Timothy F. Patterson

Committee Member
School of Mechanical Engineering
Georgia Institute of Technology

Dr. Hamid Garmestani

Committee Member
School of Materials Science and Engineering
Georgia Institute of Technology

Date Approved: 04/16/2008

ACKNOWLEDGEMENTS

This work could not have been accomplished without the help and support of many individuals. I would like to first thank Dr. Preet M. Singh for his instruction, dedication, and encouragement in advising me through the entire PhD study. I also would like to thank Dr. Richard W. Neu for his guidance, assistance, and patience during my PhD study. I am also very grateful to other committee members, Dr. Timothy F. Patterson, Dr. W. Steven Johnson, and Dr. Hamid Garmestani, for their valuable advices and supports on how to improve the planning and performing of this work. I would like to express my appreciation to Mr. Jamshad Mahmood for all his assistance with research equipments and experimental setup. Next, I would like to thank all of my lab colleagues for all their valuable suggestions and discussions on my work. I would also like to recognize Yolande Berta, David Pena, Charles Andry, and Charles Brookshire for their support during the past five years

On a personal note, I would like to thank my parents, Yingchun Shen and Yinling Yang, for the continued support and faith in me.

TABLE OF CONTENTS

LIST OF TABLES

LIST OF FIGURES

LIST OF SYMBOLS AND ABBREVIATIONS

SAC	Stress Assisted Corrosion
TGSCC	Transgranular Stress Corrosion Cracking
IGSCC	Intergranular Stress Corrosion Cracking
BCC	Body Center Cubic
FCC	Face Center Cubic
SSRT	Slow Strain Rate Test
ISSRT	Interrupted Slow Strain Rate Test
AFM	Atomic Force Microscope
CT	Compact Tensile
SEM	Scanning Electron Microscope
XRD	X-ray Diffraction
LP	Low Pressure
HP	High Pressure
IP	Intermediate Pressure
SH	Super Heater
RH	Re-heater
HIC	Hydrogen Induced Cracking
SCC	Stress Corrosion Cracking
SICC	Stress Induced Corrosion Cracking
CF	Corrosion Fatigue
ID	Inner Diameter

OD	Outer Diameter
LEFM	Linear Elastic Fracture Mechanics
FEM	Finite Element Method
SIF	Stress Intensity Factor
DO	Dissolved Oxygen
CERT	Constant Extension Rate Test
ESP	Emergency Shutdown Procedure
EPRI	Electric Power Research Institute
GBCD	Grain Boundary Character Distribution
ECD	Electrochemical Potential
BTF	Boiler Tube Failure
z	valences of solvated species
F	Faraday's constant
M	Molar
ΔK	Stress Intensity Factor Range
ΔK_{th}	Threshold Stress Intensity Factor Range

SUMMARY

Failure of carbon steel boiler tubes from waterside has been reported in the utility boilers and industrial boilers for a long time. In industrial boilers, most waterside tube cracks are found near heavy attachment welds on the outer surface and are typically blunt, with multiple bulbous features indicating a discontinuous growth. These types of tube failures are typically referred to as stress assisted corrosion (SAC). For recovery boilers in the pulp and paper industry, these failures are particularly important as any water leak inside the furnace can potentially lead to smelt-water explosion.

Previous research shows that metal properties, environmental variables, and stress conditions are the major factors influencing SAC crack initiation and propagation in carbon steel boiler tubes. A significant volume of work has also been published to show that the use of carbon steel in high temperature water applications strongly depends upon the formation and stability of a protective magnetite oxide film on the waterside of boiler tubes.

This present study is aimed at evaluating above stated variables individually and interactively to identify SAC crack initiation and crack propagation behavior in carbon steel boiler tubes. Other goal of this research is to understand the mechanism of bulbous

SAC crack formation under industrial boiler operating conditions, thus to figure out a practical way to predict and prevent SAC type failures in the industrial boilers.

In order to achieve these research goals, an autoclave with recirculation-loop was set up to simulate boiler-waterside environment in laboratory to systematically evaluate the role of key industrial boiler design and environmental parameters in initiation and propagation of SAC in the laboratory. Slow strain rate tests (SSRT) were conducted under boiler water conditions to study the effect of temperature and oxygen level on crack initiation and propagation on SA-210 carbon steel samples machined out of boiler tubes. Boiler water chemistry was controlled during a series of tests to keep the dissolved oxygen in the range of 10 ppb - 10 ppm. The magnetite film that forms on the surface has a significant role in the SAC mechanism, so coupon exposure tests were conducted to develop the magnetite film on carbon steel tube samples under different test conditions. The characteristics of film formed on the material surface were studied by atomic force microscopy (AFM) and scanning electron microscopy (SEM) technique. Heat treatments were also performed to develop various grain size and carbon content on carbon steel samples, and SSRTs were conducted on these samples to examine the effect of microstructure features on SAC cracking. A mechanism of SAC crack initiation and propagation were proposed and validated based on interrupted slow strain rate tests (ISSRT). Through these activities, significant environmental, operational, and material characteristics were identified to reduce the frequency and severity of SAC.

Simulation of boiler water conditions permitted systematic evaluation of the role of key design and environmental parameters in a laboratory system. Their individual or combined effects on SAC are quantified so that mitigation strategies can be developed to avoid SAC. Results from the tensile samples tested in boiler water with dissolved oxygen of ~3ppm and oxygen below 5-ppb have shown that SAC can be controlled by reducing the oxygen level dissolved in boiler water. Results from coupon exposure tests have indicated that the water chemistry and ratios of anode/cathode have an effect on the magnetite film morphology. Film characterization by AFM and SEM has shown that the magnetite film changes from a fine-grained porous film with tetrahedral crystals at the surface to an irregular-grained compact and protective film when the anode to cathode area is decreased. SAC crack initiation and growth mechanisms involved in boiler water environments include magnetite film damage as an important step. SSRTs on heat-treated tensile samples show that ferrite grains on the carbon steel surface is more susceptible to SAC cracks, and larger grain size, lower carbon content tend to accelerate SAC cracking. The results from SSRT and low-frequency tests indicate that crack susceptibility is found to be higher with higher mean stress, amplitude, and maximum stress, but lower with increasing cyclic frequency and the strain rate shows important influence on SAC initiation and growth in boiler water environments.

Finally, mechanisms of SAC crack initiation and propagation under industrial boiler water environment were proposed and validated based on the above stated results. The deliverables from this project can be used to control SAC in boilers: efforts were made on providing water chemistry guidelines to prevent SAC in recovery boilers and

developing a fracture mechanics model to predict SAC failure on industrial boiler tubes. Further research findings, scientific impact, and potential future work are also discussed.

CHAPTER 1: INTRODUCTION

1.1. The Evolution of Boilers

1.1.1. Design of Boilers

The power of steam had been recognized as early as 150 BC, but did not get widely utilized until the 18^{th} and 19^{th} centuries [1]. Steam was generated in closed vessels and was first used to convert chemical to physical energy, then was used to generate electricity. The development of the steam engine to drive line shafts in mills and pumps in the mines and for the propulsion of ships and locomotives led to the developments and improvements in boilers in the 1700s [1]. It was believed that the first boiler was of Greek and Roman origin. It was small and used for warming water, for heating, and for household services [2]. The boiler used with hero's engine on 130 BC was the first recorded boiler as doing mechanical work [2]. In the 1800s, boilers were most frequently built by inventors with little engineering training or education. Therefore these boilers appeared in all different shapes: oval, rectangular, round, and combinations of these. For this reason, it is more practical to classify boilers based on their mechanisms instead of on shapes. Generally there are externally-fired boilers and internally-fired boilers. Externally-fired boilers have a separate furnace built outside of the shell of the boiler,

while in the internally-fired boilers the furnace forms an integral part within the boiler structure [2]. Water-tube boiler and shell boiler are the major subjects of more concern within the externally-fired boilers. The water-tube boiler has won more acceptances over shell boilers from various industries due to the fact that water-tube boiler has better evaporative capacity, better performance under high pressures, higher thermal efficiency, and water-tube boiler is the least expensive one of all boilers for a given extent of heating surface [3]. The Babcock & Wilcox boiler, made around 1870, was the first successful water-tube boiler of sectional type [2].

1.1.2. Material of Boilers

Boiler can be defined as a closed vessel in which water is boiled by heat and thereby converted into steam, which is then available for power and heating purposes, thereby it has critical requirements for material properties. However, the materials for earlier boiler construction were limited to wrought iron, cast iron, copper, and iron, most of which were of poor quality and low strength [3]. Compared to high temperature, high pressure boiler (400^{o}F, 250 psi or above), low-pressure steam apparatus made of cast iron seems less problematic. However, cast iron becomes a dangerous material to use when high temperature and high steam pressure are concerned. This is chiefly because it is impossible to determine from its external appearance the internal conditions of a casting. Although not influenced to great degree by the temperature below 900^{o}F cast iron is not a suitable metal for boiler parts due to its low tensile strength and exceeding brittleness [2]. For this reason the American Boiler Manufactures' Association and others has excluded

cast iron more than 30 years ago from use wherever comparable tensile stresses exist [2]. The high pressures and temperatures used in power generation require a material of which the chief property shall be ductility. While strength is a desirable attribute in the structure of any boiler, the varying conditions of contraction and expansion, of shock and overpressure, and of corrosion and overheating demand a material the toughness of which will endure rough usage and give abundant warning before rupture [2]. At the same time the modern advance of steel making, especially in material toughness and homogeneity, has led to the wide adoption of puddled wrought iron as a very good material for use in pressure vessels. However, the high cost of wrought iron together with its comparatively low tensile strength, have served to eliminate it largely from use in boiler shells. With the later improvements in pressing and extruding metals in the early 1900s, most part and portion of a steam boiler can be shaped from soft steel without adding much to the expense [2]. For this reason, the modern methods of the steel foundry and annealing render the steel casting almost as homogeneous and ductile as the forging [4]. Most boilers, therefore, for severe service and high pressure, are made throughout of soft steel. At one time copper was widely used for the furnace sheets of locomotive and vertical boilers due to its ductility and immunity from corrosion [4], though the tensile strength of copper rapidly diminishes beyond 500^{o}F. Mild or low carbon steel is an alloy of pure iron with small proportions of carbon in chemical combination as iron carbides and of other elements. It is manufactured from pig iron. Mild steel has largely supplanted copper because of its relative cheapness, better ability to resist high temperatures, and all-around purposes for boiler construction [2].

As for the material selection for various parts of a boiler, it is always a function of expected temperature and related operating conditions. Take a modern recovery boiler as an example of an industrial boiler, as shown in Figure 1.1. It has two main sections: a furnace section and a convective heat transfer section, which transfers heat to the boiler water to form high-pressure steam. The furnace walls are constructed of vertical tubes set in a row. Normally economizers and water-wall sections are constructed with low or medium carbon steels, ferritic steels are typically used for super-heater/re-heater sections, and austenitic stainless steels are used to build parts with highest temperatures in the boiler due to the excellent corrosion resistance and good mechanical properties. Materials with higher corrosion resistance and better elevated temperature strength are used within limited range in boilers due to economic consideration.

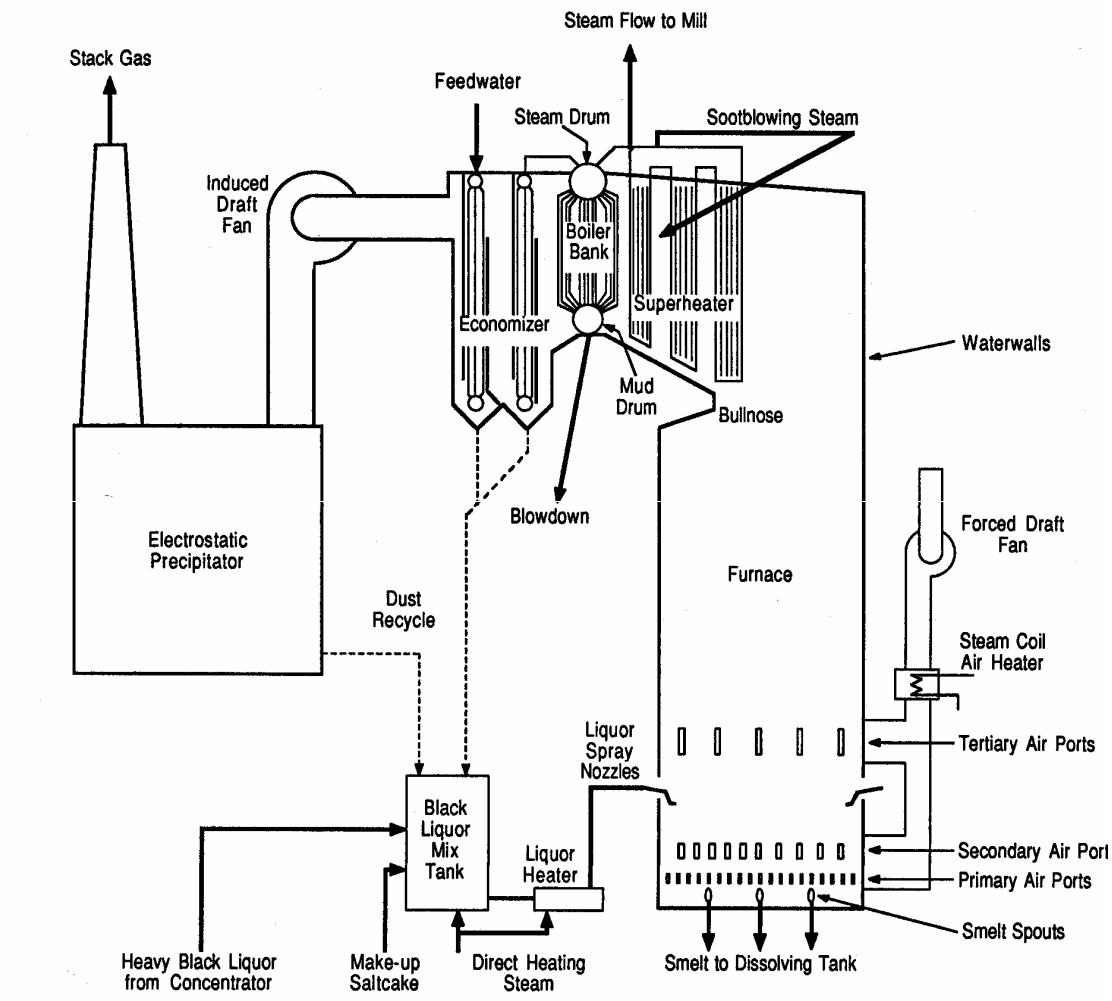

Figure 1. 1. Schematic diagram of a kraft recovery boiler [6]

1.2. Introduction of Boiler Cycle Chemistry

In most boilers, the boiler water solution is prepared to required conditions in a make up tank. Exit boiler water from the make up tank is pre-heated to a relatively low temperature by passing through a series of feed-water heaters of low pressure (LP) and high pressure (HP). Then the feed-water passes into the major part of boiler and gets heated to superheated steam. The superheated steam exits from boiler expands through the high pressure (HP) turbine, intermediate pressure (IP) turbine if present, and low pressure (LP) turbine to extract the energy/work out of the superheated steam. Exit steam from the turbines will then be condensed to lower pressure and temperature water and feed back to the make up tank. This is a typical once-through re-circulation cycle of boilers [6].

During this boiler cycle the ingress of contaminants, deposition of contaminants, and corrosion were found as the major carriers of potential problems who may have implications to the analysis of boiler tube failures (BTFs) [5]. It is generally believed that those contaminants including chlorides, sulfates, organics, oxygen, and carbon dioxide will enter the condensate part of boiler cycle and cause damages in the boiler (tube failures), or in the turbine (blade failures). The contaminant ingress was mainly found to occur during the make up process of feed-water in the tank, or whenever the feed-water was introduced into the circulation process. As a result, the deposition of contaminants was found at locations of LP&HP turbines, LP&HP heaters and the interior part of boiler.

Corrosion seems to occur at locations susceptible to contaminant deposition except at HP&IP turbines where the boiler water becomes 100% steam with probably the highest temperature [6].

The temperatures of boiler tubes also play important roles and in some level may be able to determine when/where the BTFs will occur. The temperatures of boiler tubes depend on the heat flux from the fireside and the condition of the internal fluid flow [5]. The tube of the lowest temperature is believed to come from the economizer, where the fluid is running as liquid solution. Then the liquid flow runs into the waterwall tubes as a liquid-steam mixture due to the heat transfer through the waterwalls. The fluid inside the boilers exists as liquid-steam mixture and its temperature remains constant with a typical range of 250^{o}C-450^{o}C for various boilers due to the limitation of water saturation. After exiting boilers the fluid becomes super-heated steam, the super-heated steam may get re-heated after passing through the HP turbine. At those super-heater/re-heater sections, temperature in excess of 600^{o}C (~1110^{o}F) can be reached during the final stages [5].

1.3. Boiler Tube Failures (BTF) Overview

Boiler tubes are subjected to potential degradation by a variety of mechanical and thermal stresses, and to the potential for environmental attack on both the fluid and fireside under high-temperature and high-pressure conditions. If there is no breakdown from the original design conditions, water-touched boiler tubes (waterwalls, economizers etc,) are designed for, and should have, an essentially infinite life.

Unfortunately, boiler tube failures (BTFs) remain a significant and pervasive problem in the pulp and paper industry. Especially in the paper mill, any water leak into the Kraft recovery furnace can potentially cause an explosion. Failure can occur in all boiler areas: economizers, waterwalls, super-heaters (SH) and re-heaters (RH). More than 80% of all BTFs force a facility shutdown, and a typical outage lasting three days can cost $1,000,000 for power replacement [7]. The BTF mechanisms representing the leading causes of availability loss, which come from the 16 U.S. utilities and is believed to be similar among the whole of the United States. By the early 1980s, up to 22 different BTF mechanisms had been identified and more than 80% of them were considered to be well understood [7]. Among them the BTF mechanisms which attracted most attention from researchers recently are shown in Table 1-1.

Table 1-1 Popular BTF mechanisms presenting major losses of unit availability

Corrosion Fatigue
Hydrogen Induced Cracking
Overheating
Stress Corrosion Cracking
Erosion Corrosion
Pitting Corrosion
Galvanic Corrosion
Stress Assisted Corrosion

1.3.1. Corrosion Fatigue

Damage Mechanism

Corrosion fatigue occurs by the combined action of cyclic loading in a corrosive environment and leads to brittle failure. Cyclic stresses may come from differences of thermal expansion, residual stress from manufacturing, or stress concentration effects [5]. Corrosive environments may come from dissolved oxygen or chemical cleaning during boiler shutdown. Under these conditions, crack initiation and propagation occurs more readily than it would occur under inert environments. The frequency of cyclic stress plays important role in CF cracking. Only slight, long term variations in loading are known to accelerate the onset of CF cracks, whereas high frequency loading tends to eliminate the effects of the corrosive environment.

Appearance & Location of Failure

CF failures appear as multiple, transgranular cracks that initiate from the inner surface of boiler tubes [5]. Cracks usually can be found in both waterside and fireside tube surfaces, located at attachments and/or restraints, which work as stress raisers to increase susceptibility to CF [11]. Cracks often initiate from oxygen or acid cleaning pits in the protective magnetite oxide on the boiler tube surface. Once formed, these pits may become anodic and prone to localized corrosion. These pits will also act as stress raisers. If cyclic loading continues, these surface pits will propagate along the tube wall thickness, form thick-edged fractures and eventually lead to pin-hole leaks or window-type blowout

failures [5]. Stress intensity is proportional to stress for a given crack length. Severe notches have stronger influence on the fatigue life than does corrosion alone. Surface roughening by exposing boiler tube to a corrosive environment is also well known to degrade subsequent fatigue life of them.

Root Cause and Corrective Actions

The root cause of corrosion fatigue cracking can be verified by evaluating the cyclic stresses and the environmental conditions at the failure location. A review of the water chemistry practices including chemical cleaning may be very helpful to understand the environmental effects on CF cracking [5]. Susceptibility of CF type of failures can be reduced by redesign of tube attachments to eliminate stress raisers. Conducting chemical cleaning in a timely manner can be beneficial to reduce environmental effects. However, overly aggressive chemical cleaning should be avoided. The focus should be on controlling the dissolved oxygen level to below 5 ppb and maintain pH within an acceptable range [6]. It will also be helpful to optimize the boiler shutdown/startup procedures to avoid out-of-service corrosion and minimize operation transients as much as possible. Long term prevention of BTF due to CF may require locating and replacing boiler tubes which contains cracks [7].

1.3.2. Hydrogen Induced Cracking

Damage Mechanism

Hydrogen induced cracking (HIC) is caused by penetration and diffusion of atomic hydrogen into the crystal structure of an alloy under low pH conditions, either in localized areas, such as underneath internal deposits or in terms of overall bulk water chemistry [5]. Low pH conditions make boiler tube susceptible of corrosion by removing the protective oxide film from boiler tube surface. After the atomic hydrogen entered the tube metal, it will react with the iron carbide in the steel to form methane gas, to form a local decarburized region. The methane molecules are fairly large thus may be trapped at grain boundaries. The trapped methane gas will build up the tube pressure gradually, leads to internal fissures and eventually a though-wall fracture. Aqueous hydrogen sulfide and H_2S dramatically accelerates hydrogen entry thus HIC in most alloys [7].

Appearance & Location of Failure

HIC often occurs in carbon steel waterwall tubing at locations of high heat flux and at locations where waterside deposit buildup is the greatest. HIC normally appears as discontinuous intergranular fissures and the surface of HIC may be smooth or pitted, with a thick layer of corrosion products [5]. BTFs due to HIC normally contain thick-edged-window openings which were blown out of the tube wall. A heavy internal scale may be seen unless it was removed during the rupture event [5].

Root Cause and Corrective Actions

The root cause of BTFs due to HIC can be verified by investigating into the source of the corrosive chemicals in the boiler and into the amount of deposition on the inner surface of boiler tubes [5]. The technique of tube sampling can be used to measure the relative thickness and amounts of internal buildup of deposit on the heated side of boiler tubes. Detailed tube sampling practices and related test methods can be found in ASTM standards D887 and D3483. BTFs due to HIC are often reversible [5]. Corrective actions of HIC normally involves removing the boiler tube from service, controlling water chemistry within proper range, eliminating hot spots or flow disruptors where excessive deposition occurs, and performing chemical cleaning when appropriate. Chemical cleaning should be considered after pH value was found to drop below 7 for more than one hour. By doing chemical cleaning the internal deposits are removed thus further hydrogen generation is no longer possible. HIC is especially prevalent in iron alloys because of the restricted slip capabilities in the predominantly body-centered-cubic (BCC) structure. The face-centered-cubic (FCC) stainless steels and FCC alloys of copper, aluminum and nickel are more resistant due to their inherent high ductility and lower diffusivity for hydrogen atoms, but all can become susceptible to HIC if highly cold worked [7]. The use of those materials for boiler tubes can reduce the susceptibility of HIC. Pad weld repairs may also help but should not be used for repeated failures due to HIC.

1.3.3. Overheating

Damage Mechanism

BTFs due to boiler tube overheat actually involves two mechanisms: short-term overheat, and long-term overheat. Short-term overheat occurs when boiler tubing is heated well above design temperature of the tubing material. Boiler life will drop dramatically if overheat was experienced by boiler tube. Short-term overheat damage may come from excessive local combustion, or the cooling role of steam/water flow is not fulfilled adequately. Short-term overheat damage can occur even at a temperature below the critical temperature (A_1) of material. Long-term overheat failure can also be named as high temperature creep. Long-term overheat damage usually occur with a small amount of creep deformation [5]. It also occurs when boiler tube is exposed to its creep temperature regime, and the temperature is usually above the oxidation limit of boiler tubing. Boiler tubing with higher temperature will also likely to have higher fireside ash corrosion rate and steam side oxidation rate. Ash corrosion will build up the wall-thinning effect and the hoop stress, thus lead to higher creep accumulation rates. Whereas steam-side oxide film will insulate the tube wall from steam/water cooling, resulting a much higher temperature as well as a higher creep accumulation rate [5].

Appearance & Location of Failure

Short-term overheat of boiler tubes appear as thin-edged damage, and often shows signs of tube bulging or “fish-mouth” appearance along the longitudinal direction of tubing. Long-term overheat appear as thick-edged damage, the damage also grows along

the longitudinal orientation of tubes [5]. Both short-term overheat and long-term overheat damages tend to initiate near bottom bends in vertical loops of SH/RH, or near material transitions, or anywhere the gas temperature is the highest.

Root Cause and Corrective Actions

Failure analysis or metallurgical evaluations of failed boiler tubes can not provide definite identification of overheat damages. Normally a review of plan records of failed tubing may help to identify any suspicious event which may be known to cause the damage [5, 7]. If the plan record review can not catch the root cause of failure, field measurements of temperature may be conducted to locate where and when overheat occurs. For super-heater and re-heater tubing made of ferritic materials, the measurements of tubing wall thickness and surface oxide film thickness can be used to estimate the rate of long-term overheat damage, and current status of resulted failure. Corrective actions of overheat damages involves adjusting boiler burners and re-design to improve the thermal responses of the boiler tubing with concern of possible overheat damages [5].

1.3.4. Stress Corrosion Cracking (SCC)

Damage Mechanism

SCC was reported as the so-called season cracking of brass in ammonia-bearing environments in the early twentieth century and was a serious problem in the failure of

cartridge cases for firearms during both world wars. Caustic cracking with resulting explosions of carbon steel steam-engine boilers was treated as a dangerous problem in the 1920s [7]. Historically, it has been thought that three conditions must be present simultaneously to produce SCC: a critical environment, a susceptible alloy, and some components of tensile stress. The environmental species are often specific to the alloy and may not have any effect on other alloys of different type. Not all environments cause SCC cracking of any particular alloy, but new alloy-environment combinations resulting SCC are continuously being discovered on a regular basis. Thus, many researchers are of the opinion that a specific environment may be not required for SCC [5]. Nevertheless, engineers should be familiar with those existing alloy-environment combinations that are known to produce SCC, in order to avoid them in design. Although these three factors are not usually present together, time and service conditions may conspire to produce the necessary combinations that result in surprising and expensive failures. The ingress of contaminants can provide the necessary corrosive species. The stress component may come from operation transients and residual stress stored in boiler tube during manufacturing. SCC may be initiated under corrosive environment with stress level below yield strength.

Appearance & Location of Failure

SCC cracks are most likely located on bends and straight tubing, and high stress concentration areas near welds and tube attachments. SCC cracks can grow in either transgranular or intergranular mode, usually with significant branching in crack path. The

initiation of SCC can be at inner diameter (ID), or on outer diameter (OD), along circumferential or longitudinal direction [5, 7].

Root Cause and Corrective Actions

The root cause of SCC can be verified by investigating into the source of the corrosive chemicals and the source of tensile stress. The stress level in boiler tube can be evaluated by taking field measurements, or performing stress analysis by numerical methods [5, 7]. The detailed practices can be found in ASTM Standard Practice A262 [5]. The prevention of SCC generally requires elimination of at least one of the three components of SCC. In industry the corrective actions of SCC include replacing super-heater tubing for contaminations due to improper chemical cleaning, and stress-relief annealing of bending parts and welding affected area of tubing can reduce the residual tensile stresses. Palliative may include: (i). Re-design boiler parts to eliminate service tensile stresses from critical parts. (ii). Shotpeening parts to a compressive state. (iii). The control of boiler water chemistry by adding inhibitors to lower oxidizing agents or remove the critical corrosive species. This latter palliative is probably the most effective method for eliminating SCC [5]. Coating sometimes is not effective in controlling SCC because the coated layer will not withstand aggressive chemical and physical environments associated with SCC. Choosing a different alloy which is immune to that specific environment may also help to stop SCC. Cathodic protection usually will help to reduce the rate of SCC, but sometimes will accelerate HIC.

1.3.5. Erosion Corrosion

Damage Mechanism

Erosion corrosion can be defined as a conjoint action involving corrosion and erosion in the presence of a moving corrosive fluid, leading to the accelerated loss of material [5]. Erosion is mainly caused by flow effect, when the surface layer of material is worn away by the movement of flowing fluid. Virtually all alloy or metals are susceptible to certain type of erosion-corrosion as erosion corrosion is more dependent on the fluid. Fluids that contain suspended solids and flow with high speed were often found to be responsible for erosion-corrosion. Metals or alloys which rely on a passive layer are especially sensitive to erosion-corrosion. Once the passive layer of material has been removed due to the flush or the abrasion, the bare material surface will be exposed to the corrosive environment. If the removed surface layer cannot be re-passivated quickly enough, significant damage can be seen [5].

Appearance & Location of Failure

Erosion appears as thin-edged rupture, wall thinning from inside, and “beach mark” or “orange peel” appearance. Normally the imperfections (scratch, notch, inclusion, etc.) on the tube surface can cause an eddy current which provided a perfect location for erosion-corrosion. Also, erosion corrosion is often reported to occur at economizer inlet and locations nearest to any feedwater inlet, where flow rate of fluid changes dramatically due to tube size changes [5].

Root Cause and Corrective Actions

Erosion-corrosion is caused by a combination of chemical attack and the surface physical abrasion as a consequence of the fluid motion. The best way to mitigate erosion-corrosion is to control boiler systems by maintaining a low fluid velocity and by minimizing sudden tube dimension changes and elbows. The internal corrosion in pipeline can be monitored by exposing coupons prepared from same pipe material and retrieve them from target environment after a calculated period of time. The corrosion products on coupon surface can then be analyzed with lab techniques. NACE International (http://www.nace.org) has a standard on erosion-corrosion testing. ASTM (http://www.astm.org) also has standards on erosion corrosion testing.

1.3.6. Pitting Corrosion

Damage Mechanism

Pitting can be defined as localized dissolution on material surfaces. Pitting normally starts from small imperfections in the metal surface to begin the process. Once pitting starts, the localized corrosive environment will become more concentrated around the pits, and then a "snowball" effect will take place to further develop the pitting. Pitting can grow without being detected for extended periods of time, until a failure occurs. Pits are often found as localized part-and through-wall perforations in boiler tube with the majority of the damages oriented through the wall thickness. Usually the adjacent metal around pits remains unaffected [5].

Appearance & Location of Failure

Pitting, as it sounds, appears as the formation of small pits on the surface of a metal or alloy. For pitting corrosion caused by low pH condition, the pits tend to be numerous and spaced close to each other. The cross section of pits generally appears as sharp-walled and free of corrosion products. Tube metal containing pitting corrosion damages is usually clean and free of deposits. The tube surface often appears rough and jagged. For pitting corrosion cause by high oxygen levels, the cross section of damages are usually filled with thick corrosion products. Both types of pitting corrosion often occur at inner surface of tubes where condensate can form and remain there during boiler shutdown, and also on bottoms of SH/RH tubes [5].

Root Cause and Corrective Actions

Pits can form on tubing surface due to chemical cleaning, surface defect/scratch, and surface inclusion. Generally pitting corrosion can be caused by either low pH environment or dense oxygen condition. Pitting can be mitigated by improving surface quality of materials, and conducting water chemistry control to reduce localized concentration of corrosive chemicals [5].

1.3.7. Galvanic Corrosion

Damage Mechanism

Galvanic corrosion is defined as an electrochemical process, in which two metals having different composition are electrically coupled in the presence of an electrolyte. The more reactive metal will experience preferentially corrosion while the more noble metal will be quite well protected [5].

Appearance & Location of Failure

Galvanic corrosion is a little more difficult to keep track of in the industrial world. Simply adding a screw of the wrong material can have severe consequences. Perhaps the most infamous examples of this type of corrosion are combinations such as steel and brass or copper and steel. Typically the steel will corrode the area near the brass or copper, even in a water environment and especially in a seawater environment [5].

Root Cause and Corrective Actions

The three key elements of galvanic corrosion are dissimilar metals, presence of electrolyte, and an electric circuit connecting two metals. Thus there are several ways to mitigate galvanic corrosion respectively. One way is to electrically insulate the two metals from each other. If the electrical contact is blocked, the electrochemical reaction will stop. This can be done using nonconductive plastic insulators. Another way is to eliminate the presence of electrolyte by keeping the metals dry and/or shielding metals

from ionic compounds. It is also possible to choose metals that have similar electronic potentials [5]. The more closely matched the individual potentials, the lesser the potential difference and hence the lesser the galvanic current. Using the same metal for all construction is the most precise way of matching potentials. Probably the most common way of avoiding galvanic corrosion is to electrically attach a third, anodic metal to the other two. This is referred to as cathodic protection. Finally, an electrical power supply may be connected to oppose the corrosive galvanic current. This method is usually defined as impressed-current cathodic protection [5].

1.3.8. Stress Assisted Corrosion (SAC)

SAC is very similar to CF, in terms of crack phenomena, mechanism and causes. The most popular location of SAC is the water-touched surface area near to stress raisers. The term SAC is usually used in the pulp and paper industry and CF is generally used in the power industry [11]. However, SAC is different in both crack morphology and water chemistry from CF cracks. Failure caused by SAC can be more severe as water explosion was reported in the kraft recovery boiler due to SAC. All those differences between SAC and CF indicate two different mechanisms involved in the two failures. Relatively less is known about SAC and more research need to be conducted to find out the damage mechanism and causes of SAC, and how to prevent SAC type failures in practice.

1.4. Cycle Chemistry Control to Prevent BTF

Due to the high temperature creep, BTF occurs in super-heater or re-heater sections. Other than that the major reason of BTF was the deviation or breakdown from the designed conditions of water chemistry in boilers [3]. It is generally believed that water chemistry control is the most effective and cost saving way to prevent corrosion and corrosion related failures in boilers [4]. In the 1950s United States realized this and started to work on BTF prevention by taking water chemistry treatments. In the 1960s, United Kingdom also initialized their efforts on mitigating BTF by controlling water chemistry variables [4]. It was determined by both US and UK that for most boilers the simplest and most cost-effective means of BTF prevention lies in the control options of the cycle chemistry [4]. In general for once-through units the boiler water chemistry is controlled by the feed-water treatment and for internal drum units the water chemistry is controlled by drum boiler treatment. Phosphate treatment and caustic treatment were used for a long time as control options of drum boiler treatment to provide good buffering of acids and hydroxides for drum units. However, it has been reported that phosphate treatment may cause phosphate hide out (defined as a decrease in phosphate and an increase in pH with increasing load), which can accelerate CF and lead to BTF [8]. The use of sodium hydroxide for caustic treatment in drum units seems more successful with more critical requirements on its concentration in boiler water than Phosphate treatment does. There need to be not only a minimum level of sodium hydroxide to eliminate anionic impurities and acid conditions, but also a maximum level of sodium hydroxide to avoid the damage on austentitic super-heaters and turbines due to caustic gouging from

overdosed sodium hydroxide in boiler water. The control options for feed-water treatment in many countries has consisted of adjusting pH with ammonia to 8.8-9.1 for mixed copper/iron systems, deoxygenating the feed-water mechanically in the condenser and deaerater, and deoxygenating the feed-water chemically by the addition of an oxygen scavenger [5]. It has been recommended by NACE that feedwater pH should be maintained at 9.0 or above to mitigate the potential for environmentally assisted cracking of the weld and heat affected zones of the deaerating heater and storage tank [8].

Since oxygen is not an ionizable gas, its solubility is temperature dependent. The oxygen level in boiler water was know to decrease as boiler is heated up, but it is hard to reduce the oxygen level to below 5 ppb in boiler water by using only thermal deaeration, that is why the use of oxygen scavenger becomes necessary. Hydrazine was first used as an oxygen scavenger in different industries in Germany prior to 1950 [9]. Duke Power was the first US unit to use Hydrazine for oxygen removal in utility boilers in 1951 [10]. When Hydrazine was used in feed-water system with an oxygen level far below 5 ppb, material reducing may occur to break down the protective oxide film on ferrous alloys and erosion-corrosion failures of economizer may result Sodium sulfite, another typical oxygen scavenger, was first used in 1950s to remove oxygen from boiler feed-water. Sodium sulfite reacts with water and oxidizes to sodium sulfate, which remains stable in boiler water with no reaction to other impurities at low pressures (below 250 psi) [8]. Sodium sulfate introduced through this reaction can become a problem as pressures go up, so the use of sodium sulfite is limited to lower pressure installations. Sodium sulfite also reacts with formaldehyde to form nonvolatile products so it is also suggested as a

formaldehyde scavenger in urea-formaldehyde resins used for foam insulation. Although with concerns on its slow and incomplete solubility in boiler water, sodium sulfite has become the first choice of oxygen scavenger for industry usage, and is still widely used in paper and pulp field and other industries [8].

CHAPTER 2: BACKGROUND

2.1. Motivation

The subject of interest in this study is the failure of boiler tubes due to SAC cracking in industrial boilers. SAC failures can occur in all boiler areas: economizers, water-walls, super-heats and re-heaters. Almost 90% of SAC failures force a shutdown, and a typical outage lasting few days can cost millions of dollars to replace boiler bottoms where waterside corrosion under external attachment welds has produced deep internal SAC type cracking [5]. Besides, the failure consequences caused by SAC sometimes can be catastrophic and fatal as water leaks due to SAC can cause explosions of boiler.

Failures of SAC type have been faced by all industrial boiler operators for decades, for which no complete mechanism was found to fully explain it, neither any proven remedy existed. The damage process, root causes, and corrective actions of a boiler failure may be governed by diverse BTF mechanisms as stated in previous chapter. It is very important to address that among all the BTF mechanisms, CF and SAC are very similar mechanisms, in terms of crack phenomena, failure mode, and causes. Literature review shows that research work on CF were more extensively conducted and relatively less is known about SAC. However, the review on CF research can be beneficial to SAC

study and it indicates that for SAC there is no single root cause but more likely a combined influence of various factors. Those suspected causes of SAC need to be evaluated. The magnitude of industrial SAC related failures urgently require a research program to understand the connection between SAC and CF and a comprehensive model is demanded to fully describe/predict how SAC behave under various environmental conditions. Therefore the failure analysis of recovery boilers which are known to have SAC cracks is included below to provide an initial understanding of SAC; also the rather more established understandings of CF are included here to lay an illustrative background for the SAC study.

2.2. Failure Analysis of Recovery Boiler Tubes

To evaluate the key material characteristics associated with SAC and to support laboratory simulation efforts, information from past inspection reports and failure studies of recovery boilers were analyzed. Further, tube specimens representing boilers with evidence of SAC as well as boilers with little or no evidence of SAC were examined using metallography and surface analytical techniques to find features of the base material and/or oxide film correlating with SAC.

2.2.1. Tube Sampling and Metallography Evaluation

Controlling corrosion and maintaining tube integrity in recovery boilers is a major challenge for operators. Sample tubes from failed recovery boilers were cut

longitudinally to facilitate visual inspection of the waterside of the tubing. A very smooth, uniform gray scale was found on the majority of the internal tube surfaces. However, oxide accumulations with thickness of almost 500 μm were observed in a few positions, which invariably were located on the waterside tube surface directly adjacent to an external attachment weld, as shown in Figure. 2.1. Not every attachment weld exhibited such an oxide accumulation on the tube waterside, but all accumulations were observed immediately adjacent to an attachment weld. When several tubes from a panel were examined together (such as the four-tube panel shown in Figure 2.2), oxide accumulations were observed on the inner diameter of the tube crown associated with each attachment weld location, but the degree of oxide accumulation typically varied somewhat among the attachment welds in the group. Please note that the oxide accumulation occurs only around the inner tube surfaces opposite each welding. One pair of oxide accumulations is marked with arrows, and similar pair of such accumulations is at similar locations of every tube, as shown in Figure. 2.2.

The cause of the oxide accumulations is perhaps related to subtleties of the internal heat transfer conditions at the attachment weld locations. For example, depending on the thermal efficiency of the weld attachment, the attachment may act as a cooling fin to encourage heat transfer from the tube and thereby precipitation from the water on the internal surfaces of the tube at these locations [11]. Alternate thermal conditions at the attachment might lead to slightly increased temperatures at the attachment locations encouraging more rapid growth of oxide. In any case, it is not apparent that the oxide accumulations directly cause SAC at these locations, but it is

likely the thermal conditions that contribute to the oxide accumulation also contribute to the stress concentration and corrosion conditions at these locations.

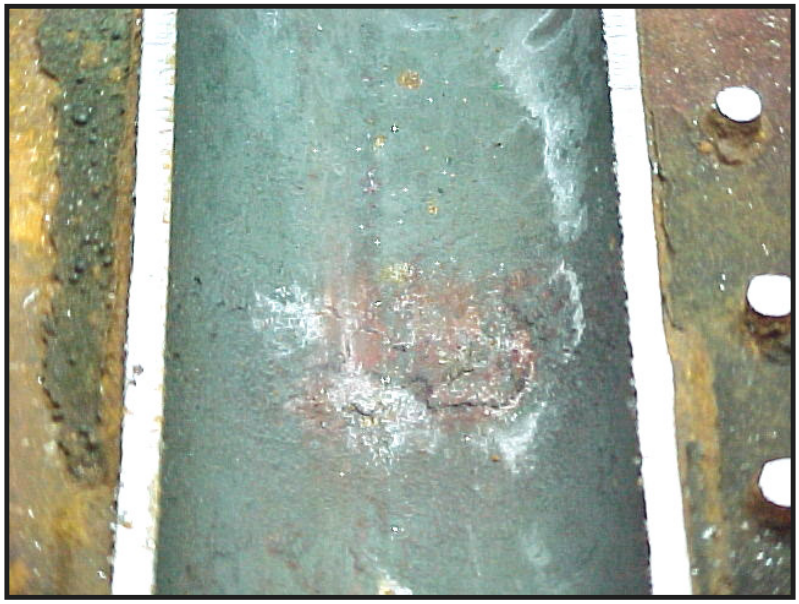

Figure 2. 1. Typical oxide accumulation on the internal surface of a boiler tube, viewed with oblique lighting. An attachment weld (scallop-type) is located immediately adjacent to the oxide build-up on the external surface of this tube.

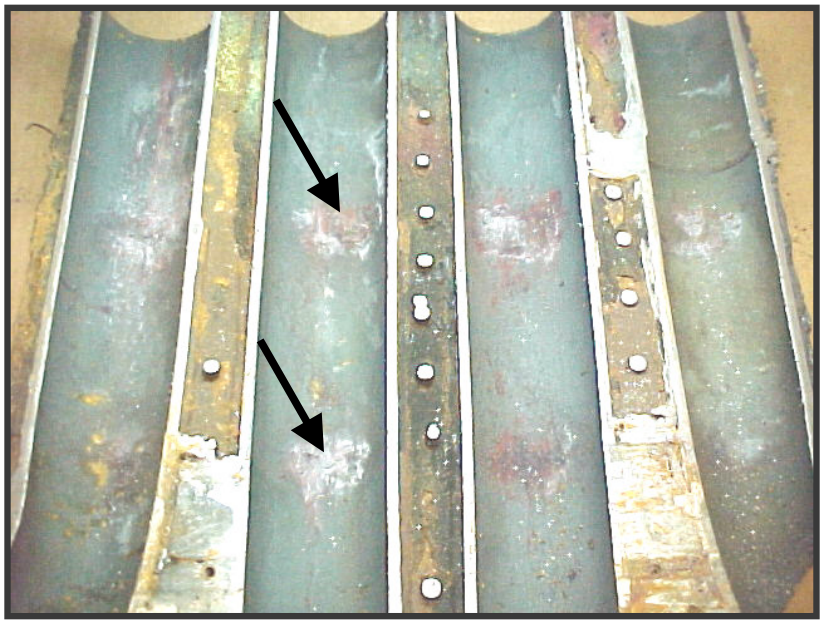

(a)

(b)

Figure 2. 2. (a) Scallop-type fillet welds associated with a tertiary windbox. (b) Internal surfaces at the fillet weld locations shown above.

One single tube sample with the oxide accumulation was cut into short lengths and chemically cleaned with inhibited hydrochloric acid (ASTM G-1-1990 procedure C.3.5) to remove the oxide with no appreciable attack of the underlying steel. A representative result was shown in Figure 2.3. Directly beneath the oxide accumulation, multiple longitudinally-oriented SAC cracks were observed. These SAC cracks appear as a cluster of short, roughly parallel indications on the ID near the tube crown, and are centered on the attachment weld location. The total longitudinal length of each cluster was less than 3 cm in every case for the tubes in this investigation.

Following the discovery of SAC under the oxide accumulations, tubes were sectioned to facilitate metallographic examination in regions with and without oxide accumulations. Figure 2.4 compares the nominal appearance of the internal oxide layer – observed over the entire boiler tube ID except for very limited areas adjacent to the attachment welds – where oxide accumulations were located. Nominally, the oxide is approximately 50 μm thick, relatively free of porosity, very adherent, and uniform in color, as shown in Figure 2.4.(a). In locations with oxide accumulations, the film tends to exhibit significant porosity (contributes to poor adhesion in some areas) and irregular thickness nominally near 300 μm but in some locations up to 400-500 μm, as shown in Figure 2.4.(b). In addition, the color of the thick films is not generally uniform, suggesting a range of oxide stoichiometries and compositions, including trace contaminants (Cu, Cl, P, and S were sporadically detected, generally near 0.1 at.%, but Cu and Cl occasionally were present up to almost 1 at.%).

Figure 2. 3. Attachment weld (top) and appearance of the internal surface opposite the weld following acid cleaning.

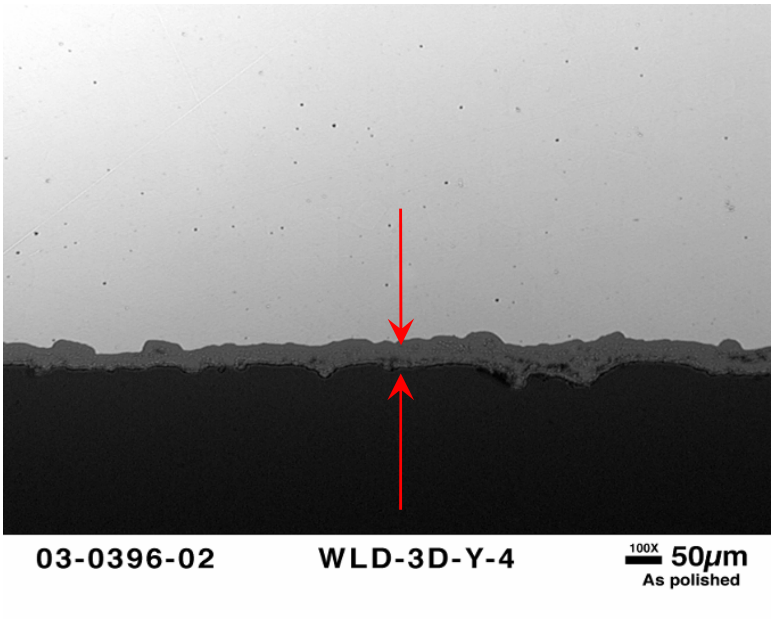

(a)

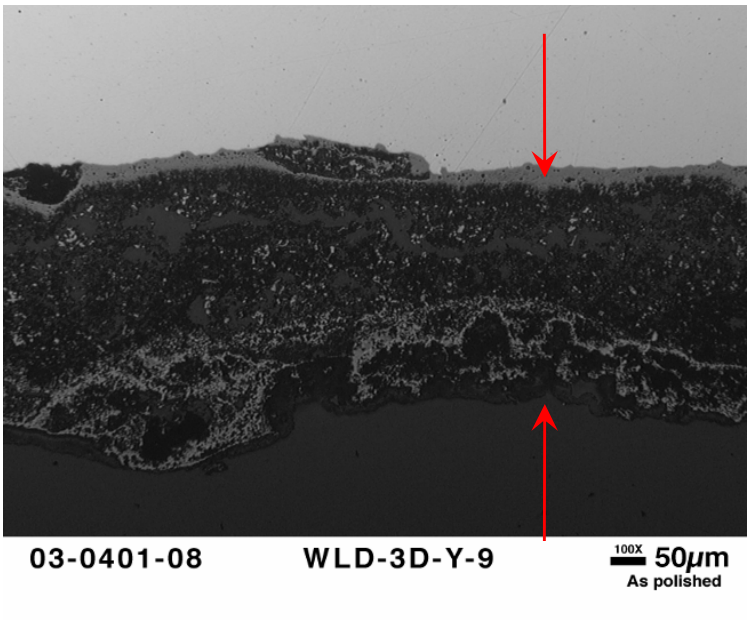

(b)

Figure 2. 4. Comparison of the nominal tube surface with the tube surface covered by oxide accumulations: (a) Nominal oxide, identified as compact & thin magnetite film, protective to SAC cracks on the tube (b) The porous & thick magnetite film, which is non-protective and associated with SAC cracks.

2.2.2. Microstructure of Material and Crack Morphology of SAC

Figure 2.5 represents the most common characteristics of the SAC indications observed in this failure investigation. The waterside penetrations are consistently transgranular, relatively straight (little or no branching), filled with an adherent, layered oxide along the crack path, with bulbous and rounded features around the tips. The relative width of the deepest penetrations varies significantly, with depth/width ratios commonly in the range 1-5. The SAC penetrations are invariably located within 1 cm or so of an attachment weld location, and the deepest penetration observed among these boiler tubes was about 30% of the tube wall thickness. In some instances, the penetrations are generally narrow with somewhat bulbous features, consistent with periodic intense corrosion events. Apparently, during periods of relatively high corrosion (probably associated with simultaneous rupture of the protective film and poor water chemistry), the penetration advances until the stress or water chemistry (or both) return to nominal levels, at which time the corrosion tends to spread laterally until full passivation is restored. In the most favorable cases, the number of "bulbs" on the penetrations can be related to the number of aggressive corrosion events [5] in the boiler.

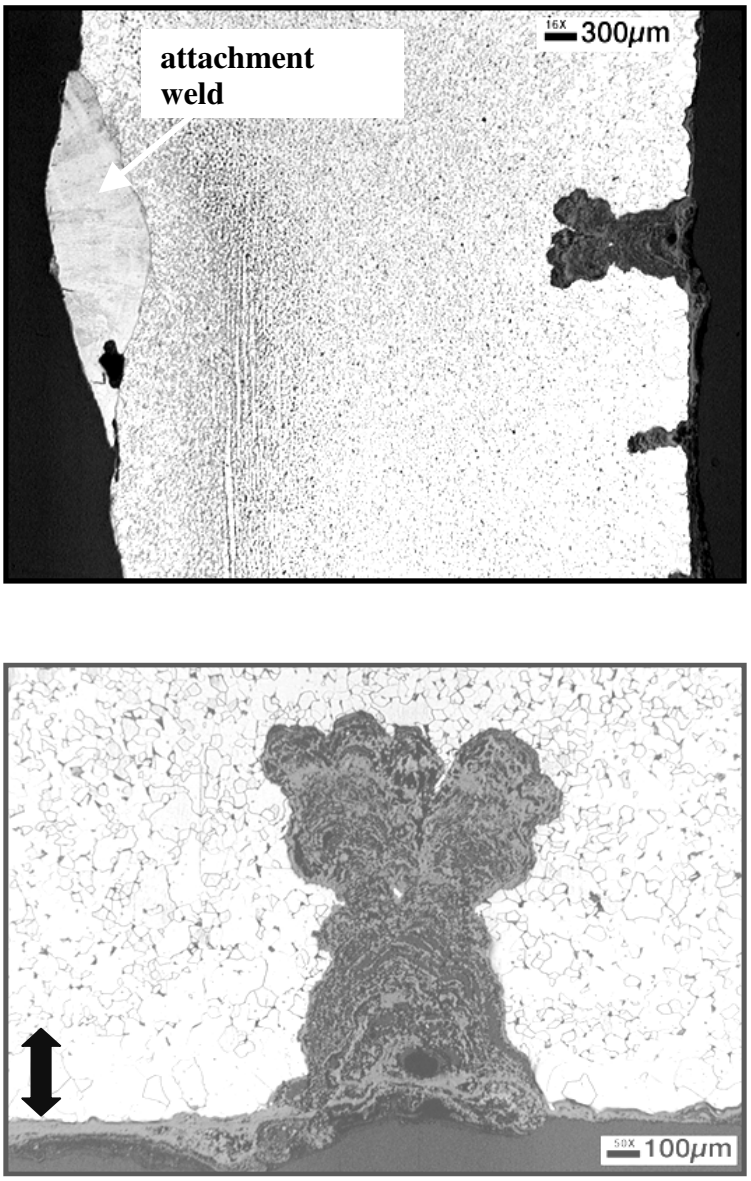

Figure 2. 5. (a) Representative photomicrographs of a tube cross section showing the attachment weld and adjacent SAC penetrations. (b) A higher magnification view of the deepest penetration associated with this particular attachment weld. A decarburized layer is marked with an arrow in the lower photograph. Note the weld-rounded features of the SAC indication and the fact that it is almost as wide as it is deep.

Another common feature revealed by the metallography in Figure. 2.5 is that the waterside surfaces rather routinely exhibit a decarburized layer approximately 200-300 μm deep in which the ferrite grains have grown significantly larger than the nominal size. Microhardness scans across the tube thickness indicate that the decarburized layer with large grains (85-100 HV) is generally somewhat softer than the nominal base material (100-115 HV). For comparison, the welds examined on these tubes exhibit somewhat higher hardness at 160-250 HV, with intermediate hardness in the weld heat-affected zone. In some regions with SAC indications, the decarburized layer was not observed on the tube waterside, suggesting sufficient general corrosion/wastage at this location to remove the thin layer of somewhat softer material. (It is also possible that tubes without the decarburization layer – potentially resulting from the original tube fabrication process – have been added in some locations as part of the periodic maintenance process). In general, the external surfaces of the boiler tubes also exhibit the decarburized layer with some grain growth (see area adjacent to the weld at the top of Figure 2.5), but where extensive surface preparation for an external attachment has occurred, the decarburized layer has typically been removed by grinding.

Additional photomicrographs emphasize other common features. Figure 2.6 is representative of the relatively common observation that only one of a group of indications tends to propagate significantly into the tube thickness. The factors that cause a specific indication to propagate are unknown, but likely are related to the combination of mechanical load at a particular location and the stress concentration associated with the specific shape(s) at the furthest extent of the indication when loading occurs. Figure

2.7 is representative of the trend that many of the deepest SAC penetrations seem to propagate from a substantial pit on the ID surface of the tube. Again, specific reasons for this behavior are unknown but stress concentration at the pit and perhaps occluded water chemistry within the pit lead to this aggressive behavior.

If the SAC process is initiated when boiler tubes experience sufficient strain to fracture the nominally protective oxide [11-17], then that process is perhaps aided by boiler tubes with a slightly weakened (decarburized, large grains) internal surface. Increased resistance to SAC might be realized by utilizing boiler tubes that do not exhibit a soft layer or, alternatively, selecting a somewhat stronger tube material in general, at least for application in areas of the boiler susceptible to SAC.

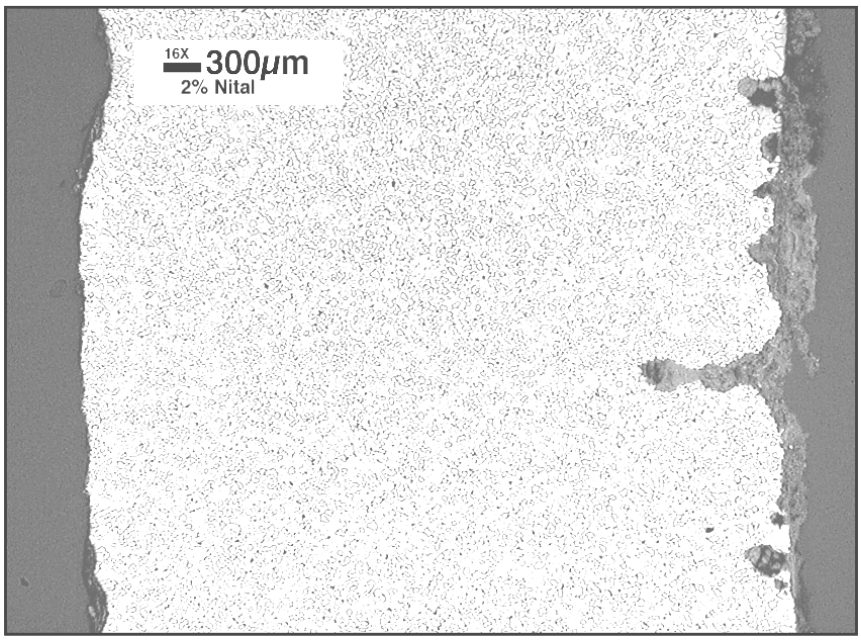

Figure 2. 6. Cluster of SAC indications on the ID of a boiler tube showing that only one indication appears to be propagating. The attachment weld in this case is just out of the photograph at the upper left. All of the indications are bulbous, rounded at the tip, and filled with oxide. Note also the thick oxide accumulation on the ID surface that tends to obscure the SAC indications from visual detection.

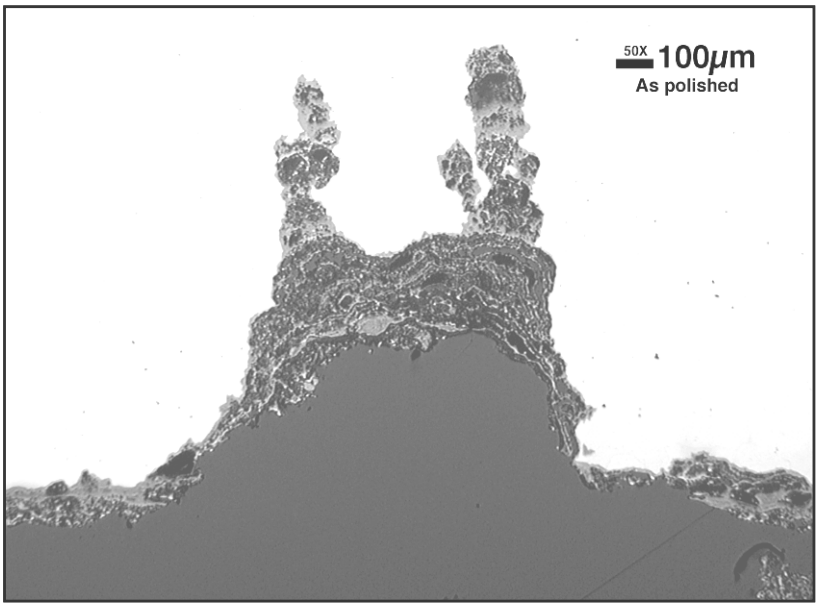

Figure 2. 7. SAC indications that appear to be propagating from a pit on the tube ID. As-polished [11].

Micrographs in Figure 2.8.(a) show the typical microstructure found in these tubes. Although there were a number of tubes where the microstructure at the tube surface was very similar to the middle of the tube but in a significant number of tubes a decarburized layer was seen near surface which had significantly larger grain size than the middle of the tube. In sections where this large grained layer was found, it was noticed that the majority of cracks seem to stop near the interface of normal microstructure and decarburized layer. This indicates that the decarburized layer with relatively large grains, with lower strength, may play some role in early initiation and propagation of SAC cracks. However, when these cracks face the stronger normal materials then the cracks do not grow further. Figure 2.8.(b) shows clearly that the layers with large grain also are soft compared to the normal microstructure in the middle of the tube. So this study will aim at evaluating how the decarburized layer and grain size difference influence SAC crack initiation and growth in industrial boilers.

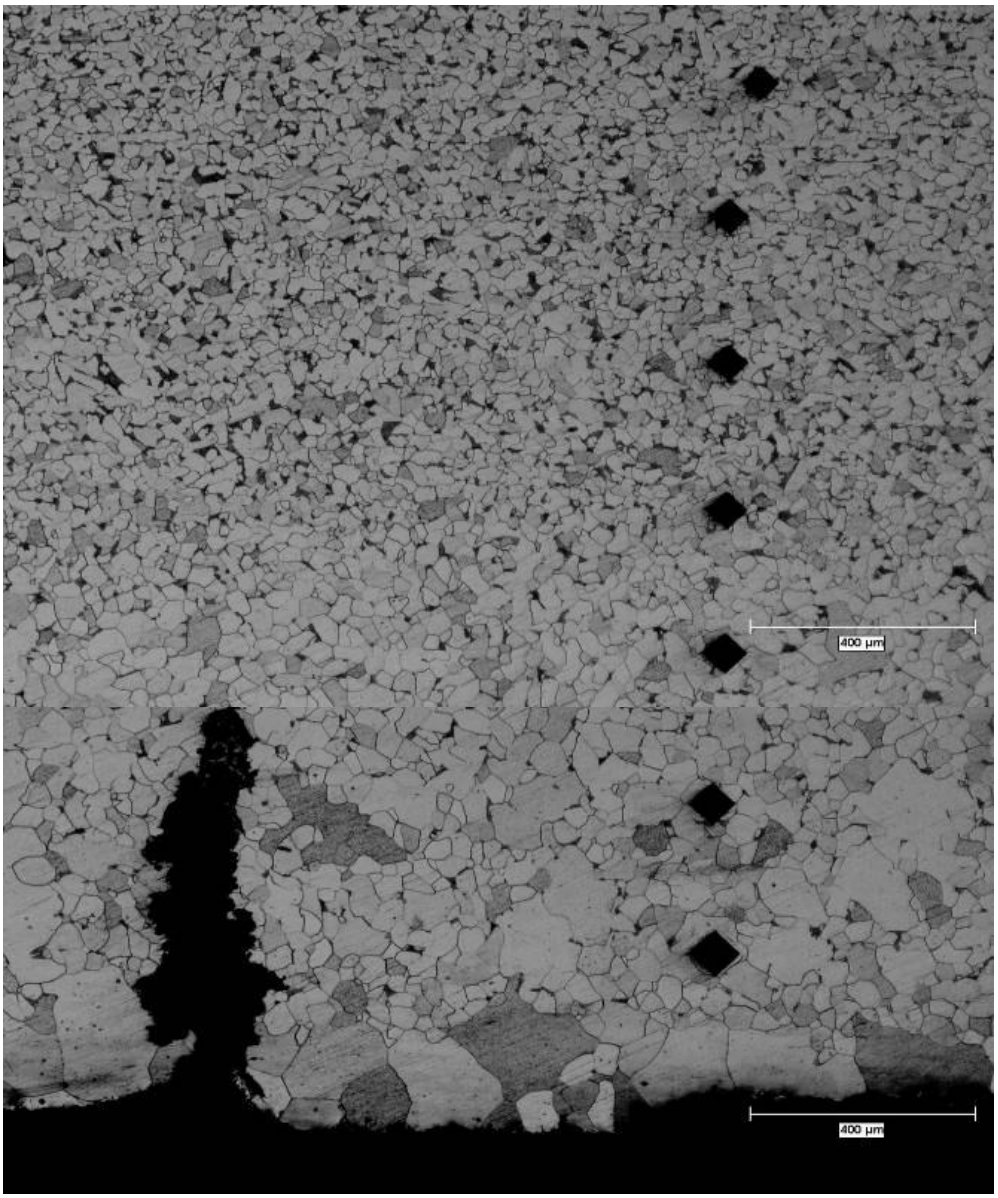

(a)

Figure 2.8 (a) Micrographs showing microhardness indents in the areas of grain growth and de-carburized layer as well as normal carbon steel tube structure. Notice that the indent size decreases away from the tube surface [11].

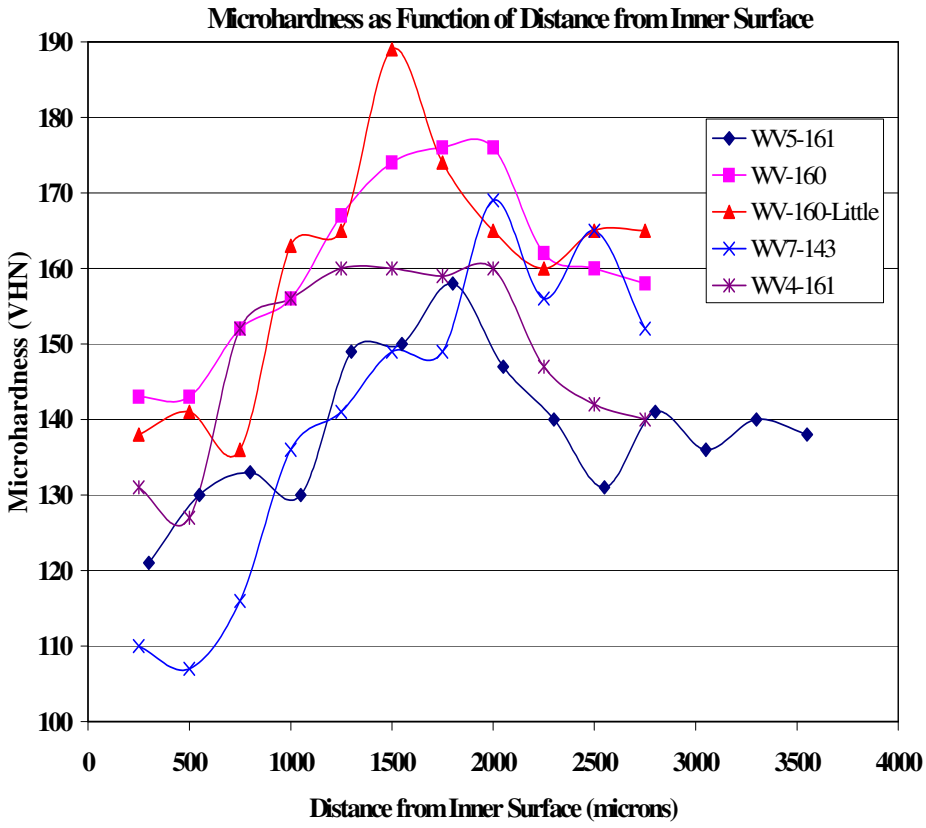

(b)

Figure 2.8 (b) Microhardness data for a set of tubes from a recovery boiler showing Vickers hardness number as a function of distance away from the inner tube surface. There is clear indication of softer layer at the inner as well as outer surface of the tube whereas the hardness is higher in the middle [11].

2.3. Research on CF Cracking of Boiler Tubes

The failure analysis of recovery boiler tubes also indicates that the mechanism of waterside SAC may be more related to CF cracking than other BTF mechanisms.

2.3.1. Introduction of CF Cracking

Waterside cracking of carbon steel tubes is one of the major reasons for water-wall tube failure in industrial and utility boilers and has also been recognized as a major cause for the boiler downtime [19-21]. As early as in the 1960s [19], some utility boilers were experiencing casing side tube leaks at attachment welds. It was assumed that those cracks originated at the outside surface of the tube, because of the proximity of the leak to the attachment weld, which was generally considered as "stress raiser". Efforts were made to modify the attachment to reduce thermally or mechanically introduced stress concentration effects which might promote outside surface crack initiation [19]. It took a while before it was recognized that actually the large majority of those leaks at attachments were originating from the inside surface of the boiler tube because leaking tubes were rarely removed and examined. Increasing awareness of similar leaks in both furnace and economizer sections was documented in some publications in the late 1970's. Quite often this type of waterside cracking was referred to as corrosion fatigue (CF) cracking and its mechanism which involves corrosion and stress (strain) was not as well understood as the other corrosion mechanisms at that time. Electric Power Research

Institute (EPRI) took a leading role in research to explain and control boiler tube problems of this type in the utility industry. In the late 1980's EPRI started a research project to study the corrosion fatigue problem in utility industry [19]. In 1992 EPRI identified corrosion fatigue as the leading cause of availability loss in fossil fuel fired utility boilers and the most popular location of this type of failure in utility boilers was the water side of pressure/non-pressure attachments in water-filled tubes. After another decade a mechanism and control scheme to avoid formation and growth of waterside CF in the utility industry was developed by EPRI. Based on the CF mechanism boiler operation guidelines were developed by EPRI to avoid CF failure in the utility boiler industry and are typically followed in the utility industry [20, 21]. However, there are significant differences in water treatment issues between utility boilers and recovery boilers (very large make-up water fraction in recovery boilers, different chemicals and treatment strategies) and the wide range of microstructural characteristics ascribed to water-side cracking of industrial boiler tubes as evidence that the details of the phenomenon and the EPRI recommendations might not apply to industrial boilers.

2.3.2. Factors Affecting Waterside CF Cracking of Boiler Tubes

Since 1983 the corrosion fatigue problem has been recognized as a major cause of tube failures and reduced availability in utility boilers [18, 19]. Prater and Coffin [22] reported that the temperature, dissolved oxygen level, and load frequency have significant effects on the life of fatigue crack initiation in high temperature water environments. Based on "the worst case" assumption, they [22] also provided a good

prediction of the ASME fatigue data curve from the ASME crack growth curves in air, for carbon steel. However, there were no systematic conclusions on the fatigue behavior of carbon steel under environmental effects due to his limited data. A significant amount of work has been published on corrosion fatigue crack initiation and propagation by other researchers [23-33]. The waterside corrosion fatigue in utility boilers was found to be strongly influenced by boiler water chemistry, particularly oxygen content, pH, chloride and sulfate content, as well as by number of start-ups, operating hours and chemical cleans. In order for corrosion fatigue to occur, a susceptible material, an environment that will cause cracking of that material and a high enough stress or stress intensity factor are required. However, because of the myriad of stress and water composition variables involved, no specific factors have been found to be universally associated with SAC, no specific rate (or even bounding rate) has been determined for the SAC processes. How SAC cracks formed in industrial carbon steel tubes is not clear either due to limited research work on this subject within the pulp & paper and other industries. But the conclusions above drawn from corrosion fatigue research can consequently provide us some possible directions we can follow during the investigation on SAC cracking problems of industrial boilers.

Industrial boilers have been traditionally defined as steam generators in which vaporization occurs in a convective section and in water wall tubes, which heat transfer occurs principally through radiation. A myriad of boiler designs can be shop assembled or field erected and can burn a wide range of fuels. Traditionally the majority of these boilers have been operated below 900 psi. Due to the change of market conditions later,

the owners and operators of industrial boilers have shifted to solid fuel burning for higher efficiency and simultaneous generation of process steam and electric power. With regard to cogeneration, users strive to extract maximum heat from the fuel. Therefore, industrial firms will more frequently select higher pressure and higher temperature steam cycles to optimize the amount of electrical power and steam produced. Until recently, the industrial trend toward higher pressures (up to 1800 psi) and temperatures presents new challenges for the boiler users/operators with respect to technology awareness and operational and maintenance requirements. Generally carbon steels become more brittle at lower temperatures. Several studies have dealt with the effect of temperature on corrosion fatigue [24-27, 30, 34-36], and most have shown that over a relatively wide range of temperatures, a rather mixed response is observed. Temperature effect is not a unique and straightforward manner. The effect of temperature on SAC cracking can be either way, with maxima, or minima value in between, depending on the actual situation. As James and Van Der Sluys [36] concluded that fatigue growth rates may either increase or decrease with increasing temperature, and maxima or minima in fatigue crack propagation rates often occurs at intermediate temperatures. Temperature effect is also more prominent in low cycle fatigue, compared with high cycle fatigue.

Oxygen concentration in utility boiler environments has a significant effect on corrosion fatigue cracks in carbon steels. For carbon steel boiler tubes, Dooley [20] reported that the corrosion fatigue is strongly influenced by water chemistry with oxygen concentration being the major factor. Results from phosphate water-chemistry tests indicate a two-orders-of-magnitude increase in dissolved oxygen from 10 to 1000 $\mu g \cdot kg^{-1}$

may decrease the number of thermal cycles required to initiate corrosion fatigue cracks by one-order-of-magnitude (from 1000 to ~ 100) [20]. This type of increase in oxygen concentration is associated with the boiler startup, when oxygen may enter the water and the thermal strains are also the greatest. This study also shows that the stress range needed for initiation of corrosion fatigue depends upon the water chemistry variables. Nakao et al. [37] noticed that fatigue life of carbon steel STS410 in BWR water started to decrease at temperature above 200 ^{o}C and with dissolved oxygen higher than 0.1 ppm. An empirical P-value equation based on their data was proposed to predict the fatigue life for this material for a certain environmental conditions 100-290 ^{o}C). In Perkins and Bache' [33] load control fatigue test at 120 ^{o}C de-ionized water, it was noticed that the addition of 4 ppm oxygen might produce an approximate 30% drop in fatigue strength. Chopra and Shack [38] found that a significant fatigue life decrease of carbon and low-alloy occurs only when five conditions are satisfied simultaneously. Those conditions are described as applied strain range, temperature, dissolved oxygen in the water, and sulfur content of the steel are higher than some threshold level and the loading strain rate should be lower than a threshold value [38].

Performance of carbon steel tubes in high purity water strongly depends upon the formation and stability of protective magnetite, oxide film on the waterside surface of boiler tubes [39, 40]. Chemical or mechanical disruption of the magnetite film may lead to the initiation of local corrosion or cracks. Rupture of the protective film by fatigue-generated strains may also depend upon the film composition and properties along with the magnitude of strain.

The extraordinary ability of boiler tube materials to function in boilers is due primarily to the formation of oxide film on material surface. Generally there are three stable, solid forms of oxide film that occur as a result of the reaction of iron and water/steam under temperature and pressure conditions relevant to boiler practice: wustite (FeO), magnetite (Fe_3O_4), and hematite (α -Fe_2O_3) [5]. Among these three types of film, wustite is formed with lowest oxygen concentration but not stable at temperatures typically below 500^{o}C. Hematite forms with highest oxygen concentration and normally exists as the outermost layer of the oxide. Magnetite is the most predominant form of oxide and exists over a wide range of oxygen partial pressures and temperatures [41]. When the oxide film grows, it also impedes transport and diffusion of the ions produced by the reaction of iron with water/steam. As a result, the rate of transport decreases with time. Similarly the rate of oxide film formation is initially high but decreases as the film thickness increases and become self-limiting [41]. How one of those three types of film forms depends upon a number of variables including: oxygen concentration, temperature and pH value [42]. Most time in actual practice only one layer of surface film will form because the possible extra layer of film tends to be taken away by the boiler water flow and gets re-deposited with feed-water corrosion products in other regions. Though the surface film grows as slow as only 10-15 μm after years, it still can provide enough protection from corrosion until mechanically disrupted or flushed away.

Mechanism of magnetite film growth on iron/carbon steel surfaces in caustic solutions or boiler water environment, and the resulting morphology, has been reported by a number of researchers [30, 32, 38-40, 43-45]. There is some discrepancy among the

results reported from magnetite growth experiments under similar test conditions. Magnetite film grown by Potter and Mann [30] under neutral and alkaline solutions in autoclaves or flowing water loops was reported to be thick & relatively porous duplex film whose growth follows a parabolic time law, and the magnetite film grown by Bloom and Newport [39] in neutral and alkaline solutions in closed ampoules was reported to be thin, compact and protective film whose growth follows logarithmic time law. In acid solutions, the growth of a thick multi-laminated film according to a linear time law was reported [32]. Some investigators used strong alkaline solutions to develop thicker oxides, but have reported that the morphology of the magnetite developed under these conditions was similar to the magnetite film formed on boiler tube surfaces under normal boiler operating conditions [43]. In simulated ground water solutions, the formation of magnetite film on iron surface was reported to grow by a dissolution/precipitation mechanism with the separation of anodic and cathodic sites across the surface film [45].

The growth mechanism involves a transport of iron ions from the steel to the outside interface of the oxide and an equal transport of oxygen ions from the boiler water to the steel surface. And the iron ions may be transported in two possible processes. The two processes in concentrated solution of NaOH were reported [40] as (i) solid state diffusion of iron and (ii) loss of iron by aqueous dissolution. There have also been discussions about how one process was chosen over the other in various environmental conditions. According to Mann et al. [30, 32, 40], the formation of either porous or compact film might be determined by which of the two processes occurred dominantly under the initial oxidation conditions. If solid state diffusion of iron acts as the rate-

limiting process under the initial oxidation conditions, it will more likely lead to formation of thin and continuous film. Whereas in initial conditions of iron transport by dissolution being the rate-limiting process, the system will tend to create porosity in the oxide film.

Magnetite film formed on the carbon steel surface acts as a protective barrier against further corrosion reaction. Corrosion fatigue or stress-assisted corrosion crack growth will also depend upon the breaking and formation kinetics of this layer in local areas with strain concentration. Attachment welds are such areas in boilers. Finite element modeling results have shown that the strain during boiler shutdown is concentrated on the inner surface of the boiler tubes in the vicinity of attachment welds [46]. Dynamic straining is experienced by the boiler tubes not only during boiler shutdown and startup but also during regular operations. These cyclic strains may help locally damage magnetite film if the strains are higher than the threshold strain values required for scale damage. Scale properties may also influence the value of strain required for scale damage. Dooley's study [20] shows that the stress range needed for initiation of corrosion fatigue depends upon the water chemistry variables, as the water chemistry deviates from the optimum values, the stress required to initiate corrosion fatigue decreases. This may explain the large variation in corrosion fatigue occurrence from one boiler to another or from one area in a boiler to another due to possibilities of variation in water chemistry as well as local tubes stress due to attachment welds or other sources [20].

For CF cracking, cracks grow under both stress and chemical attack at the same time. 55% of the stress sources causing failures were mechanical stress, the rest 45% failures were caused by resonance and/or vibration and cyclic thermal stress [21]. The chemical attacking only occurs on exposure of passive film free material to the aqueous environment. Although attacking of the oxide film may occur upon initial loading in static load stretching, re-passivation is likely to form on material surface very rapidly [40]. Therefore, the application of cyclic stress appears necessary to induce damage in the oxide film, the amount being dependent on cycle shape and duration. Research on electrochemical and physical mechanism of oxide film rupture/re-passivation and its influence in surface pitting is an ongoing topic, the investigation of the mechanical behavior of the material under various mechanical loading conditions is therefore essential to a better understanding of SAC.

Parkins [47, 48] pointed out that the crack tip strain rate, which can be calculated from the applied strain rate and crack density, is an important variable in determining the stress corrosion crack growth in systems where the film rupture plays an important role in overall mechanism. The crack tip strain rate should not be too low as the protective film will cease the crack tip dissolution, thus may stop crack growth, or too high because high straining will likely cause overload failure. The appropriate applied strain rate at which SAC cracks frequently occurs in pipeline steels ranges from $5x10^{-8}$ to $5x10^{-6}$ Hz [47]. The processes of metal dissolution, film formation and film rupture collectively determine the average crack growth rate. The average crack velocity may be expected to be strain rate dependent because straining can rupture films, or create bare metals at a rate

that exceeds the film growth rate, to continue the crack growth [48]. However, there is an obvious difficulty in relating the strain rate effects indicated above for laboratory tests to structural systems in service conditions. It is hardly likely that the required strain rate to initiate a SAC will be sustained until the environmental requirement for SAC are established, which may take years. In the strictest sense, the occurrence of SAC may be independent of the boiler age [28], but it tends to be a relatively slow process and is most commonly found in boilers that have been operating for at least ten years [21, 27]. The answer for how the needed strain rate for SAC is achieved in service conditions lies in cyclic loading, to which structures are subjected due to varying temperatures, and which can sustain creep or strain rate beyond that under static loading conditions for the same maximum stress [48].

The fatigue strength of a material in a corrosive environment can be strongly affected by test frequency, with a decrease in frequency generally producing a decrease in fatigue strength of the material [49, 50]. However, Endo and Komai [51] suggested it is not the number of stress cycles, but the period of changing stress that affects the corrosion fatigue strength of a material. The practical failures due to SAC or CF occurred over a wide frequency range from 5 kHz of a marine turbine blade and 3 kHz of a noise reduction plate to 3.8×10^{-7} Hz of a cylinder cover in marine diesel engines, and the cyclic thermal stress resulted from temperature variation can exceeds the yield strength [45, 52], so the stresses induced by resonance and/or vibration and cyclic thermal stresses should not be neglected due to their amplitude or small number of cycles.

A positive mean stress has detrimental effects on the cyclic fatigue life of materials [52-55]. The influence of tensile mean stress on crack propagation threshold and propagation behavior of ultra-fine grained low carbon steel was analyzed by M. D. Chapetti et al. [55]. Their results indicate that higher mean stress enhances crack initiation but show no significant effect on fatigue propagation. The number and size of the corrosion pits was also found to be dependent upon the applied stress, with the greater amount of damage produced on the test specimen at higher mean stress, and no pitting on the specimen under constant load or when the mean stress is too low [33].

It was reported that metallurgical factors such as grain size, carbon content, etc. might also affect CF behavior on carbon steels. Microstructure effect on fatigue and corrosion fatigue has been studied in various ally systems. The effect of microstructure change on fatigue behavior has been reported by Yong Gao et al. [56]. In their work, the grain size and grain-boundary character distribution (GBCD) of a nickel-based superalloy, ME3, has been controlled by a grain boundary engineering approach. The fatigue thresholds and near-threshold growth rates were shown to be significantly affected by grain size at room temperature and the crack growth resistance was improved significantly by increasing the fraction of special grain boundaries [56]. For carbon steels, different microstructure gradients were shown to affect both crack growth behavior and fracture mode (transgranular/intergranular). For corrosion fatigue, effect of microstructure on crack initiation and propagation may vary with the environment. The SEM examination by Perkins and Bache [33] for carbon steel in carbonate/bicarbonate solutions showed that in general corrosion fatigue cracks start with a mixed

intergranular/transgranular cracking mode near the initiation site and proceed in a transgranular manner. The fatigue crack propagation was proposed to be governed by plastic deformation characteristics and hence be a function of the given microstructure [57].

Corrosion fatigue was very useful in determining the durability and reliability of boiler tubing and other engineering structures. However, corrosion fatigue is defined as a cracking behavior in materials under combined action of cyclic stress and a corrosive environment. By this definition, corrosion fatigue is restricted to the simultaneous action of a variable mechanical stress and a corrosion process. The following damage mechanisms are not covered by CF: (a) Purely mechanical stress followed by a corrosive action in the unstressed state; and (b) corrosion in a stress-free state, followed by purely mechanical cyclic stressing without interaction of corrosion. Although linear elastic assumptions are still considered to be valid in studying the initiation and propagation mechanism of CF cracking, it is also generally believed now that linear elastic fracture mechanics (LEFM) only deals with one aspect of the multifaceted problem of corrosion fatigue, which normally involves chemistry and metallurgy and more broadly, material science. Thus the effect of corrosive environment on fatigue cracking needs to be emphasized in this SAC study, information from CF research in power industry can also be used to build hypothesizes and related experiments for SAC investigation.

2.4. Research on SAC Cracking of Boiler Tubes

2.4.1. Introduction of SAC Cracking

Water-side tube cracking was reported in industrial boilers in the late 1980's, when cracks were found in kraft recovery boilers [20]. These cracks were different in morphology from CF cracks and manufacturers of recovery boilers described these "cracks" as "stress-assisted corrosion". The word "crack" seems inappropriate here compared to "corrosion" because it may incorrectly convey the thought that the metal has pulled apart. Due to the fatal rupture of a floor tube in a recovery boiler in May 1991, concerns were raised about SAC failures in other industrial boilers. During the past twenty years, a significant number of lower furnace tubes and recovery boiler tubes were replaced due to SAC problems. The term "stress-assisted corrosion (SAC)" was continuously used in the paper industry till now.

Stress-assisted corrosion (SAC) cracks and corrosion fatigue (CF) cracks have different morphologies which points to different mechanisms involved in the two failures. The typical CF cracks found in utility boiler are generally un-branched, long and sharp, as shown in Figure 2.9.(a). However, SAC cracks in industrial boilers typically found in the areas with heavy attachment welds on the outer surface of waterwall, are typically blunt, with multiple bulbous features indicating a discontinuous growth, as shown in Figure 2.9.(b). The scanning electron microscope (SEM) examination from Perkins and Bache [33] showed that in general corrosion fatigue cracks start with a mixed

intergranular/transgranular cracking mode near the initiation site and proceed in a transgranular manner for 12%Cr stainless steel in pure water. Typically, utility boilers operate at higher temperatures and pressures compared to the industrial boilers. There are differences in the water chemistry and frequency of upsets in the operating conditions between the high-pressure power boilers and lower pressure industrial boilers. It has been speculated that the water chemistry in utility boilers, during operating and shutdown, may be tightly controlled as compared to most low pressure industrial boilers. Boiler tube leak in utility boilers may lead to lower energy efficiency for the boiler but may not always force the utility boilers to shutdown. However, in some boilers where SAC is expected or is detected, boiler pressures have to be reduced to avoid failures or the boiler has to be shut down to remove and replace affected tubes. If water leaks into the furnace, some of the industrial boilers like kraft recovery boilers in the pulp and paper industry may even experience a smelt/water explosion and lead to fatal accidents [11].

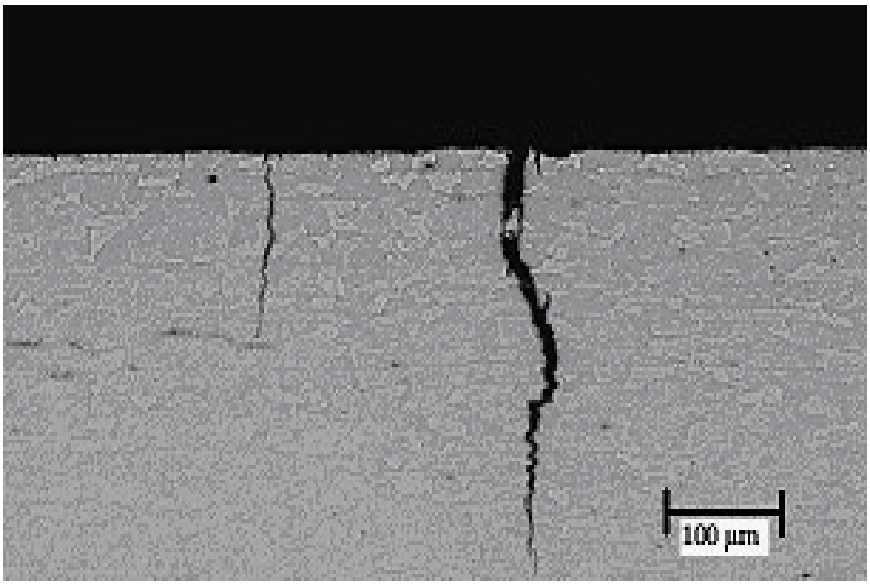

(a)

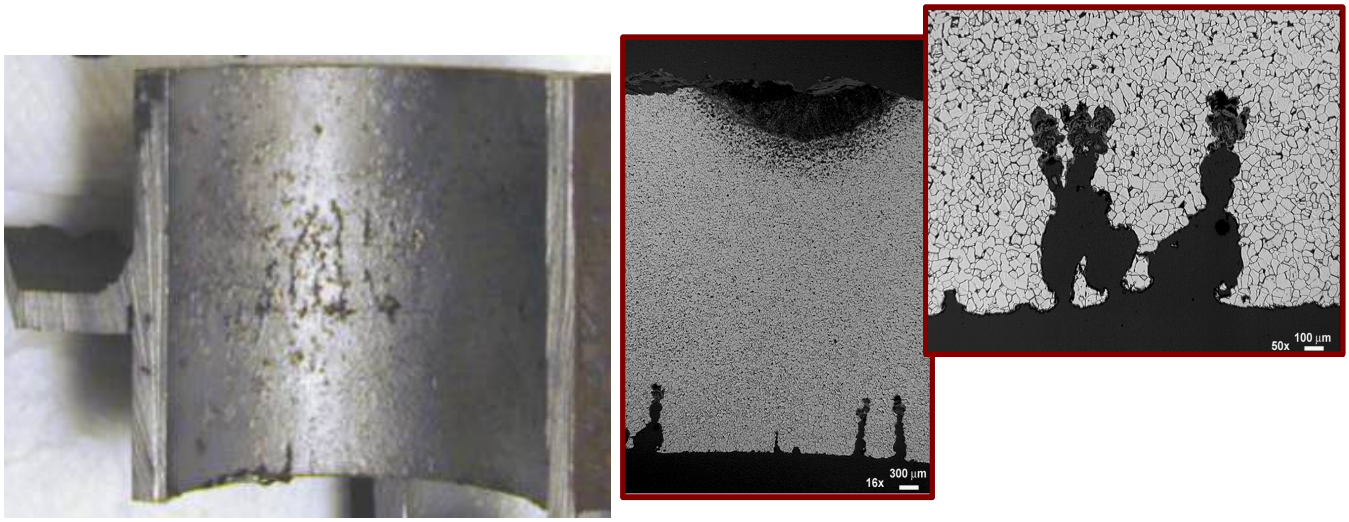

(b)

Figure 2.9. (a) Sharp corrosion fatigue cracks, typically found on carbon steel tubes in high pressure utility boilers. (b) Blunt SAC cracks with bulbous appearance, typically found in industrial boilers [18].

2.4.2. SAC Cracking in Industrial Boilers

Compared to the significant amount of work published on the initiation and propagation of sharp CF cracks, relatively less is known about the initiation and propagation mechanisms of blunt SAC cracks [58], though in recent years there has been a considerable increase of interest in SAC [11-18, 45, 52, 59-66]. Sharp [60, 61] has reviewed the SAC problem in the pulp and paper industry. The term "Stress Assisted Corrosion" was generally adopted by the pulp and paper industry and other industrial boiler operators, which affirmed that SAC is a different phenomenon from the corrosion fatigue cracking studied by the Electric Power Research Institute (EPRI). Esmacher et al. [63, 64] also summarized the probable causes of and recommendations to minimize SAC in boilers. Both mechanical stress and corrosive environment are necessary to initiate SAC. The dissolved oxygen and/or pH excursions are the major water chemistry variables contributing to SAC. SAC cracks are most frequently found in areas near heavy field attachments to the tube surfaces [45]. To avoid conditions that contribute to SAC, the disruption of the magnetite (Fe_3O_4) surface film and the corrosive aqueous environment need to be avoided. Sidey et al. [65] states that corrosion is the dominant process for SAC growth and cyclic stress is not needed. Hargrave et al. [64] proposed that SAC can propagate by successive pit development and provided some evidence for a mixed mode attack on the waterside surface, where there appears to be an interaction between SAC and the corrosion fatigue. Labuda and Bartholomew [66] believed that the

SAC mechanism does not have to involve simultaneous action of corrosion and stress, but consecutive actions of stress and corrosive environment may lead to SAC failures.

2.4.3. SAC Cracking in Deaerator Vessels/Nuclear Industrial Equipments

Also related cracking phenomenon of carbon steel in high purity water has been reported and studied in deaerator vessels and nuclear industry equipment [67-73]. Mechanisms for the crack initiation and growth have been studied in these systems and are relevant to the SAC in industrial boilers. Bulloch [67] reported that deaerator feedwater storage weldment cracking initiated from the bottom of corrosion pits. Scott and Tice [68] reviewed literature on crack initiation and propagation in low alloy steels in high temperature aqueous environments and concluded that the cracks may initiate from corrosion pits under environmental conditions which may have deviated from the normal operating conditions. They further emphasized that dissolved oxygen may play an important role in stress corrosion cracking (SCC). Bulloch [67] attributed the crack growth to a combination of environmental assisted cracking and mechanical fatigue crack growth, whereas the final failure was found to be due to fast fracture of steel. Wright [69] reviewed the SCC of carbon and low-alloy steels in nuclear power plant pressure vessels and piping and concluded that the dynamic straining and electrochemical potential (ECP) play critical roles in the early stage of cracking in these systems.

SAC of carbon steels in high temperature aqueous environment may not initiate under completely static loading [69]. Surface film characteristics may influence the local

electrochemical potentials, thereby affecting the local corrosion behavior of steels. Importance of dynamic strain in crack initiation and growth of carbon steels in high purity water was further supported by Hickling and Blind [70], who proposed that the term strain-induced corrosion cracking (SICC) should be used rather than SCC. Lenz and Wieling [71] developed three-dimensional diagrams to show SICC susceptibility of steels in light water reactor where the cracking was shown to depend on dissolved oxygen, temperature and strain rate. Results indicated that the key to reduce cracking susceptibility in these systems is to minimize strain events and control water chemistry so that straining does not occur when the environmental conditions for cracking exist.

Although the research activities cited above have enlarged our knowledge on SAC of carbon steel tubes in industrial boilers, deaerator vessels, and nuclear industry equipments, the mechanisms of SAC cracking are still not clear. No technology or guidelines were found to be able to control SAC either. However, the reviews above (section 2.2-2.3) indicate that the investigation on SAC problem of carbon steel tubes in boiler water conditions should be organized and conducted by individually studying the roles of different factors affecting SAC cracking, and the SAC mechanism should be derived from a combined understanding of the roles of these different factors.

2.5. Numerical Modeling of SAC Cracking

The modeling of fatigue crack growth in stressed carbon steel under various mechanical conditions has been extensively studied. Normally pure mechanical fatigue cracking of carbon steels without considering environmental effects can be numerically simulated by finite element methods (FEM). Stress distribution and stress intensity factor (SIF) at a set of points along the crack front can be calculated by applying LEFM to FEM model, and the SIF values at the next crack front can be predicted by implementing automatic re-meshing techniques, which apparently requires more time [74]. The combined use of the level set method and extended-FEM approach by Stolarska et al. [75] allowed them to simulate the crack growth without the re-meshing step. Due to the gross plasticity accompanied with plastic straining, in circumstances where single cracks grow beyond three times of grain size, J-integral method can be introduced to help predict the fatigue life of carbon steel structures. Considering only elastic responses from the material, J-integral values may be converted to SIF based on either plane strain or plane stress assumption on elastic structures [74].

However, SAC or CF type of cracking is caused by interactions of electrochemical, metallurgical, and mechanical processes at the crack tip area under specific environmental conditions. Though the mechanical part or sometimes even metallurgical process of SAC or CF cracking can be effectively modeled by FEM based approach, the electrochemical process which accounts for various environmental factors

such as temperature, dissolved oxygen level, and surface film formation is more complicated. Thus the efforts of modeling corrosion related cracking are generally not limited to FEM-related modeling methods only.

From the electrochemical perspective, some corrosion crack initiation and growth models have also been proposed over the past decades [76-79]. Agrawal and Raj [76] have proposed a model capable of evaluating the interfacial shear strength of the surface film-substrate system. Then Chen et al. [77] further developed this model to approximate the shear stress distribution on the interface between an elastic film and a ductile substrate. The model demonstrated that the predicted interfacial shear strength is of the same order of magnitude as the yield shear strength of the substrate. The model was also validated as credible by experimental data from TiN coating-304 stainless steel system but was still restrained to the level of trying to model an electrochemical process by applying only mechanical concepts. Kanasaki et al. [78] used the modified rate approach which was first developed by Higuchi and Iida [79] to predict the fatigue life reduction under changing temperature conditions. They successfully simulated the effects of both in-phase and out-phase temperature changes on fatigue life, and this fatigue life prediction model was shown to agree well with their experimental results. However, the model can only work under conditions of dissolved oxygen and strain rate values being constant.

As more recently, the implementation of new technology to stress corrosion crack modeling gives semi-quantitative and statistical results based on the fast development of

molecular mechanics and empirical methods. Jonas [80] have applied equations derived from classical physics and empirical methods based on quantum mechanics to model the interactions of molecules and atoms on magnetite and hematite covered surface under various corrosive environments. By his work, the rate processes of crack initiation and propagation can be evaluated from simulating generation/diffusion of atomic hydrogen, mass transportation towards or away from the crack tip, and passivation process on material surface. The model was developed without any representations of pitting process because the technology for modeling pitting is not sufficiently advanced, and effects of temperature/pressure and stress conditions were not considered in this work either. Ramsanooj and Shugar [81] took both electrochemical corrosion and mechanical fatigue into consideration in their work of modeling CF cracking based on one assumption that the rate of corrosion fatigue was assumed to be the sum of the rates of crack growth in lab air and that in an aggressive environment. The effects of Young's modulus, fracture toughness, the yield strength, and threshold SIF, plus SCC velocity under stressed and environmental conditions were all included in this model, and the model predictions matched favorably with the published data on CF of some typical metals [81]. However, the stress corrosion rate was simply treated as required input instead of calculating it from other provided information. A similar superposition model including fatigue and SCC components was proposed by Lambert et al. [82] in 2000 and the resulting predictions of the growth behavior of single cracks in stressed pipeline steel under simulated field conditions were also found reasonable. Another two parameter (Kmax and ΔK) driving force model proposed by Kujawski and Stoychev [83] seems rather interesting. The relationship of crack growth rate (da/dN) versus SIF range (ΔK), and the relationship of

SIF range (ΔK) versus the maximum stress intensity factor (K_{max}) was extracted from experimental data respectively. Those given experimental data were plotted as a 3-Dimentional table in terms of da/dN, ΔK, and K_{max}. Then the crack growth rate values (da/dN) of any combination of ΔK and K_{max} extrapolated from above relationships could be located from the calculated table [83].

With growing interests in predicting the remaining life of industrial boiler tubes, the modeling of SAC crack initiation and propagation has acquired urgency to be able to extend the life of a boiler beyond its design life. As described in chapters 1-6, mechanisms of SAC in boiler water environment were identified as function of the interactions of environmental factors (temperature, dissolved oxygen), material properties (grain size, tensile strength), and parameters of stress conditions (frequency, amplitude, mean stress, and strain rate). All of those stated variables need to be considered in establishing required conditions to duplicate SAC cracking in a laboratory, as well as in putting up a numerical model to predict the cracking behavior of SAC. This is important so that appropriate environmental (water treatment and chemical cleaning), operational (thermal stresses, attachment weld design/location), and material (mechanical properties, composition of base material and oxide films) options can be selected to reduce the severity and frequency of SAC. Further, a good estimation of the remaining life of boiler under given conditions can also be used to identify the boilers with certain “higher risk factors” for SAC. Thus risk-based inspections encompassing frequency and scope for individual boilers can be arranged to best protect the equipment, personnel and reduce catastrophic boiler failures.

2.6. Research Objective

Main objective of this project was to examine the mechanism of stress assisted corrosion cracking (SAC) in recovery boiler tubes. To understand the effect of key environmental and stress related parameters on SAC initiation and propagation, the overall objective of this project was further divided into specific tasks, which are:

1. **To develop a test facility to simulate industrial boiler waterside environment and be able to change key variables.**
2. **To evaluate the effect of environmental factors such as temperature and dissolved oxygen (DO) on SAC initiation and propagation under industrial boiler water environment.**
3. **To evaluate the effect of stress parameters such as mean stress, amplitude, frequency, and strain rate on SAC initiation and propagation under industrial boiler water environment.**
4. **To evaluate the effect of carbon steel grain size and decarburization on SAC initiation under industrial boiler water environment.**
5. **To evaluate the effect of surface film characteristics on SAC initiation and propagation under industrial boiler water environment.**

6. **To propose and validate the mechanism for SAC initiation and propagation under industrial boiler water environment, and provide some suggestions on how to mitigate SAC.**

To understand the SAC type failures, the research objectives also included failure analysis of boiler tubes and to develop a model for predicting the overall life of boiler tubes under a given set of service conditions based on the understanding of initiation and propagation mechanisms of SAC cracking.

Corrosion fatigue (CF) of boiler tubes and stress assisted corrosion (SAC) are related phenomenon as both type of failures are result of combined effect of mechanical loading and corrosive environment. But the differences in crack morphology, water chemistry variables, operation procedures and working temperature for CF and SAC indicate that two different mechanisms are involved in the two types of failure. However, corrosion fatigue perhaps represents the clearest example of the failure problems which take surface film rupture as the initial step. Since the key water chemistry variables can affect the stability of the protective oxide film which is related to the severity of corrosion fatigue, it makes a fair assumption that the formation of oxide film on material surface is related with the initiation and severity of SAC cracking. Therefore the knowledge from CF study and other assumptions related to the kinetics of oxide film may be adapted with caution in this study to help understand the relationship between the water chemistry and initiation of SAC.

In general all cracking phenomena can be separated into two distinct stages; crack initiation and crack propagation. Boiler tube cracking processes in these stages further depend upon the environmental factors like temperature and water chemistry, as well as on the material microstructure features and stress conditions of boiler tubes. The relationship among those environmental factors regarding their influences on CF or SAC cracking can be illustrated in a chart, as shown in Figure 2.10. The research plan of this project was designed and conducted accordingly.

2.7. Research Organization

Main objective of this research was to understand the mechanisms involved in the SAC crack initiation and propagation in carbon steel under boiler water conditions. To understand the mechanism, it is important to understand the effect of various possible parameters involved. Work was planned to study the parameters such as stress conditions (frequency, strain rate, amplitude, mean stress, and maximum stress), water chemistry (i.e. oxygen concentration, pH or conductivity, etc.), and material microstructure (grain size, carbon content) individually or in select combination under controlled environmental conditions.

Under the simulated industrial boiler water conditions: Slow strain rate tests (SSRT) were conducted to study the effect of temperature and oxygen level on crack initiation and propagation on SA-210 carbon steel samples made out of boiler tubes. SSRTs were also conducted under various combinations of frequency, mean stress,

amplitude, and strain rate to study the effects of stress parameters on SAC cracking. Heat treatments combined with SSRTs were performed on tensile samples to examine the effect of material microstructure; image analysis technique was used to quantify grain size and carbon percentage of material. Magnetite film formed on the surface has a significant role in the SAC mechanism, so coupon exposure tests were conducted to study the characteristics of film formed due to environmental effects. Through these activities, significant environmental, operational, and material characteristics were identified to reduce the frequency and severity of SAC.

Based on the experimental results and subsequent analysis from the tests stated above, the role of key industrial boiler design and environmental parameters on initiation and propagation of SAC in the laboratory was systematically evaluated. The SAC mechanism on carbon steel boiler tubes under industrial conditions was then be obtained by developing those correlated roles into a quantitative understanding of SAC cracking within the framework of the LEFM. Interrupted slow strain rate tests (ISSRT) were designed and conducted in lab to validate the proposed mechanisms of SAC cracks initiation and propagation under industrial boiler water environment. Finally, efforts were made to develop a numerical model to predict SAC failure on industrial boiler tubes under given service conditions.

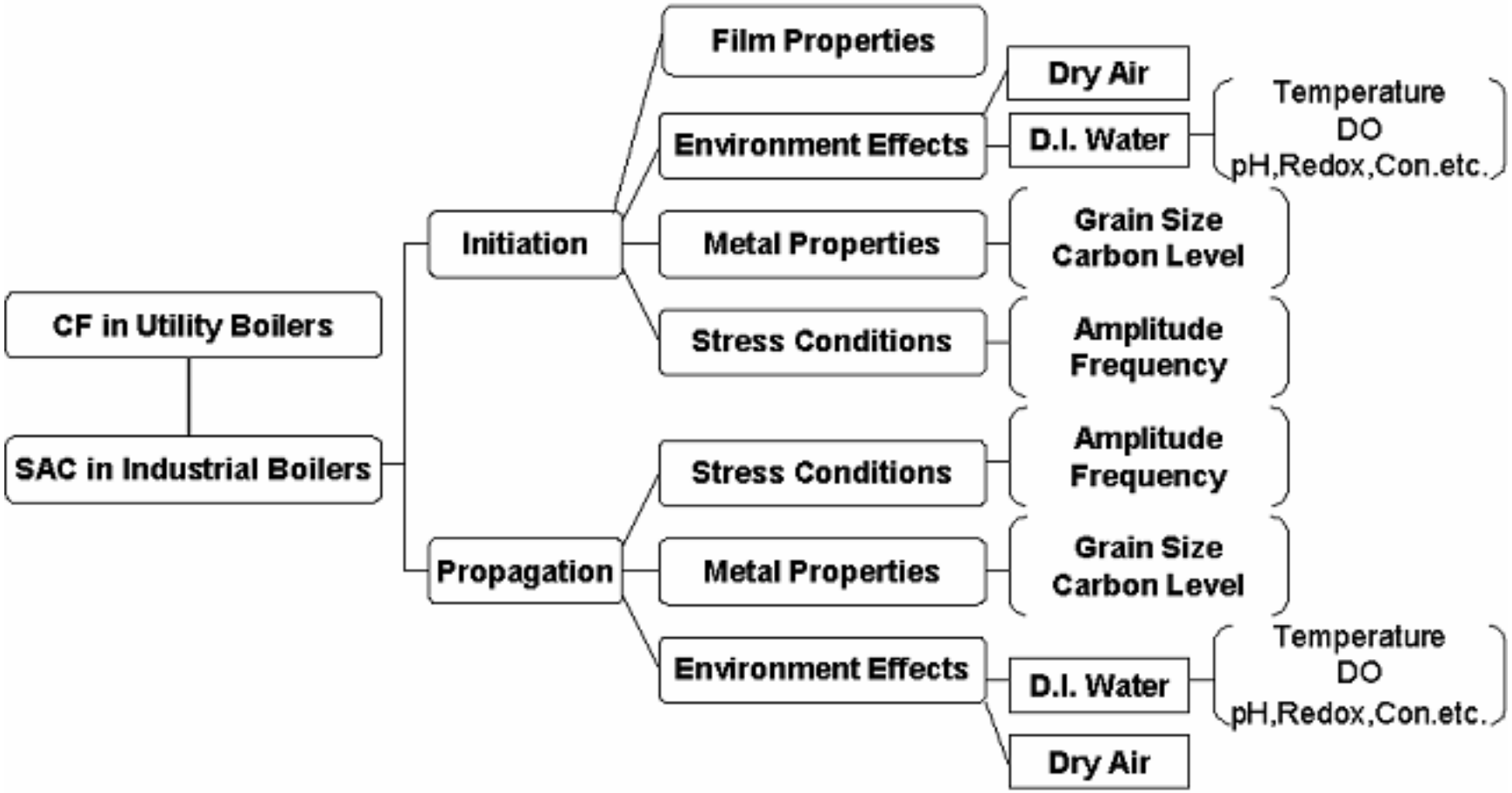

Figure 2.1 1. Schematic of effects of environmental variables on SAC & CF crack initiation and propagation

CHAPTER 3: GENERAL EXPERIMENTAL SETUP

3.1. Materials

Carbon steel is widely used for industrials and utility boiler tubes because of its low cost, high strength, good thermal conductivity and the ease of construction and welding in field. Therefore the material used in all SSRTs in this study was SA-210 carbon steel, typically applied for industrial boiler tubes, with a nominal composition listed in Table 3-1. The mechanical properties for SA-210 carbon steel as a function of temperature extracted from SSRT tests are listed in Table 3-2, and are shown in Figure 3.1. Compact tension (CT) samples for fatigue tests under air condition were carried out using 516 Gr70 plate instead of SA-210 tubes as SA-210 is commercially available only in the tube form. Both carbon steels have similar nominal composition, as shown in Table 3-1.

3.2. Experimental Setup for SAC Simulation

SAC initiation and propagation may take years to establish on carbon steel boiler tubes under real service conditions. Therefore effects of environmental conditions on SAC susceptibility of boiler tubes are not very apparent from the field data. A laboratory facility was developed where the boiler environmental conditions could be simulated to study SAC cracking within reasonable exposure time [62]. This included an autoclave

with recirculation-loop which allowed us to systematically evaluate of the role of key industrial boiler design and environmental parameters in initiation and propagation of SAC in the laboratory.

The Hastelloy-C autoclave, as shown in Figure 3.2, has a capacity of three liters with the design pressure of 2500 psi and design temperature of 350^{o}C. It is wrapped by 3-zone heating element, which could control the temperature within ±1^{o}C of the test temperature. Typically chemically treated de-ionized water (DI water) is used in industrial boiler. In DI water, dissolved oxygen (DO) is the major variable of focus as it plays the most important role in the industrial boiler water environment. To reduce the possibility of other dissolved elements influencing the test results, double de-ionized water (high purity water) was selected for making the test solution. For all autoclave tests in this study the volume of test solution was 2.5 liters in a 3.5 liters autoclave so that a mixture of steam/water solution is maintained inside the autoclave.

Nitrogen is well known to reduce the amount of DO in the water solution by displacement [23]. Nitrogen bubbling is a good way to control dissolved oxygen in laboratory but is not affordable for the large volume of makeup water in an industrial boiler. Therefore in some tests Na_2SO_3 was also used as an alternative oxygen scavenger to adjust the oxygen level in high purity water. Figure 3.3 shows the schematic of the recirculation-loop along with the autoclave. A 100-liter storage/makeup tank was used to control DO level and to add other chemicals needed to simulate different boiler chemistries. A high pressure pump with pressure valve controls the recirculation loop

pressure between the autoclave and the makeup-tank. Water exiting the autoclave is used in a heat exchanger to pre-heat the water entering the autoclave. Water flow rates can be controlled up to 10 liters per hour. Water exiting the autoclave is further cooled by using a series of heat exchangers where the temperature of water is controlled below 50^{o}C. Various on-line sensors are used in the recirculation loop to real-time monitor and control the water chemistry which includes oxygen concentration, pH, redox potential, and conductivity.

Stress is an important component for stress assisted corrosion. In laboratory, constant strain samples, as in U-bend or rigid-fixture tensile samples may be used to study the stress corrosion susceptibility. Initial SAC tests consisted of carbon steel tensile samples strained to a constant strain value in the rigid fixture and coupon samples exposed to the high purity water environments [62]. However, these tests did not reproduce stress conditions experienced by the boiler tubes as the industrial boiler tubes normally undergo a series of dynamic loading, especially during startup and shutdown. To simulate these stress conditions, constant extension rate test rig was designed where a tensile sample could be exposed to the simulated boiler water environment and tested under different strain rates or under low frequency fatigue conditions. Initial constant extension rate tests or slow strain rate tests (SSRT) conducted with the tensile test rig also showed more reproducibility than the constant strain technique. Therefore, along with the recirculation-loop autoclave, a tensile test rig is used to test materials in simulated boiler water environment.

The tensile test rig developed is shown in Figure 3.4. Special cooling and sealing systems were designed to prevent any leak during the test and still be able to strain the tensile sample at a variety of initial slow strain rates. Load on the sample was continuously monitored by using a load cell in the load train, as shown in Figure 3.5. Signal from the load cell was fed into a computer for continuous monitoring and recording. The signals from the temperature and motor controller were also recorded continuously throughout each test.

Recirculation-loop and autoclave was tested for maximum temperature and pressure and under static and flow conditions before actual tests were started in this facility. Safety shield was used to protect operators against any unexpected steam leak or circulation line failure. All sensors were placed outside this shield such that the operator did not have to enter the safety shield for any control or measurement; the photograph of the whole setup was shown in Figure 3.6 and Figure 3.7.

The autoclave along with the re-circulation loop set up was introduced here as a general experiment set up to mock up the industrial boiler conditions in this study. There are other special designed experiments and related equipment set up for each particular research task described in section 2.6. These research tasks are discussed separately along with the experimental details, results and discussions.

Table 3-1 Nominal composition of carbon steels used in this study (in wt %)

	C	Mn	S	P	Si	Ni	Cr	Mo
SA210	0.27 max	0.93 max	0.058 max	0.048 max	0.10 min	0.03	0.09	0.01
516G70	0.27 max	0.79-1.3	0.040 max	0.035 max	0.13-0.45	0.01	0.02	0.03

Table 3-2 Mechanical Properties of SA210 tested at different temperatures

Temperature (^{o}C)	UT Strength (MPa)	Yield Strength (MPa)	Fract. Strain (%)	Elastic Modulus (GPa)
24.5	473	369	39.7	203.4*
110	452	350	32.6	198.6*
150	479	348	31.1	_
200	528	347	31.4	190.9*
240	539	335	_	_
250	490	339	30.1	_
275	491	341	31.8	_
280	475	340	_	_
300	457	326	27.8	184.1*
320	428	311	29.7	_

* From eFunda (online engineering fundamental database)

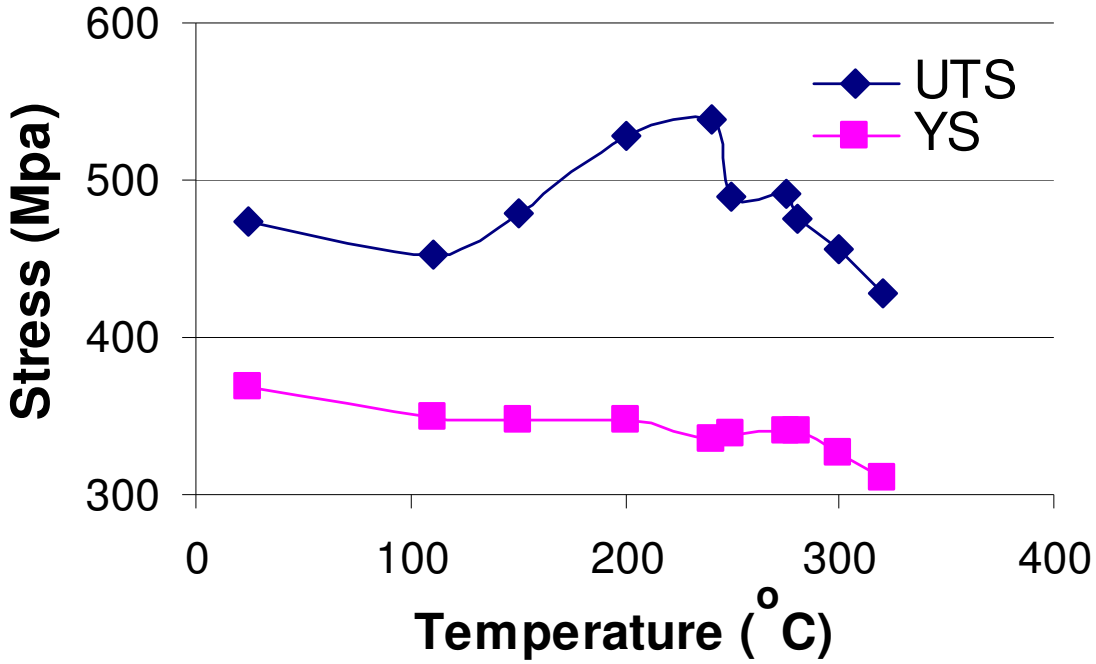

Figure 3. 1. Mechanical Properties of SA210 Carbon Steel

Figure 3. 2. Autoclave used for boiler water environment simulation

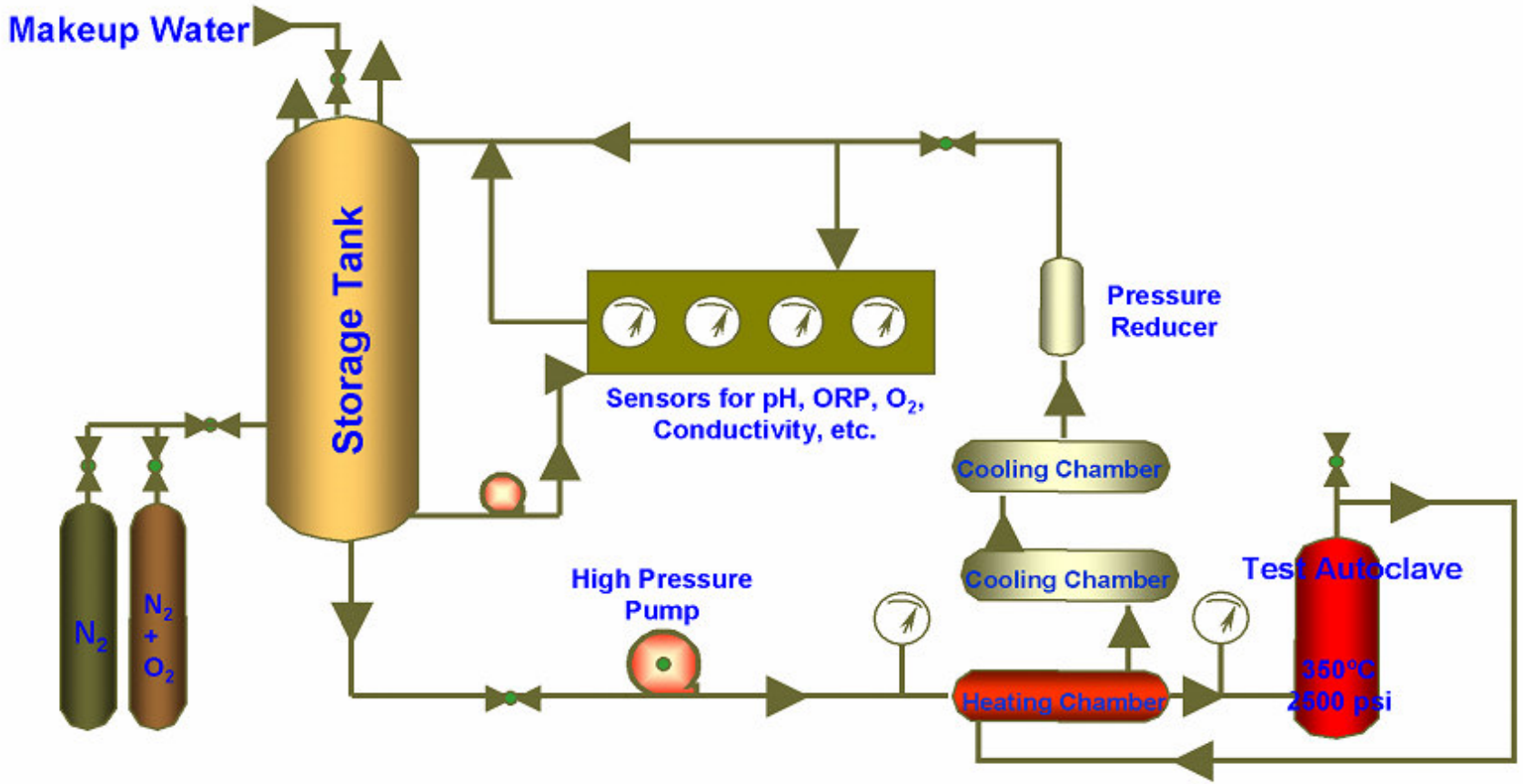

Figure 3.3. Schematic of the recirculation loop and autoclave to simulate boiler environments to study SAC

Figure 3. 4. A constant extension rate or slow strain rate test rig fitted with autoclave and recirculation loop was used for SAC tests.

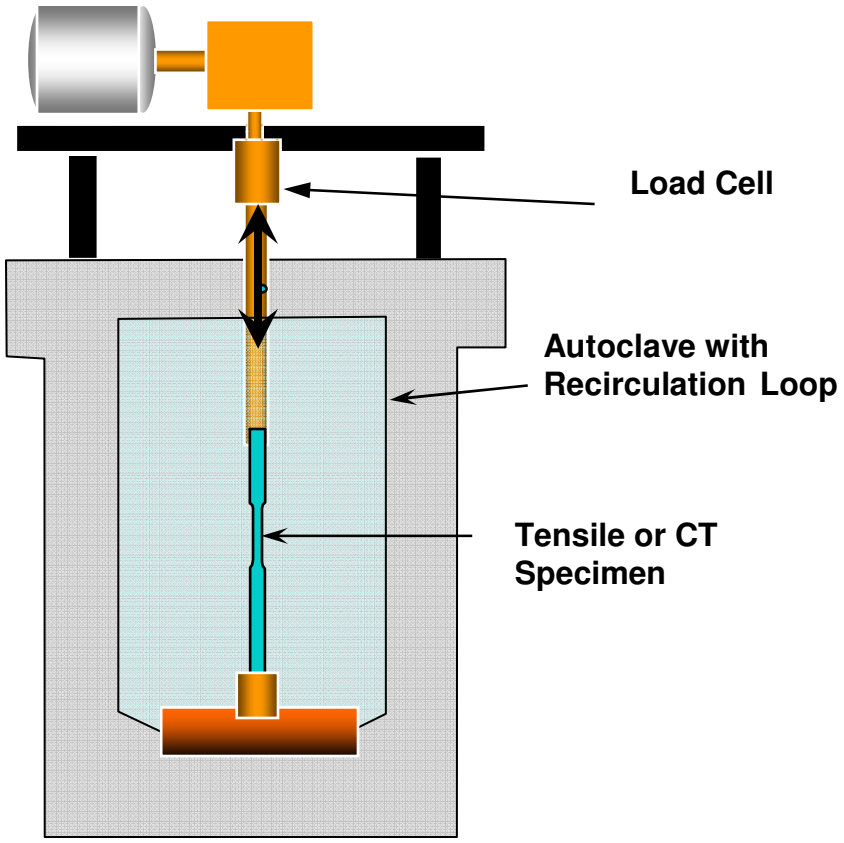

Figure 3. 5. Schematic of the autoclave showing the load-train and tensile sample fixtures. Load on the test sample was measured outside the autoclave

(a) **(b)**

Figure 3. 6. (a) Autoclave, heat exchangers and make-up tank within protection shield. (b) Sensors and controllers for measuring pH, redox potential, temperature, conductivity, and DO in boiler water simulations.

Figure 3. 7. Control panel and protection shield for autoclave and recirculation loop. Data from sensors was recorded in a data acquisition system.

CHAPTER 4: ROLE OF ENVIRONMENT ON SAC CRACKING

4.1. Experimental Details

Typically industrial boiler water environment has a near neutral pH value which is relatively easier to maintain, and thermal conductivity only indicates how well the water treatment was done in boilers, therefore the study of the role of water chemistry is mainly focused on how dissolved oxygen and boiler temperature will affect SAC cracking. Values of pH and thermal conductivity, etc. were monitored during tests to make sure that the water chemistry treatments worked as desired.

Water chemistry in laboratory autoclave was maintained to control the dissolved oxygen (DO) below certain level. A number of different approaches are available to control the dissolved oxygen level but the main aim is to scavenge the oxygen either by chemical reaction or by displacement. After the desired temperature and DO level were reached and maintained, slow strain rate tests were conducted in the autoclave to investigate the effect of temperature and DO on SAC cracking. Coupon exposure tests were also conducted to study the effect of DO on the surface film formation on steel surface.

4.1.1. Materials & Equipments

Smooth tensile specimens with 0.125 inches diameter and 0.5 inches gage length, as shown in Figure 4.1., were machined out of SA-210 carbon steel tubes. The specimens were machined with the tensile axis oriented along the pipe length. Tensile specimens were polished to a 2000-grit finish and cleaned with acetone before testing.

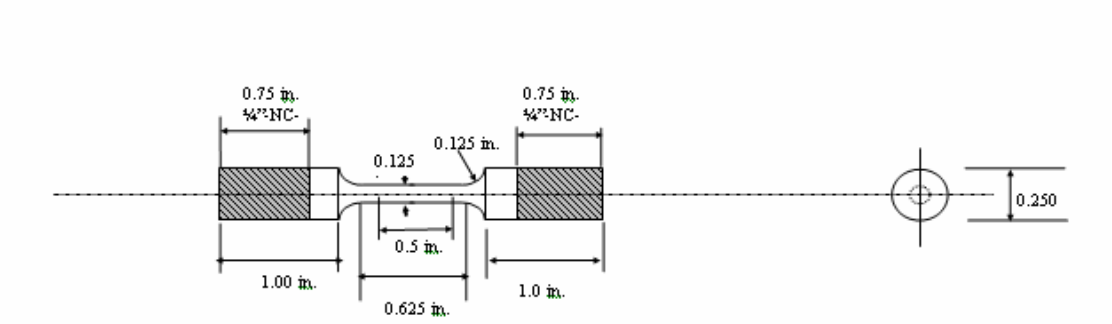

Figure 4. 1. A typical slow strain rate specimen showing the gage length & diameter

4.1.2. Slow Strain Rate Test (SSRT)

Stress assisted corrosion (SAC) cracks and corrosion fatigue (CF) cracks can generally be distinguished as the CF cracks are sustained at high cyclic loading frequency while SAC cracks are more often observed with static, monotonic, or low frequency cyclic loading. However, under relatively low frequency environment, the failure promoted by cyclic loading can be difficult to distinguish from that obtained in slow strain rate tests on ferritic steels. So an assessment of environmental induced cracking by slow strain rate tests might provide data pertinent to understanding the mechanism of SAC. Slow strain rate tests are also known as constant extension rate tests (CERT). Water chemistry parameters (i.e., dissolved oxygen (DO), temperature, pH and conductivity, etc.) were individually monitored and controlled, by either passing Nitrogen into the water environment at a certain flow rate, or combined use of passing Nitrogen through the water solution and addition of different amounts of oxygen scavengers like Na_2SO_3. Test temperatures for autoclave tests ranged from 110 ^oC to 320 ^oC. Once the required water chemistry was achieved in the recirculation loop, heating was started to obtain initial test conditions. Slow strain rate loading were started after the initial environmental conditions were stabilized. Pressure for these was controlled by the test temperature in the autoclave; a 50 lb preload was applied on the load assembly to avoid the slag between tensile sample and grip of fixture. An initial strain rate of 2×10^{-6} s^{-1} was used for each test. After each test, the one half of the broken tensile sample was mounted and polished to quantify crack velocity, crack density, percentage fracture strain, and percentage area reduction.

4.2. Results and Discussions

4.2.1. Control and Stability of DO of High Purity Water

Results from this study have shown that the level of dissolved oxygen in high purity water has a significant effect on SAC cracking of carbon steel boiler tubes. The concentration of oxygen in high purity water was monitored by oxygen probe located on the recirculation-loop wall. The oxygen probe was calibrated against a standard given in the probe manual, before each test.

To check the oxygen solubility of naturally saturated, as received, high purity water, the real time measurement was started from the moment the oxygen probe was dipped into the high purity water. The reading of the oxygen probe versus time was recorded, as shown in Figure 4.2. It took ~0.5 hour for the oxygen level of ~5 ppm to become a stable value of ~3.2 ppm. Values became constant upon leaving the water and the probe undisturbed. Stirring of water was found to again increase the oxygen level in the water.

Three exactly same tests were done under same conditions to check the oxygen solubility test reproducibility; the relative error of each measurement was found to be below 4%. When the measurement was disturbed by bubbling nitrogen into the test

solution, initially the oxygen level went up very quickly to 3.5-3.7 ppm. The sudden increase of oxygen level due to the disturbance corresponded to the flow rate of Nitrogen, as shown in Figure 4.3. Since the test solution in the autoclave of recirculation loop is not always absolutely stagnant, DO ~3 ppm was determined as the baseline value for as received high purity water used in this study. While Nitrogen was continuously bubbled through the test solution, the level of DO decreased significantly and came to equilibrium, depending on the flow rate and time. For the flow rate of ~0.5 liter per minute, DO dropped quickly and reached a stable value of 3.5 ppb in ~ 1.5 hour; for the flow rate of ~0.05 liter per minute. However, for the flow rate of ~0.005 liter per minute, the DO level dropped more gradually and reached a stable value of 4.7 ppb in ~3.5 hours; and further decreased after 5 hours; as shown in Figure 4.3. After another 2 hours, the level of DO, with the Nitrogen flow rate of ~0.005 liter per minute, reached at a stable value of 0.46 ppm, as shown in Figure 4.4.

In order to check the Na_2SO_3's ability of reducing DO in high purity water, measured amounts of Na_2SO_3 were added into the test solution to create a Na_2SO_3 concentration of 0.0001 gram per liter. It was found that the level of DO quickly increased to 0.52 ppm, then decreased to a stable value of 0.29 ppm; after another addition of Na_2SO_3 to create a Na_2SO_3 concentration of 0.0002 gram per liter in the test solution, DO level quickly went up to 0.32 ppm, then dropped to a stable value of 0.28 ppm; after another 3 addition of Na_2SO_3 , of equal amounts, to create a final Na_2SO_3 concentration of 0.0005 gram per liter, the DO level of test solution stopped decreasing and reached a steady final value of 0.26 ppm. The results of DO versus time by passing

Nitrogen, and by addition of Na_2SO_3 are shown in Figure 4.4. When plotted on logarithmic scales for both X and Y axis, the rate of DO drop VS time showed linear characteristics, as shown in Figure 4.5, with a linear regression given by Eq.4.1 to Eq.4.3.

$$\log(DO_{0.005L/M}(t)) = -0.8099 \cdot \log(t) + 0.4352 \quad \textbf{(4.1)}$$

$$\log(DO_{0.05L/M}(t)) = -4.0387 \cdot \log(t) + 0.1948 \quad \textbf{(4.2)}$$

$$\log(DO_{0.5L/M}(t)) = -8.6595 \cdot \log(t) - 1.1040 \quad \textbf{(4.3)}$$

If plotted on linear axes, those equations above can be written as:

$$DO_{0.005L/M}(t) = 2.7239 \cdot t^{-0.8099} \quad \textbf{(4.1*)}$$

$$DO_{0.05L/M}(t) = 0.6386 \cdot t^{-4.0387} \quad \textbf{(4.2*)}$$

$$DO_{0.5L/M}(t) = 0.0787 \cdot t^{-8.6595} \quad \textbf{(4.3*)}$$

Thus, it was concluded that both Nitrogen and Na_2SO_3 can work efficiently to reduce the level of DO in test solution. The flow rate at which Nitrogen was bubbled through the test solution had great influence on the controlling the speed and the final level of DO, if more reduction in the dissolved oxygen was required after the usage of nitrogen, Na_2SO_3 could be used to further reducing the DO to a lower level.

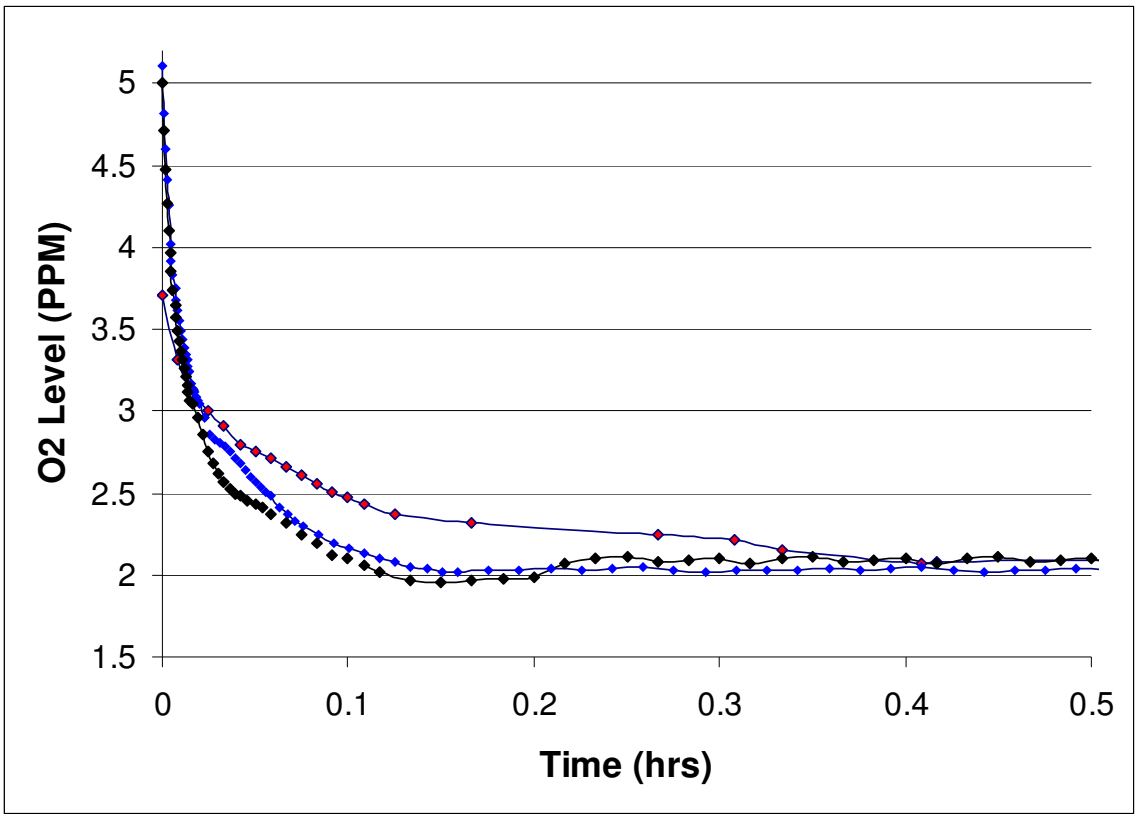

Figure 4. 2. Measurement and reproducibility on DO level in high purity water (As received)

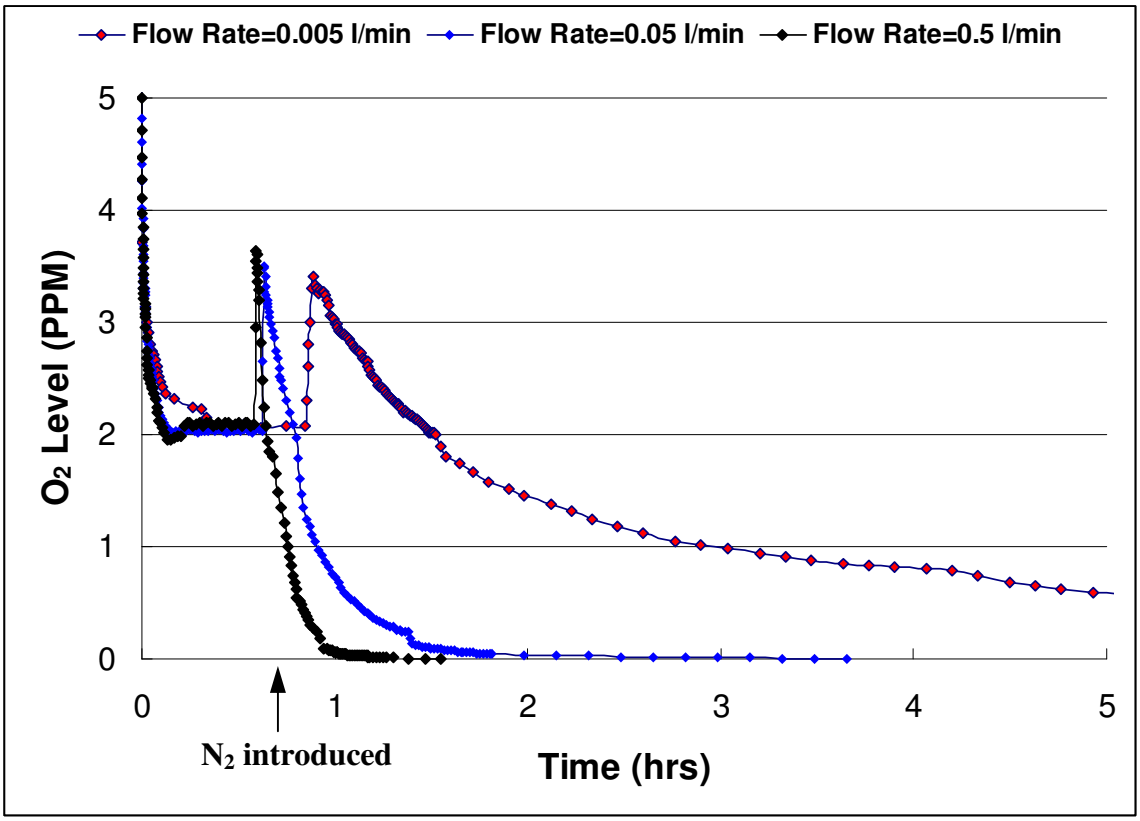

Figure 4. 3. DO level changes VS time of Nitrogen passing into the test solution at certain flow rates

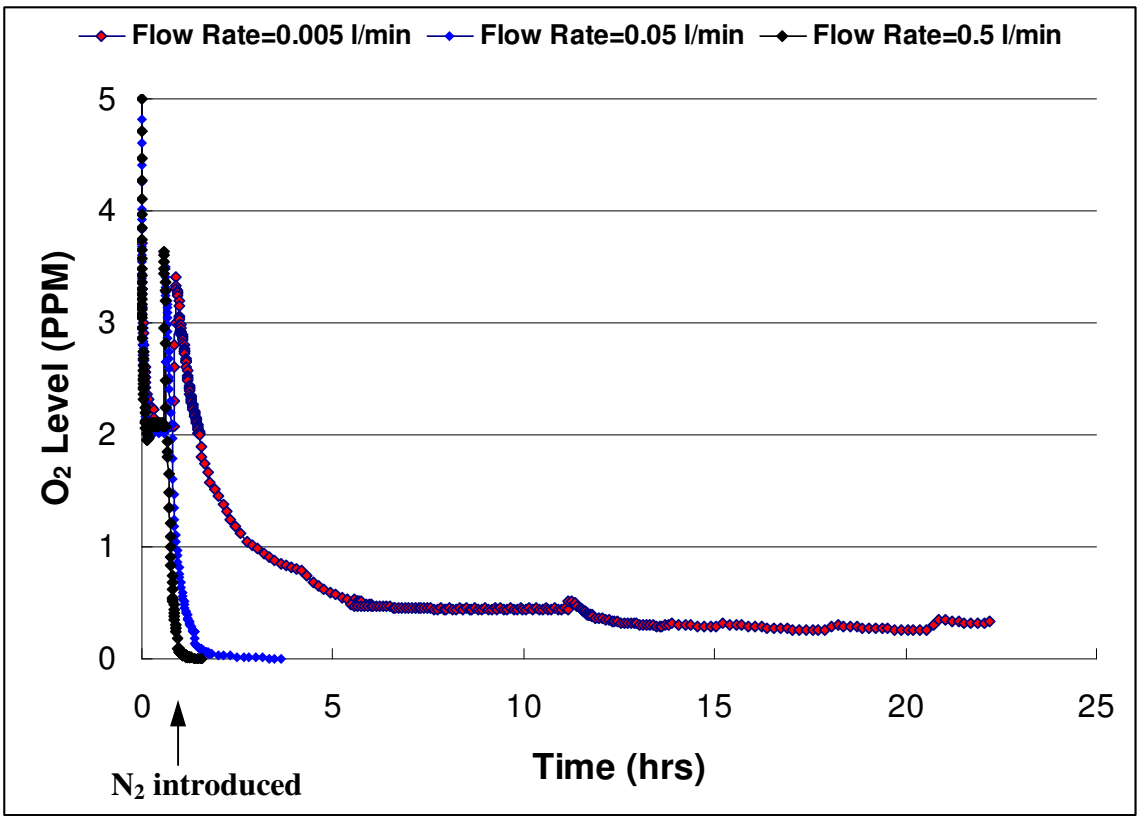

Figure 4. 4. DO level changes VS time of Nitrogen passing into the test solution at certain flow rates

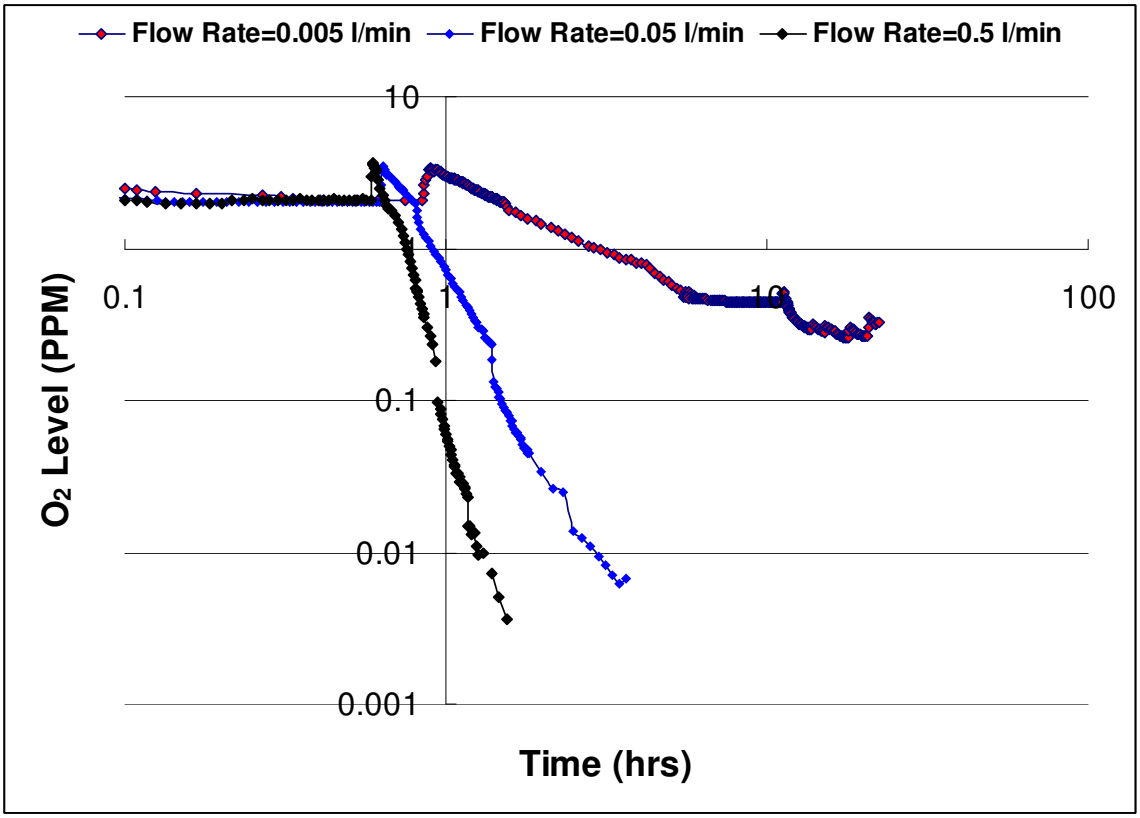

Figure 4. 5. DO level changes VS time of Nitrogen passing and addition of Na_2SO_3 into the test solution at certain flow rates

4.2.2. Effect of Temperature and DO on SAC Cracking in High Purity Water

Initial slow strain rate tests (SSRT) were carried out under different environmental conditions to check the reproducibility of SSRT results at room temperature. The resulted stress-strain curves from environments of oxygenated water, sand, and room air at room temperature were shown in Figure 4.6. The tests under oxygenated water and room air were done in the autoclave with the test rig shown in Figure 3.4 and Figure 3.5, and the test in sand was performed on a similar slow strain rate test rig used by Bhattacharya and Singh [84]. All three curves showed similar features of initial linear elastic deformation, then double yield point, which is typical for low carbon steels, and similar stress strain behavior of duplicate samples. These results indicate that the procedures for sample preparation and general procedures used for SSRT were reproducible.

Two more SA-210 carbon steel samples were tested by SSRT in oxygenated water with DO ~ 3 ppm and with high pure water with DO ~ 5ppb at 110^{o}C in the autoclave. No significant differences were found between the resulted stress-strain diagrams shown in Figure 4.7. One half of the fractured tensile samples were mounted, polished, and checked under optical microscope after the tests. Only one surface crack, of almost ~30 μm length, was found on the sample tested under oxygenated water with DO ~ 3 ppm at 110^{o}C. These results indicated that the oxygen effects are not important at relatively low temperatures (< 110^{o}C) for SAC cracking of carbon steels.

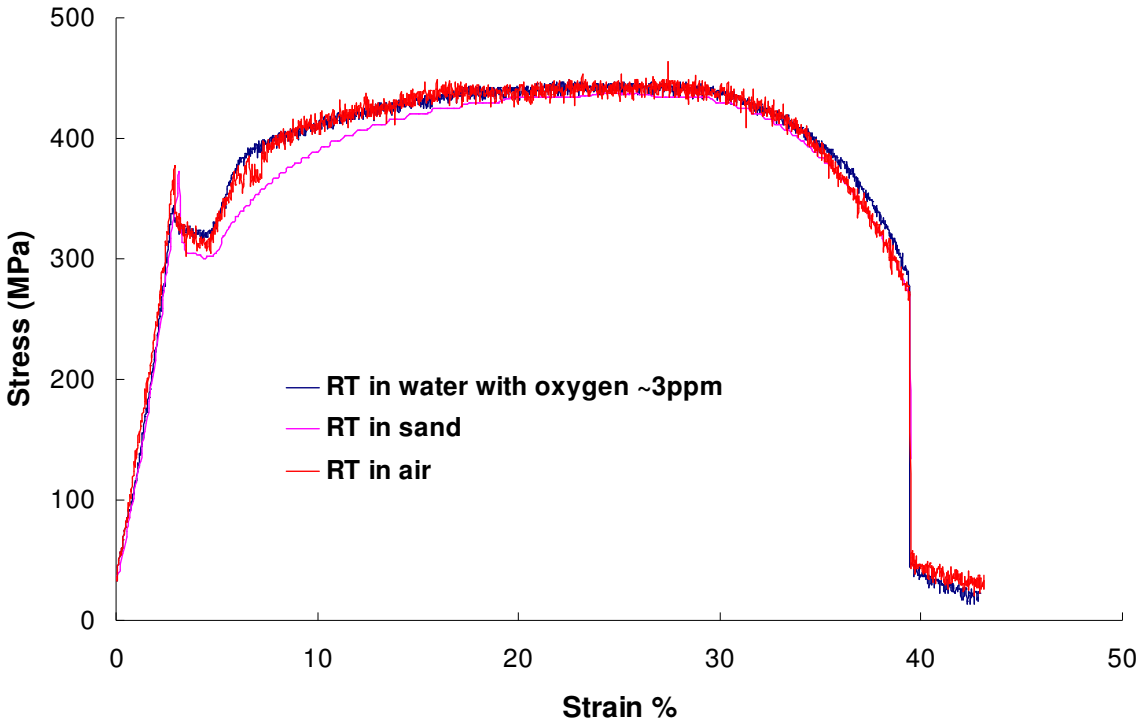

Figure 4. 6. Stress-strain behavior of SA-210 carbon steel from SSRTs under different test environments at room temperature.

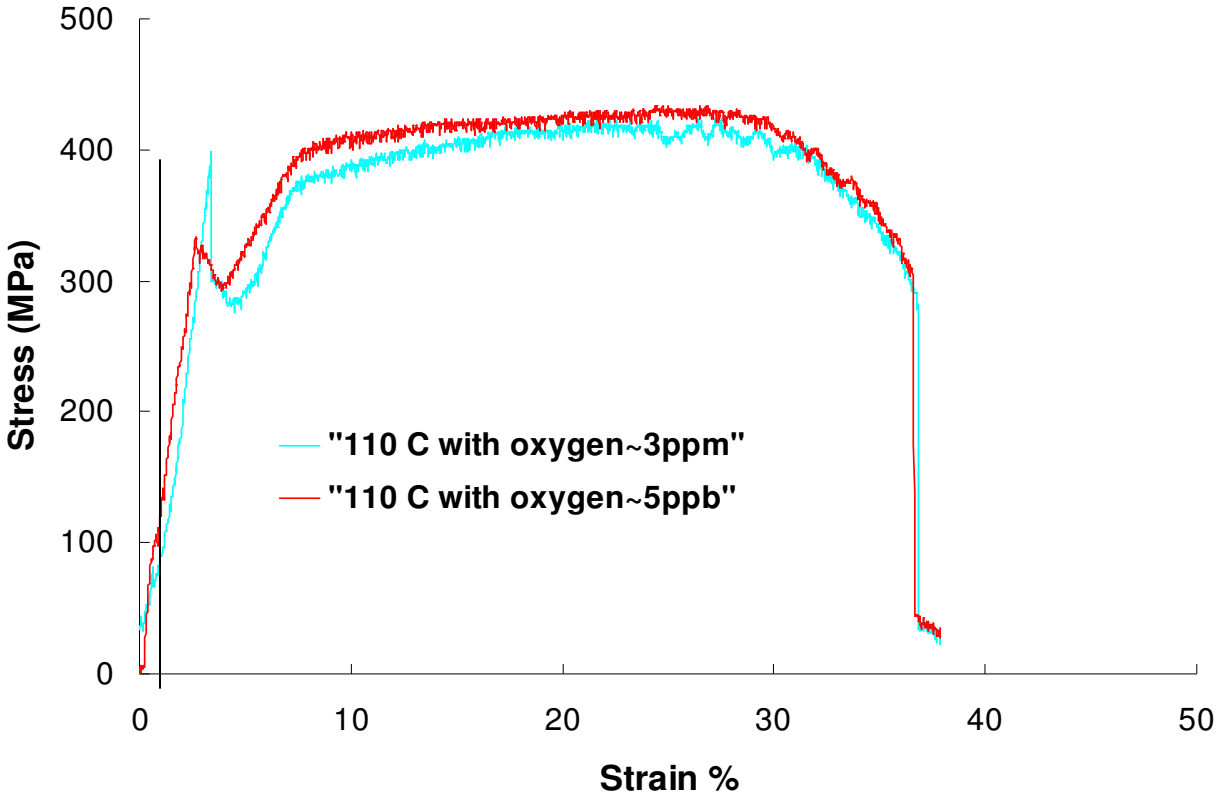

Figure 4. 7. Stress-strain behavior of SA-210 carbon steel samples tested by SSRTs in oxygenated water and pure water at 110^{o}C

Further slow strain rate tests (SSRT) were carried out where the carbon steel samples were tested in an environment with controlled water chemistry at different test temperatures. DO was controlled between ~ 3 ppm in untreated water and ~ 5ppb in different tests. To guarantee a DO level below 5 ppb, the combined use of passing Nitrogen through (0.05 l/min) and addition of Na_2SO_3 (0.0005 g/l) was adapted in the oxygen removal environment. Typical stress strain curves from these tests are shown in Figure 4.8. Tests carried out without removal of oxygen (~3 ppm of DO) showed cracks on the sample surface, whereas tensile samples tested in water with DO controlled ~ 5ppb did not show any sign of surface cracks and had ductile failure, as is shown in Figure 4.9. When the test water had ~ 3 ppm of DO in it, the length of the largest crack found on tensile samples, besides the crack associated with the final fracture, increased from 30μm at 110^{o}C to 1030μm at 320^{o}C, as shown in Figure 4.10. And the crack velocity as well as crack density of smooth tensile specimens increased with an increase in the test temperature; this is evident from the results shown in Figure 4.11.(a) and Figure 4.11.(b).

The increased crack density can affect the overall crack growth rate due to crack interaction and coalescence of multiple cracks. As expected, the carbon steel samples showed a decrease in ductility (as measured by the %-elongation or %-reduction in area of failed samples) with an increase in cracking susceptibility. Tendency for the material to undergo environmental sensitive fracture can be correlated to its percentage reduction in area (%RA) during a tensile test. When the DO was controlled at ~ 5ppb in

water, the %RA of carbon steel sample did not change much with an increase in the test temperature from 250°C to 320°C. However, when the DO in the test water was ~ 3 ppm, both %RA and fracture strain decreased with the test temperature (from 110°C to 320°C), as shown in Figure 4.12.a. This decrease in ductility is an indirect indication of an increase in cracking due to environmental effects.

A series of tests were carried out at 300°C and 320°C, where the oxygen level was varied by use of nitrogen and chemical treatment to determine the effect of DO on cracking susceptibility in pure water at high temperatures. %RA and fracture strain for the carbon steel decreased with an increase in the DO under boiler conditions, as shown in Figure 4.12.(b).

As shown in Figure 4.13., the crack velocity of SAC decreased in almost a linear way as the level of DO decreased. When the DO level was controlled around 20 ppb, the SAC cracks disappeared from the surface of the tensile samples, indicating that 20ppb can be taken as the threshold value of DO below which no SAC would occur. The results from the work by Congleton et al. [85] were plotted in the same Figure 4.13 to compare our results with the published data. The crack velocity of stress corrosion cracking (SCC) on reactor pressure vessel steel in high temperature water showed similar trend as results from the present study on carbon steel. The difference between Congleton's curve and our data is probably due to the Congleton's tests were performed on reactor pressure vessel steel in 286°C water, and our tests were performed at 300°C water. From the

curve-fitting of the data shown in Figure. 4.13, the quantified relationship between SAC crack velocity and DO level can be recorded as:

$$Y=6.06 * 10^{-7} x^{2.1354} \quad \textbf{(Eq. 4.4)}$$

Where: Y= crack velocity of SAC (mm/s); X= level of DO (ppm).

Also from the line-fit of the data shown in Figure 4.14, the quantified relationship between SAC crack density and DO level can be recorded as:

$$Y=2.4943 x^{0.9204} \quad \textbf{(Eq. 4.5)}$$

Where: Y= crack density of SAC (1/mm); X= level of DO (ppm).

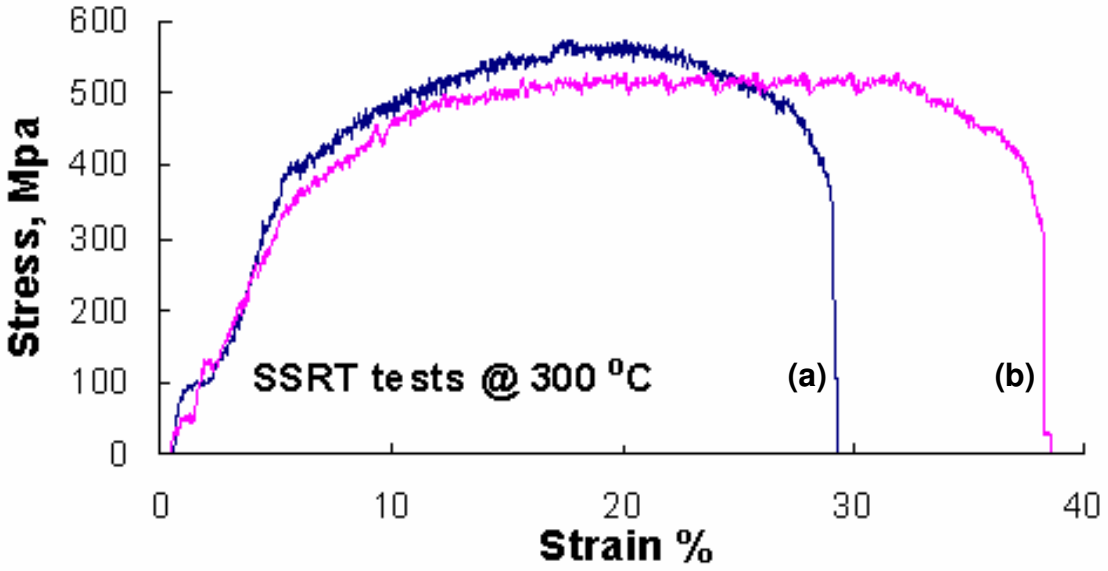

Figure 4. 8. Stress-strain curves for SA210 carbon steel samples tested at 300°C in water with (a) ~3 ppm and (b) ~5ppb DO.

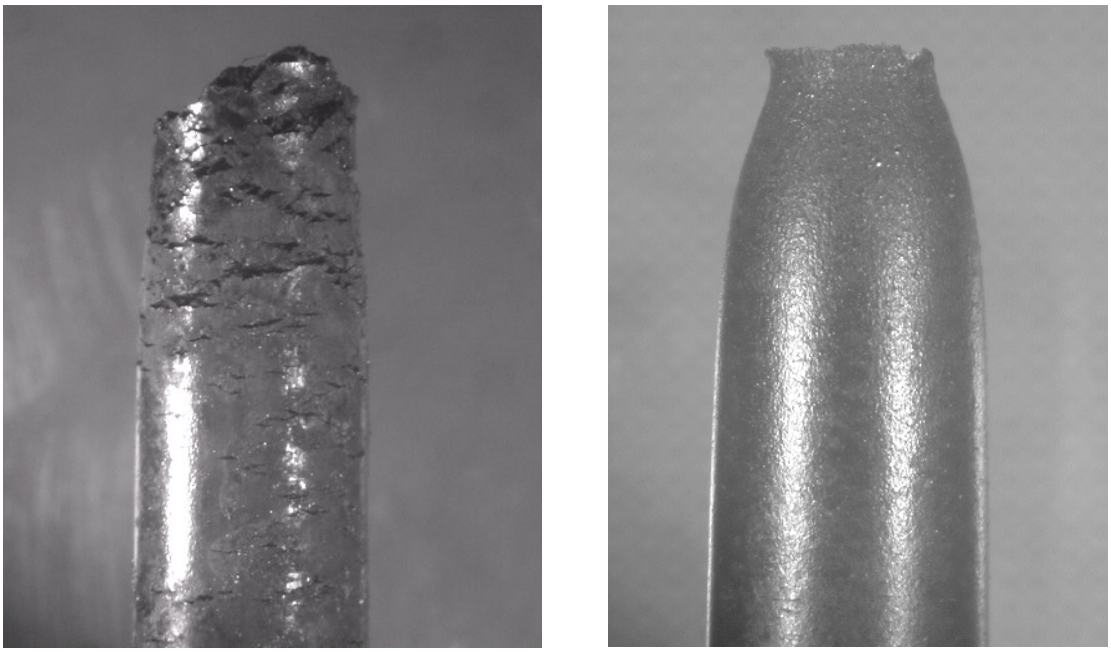

(a) **(b)**

Figure 4. 9. SA210 carbon steel samples tested at 300°C in water with (a) ~3 ppm and (b) ~5ppb dissolved oxygen.

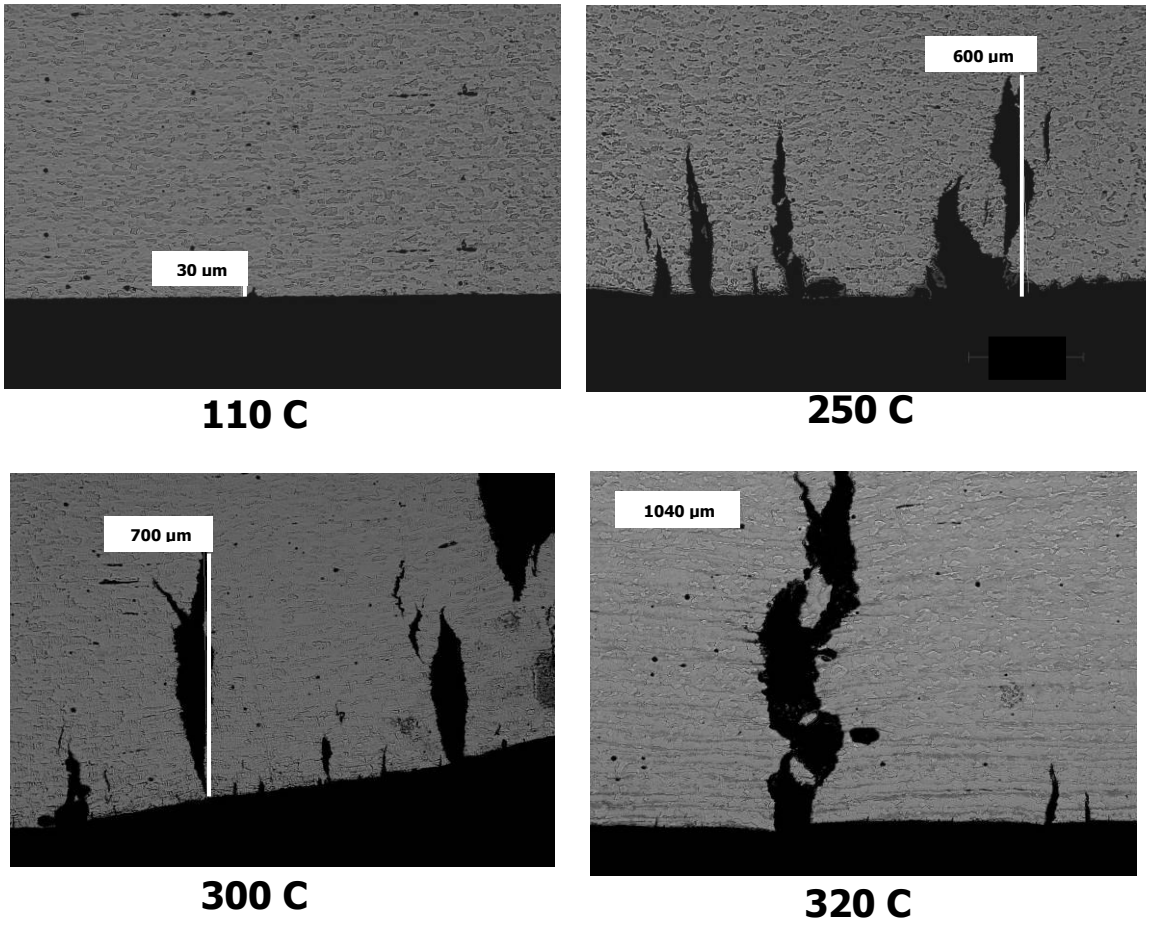

Figure 4. 10. Effect of Test temperature on crack length for SA210 carbon steel samples tested by SSRT method in boiler water with ~3 ppm dissolved oxygen.

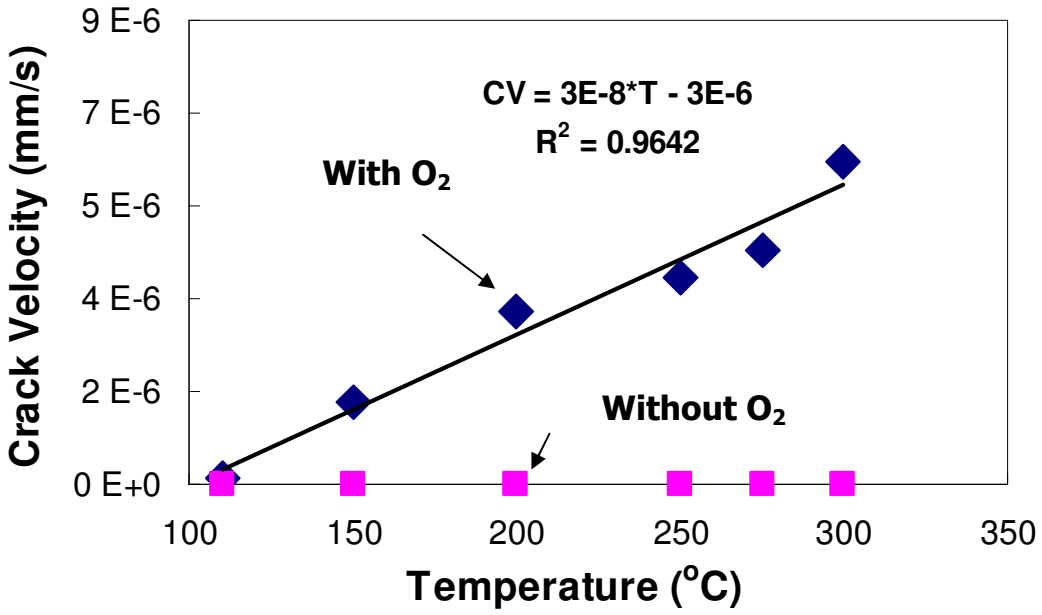

(a)

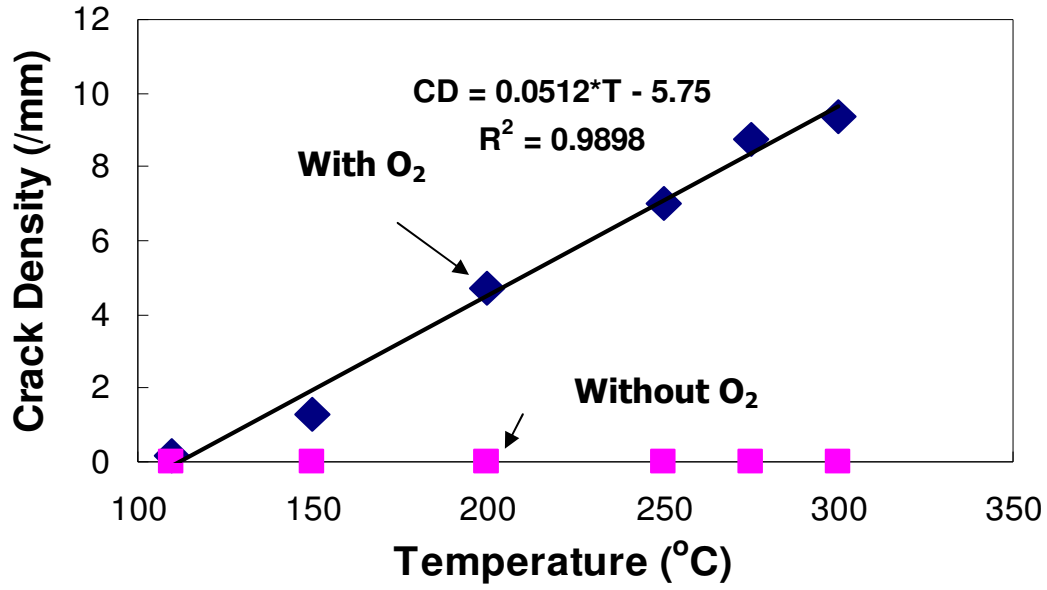

(b)

Figure 4. 11. Effect of test temperature (a) on crack velocity (b) on crack density for SA-210 carbon steel specimens tested in pure water without oxygen removal treatment.(Threshold value of temperature ~110^{o}C, no SAC will occur below ~110^{o}C)

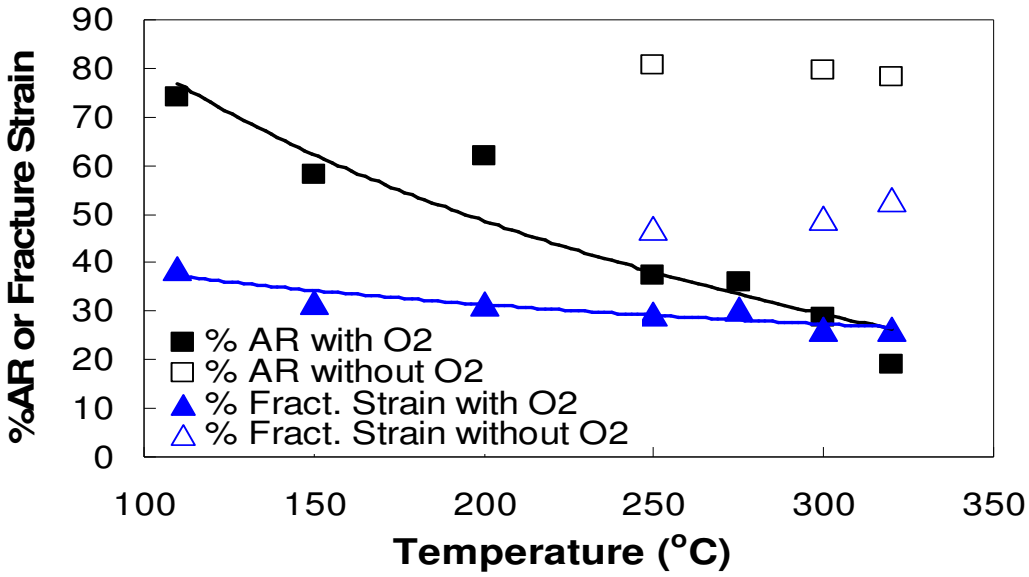

(a)

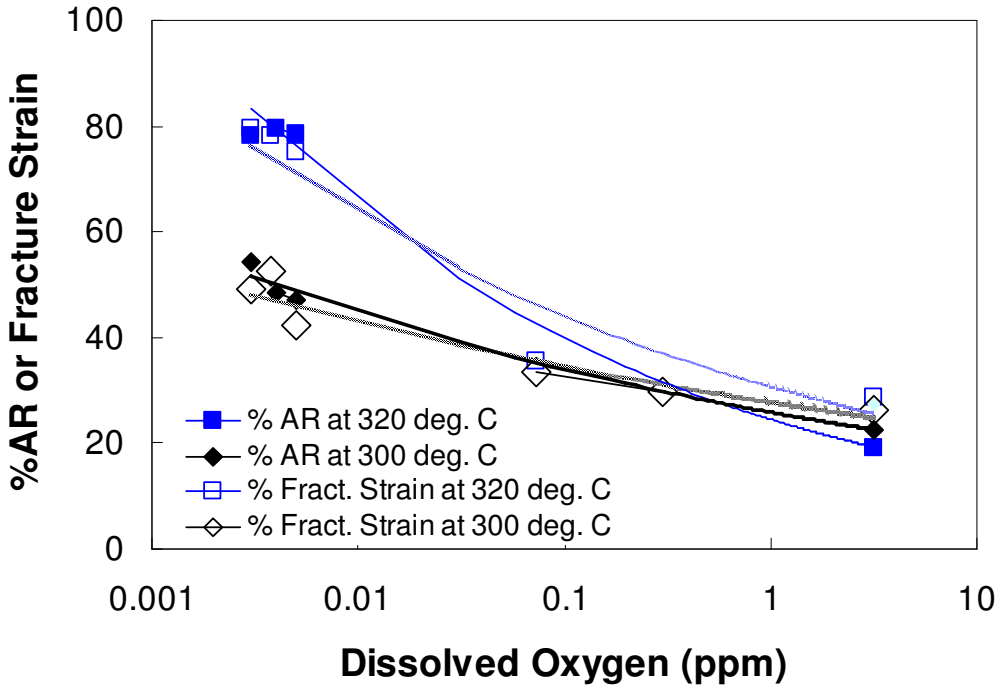

(b)

Figure 4. 12. (a) Effect of test temperature on fracture strain and % reduction in Area (AR) for SSRT samples (b) DO on the ductility of SA-210 specimens tested by slow strain rate of $2x10^{-6}$ s^{-1} in high purity water

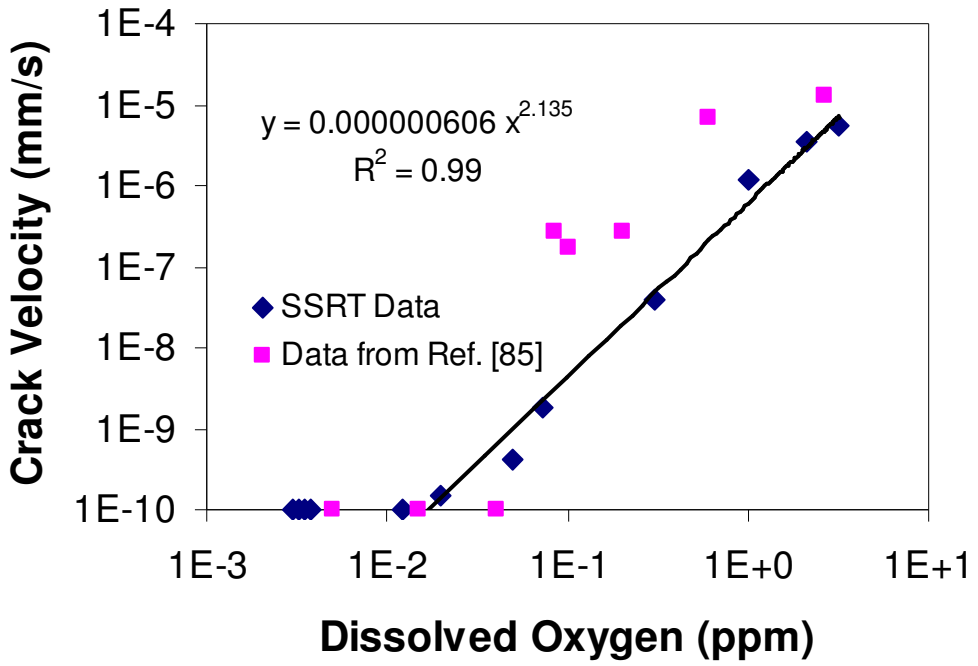

Figure 4. 13. Effect of DO on crack velocity of SAC of SA-210 samples tested at 300°C by slow strain rate of $2x10^{-6}$ s^{-1} in pure water. (DO threshold value: 20ppb)

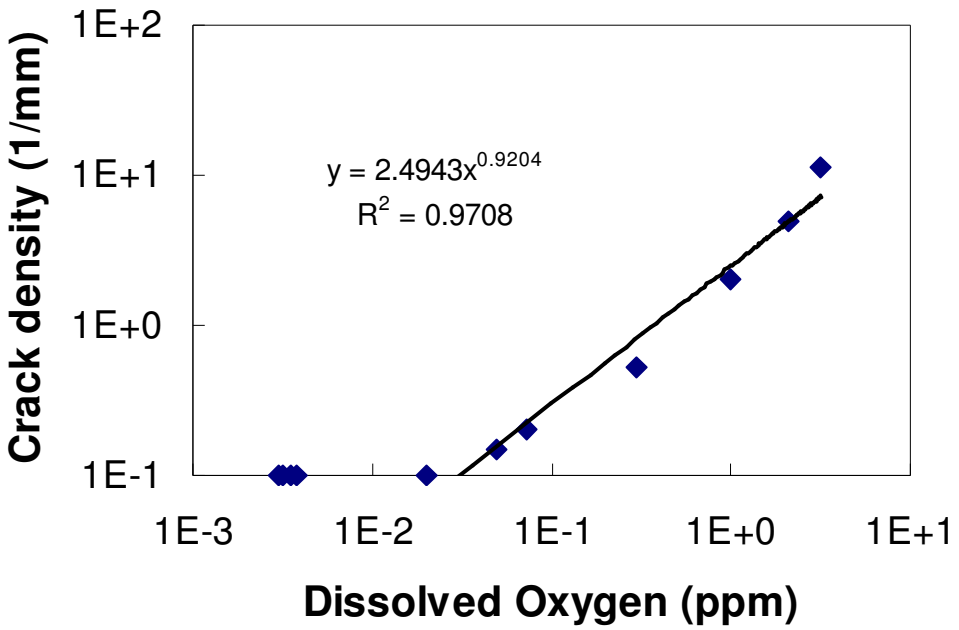

Figure 4. 14. Effect of DO on crack velocity of SAC of SA-210 samples tested at 300^{o}C by slow strain rate of 2x10^{-6} s^{-1} in pure water. (DO threshold value: 20ppb)

CHAPTER 5: ROLE OF STRESS CONDITIONS ON SAC CRACKING

Previous experience with SAC in recovery boilers indicates that suspected regions are typically associated with attachment welds on the cold side of the furnace, although SAC also has been identified on the fire side of tubes near hanger welds associated with construction. No theory had earlier been developed to account for specific weld designs and features but the combination of residual and operating stresses (>0.2% strain identified as significant) associated with the welds, as well as perhaps increased restraint associated with thermal excursions, contribute to cracks in these locations. To support this information, strain gages, and thermal couples (TCs) were placed on the cold side of an operating boiler to measure total strains and nominal fluctuations for over one year, those measurements are summarized in Table 5-1, and the representative measurements are shown in Figures 5.1.-5.3. Modeling to determine stresses/strains on the inside of the tubes was undertaken to relate the external measurement to the value of interest and to assess potential for the propagation of cracks. Different types of cyclic loadings experienced by industrial boilers during the operation process are described as next.

Considering the initial pressurization of the boiler tubes along with significant changes in temperature (and development of temperature gradients), start-up of the boiler is considered an aggressive stress/strain event that perhaps contributes to the initiation

and propagation of SAC. Figure 5.1 is a set of data representing the initial start-up of the boiler after the strain gages and TCs had been installed. In the start-up process, the temperature recorded by the TCs changes from near ambient to over 250ºC in only 3-4 hours. Following some equipment "shakedown" that caused the water temperature to be somewhat irregular over the subsequent ~30 hours, the boiler approached steady state operation.

The second type of cyclic loading the boiler might experience in service can be defined as emergency shutdown procedures (ESPs). ESPs typically occur when an off-normal safety measurement is detected; for example, an abnormal pressure or temperature in the coolant system that might indicate a leak of coolant into the boiler. Whatever the initiator, the goal of the ESP is to cease boiler operation as quickly and safely as possible. Due to the sudden change in boiler load – both stopping the operation and the subsequent restart – these events have long been suspected of representing a very aggressive strain on the boiler, which perhaps could exacerbate SAC tendency. Figure 5.2. shows a representative strain and temperature profile for one of the ESP events at the mill.

During normal boiler operation process, the boiler tube temperature leading up to the ESP is essentially constant/uniform and varies only 2-3ºC, as shown in Figure 5.3. Correspondingly, the boiler tube surfaces represented by the strain gages experience no significant change in stress/strain during these "calm" periods. This type of cyclic loading can be defined as small amplitude cyclic loading due to thermal fluctuation, which is experienced by the boiler continuously during normal operation. The results from initial

slow strain rate test indicated that even small amplitude fluctuating stresses can affect both crack initiation and propagation mechanisms at 300°C in oxygenated water and thereby can reduce the time to failure.

There is, however, one brief temperature excursion of about 11-12°C that occurred 4-5 hours prior to the ESP, which has a small relatively modest strain change associated with it. These small temperature/strain excursions represent some type of modest process upset and occurred periodically during the year of data gathering. Figure 5.3 is a representative example of the characteristics of the modest (in terms of temperature/strain excursion) process upsets. In this particular case, the size of the temperature excursion is relatively large (about 60°C) and has a very typical total duration of 5-6 hours. The measurements of cyclic stress experienced by a recovery boiler over 55 weeks of operation are listed in Table 5-1.

Table 5-1 Typical cyclic loading experienced by industrial boilers

	Boiler Start	Boiler Shutdown	Emergency Shutdown Procedures	Process Upsets avg=60°C	Process Upsets avg=20°C	During Boiler Operation
Relative Strain (%)	0.077	0.077	0.04	0.02	0.008	0.002
Temperature (°C)	290	290	290	290	290	290
Dissolved Oxygen (ppm)	3-4	3-4	3-4	< 3	< 3	< 3
Max Stress (MPa)	370	370	310	275	255	250
Mean Stress (MPa)	220	220	230	235	240	245
Amplitude (Mpa)	300	300	160	80	40	10
Occurrences in 55 weeks	1	1	2	8	33	___
Equivalent Frequency (Hz)	3.5E-05	3.5E-05	3.5E-05	4.6E-05	1.4E-04	0.001
Equivalent Strain Rate (s^{-1})	2.3E-6	2.3E-6	1.2E-6	3.7E-7	1.1E-7	2.2E-8
Duration (Hours)	3-4	3-4	6-8	5-6	2	~ 8000

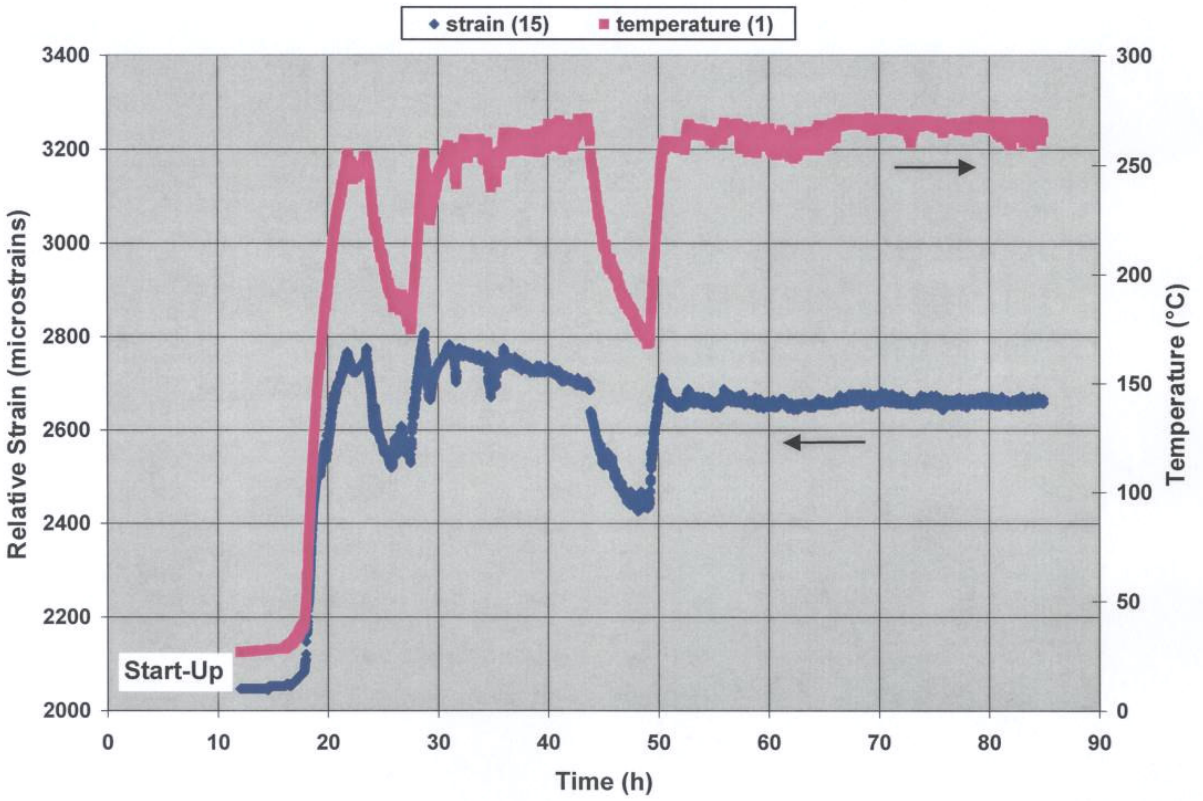

Figure 5. 1. Strain (gage #15) and temperature (TC #1) profiles representing the initial boiler start-up following installation of the gages.

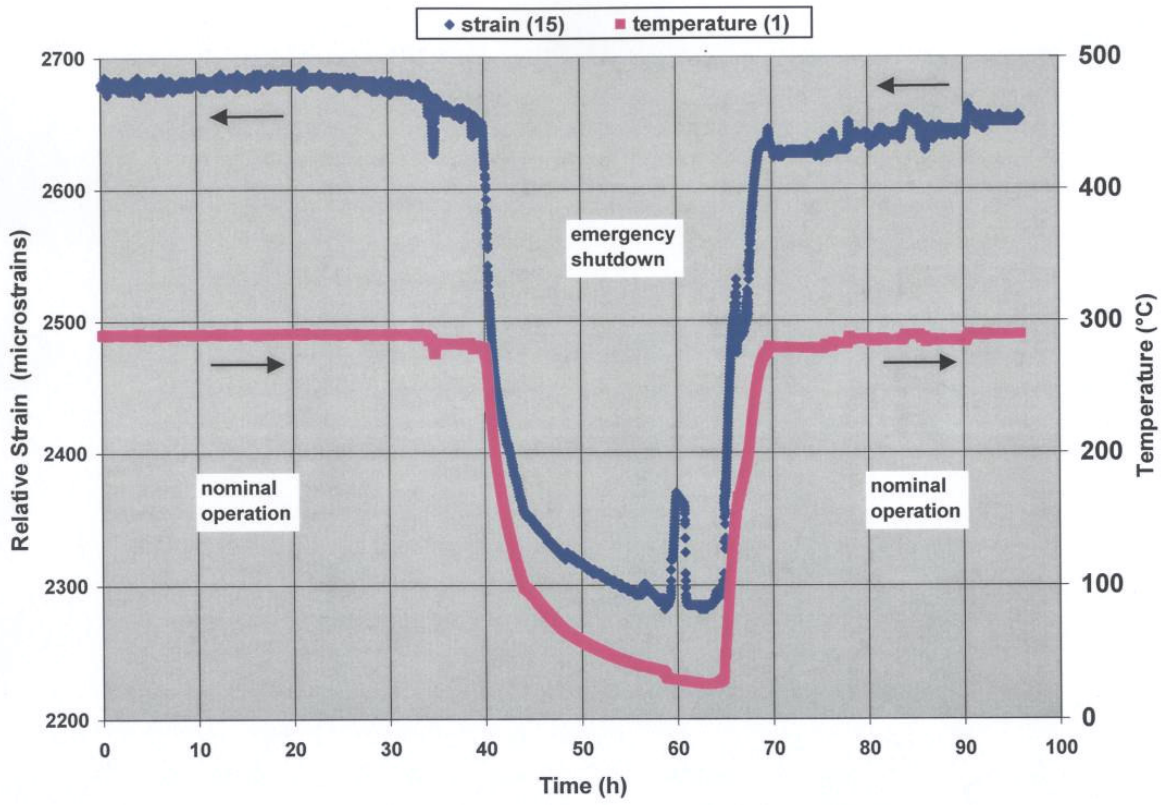

Figure 5. 2. Strain (gage #15) and temperature (TC #1) profiles representing the emergency shutdown and restart conditions in the boiler.

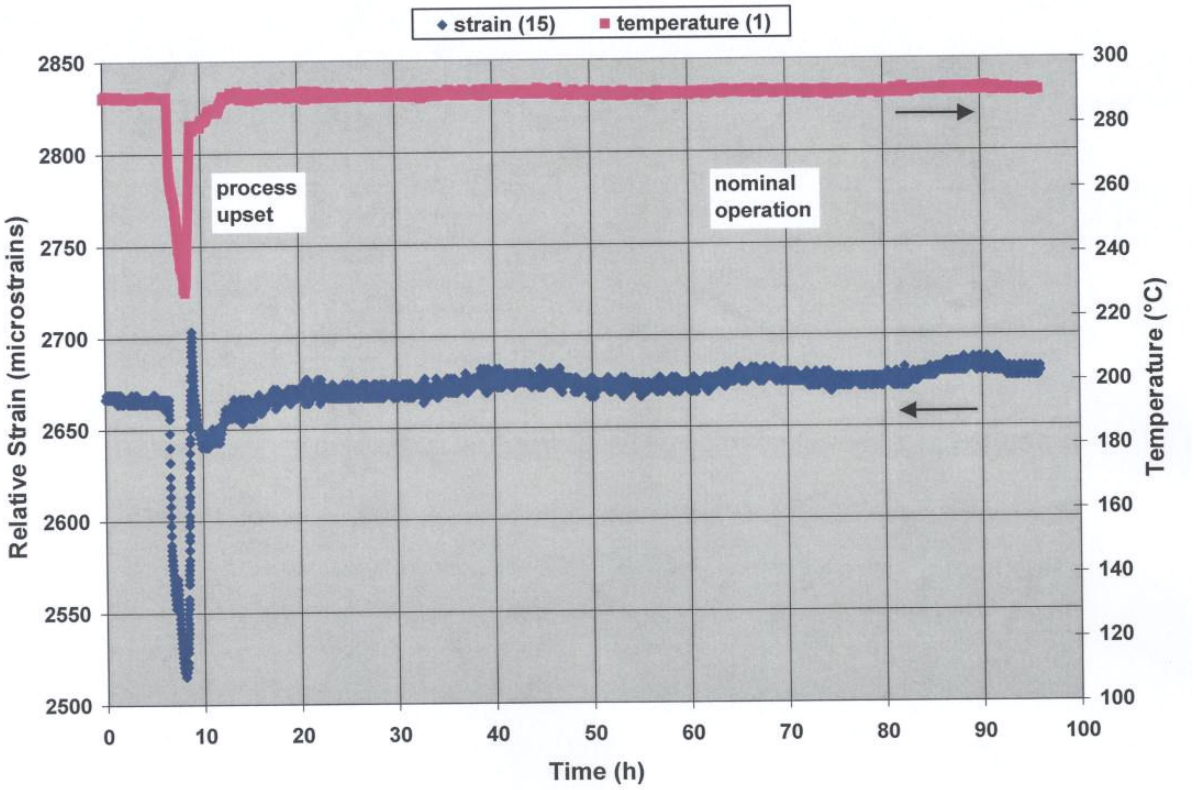

Figure 5. 3. Strain and temperature profiles representing a relatively modest process upset with a temperature change of about 60ºC.

The present research project was aimed at examining the details of crack initiation and propagation of SAC in industrial boilers with special emphasis on the recovery boilers in the pulp and paper industry. By simulating the stress conditions on a slow strain rate rig in a pressurized recirculation-loop autoclave facility [18, 62], this study evaluated the effect of mean stress, stress amplitude, frequency, and strain rate on initiation and growth of SAC in industrial boilers.

5.1. Experimental Details

Smooth tensile specimens with 0.125 inches diameter and 0.5 inches gage length were machined out of SA-210 carbon steel tubes. The specimens were machined with the tensile axis oriented along the pipe length. Tensile specimens were polished to a 2000-grit finish and cleaned with acetone before testing. Water chemistry parameters (i.e., dissolved oxygen, temperature, pH and conductivity, etc.) were individually monitored and controlled, as described in Chapter 4. Test temperatures for autoclave tests ranged from 110^{o}C to 320^{o}C. Dissolved oxygen in the pure water was controlled between 5 ppb to 2 ppm in different tests by, individual or combined use of, passing N_2 through the solution or additions of different amounts of Na_2SO_3. Slow strain rate tests under different stress conditions (with various combinations of mean stress, stress amplitude, and frequency) were conducted to investigate their influences on SAC cracking. For majority of slow strain rate tests, an initial strain rate of 2×10^{-6} s^{-1} was used, however, strain rate of 2×10^{-7} s^{-1} and strain rate of 6×10^{-6} s^{-1} were also used to evaluate the effect

of strain rate on crack velocity and crack density. After each test, one half of the failed tensile specimen was mounted and polished to quantify crack velocity, crack density, percentage fracture strain, and percentage area reduction.

5.2. Results and Discussions

Industrial boiler ratings range from low pressure (600 psi) to high pressure (1500 psi) with corresponding operating steam temperatures in the furnace tubes between 250^{o}C to 320^{o}C. Most of utility industry boilers are high-pressure boilers. Water chemistry for all boilers is controlled by chemical treatments so as to control the dissolved oxygen levels and pH of boiler water in safe range to avoid general corrosion of tubes. Carbon steel boiler tubes rely on the formation and stability of a protective magnetite film on the tube surface. Any boiler upset, chemical or mechanical can destroy or disturb the protective magnetite film and cause localized corrosion or may lead to crack initiation in the presence of tensile stresses. Boiler tubes experience residual stresses due to manufacturing operations as well as operational stresses from steam pressure and boiler loading. Strain measurements on boiler tubes and calculations have shown that the strains up to 0.15% may be experienced by tube surface near attachment welds, depending upon the attachment configuration [37] during shutdowns and startups.

Results from the lab simulations as well as from the strain measurements have indicated that the stress assisted corrosion in boilers may occur due to "upsets" in the boiler water chemistry and especially during boiler shutdown and startup periods.

5.2.1. Effect of Stress on SAC Crack Initiation

Magnetite film on the boiler tube surface protects it from further corrosion under boiler operating conditions. However, the magnetite film is a brittle film and can become damaged locally by mechanical stresses or chemical reactions exposing carbon steel to corrosive environments. Recent work [11-18] on boiler water along with the work done by Potter and Mann [30, 32, and 40] and Bloom and Newport [39] in caustic solutions has shown that if the film gets damaged the new magnetite film formed is porous and non-protective due to large cathode to anode ratios for this situation. Critical strain required to initially damage a compact and protective magnetite film may be different from the strain required to damage a porous film. However, if strains are lower than the required strain to damage the magnetite film, then the crack may not initiate or propagate.

In order to determine the critical stress/strain for SAC crack initiation, a series of SSRT samples were loaded to different initial stress in the elastic region strain under a constant strain rate (2×10^{-6} s^{-1}) at 300^{o}C in simulated boiler water. After attaining the desired stress on the sample, the loading machine was stopped and the samples were held at that stress for 70 hrs and the sample was unloaded after that time. Results from these tests are shown as the diamond symbols in Figure 5.4.(a). The cracks were found to initiate after about 10-12 hours of straining at the strain rate of 2×10^{-6} s^{-1}, which

corresponded to a stress of 370 MPa, indicated that the stress applied on SA 210 samples by constant strain rate loading need to be larger than material yield strength (330 MPa) to initiate SAC cracks at 300^{o}C in simulated boiler water with dissolved oxygen ~ 3 ppm. The results of some slow strain rate tests conducted at different temperatures (room temperature to 320^{o}C) are also plotted as the square symbols in figure 5.4.(b). The maximum crack length in a sample increased and the time to fracture decreased with an increase in the test temperature. Maximum crack length for the SSRT tests carried out at different temperatures (shown as square symbols) was similar to the constant strain tests (shown as diamond symbols) after initial straining time of 37-40 hrs, temperature~300^{o}C.

5.2.2. Effect of Cyclic Stresses on SAC Crack Initiation

To determine the effect of low amplitude, frequent, cyclic stresses on waterside cracking of carbon steel, slow strain rate tests with fluctuating stresses were carried out. There were two main questions while designing these tests were first, whether the cracks will initiate in the boiler water with 5ppb oxygen in the presence of fluctuating stresses; second if the crack density and overall crack velocity will change with cyclic stresses in water with ~3 ppm oxygen. Initial SSRT tests with low cyclic loading (Frequency = 0.001 Hz, Amplitude = 80 MPa, R = 0.85) were conducted at 300^{o}C to compare with a monotonous SSRT test without cycling load superposed. The results from these tests are given in Table 5-2. Both crack velocity as well as crack density on carbon steel samples under cyclic loading were found to be slightly higher than for the ones tested under monotonous SSRT loading in oxygenated boiler water. Total test time or the time for the specimen to fracture was reduced due to the cyclic loading effects. These results indicate

that even small amplitude fluctuating stresses can affect both crack initiation and propagation mechanisms at 300°C in oxygenated water and thereby can reduce the time to failure.

Table 5-2 Effect of Cyclic Loading on SAC Cracking

Environment Description (Temp, O_2 Level, etc)	Max Stress (MPa)	Stress Amplitude (MPa)	Frequency (Hz)	R-ratio	Crack density (/mm)	Crack velocity (mm/s)	Time to fracture (hrs)
300 °C Untreated Pure Water	550	monotonous SSRT	N/A	N/A	9.4	6.2×10^{-7}	42.6
300 °C Untreated Pure Water	550	80	0.001	0.85	11.2	6.3×10^{-7}	36.7

Other type of cyclic loading that boiler tubes experience is related to boiler shutdown and startup. The high amplitude cycles have very low frequency in boiler tubes. To see their effect of low frequency cycling on crack density and crack growth rate, a series SSRT tests under different stress conditions (with various combinations of mean stress, stress amplitude, and frequency) were conducted to investigate their influences on SAC cracks. Test samples were loaded to the maximum stress values using normal slow strain rate (2×10^{-6} s^{-1}) and then the cycling was started accordingly. Tests were stopped after 70 hours and were examined for crack density and length.

Results from the tests conducted with different values of mean stress and stress amplitude are shown in Figure 5.5.(a-b) and Figure 5.6.(a-b). As the mean stress value of the cyclic loading was increased from 150 MPa to 350 MPa, or the stress amplitude was increases from 0 MPa to 500 MPa, both crack velocity and crack density for the tested carbon steel specimen increased significantly. However, both crack velocity and crack density decreased as the loading frequency was increased from 5×10^{-6} Hz to 0.001 Hz, as is shown in Figure 5.7.(a-b). These results indicate that the damage on test sample in

terms of crack density per cycle or crack length per cycle is greater at lower frequencies. Results from this study are similar to the ones reported by Barsom [51, 52] who suggested that a decrease in cyclic frequency generally produce a decrease in the fatigue strength of the material in corrosive environments. Endo and Komai [53] also suggested that it is not the number of stress cycles, but the period of changing stress that affects the corrosion fatigue strength of a material.

The maximum stress (mean stress + 50% of amplitude) shows a significant effect on cracking susceptibility. Corrosion fatigue cracks were found to initiate on the smooth carbon steel tensile samples under high amplitude, low frequency loading with maximum stress of 280 MPa, as shown in Figure 5.8.(a-b). Results indicate that the environment induced cracking can initiate below the yield strength (330 MPa) of SA-210 under tested temperatures under cyclic stress conditions. It should be noted that after the maximum stress reached to certain value, the change of amplitude started to show stronger effect on the crack velocity due to a larger ΔK value it produced than the change in mean stress did. There is little difference in the respective effect of mean stress and amplitude on crack initiation as long as the combined maximum stress overcomes the critical strain to break the magnetite film locally. And a threshold strain value is found to lie between 0.027% and 0.051% to fracture the surface oxide film on mild steel in the temperature range 500-570^{o}C [48]. Critical stress under cyclic loading conditions was found to be less than the value for monotonous loading conditions, which was found to be roughly 330 MPa (corresponded to a critical strain of 0.15%) as the minimum threshold stress value to initiate SAC in this study, as shown in Figure 5.4.a.

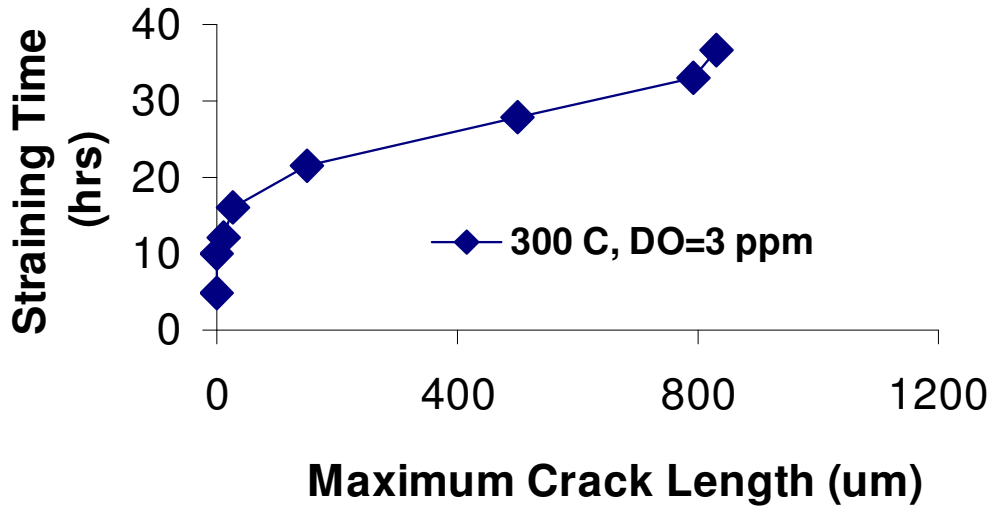

(a)

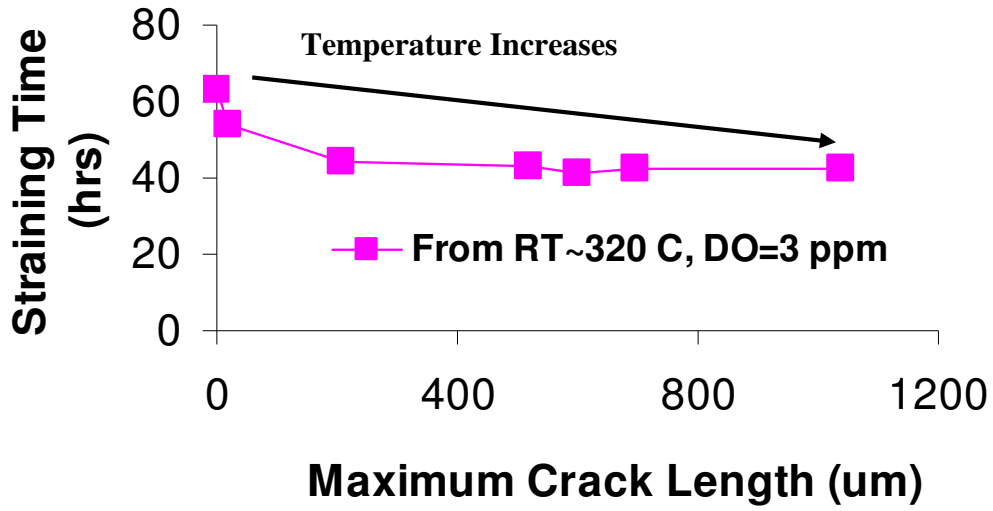

(b)

Figure 5. 4. Straining time versus maximum crack length for SSRT samples in (a) boiler water (3 ppm, 300°C, critical strain ~0.15%) (b) Boiler water (3 ppm, room temperature to 300°C)

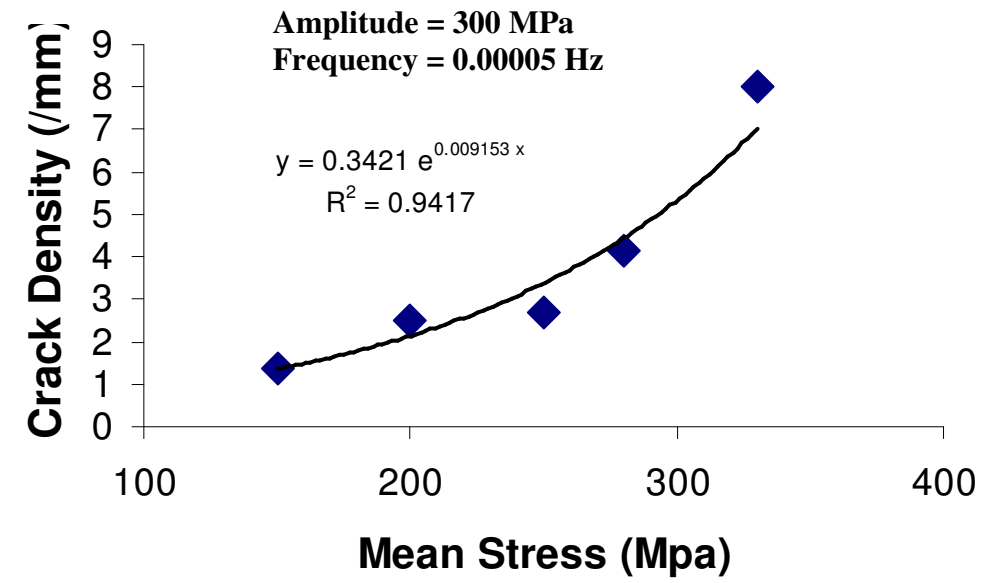

(a)

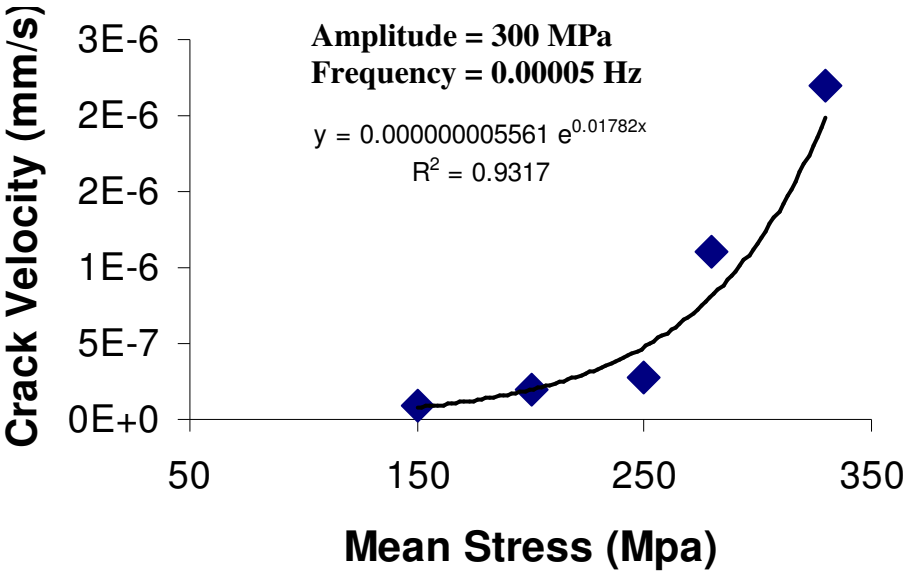

(b)

Figure 5. 5. Effect of mean stress on (a) crack density (b) on crack velocity for SSRT samples tested at 2×10^{-6} s^{-1}

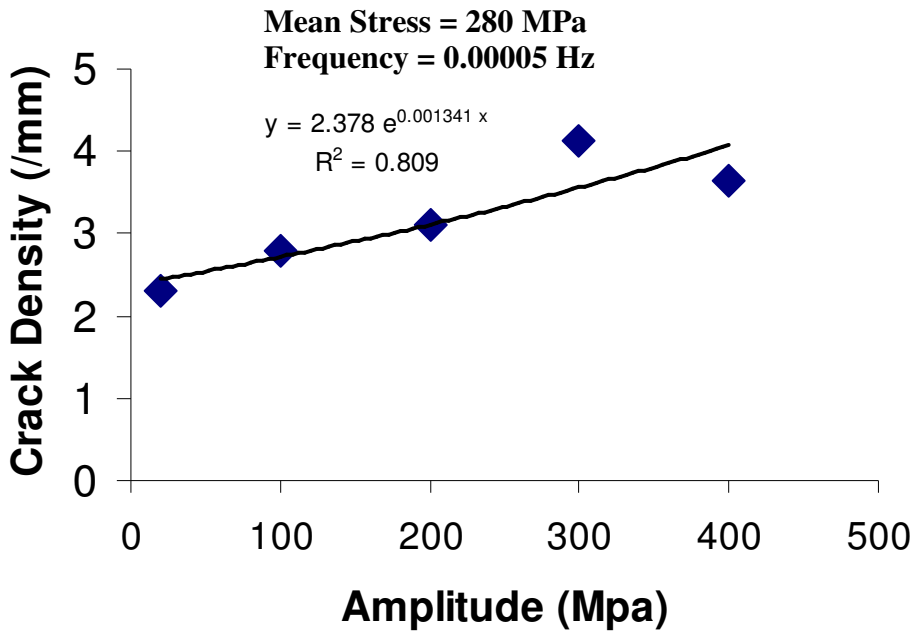

(a)

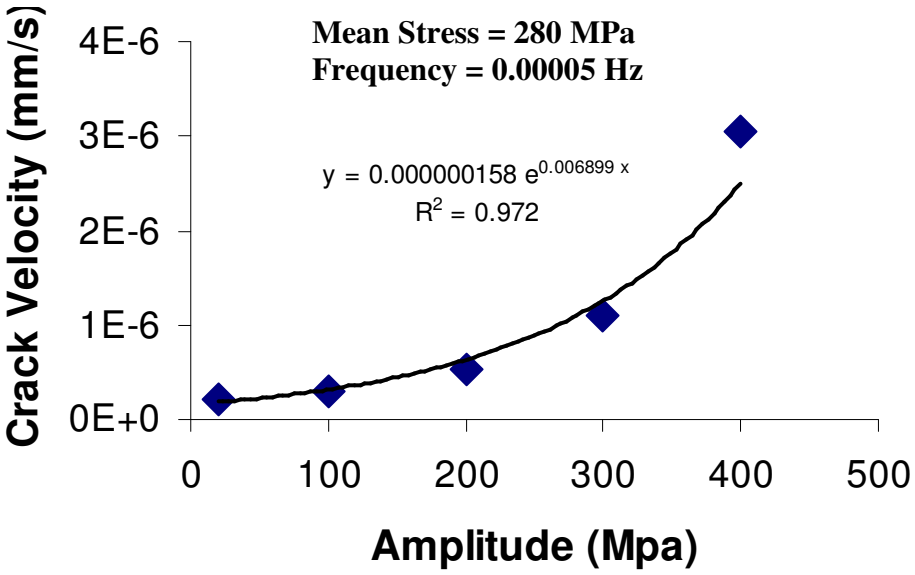

(b)

Figure 5. 6. Effect of stress amplitude on (a) crack density (b) on crack velocity for SSRT samples tested at 2×10^{-6} s^{-1}

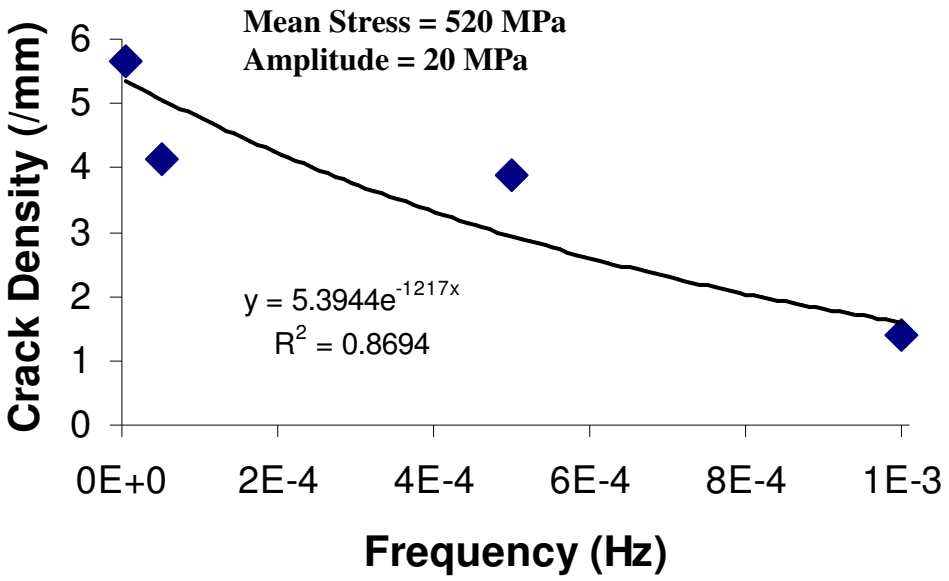

(a)

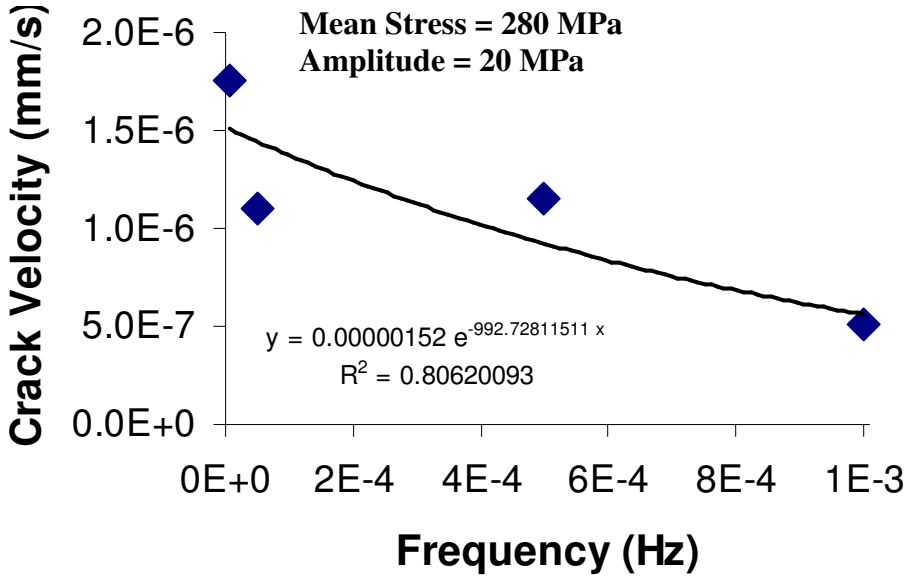

(b)

Figure 5. 7. Effect of cyclic frequency on (e) crack density (f) on crack velocity for SSRT samples

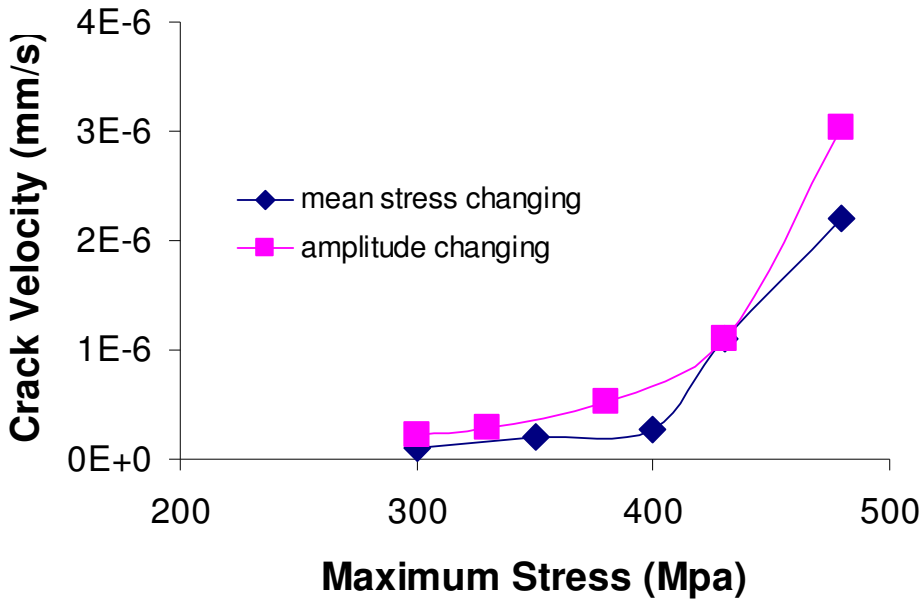

(a)

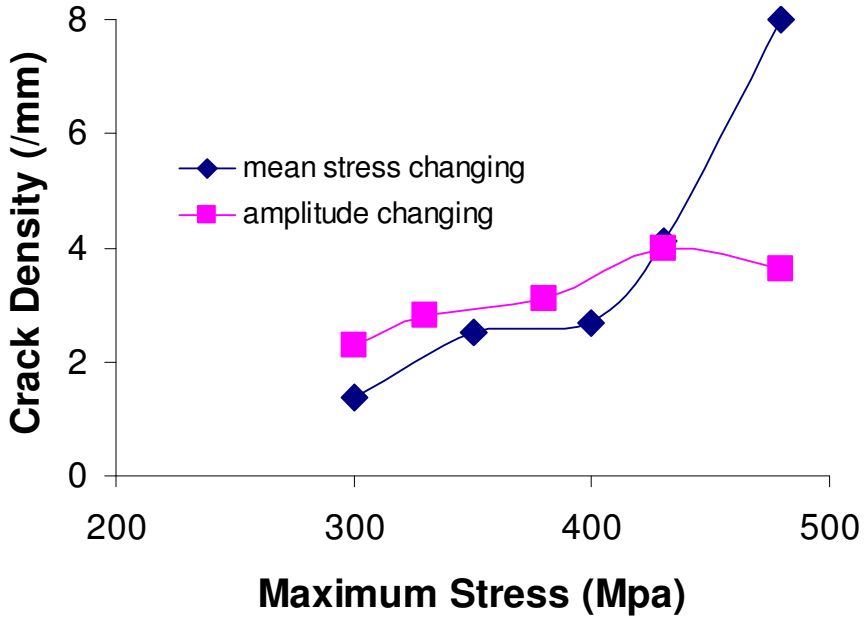

(b)

Figure 5. 8. Effect of maximum stress on (g) crack density (h) on crack velocity for SSRT samples tested at 2×10^{-6} s^{-1} (all SSRT tests in this Figure were done in 300°C boiler water on SA 210 samples)

5.2.3. Effect of Strain Rate on SAC Cracking

Results from the corrosion fatigue tests carried out at different frequencies indicate that the crack density and crack growth rate are affected by the cyclic loading parameters. These results also suggest that the strain rates may also have an impact on stress corrosion cracking of carbon steel in boiler water environments. A series of SSRT tests with four different strain rates (strain rate = 2×10^{-7} s^{-1}, 2×10^{-6} s^{-1}, 4×10^{-6} s^{-1}, and 6×10^{-6} s^{-1}) were conducted in pure water at 300^{o}C. As is shown by the results in Figure 5.9, no cracks were found on tensile samples under different constant strain rate loading when the dissolved oxygen concentration in boiler water was controlled around 5 ppb level. However, in the presence of 3 ppm dissolved oxygen in the water, stress corrosion cracks appear on the surface of tensile samples. Crack density decreases as the strain rate goes up. With strain rate of 2×10^{-7} s^{-1}, crack density was about 16 cracks/mm compared to the roughly 1 crack /mm at strain rate of $6x10^{-6}$ s^{-1}. One important reason for this may be that exposure time increases with low strain rates. However, the trend is not the same for crack velocity. Crack velocity was found to be the maximum at the strain rate of $2x10^{-6}$ s^{-1}compared to the lower and higher strain rates tested. This may be due to competing mechanisms involved in the overall stress corrosion cracking where the magnetite film breaking and passivation rates are competing mechanisms and may dominate at higher and lower strain rates respectively. Whereas the two mechanisms seem to have optimum effect at a strain rate of $2x10^{-6}$ s^{-1}. At higher strain rate (6×10^{-6} s^{-1}), there is lesser time for the passive film to form on the surface and the failure may be

more due to mechanical effects than environmental effects. At the same time there are lesser number of cracks on the sample surface tested at higher strain rate which may affect the maximum crack velocity as there will be lower chances of crack interaction and coalescence. This may explain why the crack velocity & density are low on carbon steel samples tested at high strain rate of 6×10^{-6} s^{-1}, as shown in Figure 5.9.(a) and Figure 5.9.(b). The present results indicate that SAC cracks initiate due to the local fracture on magnetite surface film. Cyclic stresses may facilitate magnetite film damage at lower stresses.

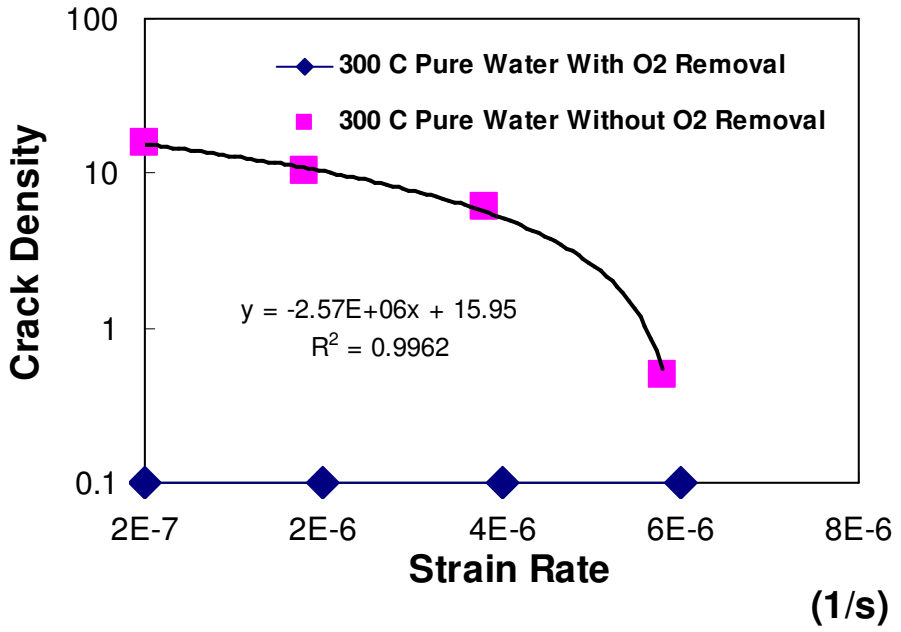

(a)

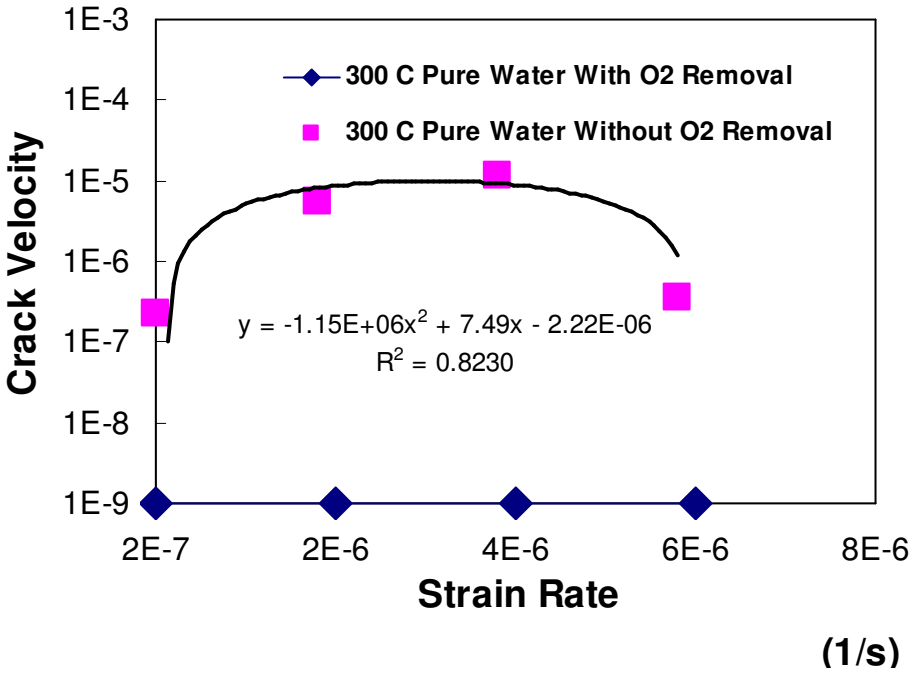

(b)

Figure 5. 9. (a) Effect of strain rate on crack density for SA-210 samples tested by SSRT at 300°C in boiler water. (b) Effect of strain rate on crack velocity for SSRT samples tested at 300°C.

CHAPTER 6: ROLE OF MICROSTRUCTURE ON SAC CRACKING

The relationship between microstructure and corrosion fatigue behavior of carbon steels has been the subject of extensive research for some time. In high carbon steels it was found that fracture toughness and material ductility may vary inversely with austenite grain size [86]. The failure analysis in section 2.2 has indicated that grain size and carbon content may also influence SAC susceptibility of low carbon steels. To find out how those microstructure features of low carbon steel affect SAC cracking under simulated industrial boiler conditions, a series of specimens with different microstructure features generated by varying the heat-treatment process. Heat-treatment tests and SSRTs were conducted in lab. The quantified relationship between microstructure and SAC cracking was then developed from the experimental results.

6.1. Experimental Details

6.1.1. Material & Sample configuration

Crack initiation and propagation susceptibility in heat-treated carbon steel samples was evaluated by slow strain rate test (SSRT) method. SSRT were conducted on tensile samples made of SA-210 carbon steel, a typical material for industrial boiler tubes.

Fatigue tests were also carried on differently heat-treated compact tension (CT) specimens made of 516 G70 carbon steel. CT samples (2.9 inches x 2.5 inches x 0.5 inches) were machined out of 0.5-inch-thick plates. 516 G70 plate was used instead of SA-210 tubes as SA-210 generally is available in tube form and both materials have similar nominal composition, as shown in table 3.1.

6.1.2. Heat-treatments to Change Microstructure

To explore the role of carbon steel microstructure on SAC, baseline tests were carried out with as received pearlitic microstructure. Carbon steel tensile samples were given different heat-treatments under Argon gas environment in the ceramic tube furnace to develop different microstructures. The tensile samples were Alumina cement sealed into a small ceramic tube to avoid oxidation during the heating. Then the small tube with sample was put into the ceramic furnace with argon flowing throughout the test. For carbon steel, the first step of the heat-treatment was to austenitize at $1100^{o}C$ and the temperature was held for different times for grain growth after the furnace was Argon purged for 2-3 hours to get rid of the oxygen in furnace. The cooling rate curve for each sample heat-treatment in this study was monitored and was the same, as shown in Figure 6.1.(b). A ceramic tube furnace, with argon gas flowing through it, was used for heat-treatments to produce different microstructures on tensile and CT samples. Heat-treated tensile samples were removed from the sealed ceramic tubes and polished to 2000-grit finish for stress corrosion susceptibility tests. SSRTs were conducted on these tensile samples to study the effects of grain size and decarburization on SAC cracking. CT specimens of carbon steel 516 G70 were also given similar heat treatments under inert

atmosphere to vary the grain sizes and fatigue tests were done in lab air to study the grain size effect on the threshold stress intensity for initiation and crack growth rates of carbon steels. According to the cooling curve in Figure 6.1.(b) and the time-temperature transformation curve in Figure 6.1.(a), two phase (ferrite/pearlite) microstructure were expected on heat-treated tensile and CT samples as 0.2% carbon steel, 516 G70, and SA-210 have almost the similar composition and carbon content. Ends of tensile samples were mounted, polished, and etched after the SSRT were over. Image analysis was used to quantify grain size and other microstructural features.

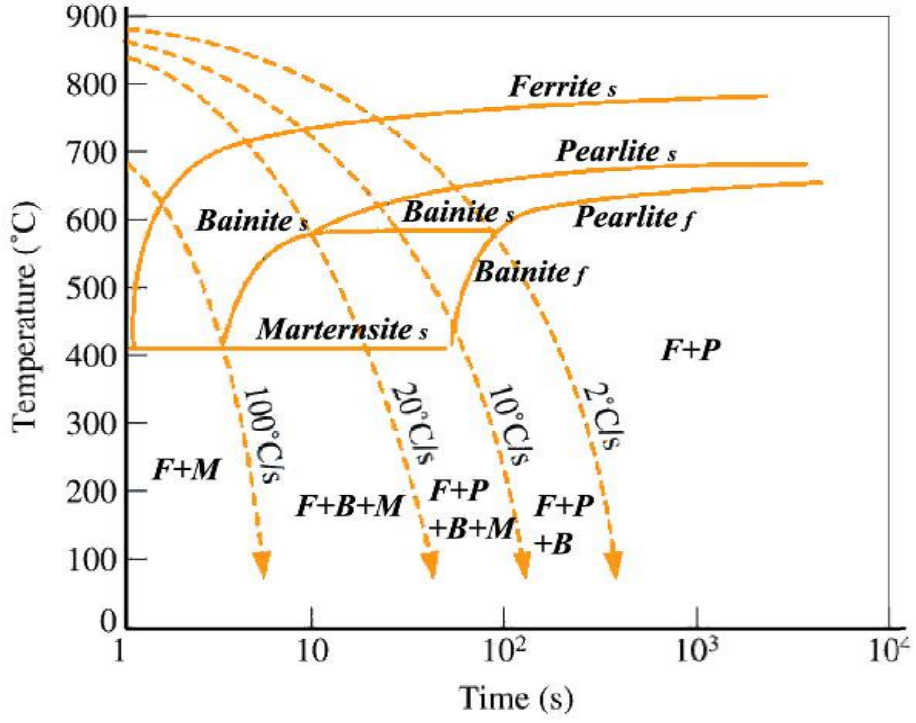

(a)

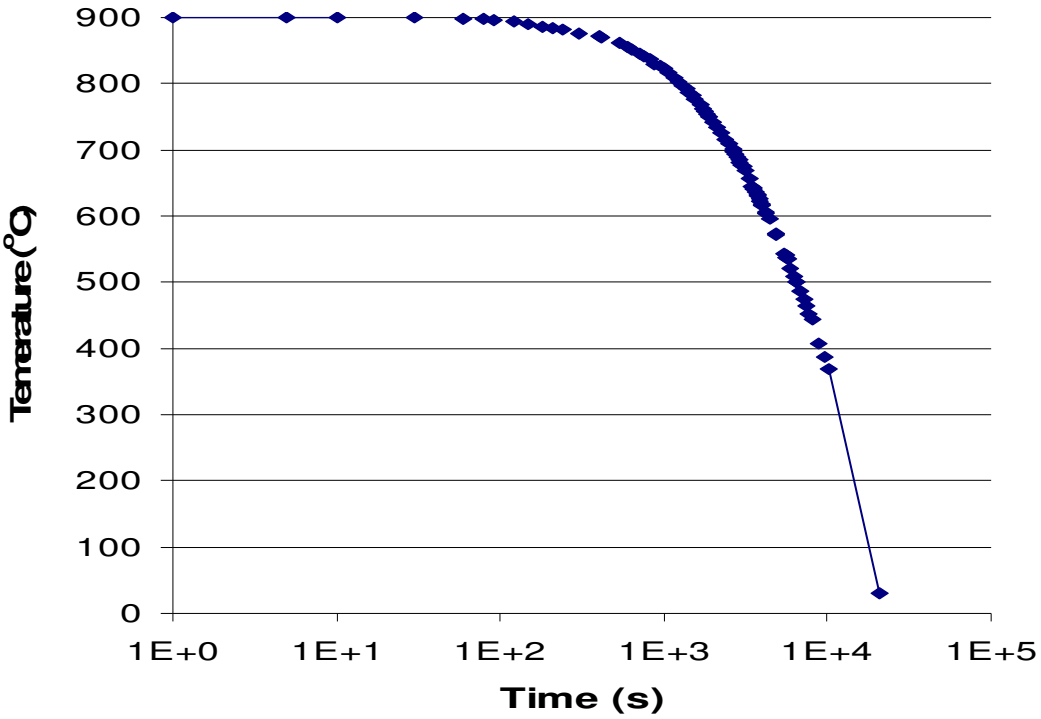

(b)

Figure 6. 1. (a) CCT curve of 0.2% carbon steel [87] (b) Cooling curve of heat-treatment tests

6.1.3. Slow Strain Rate Tests

After heat-treated, the tensile samples were polished to a 2000-grit finish and cleaned with acetone before slow strain rate testing. A set of SSRT conditions (constant strain rate of 2×10^{-6} s^{-1}, constant test temperature of 300^{o}C, and dissolved oxygen was controlled ~3 ppm) were applied on heat-treated samples in simulated boiler water conditions. After each test, one half of the failed tensile sample was mounted and polished to quantify crack velocity (defined as length of the second largest crack/loading time), crack density (defined as crack number/ length of mounted sample), percentage fracture strain, and percentage area reduction.

6.1.4. Fatigue Tests

After heat-treated, the CT samples were also polished to a 2000-grit finish and cleaned with acetone before slow fatigue testing. The fatigue crack growth tests were conducted on heat-treated CT samples by using a servo-hydraulic closed-loop testing machine (MTS) under sinusoidal cycles with displacement control at a frequency of 20 Hz and R-ratio of 0.3. The fatigue crack growth tests were performed only in lab air at room temperature (24^{o}C). Crack growth was monitored using a traveling microscope unit attached to the test rig. The precision of the traveling microscope units was 0.01 mm. Pre-cracked CT specimens were subjected to fatigue conditions to measure crack growth rate.

Stress intensity values (K_I) were calculated from the load values and crack length at a given time, as described in ASTM standard E647..

6.2. Results and Discussions

6.2.1. Effects of Microstructure on SAC under Industrial Boiler Conditions

Initial SSRTs were conducted on heat-treated tensile samples under simulated industrial boiler water conditions with initial strain rate of 2×10^{-6} s^{-1}. These tests were conducted at 300 ^{o}C, with dissolved oxygen in doubly deionized water controlled ~3 ppm. The fractured tensile samples after the test were polished to a 2000-grit finish, etched with 2% Nital solution, and cleaned with acetone before examining them under optical microscope and using image analysis to quantify microstructure. The grain size was measured by intercept method using image analysis software Clemex Vision PE/Lite. The resulting microstructures and corresponding SSRTs loading curves are shown in Figure 6.2. Grains in the as received pipeline steel were elongated along the tube length. As the annealing time at 1100^{o}C increased from (0 to 7 days), the grain size increased (the average grain length increased from 14.6 µm to 68.5 µm; and the grain width increased from 7.8 µm to 52 µm) significantly. As a result, the yield strength of material became lower and the material acted as less ductile material as the its fracture strain decreased significantly. The microstructures of as received sample and sample with annealing time of 1 hour indicate that heat-treatment also changed the grain shape from elongated grain to a more equiaxed grains, as shown in Figure 6.2.

Data shown in Table 6-1 indicates that both SAC crack density and velocity increased with increase in the grain size and decarburization of the material, validating the observations from failed waterwall tubes showing cracking in the large grained materials. This indicates that the carbon steel microstructure does influence SAC cracking under industrial boiler water conditions. Lower carbon level in the surface layer of material was believed to have some contribution to the accelerated SAC cracking as well. Narasaiah and Ray [88], and Taylor [89] have shown that fatigue properties of carbon steel depend upon the carbon content of steel. They reported that fatigue threshold increases with increasing pearlite percentage or carbon content in ferrite-pearlite carbon steels.

Material with larger grain size is expected to show more ductility along with the lower yield strength. However, when these materials are exposed to the boiler water environment, results from this work show that the yield strength decreased with an increase in the grain size and decarburization but, as shown in Figure 6.2, but the larger grain size materials were found to have lower fracture strain, indicating more brittle material behavior or more susceptibility to SAC. Under inert environment, ductility would have increased with grain size but due to higher susceptibility of crack initiation and growth due to the environmental effects has resulted into lower fracture strain. The dependences of crack velocity and crack density on grain size are plotted in Figure 6.3.(a) and Figure 6.3.(b), which indicate that both the number of cracks and their growth seem to increase linearly as the material grain size grows. By line-fitting, both crack velocity and crack density can be derived as functions of grain size, as shown in Figure 6.3.(a-b).

The microstructure of as received sample did not show any grain growth under the SSRT process with a dissolved oxygen level of 3 ppm. The working temperature of industrial boilers is 300^{o}C to 350^{o}C, which is far below the critical temperature (727^{o}C), and the required annealing temperature of 0.2% carbon steel (AISI 1020). So the grain growth on the failed boiler tube was most likely from the boiler tube manufacturing/processing and not during the boiler operation. This indicates that the possibility of SAC crack initiation could be decreased by quality control and eliminating tube with large grained microstructure at its inner surface.

As mentioned earlier, the heat-treated microstructures of SA-210 carbon steel shows two phases (ferrite/pearlite) features. The SAC cracks seem to initiate from ferrite grain sites and grow in a transgranular mode. The pearlite phase structure seems to have stronger resistance of SAC crack growth as quite often the SAC cracks were found to arrest before or avoid pearlite structure, as shown in Figure 6.4. and Figure 6.5. This type of phenomenon was also reported by other researchers. Fowler and Tetelman [90] reported that the fatigue crack path was deflected by presence of ferrite along the prior austenite grain boundaries, and Narasaiah and Ray [88] reported that fatigue cracks tend to take large deflection along the ferrite-pearlite interface prior to passing through the pearlite colony. It is also shown in Figure 6.4.(a-b) that most SAC cracks appear to be transgranular, which indicates the grain boundary region of low carbon steels may be as susceptible as in-grain regions to the SAC cracking under environmental effects.

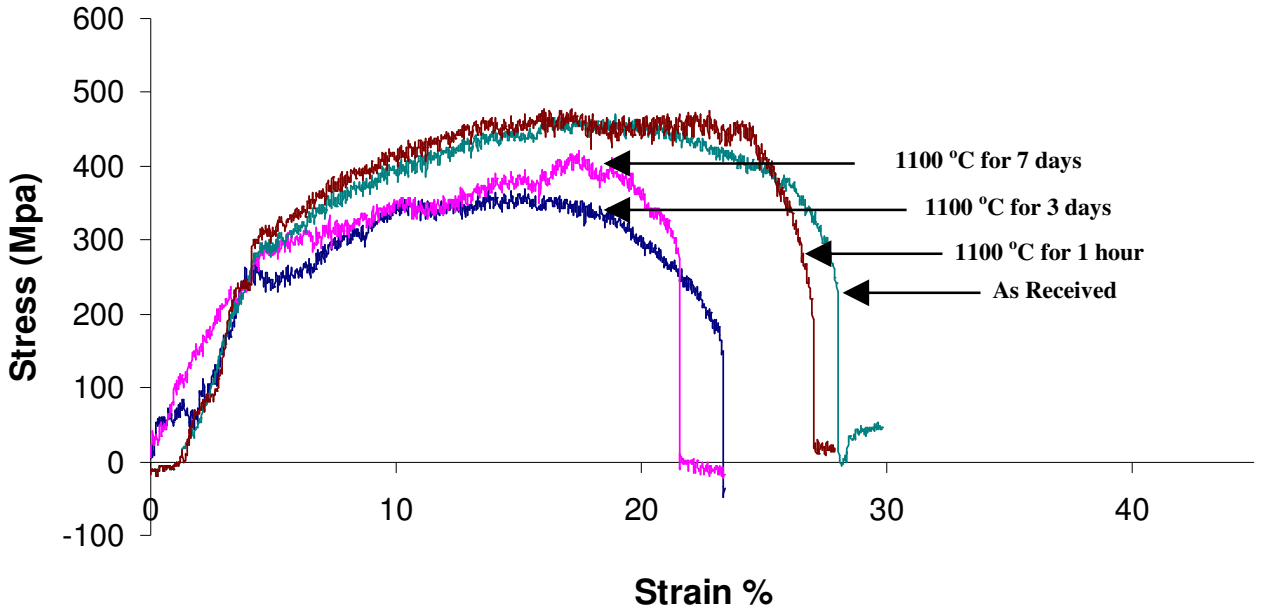

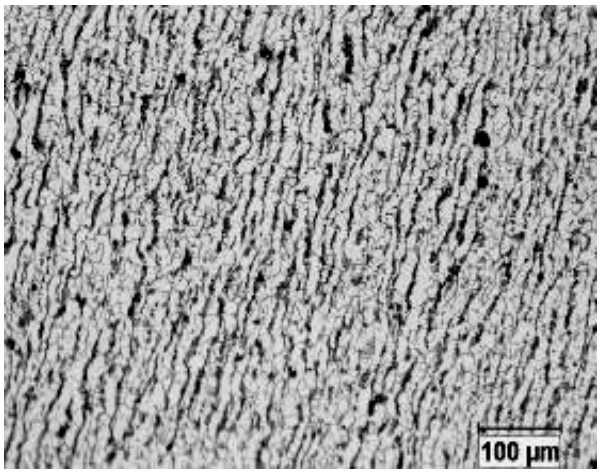

As received

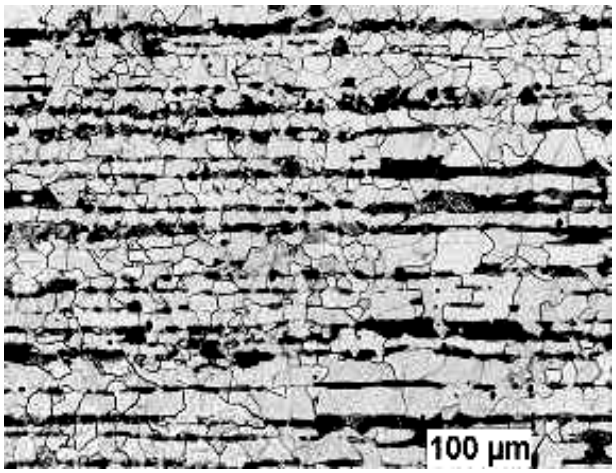

1100°C for 1 hour

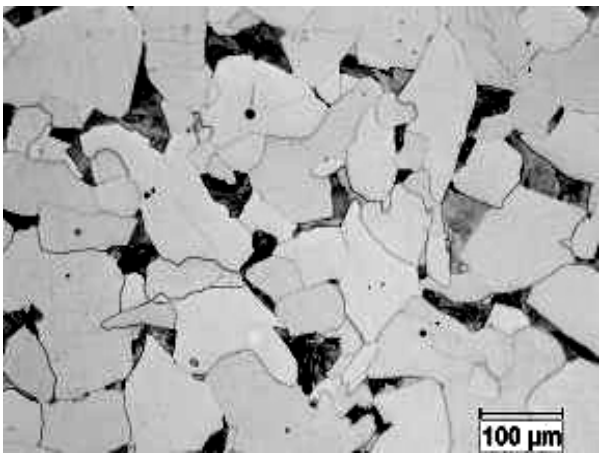

1100°C for 7 days

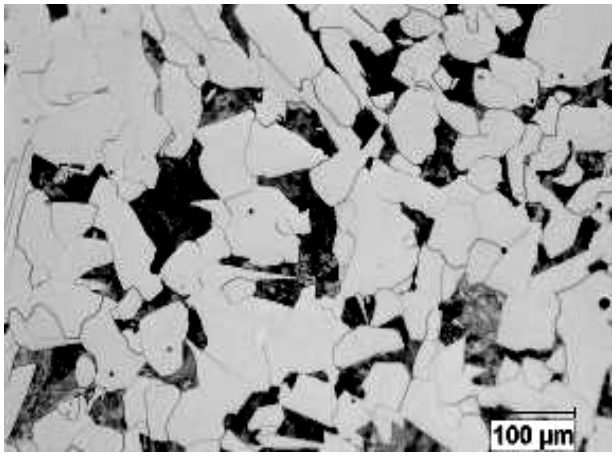

1100°C for 3 days

Figure 6. 2. Effects of grain size and carbon content on SAC cracking

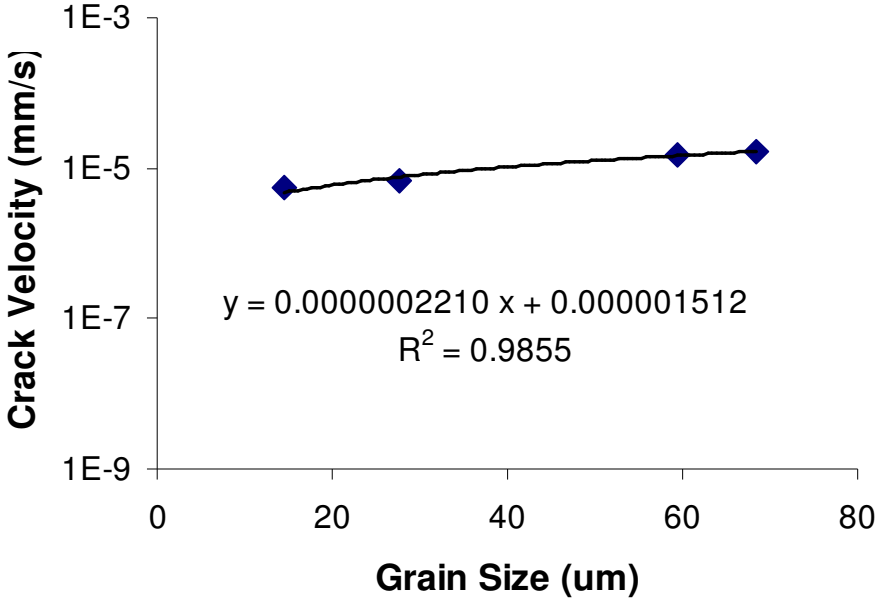

(a)

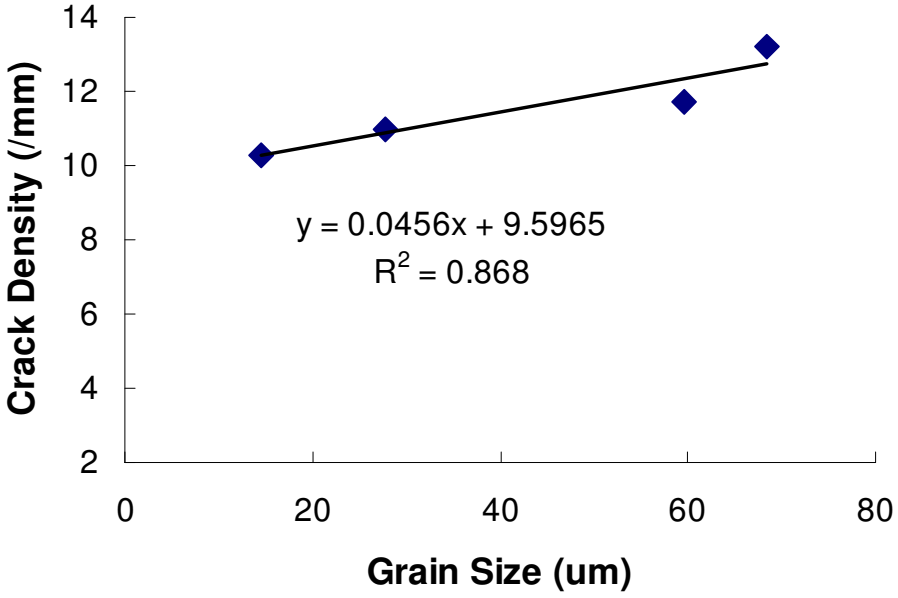

(b)

Figure 6. 3. (a) Effect of grain size on crack density for SA-210 samples tested by SSRT at 300°C in boiler water. (b) Effect of strain rate on crack velocity for SSRT samples tested at 300°C.

Table 6-1 Heat-treatments and resulting microstructure features of SA210

Time at 1100°C (hours)	Grain Length (μm)	Grain Width (μm)	Pearlite/Ferrite (Area ratio %)	Crack Velocity (10^{-6}mm/s)	Crack Density (/mm)	Fracture Strain (%)
0	14.6	7.8	33.8	6.3	10.3	28.4
24	27.7	12.7	32.2	6.7	11.0	27.0
72	59.5	47.4	25.6	15.0	11.7	23.4
168	68.5	52.0	14.0	16.6	13.2	21.8

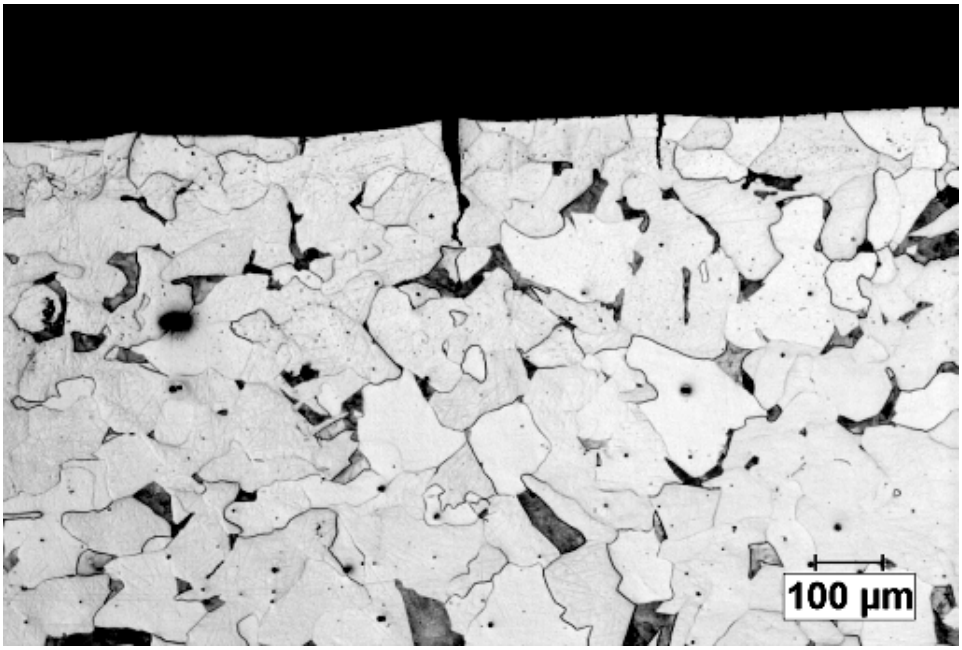

(a)

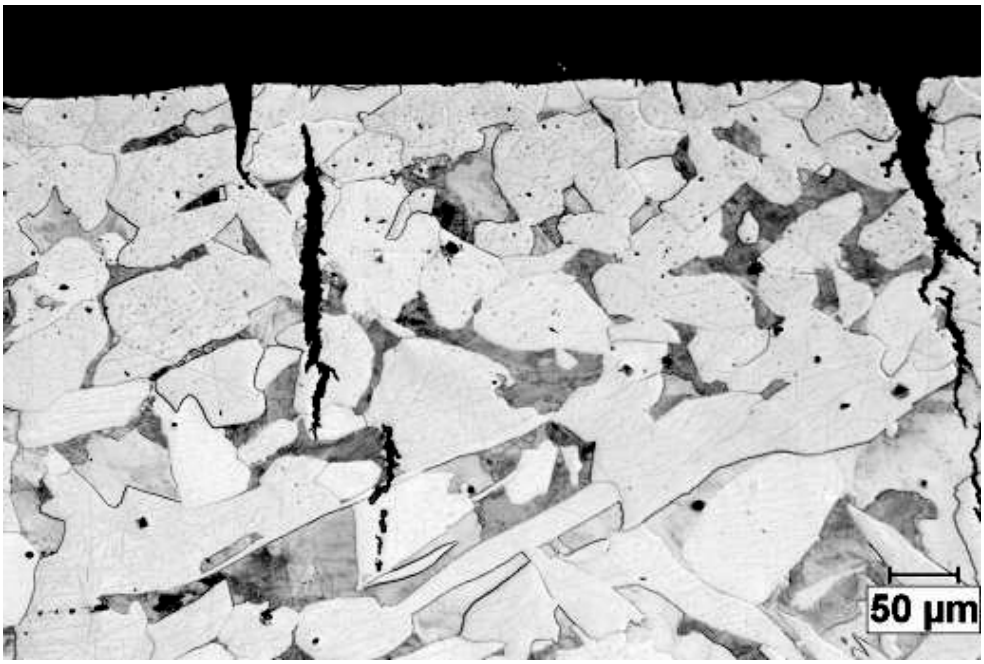

(b)

Figure 6. 4. (a) SAC resistance of ferrite/pearlite structure of SA-210 carbon steel (b) SAC resistance of ferrite/pearlite structure of SA-210 carbon steel

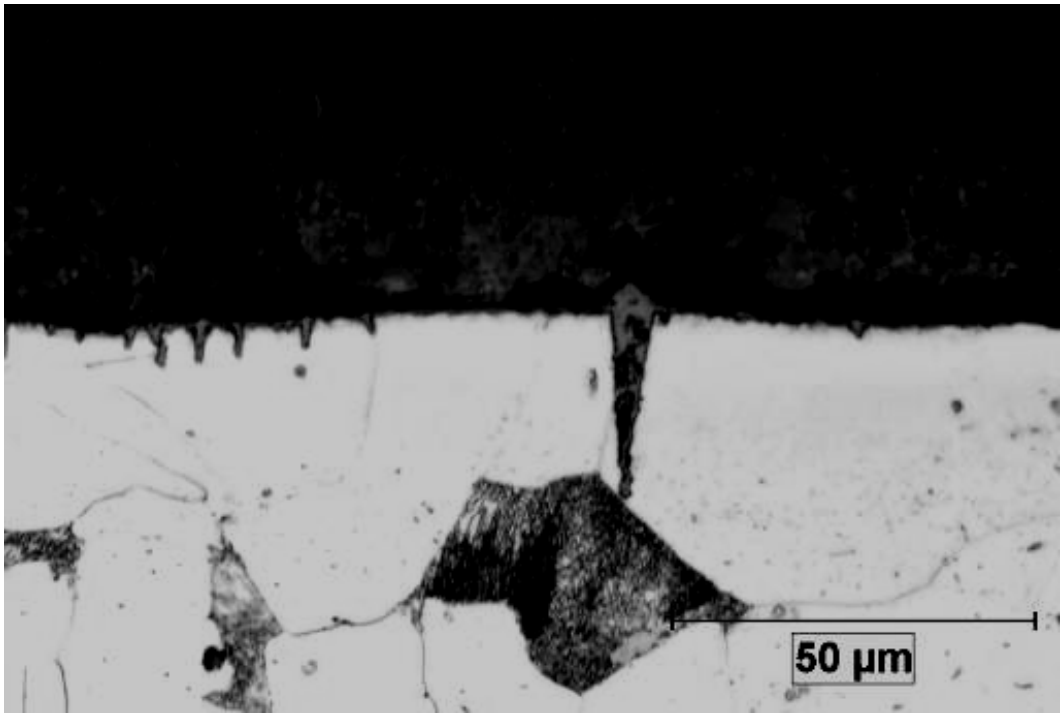

(c)

Figure 6. 5. SAC resistance of ferrite/pearlite structure of SA-210 carbon steel

6.2.2. Effect of Microstructure on Fatigue Behavior in Lab Air Conditions

Work was carried out to quantify the effect of grain size on threshold stress intensity factor for crack propagation. These tests were carried out in lab air to develop understanding of the effect of metallurgical parameters on fatigue behavior of carbon steel. The annealing temperature and times to heat-treat CT samples are shown in Table 6-2. The microstructure and properties (grain size, hardness) after different heat-treatment are also listed in Table 6-2. Image analysis data indicates that the ferrite/pearlite ratio in all heat treated samples was similar. After heat-treatment the CT specimens were polished to a 2000-grit finish, and cleaned with acetone before put on fatigue testing on the servo-hydraulic MTS machine. Results in Figure 6.6 show that as the time at annealing temperature increased the value of $\Delta K_{threshold}$ for crack propagation increased accordingly. From the Figure 6.6 steady state crack growth rate region, linear zone of the curve can be described by Paris' Law equation: $da/dN=A*(\Delta K)^p$ As the hardness and grain size changed, the slopes of Paris region for different compact tension specimens did not show significant difference, which means the rate of crack propagation did not change much with the change of microstructure characteristics described in table 6-2. Results clearly show that that crack propagation started at higher threshold stress intensity values for carbon steel with larger grain size or lower strength. However, in these CT tests the carbon steel samples were not exposed to the industrial boiler water and did not see the effect of environment on SAC crack propagation. This result is consistent with the well-known oberservation from W. V. Vaidya [57]. Vaidya observed that material microstructure has stronger influence on crack initiation and final fast fracture, but no significant effect on the crack propagation region which is governed by

Paris Law [57]. Whereas the results from SSRTs indicate that SAC cracking in the presence of industrial water is more severe so the microstructure seems to have very significant effect on the crack initiation and crack propagation in presence of industrial water. So a steel with inherent crack growth resistance (with higher threshold stress intensity in air) may be susceptible to SAC cracks with a low stress intensity value under boiler water conditions, and the SAC cracks will likely lead to a brittle fracture during SSRT tests.

Table 6-2 Heat treatments used to vary grain size of carbon steel

Conditions	Heat-treatments	Grain Size (μm)	Hardness of Surface (VHN)	Lab air ΔK_{th} R= 0.3 ($MPa/m^{1/2}$)
A	As Received	27.0	245	9.1
B	45 min. /1000 ^{o}C + air cooled to room temperatur	28.5	211	10.0
C	90 min. /1000 ^{o}C + air cooled to room temperatur	30.2	156	10.7
D	24 hours/1000 ^{o}C + air cooled to room temperatu	37.2	141	13.2
E	60 hours /1000 ^{o}C + air cooled to room temperatur	53.1	140	14.9

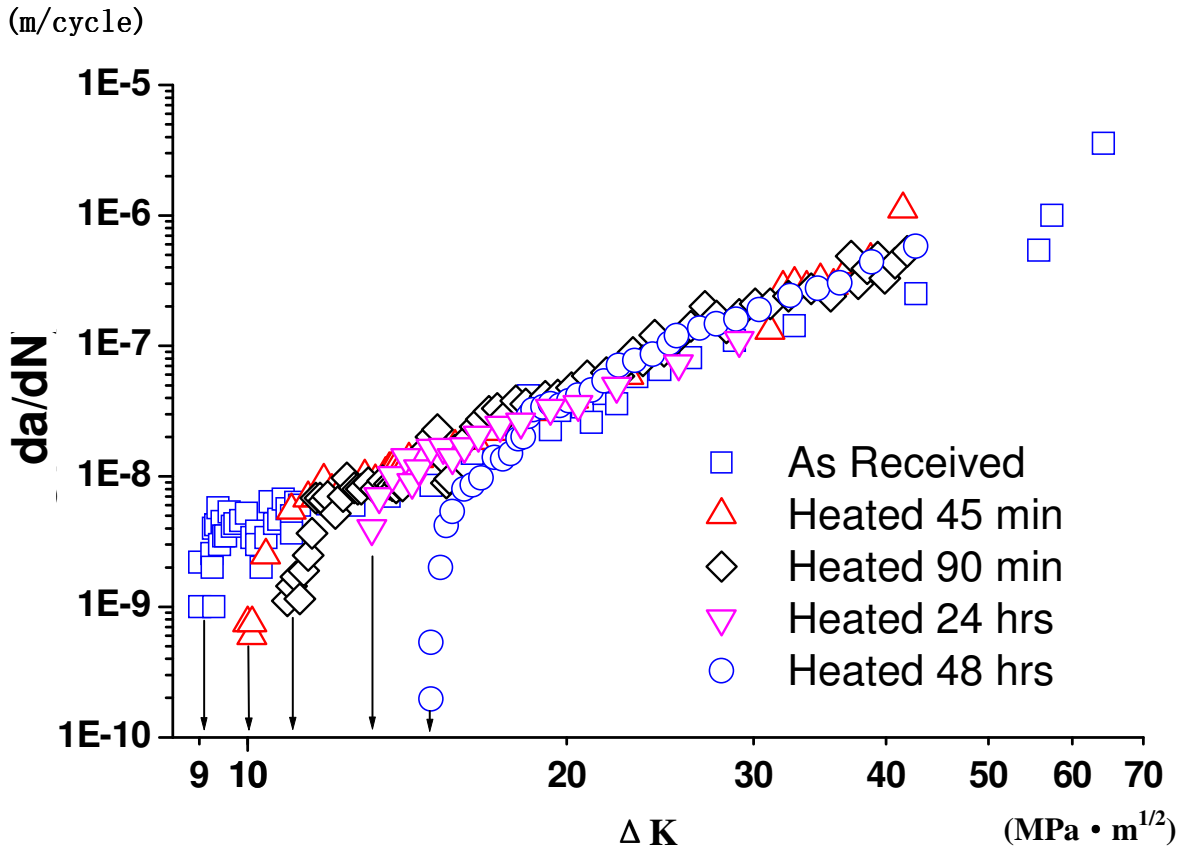

Figure 6. 6. Effect of heat treatment (and resulting grain size) on fatigue behavior of 516 G70 carbon steel

CHAPTER 7: MECHANISM STUDY OF SAC CRACKING

Previous chapters described the crack initiation and propagation behavior of SAC on carbon steel SA-210 under different environment variables. SAC behavior was examined by conducting various specially designed tests and subsequent analysis under simulated industrial boilers conditions. Dissolved oxygen, mechanical stress, and temperature were identified as necessary conditions with a threshold value for these variables for SAC initiation, showing that no occurrence of SAC type of cracks is expected if any of those three variables were controlled below a certain value for either of them. As indicated by the failure analysis of failed boiler tubes, stability of magnetite film on the tube surface seems to be another important variable for the establishment of environment for SAC to initiate.

In order to investigate how dissolved oxygen, mechanical stress, and environmental temperature interact with each other, and affect the magnetite film formation, coupon exposure tests were conducted under designed test conditions. Surface film characterizations were done with AFM/SEM techniques. In this chapter, the mechanism of SAC crack initiation was proposed based on the result analysis of exposure tests, and verifications of the proposed mechanism were also performed experimentally.

7.1. Experimental Details

7.1.1. Samples Preparation

Two different types of tests were conducted to evaluate the effect of magnetite film, on SA-210 carbon steel surface, on SAC initiation and propagation. Flat samples were used to grow and characterize magnetite film under different environmental conditions. Whereas, interrupted slow strain rate tests were conducted to understand the crack morphology of SAC cracks.

As shown in Figure 7.1, smooth coupon plate with 1 inches length, 0.5 inches width, and ~0.12 inches thickness, were machined out of SA-210 carbon steel tubes. The length of the coupon was also along the longitudinal direction of the tubes. The exposure coupons were polished to a 1000-grit finish and cleaned with acetone before put into the autoclave for the coupon exposure testing. Smooth tensile specimens with 0.125 inches diameter and 0.5 inches gage length were machined out of SA-210 carbon steel tubes, as shown in Figure 4.1. The specimens were machined with the tensile axis oriented along the pipe length. Tensile specimens were polished to a 2000-grit finish and cleaned with acetone before testing.

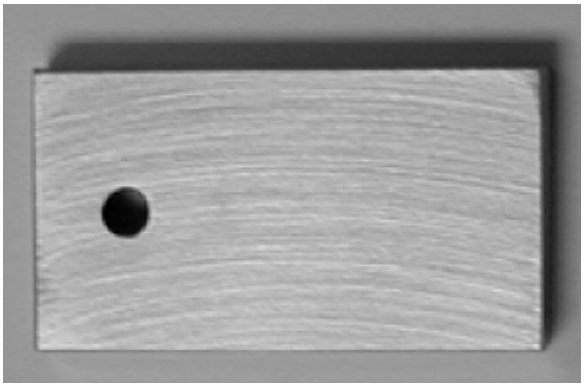

Figure 7. 1. A typical coupon sample for exposure test in simulated boiler conditions

7.1.2. Coupon Exposure Test

Under normal operation, boiler tubes are protected by a magnetite film on the steel surface. Previous work has suggested that damage to the magnetite film plays a important role in SAC initiation and growth [11-18]. A series of tests were carried out to characterize the formation and growth of oxide film on the medium carbon steel, SA-210 samples under different environmental conditions in the autoclave system. Dissolved oxygen level was controlled from ~3ppm to ~5 ppb by either passing Nitrogen into the water environment at a certain flow rate, or a combined use of passing Nitrogen through the water solution and addition of different amounts of Na_2SO_3 as an oxygen scavenger. Test temperature was controlled from 110^{o}C to 320^{o}C for time periods of 30 to 70 hours by pre-programming on the heater controller. Industrial boilers typically operate with water temperature in this selected range. The carbon steel samples were polished to 1000 grit finish, after which they were cleaned with acetone, weighed, and prepared for exposure. Once the required water chemistry was achieved in the recirculation loop, heating was started to obtain initial test conditions. Pressure was determined by the test temperature and was not controlled.

Some polished coupons were exposed to the boiler water environment to check if the conditions were correct to develop magnetite scale similar to the one found on the surface of boiler tubes in the field. Some other polished coupons were exposed to the boiler environment with different anode to cathode area ratio, by putting one coupon

sample into an isolated ceramic holder to simulate the new or acid-cleaned tubes (anode/cathode area ratio = ~1), and putting another coupon sample on the surface of the metal fixture to simulate the damaged film area where bare metal acts as a small anode (anode/cathode area ratio = ~1/200). At the end of each test, the coupons were removed without disturbing the surface film on carbon steel samples. Surface film was first examined using an optical microscope and then characterized using X-ray diffraction method. X-ray diffraction pattern provided information on the type of oxide film and phases present but did not provide information on the morphology of the film. The film morphology was characterized by use of AFM and SEM on sectioned and polished samples.

7.1.3. Interrupted Slow Strain Rate Test (ISSRT)

To simulate the operating environments of real boiler tube, an interrupted slow strain rate test (ISSRT) was designed and carried out in laboratory conditions, by adding a 15-hour-interval with constant temperature of 80°C, constant loading of 30% yield strength, and a 10-minute-O_2 introducing, into SSRTs after each 15 hours loading at a constant strain rate of 2×10^{-6} s^{-1}, as shown in Figure 7.2. The water chemistry parameters for ISSRTs were designed as: test temperature ~ 300°C, dissolved oxygen in coupon exposure test solution was controlled as ~2ppm and ~5 ppb different for different tests. After each test, one half of the failed tensile specimen was mounted and polished to quantify crack velocity, crack density, percentage fracture strain, and percentage area reduction. The crack morphology produced by interrupted slow strain rate test was studied and used to validate our proposed SAC crack initiation & propagation mechanism.

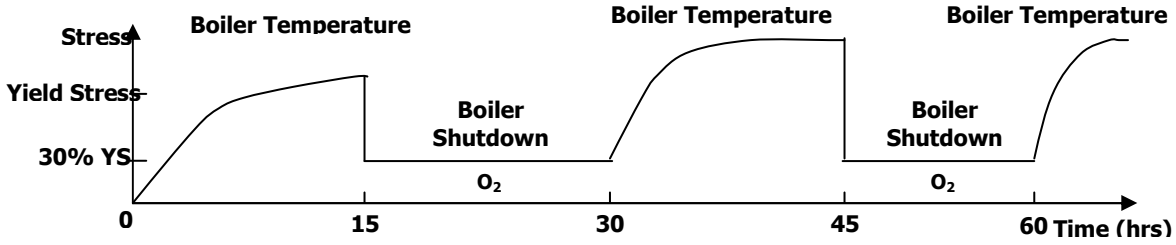

Figure 7. 2. A typical interrupted slow strain rate test-loading curve

7.2. Results and Discussions

7.2.1. Effect of Dissolve Oxygen on the Formation of Surface Film

Water chemistry variables of the simulated industrial boiler environment (300-320^{o}C, 1100-1500 psi) were measured and recorded. Those measurements were then analyzed and marked as the red rectangular area on the Pourbaix diagram of carbon steel tubes in boiler water conditions, as shown in Figure 7.3. Iron was known to react with oxygen-free neutral or slightly alkaline water to form magnetite film at a temperature above 230^{o}C [62]. The reaction can be summarized by following reaction:

$$\mathbf{3\ Fe + 4\ H_2O \rightarrow Fe_3O_4 + 4\ H_2}$$

According to the Pourbaix diagram shown in Figure 7.3, the iron in mild steel is thermodynamically unstable in the presence of high temperature water and tends to form magnetite film with liberation of hydrogen under typical industrial boiler conditions. The reaction product, magnetite, in slightly alkaline water forms a protective layer at the surface which ensures that thinning of the tube wall is negligible under normal operating conditions. Use of carbon steel for high temperature water applications strongly depends upon formation and stability of protective oxide film of magnetite, Fe3O4, on the waterside surface of boiler tubes

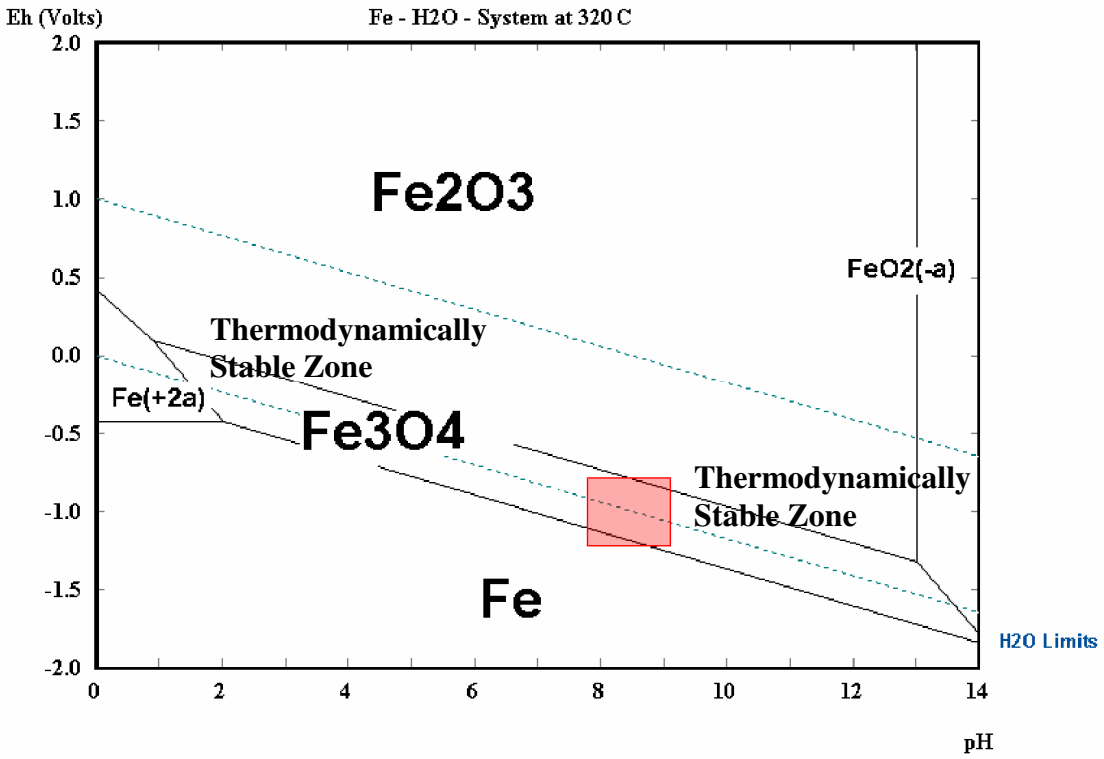

Figure 7. 3. Pourbaix diagram of industrial boiler water environment

X-ray diffraction technique was used to characterize the surface film product formed on unexposed and exposed SA-210 carbon steel sample. As is expected, prominent peaks for the unexposed carbon steel sample in this diffraction pattern corresponded to iron (Fe BCC). Further exposure tests were also done on exposed SA-210 carbon steel samples to extend the simulation of some typical industrial boiler conditions, as summarized in Table 7-1.

Table 7-1 Simulated conditions for exposure tests of carbon steel samples

ID of Condition	Temperature (^oC)	Anode/cathode (ratio)	Dissolved O_2 in boiler water	Exposed time (hours)
i	**300**	**1:1**	**~3 ppm**	**150**
ii	**300**	**1:200**	**~3 ppm**	**150**
iii	**300**	**1:1**	**~5 ppb**	**150**
iv	**300**	**1:200**	**~5 ppb**	**150**

Figures of 7.4.(a-h) are x-ray diffraction patterns of surface films developed at 300^{o}C with dissolved oxygen levels of ~3 ppm and ~5 ppb respectively, on both surfaces of samples, bottom surface and top surface, which were exposed to simulated environments of different anode/cathode ratios. The compositions of the surfaces on all test samples exposed to conditions i-iv were found to be predominately magnetite, Fe_3O_4, which indicate that laboratory test conditions were similar to those in industrial boilers.

The diffraction patterns from the samples with simulated new or acid-cleaned surfaces (anode/cathode area ratio = ~1:1) tested under condition i and condition iii are shown in Figure 7.4.(a-d). The relative intensities and locations of iron peaks along with the magnetite peaks of the top surface matched very well with the bottom surface of the exposed sample (as shown by comparing Figures 7.4.(a) and 7.4.(b) for condition i

simulation, and by comparing Figures 7.4.(c) and 7.4.(d) for condition iii simulation), which indicate good re-productivities of the exposure process and x-ray diffraction tests.

The diffraction patterns from the samples exposed to condition ii and condition iv to simulate the tube area with broken surface film (anode/cathode ratio= ~1:200) are shown in Figure 7.4.(e-h). However, for both conditions the bottom surface of the exposed samples did not show good match of relative intensities but had more prominent magnetite peaks than the top surface of the same sample, as were shown by comparing Figures 7.4.(e) and 7.4.(f) for condition 2, and by comparing Figures 7.4.(g) and 7.4.(h) for condition iv. There may be two reasons for this; bottom surface was directly in contact with a large cathode, thus current densities at this surface will be higher than at the back surface; also due to crevice formed between the touching surfaces, a small amount of water can get into the space between the metal fixture and bottom surface of exposed samples, thus the flow rate of boiler water may not affect the film dissolution.

The samples exposed under condition i and condition ii were found to show more prominent magnetite peaks than corresponding samples exposed under condition iii and condition iv, as seen from the comparison of the diffraction patterns of Figures 7.4.(a) : and 7.4.(e), Figures 7.4.(b) and 7.4.(f), Figures 7.4.(c) and 7.4.(g), and Figures 7.4.(d) : and 7.4.(h). It indicates that higher concentration of oxygen in industrial boiler environment may promote higher rate of reaction of iron with water forming magnetite film at the surface.

As mentioned earlier, the magnetite film grown under very similar conditions can either be thick and relatively porous or it may be thin and compact. Marsh [43] concluded that depending upon the cathodic area in contact with the test sample, the morphology of magnetite can be changed. Although the x-ray diffraction technique can only provide information to identify the composition or the consistence of compounds of material surface, the comparison of the diffraction pattern of isolated samples exposed under condition i to those exposed under condition ii did show that different anode/cathode area ratio may result to prominence difference of magnetite peaks, as shown from comparing Figures 7.4.(a) and 7.4.(c), and from comparing Figures 7.4.(b) and 7.4.(d). Other techniques such as AFM and SEM are used later for further information on morphology or thickness of magnetite film formed on industrial boiler tube surface,

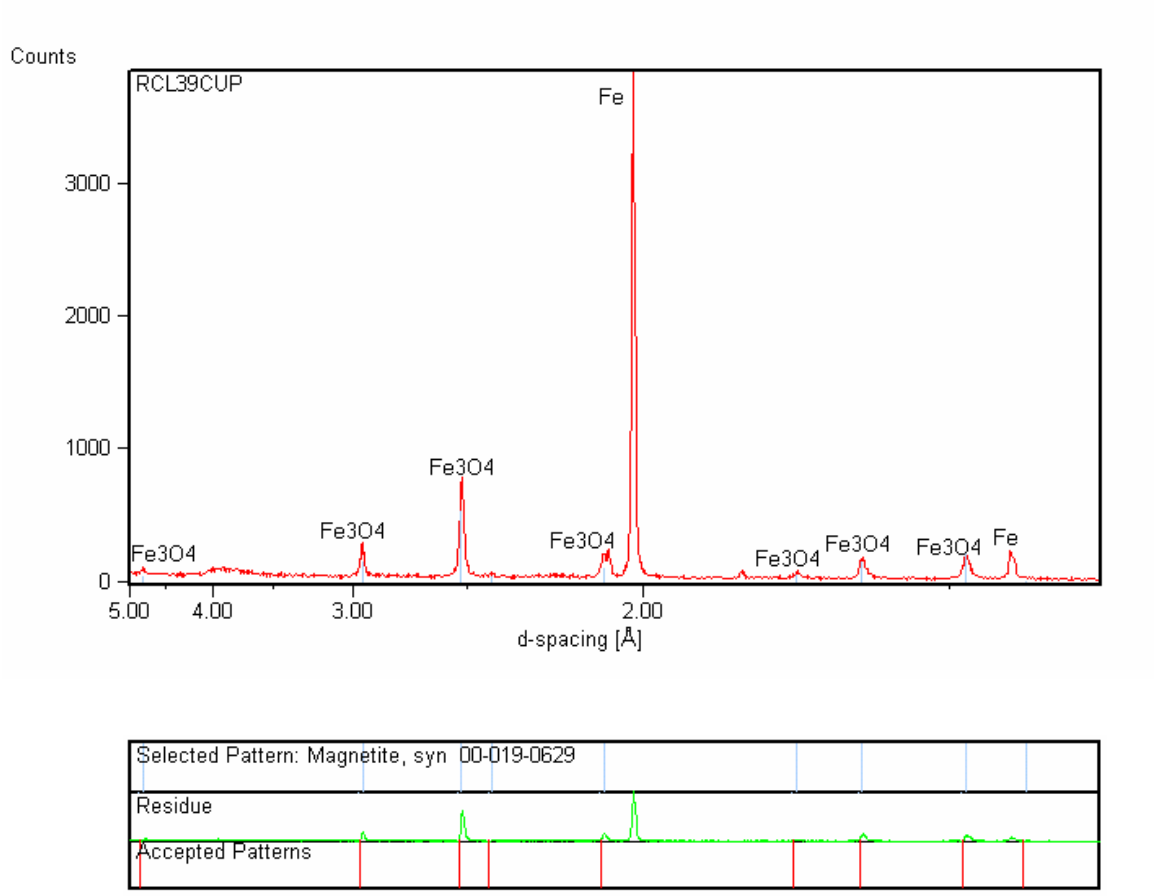

Figure 7.4. (a) X-ray diffraction pattern of the top surface film for SA-210 carbon steel (on contact with metal fixture) exposed to pure water with dissolved oxygen ~3ppm at 300^{o}C for 30 hours

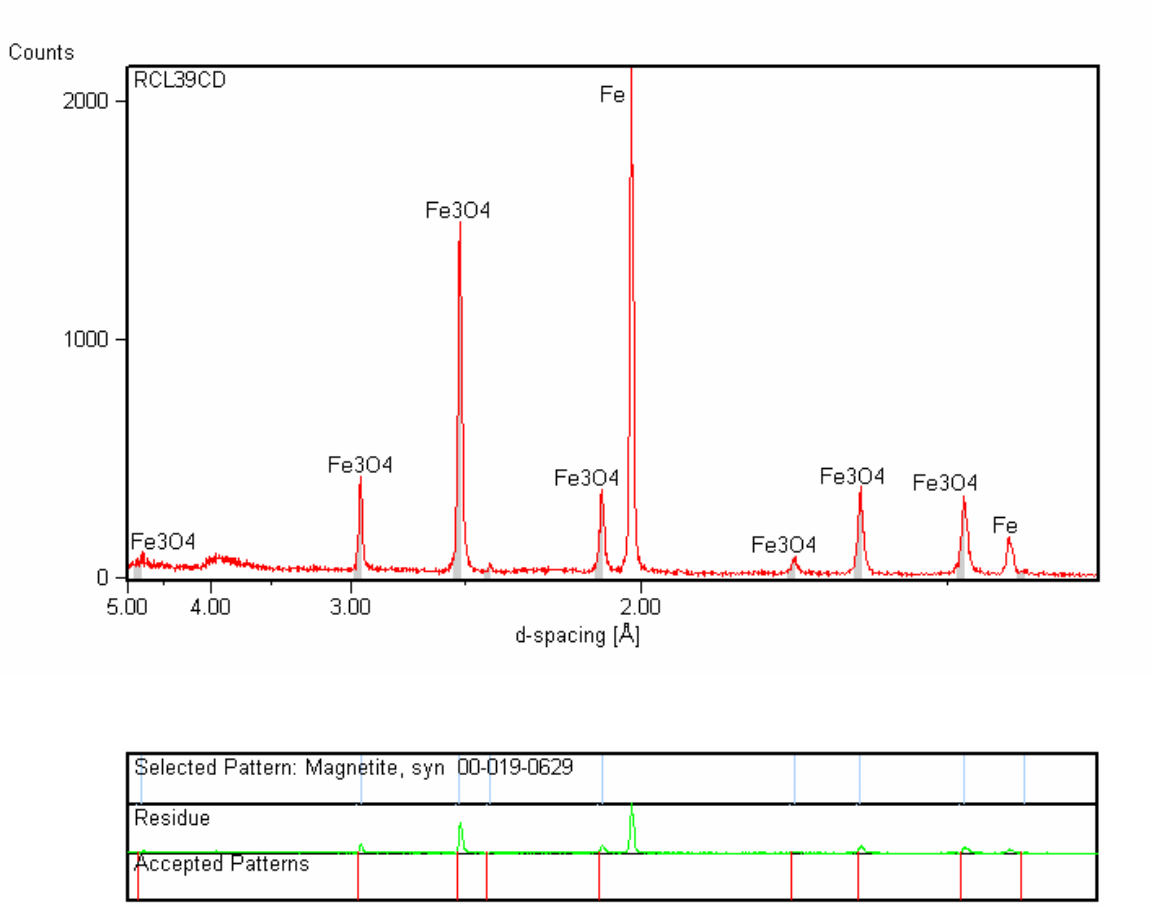

Figure 7.4. (b) X-ray diffraction pattern of the bottom surface film for SA-210 carbon steel (on contact with metal fixture) exposed to pure water with dissolved oxygen ~3ppm at 300°C for 30 hours

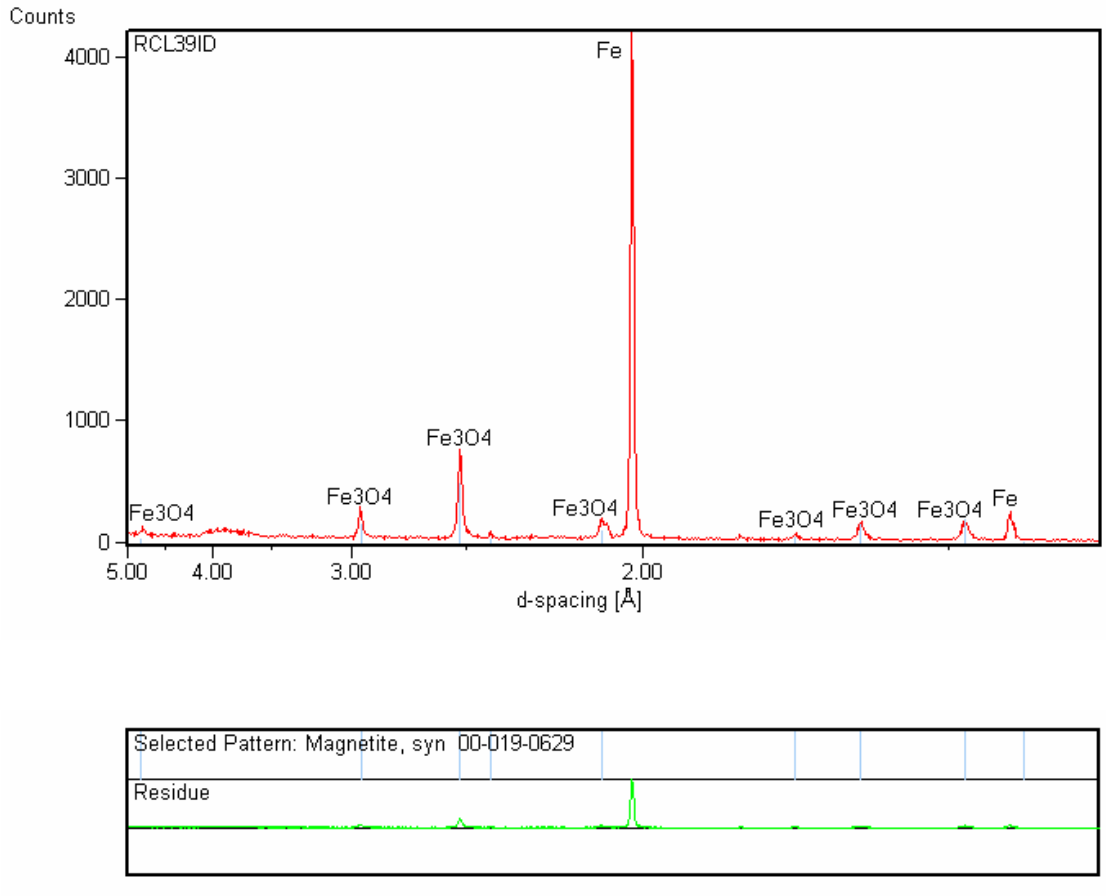

Figure 7.4. (c) X-ray diffraction pattern of the bottom surface film for SA-210 carbon steel (isolated in ceramic holder) exposed to pure water with dissolved oxygen ~3ppm at 300^{o}C for 30 hours

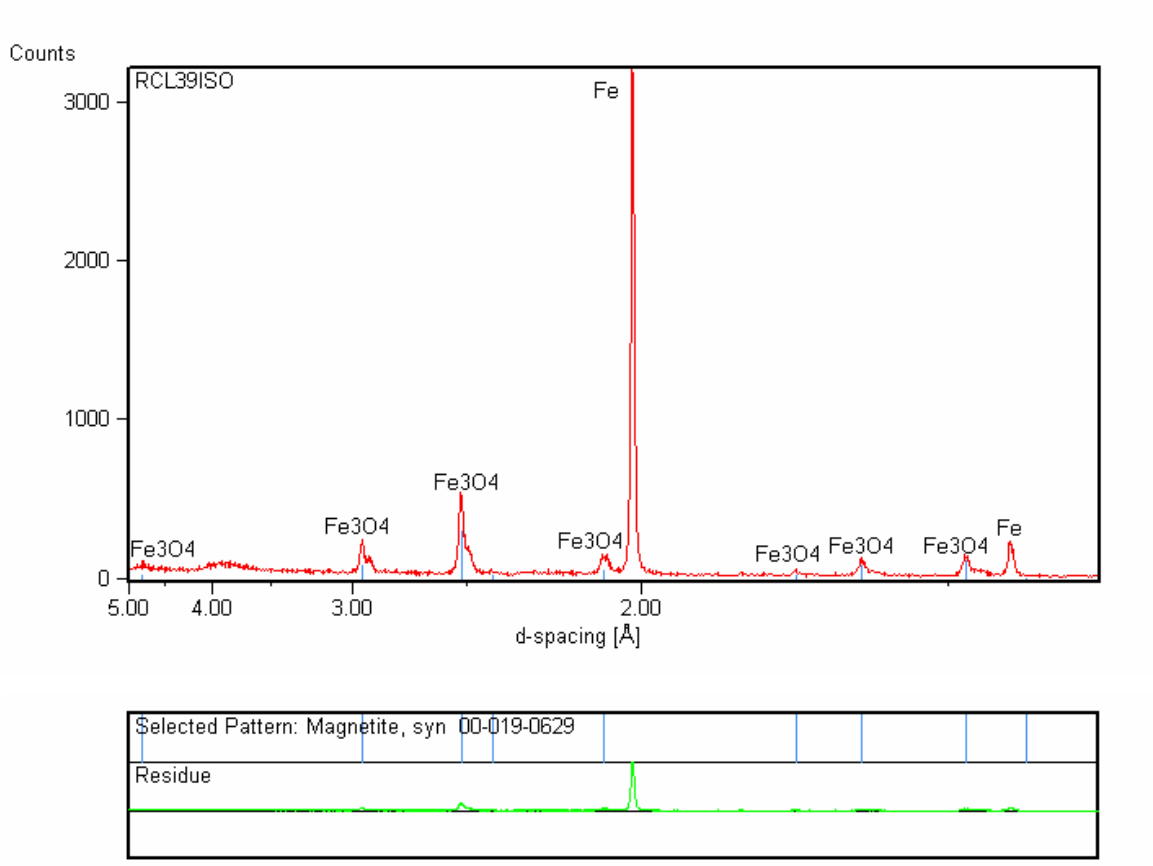

Figure 7.4. (d) X-ray diffraction pattern of the top surface film for SA-210 carbon steel (isolated in ceramic holder) exposed to pure water with dissolved oxygen ~3ppm at 300°C for 30 hours

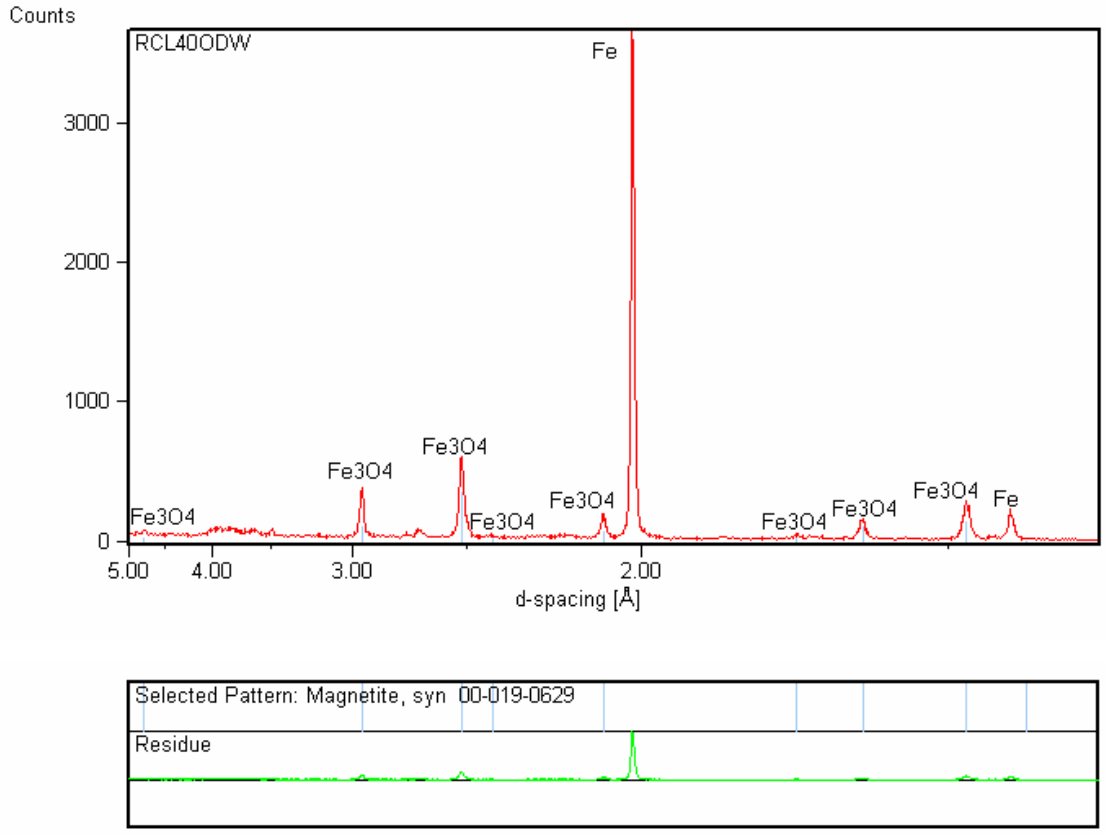

Figure 7.4. (e) X-ray diffraction pattern of the bottom surface film for SA-210 carbon steel (on contact with metal fixture) exposed to pure water with dissolved oxygen ~5ppb at 300°C for 50 hours

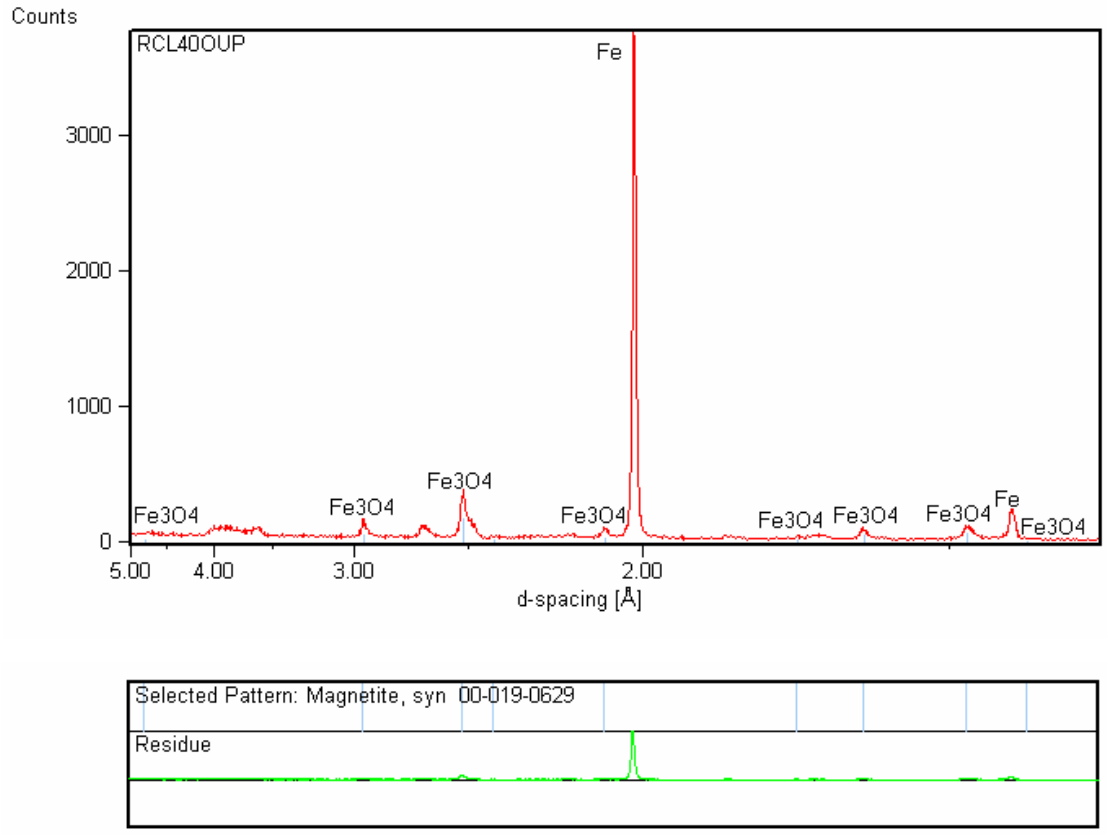

Figure 7.4. (f) X-ray diffraction pattern of the top surface film for SA-210 carbon steel (on contact with metal fixture) exposed to pure water with dissolved oxygen ~5ppb at 300°C for 50 hours

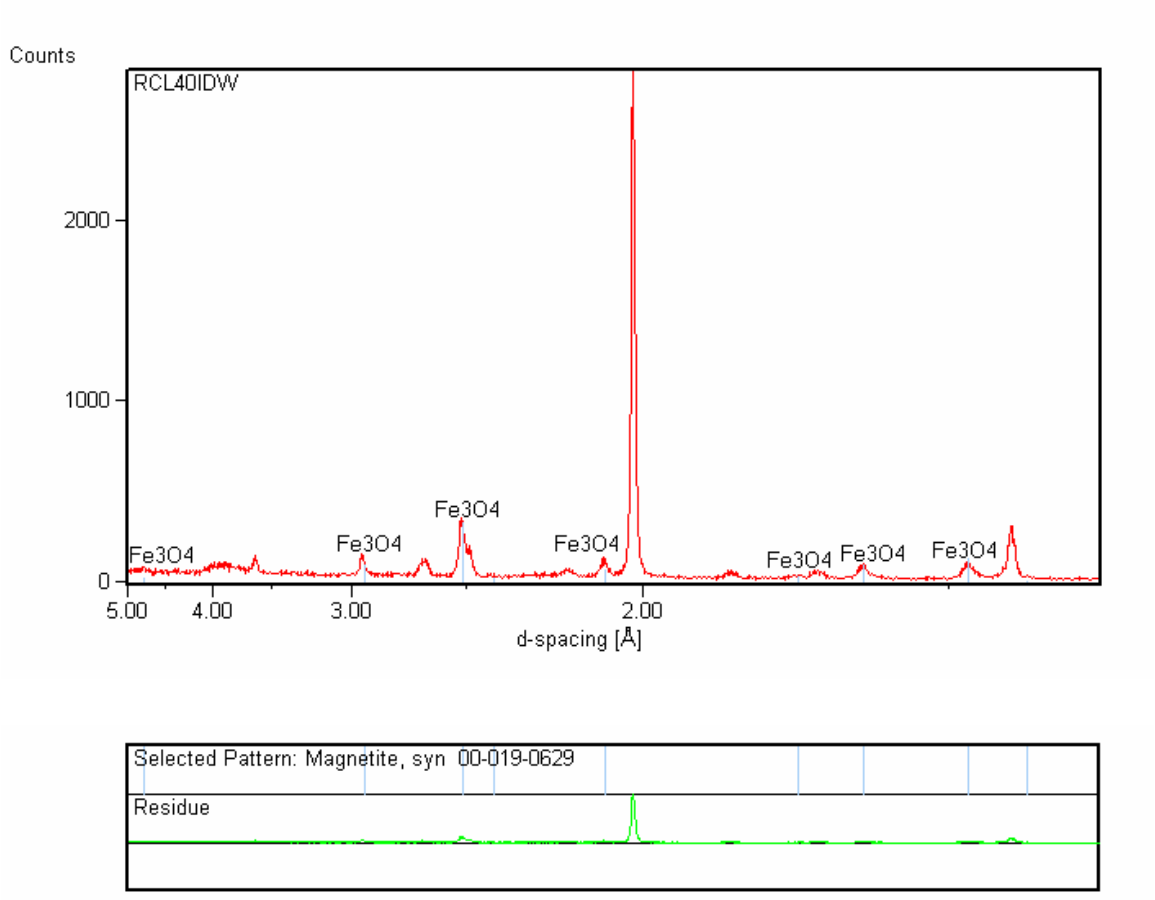

Figure 7.4. (g) X-ray diffraction pattern of the bottom surface film for SA-210 carbon steel (isolated in ceramic holder from metal fixture) exposed to pure water with dissolved oxygen ~5ppb at 300^{o}C for 50 hours

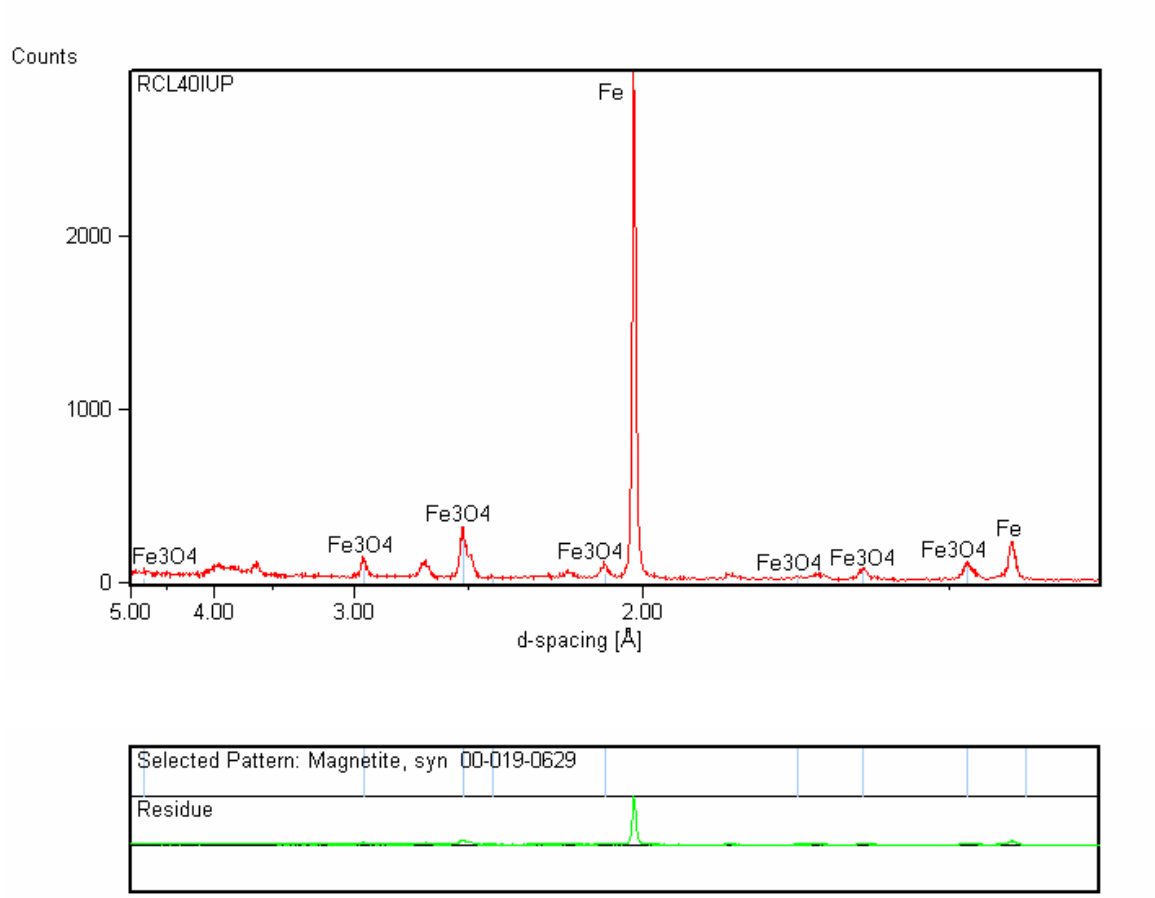

Figure 7.4. (h) X-ray diffraction pattern of the top surface film for SA-210 carbon steel (isolated in ceramic holder from metal fixture) exposed to pure water with dissolved oxygen ~5ppb at 300°C for 50 hours

7.2.2. Effect of Anode/Cathode Area Ratio on Formation of Surface Film

Initial observations from the SEM study have shown that the un-strained samples exposed to the environment where SAC was observed on the tensile samples, had a single layer of magnetite on the surface [45]. As mentioned earlier and suggested by Odziemkowski et al. [45] and Bloom and Newport [39], the morphology of a magnetite film is dependent on relative area ratios of anode to cathode. Our previous work on carbon steel in boiler water [15, 16] at 320^{o}C and published work on carbon steel in concentrated caustic solutions [18, 40-43] have shown that if the carbon steel sample has no contact with a suitable cathodic surface, or only comparable cathode to anode areas, then a compact, non-porous film is formed in high temperature water environment, as shown by AFM micrograph in Figure 7.5.(a). This film may provide greater protectiveness and is also significantly thinner. However, if the carbon steel samples were attached to a large cathode (area ratio 1:200) and exposed to pure water at 320^{o}C, a rough and porous magnetite film tend to form on the carbon steel sample, with tetrahedral crystals on the surface, as shown in Figure 7.5. (b). The film growth rates may be higher for this type of porous oxide film [30, 32].

Figure 7.6 shows the temperature dependence of crack velocity in carbon steel samples, which follows an arrhenius relationship ($CV=C\ e^{-E/RT}$, where CV stands for crack velocity, R stands for gas constant, C is a constant, T stands for temperature, E stands for thermal activation energy), from which the thermal activation energy was calculated as 17.4 KJ/Mol. Robertson [24] reviewed literature to propose a mechanism

of high temperature aqueous corrosion of carbon steels in deoxygenated water. He reported a temperature dependence of corrosion rates. The activation energy of the magnetite film growth by the solution-pores model was found to be between 15 KJ/mol and 20 KJ/mol and Robertson [24] attributed this to the diffusion coefficients of the aqueous ions. Whereas in presence of steam, with or without oxygen or carbon dioxide, at high temperature ($T > 350^{o}C$), the activation energy was reported to be: 142 KJ/Mol for 10^{-6} bar O_2; 116 KJ/Mol for CO_2; 120 KJ/Mol for the steam [24]. In the case of steam, the rate-controlling step was attributed to be diffusion of iron ions through the oxide (magnetite) grain boundaries. Activation energy for the crack growth in our study was found to be 17.4KJ/mol from Figure 7.4, which suggests that the SAC crack growth mechanism may involve diffusion of ions through solution for the formation of magnetite film at the crack-tip and act as a rate controlling step in this environment sensitive fracture mechanism. According to Potter and Mann [30, 32] and Castle and Mann [40], the aqueous corrosion limited by solution transport process will most likely produce a single porous layer of magnetite film on the surface of carbon steel. Potter and Mann [30, 32] also reported that under certain conditions the protective oxide film may consist an inner layer of fine-grained oxide and an outer layer of loosely packed, larger grains which appear to have precipitated from solution. The boundary between the layers is found to be at the original metal surface, which indicates that the inner layer grows at the metal-oxide interface, while the outer layer grows at the oxide-solution interface. Normally the inner layer retains more protective components [24], and the outer layer may not be visible as sometimes 80% or more of this material can be deposited elsewhere in the system other than the surface of sample, which is probably what happens in our case during this study.

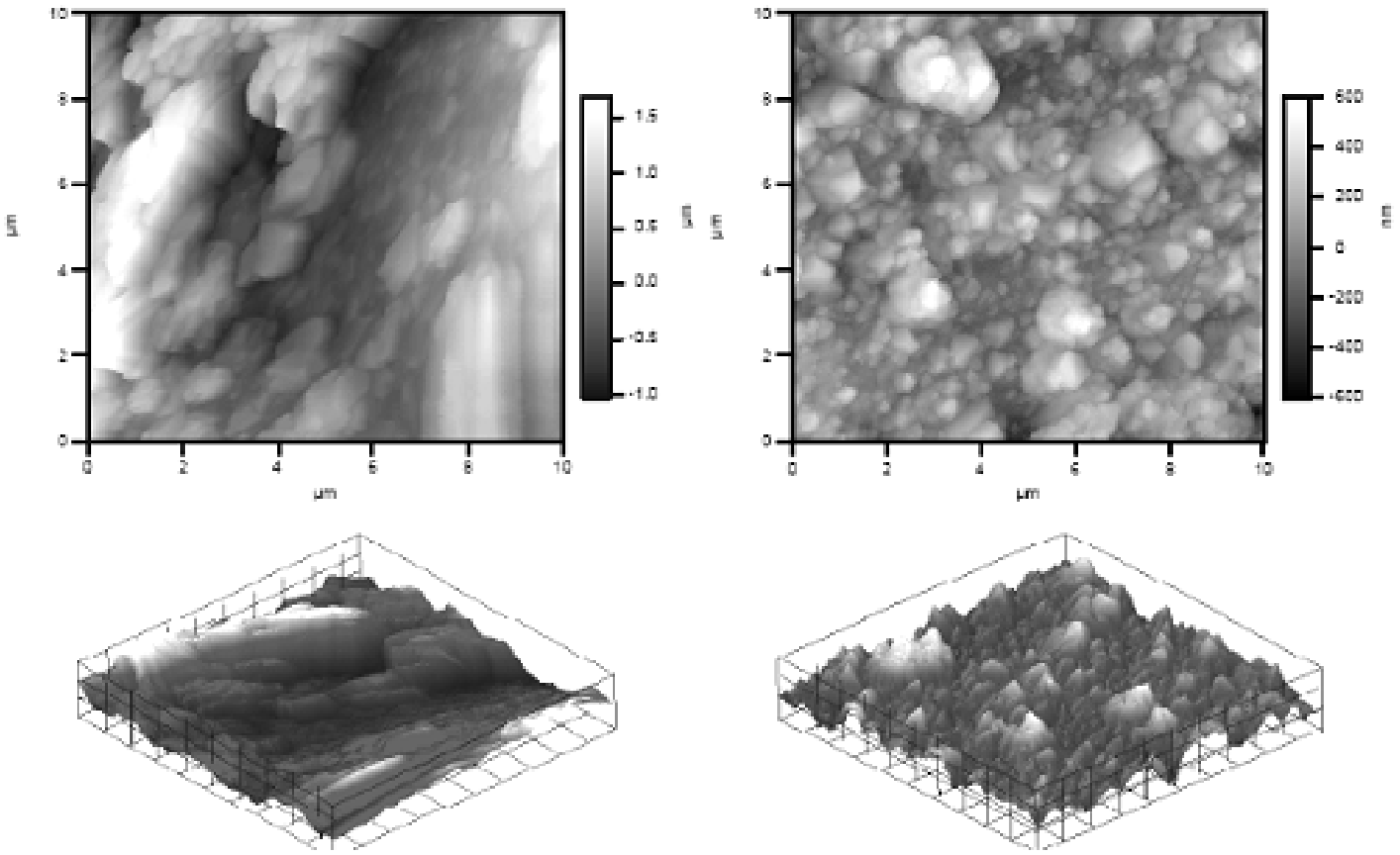

(a) **(b)**

Figure 7.5. (a) Magnetite film on the surface of an electrically isolated carbon steel coupon (Anode/Cathode area ratio = 1) (b) Surface of a test coupon in-contact with a large cathode (Anode/Cathode area ratio =1/200) showing tetrahedral crystals

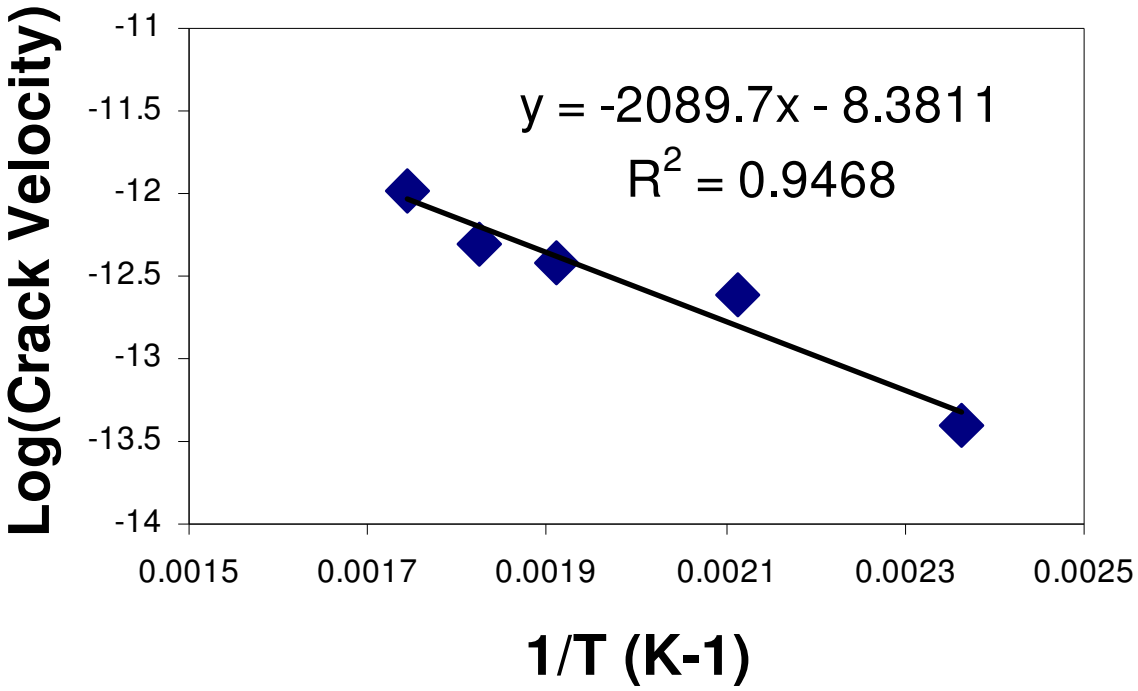

Figure 7. 6. The temperature dependence of crack velocity for carbon steel SA-210

7.2.3. Surface Film under Simulated Boiler Shutdown Conditions

The AFM micrograph and derived Arrhenius relationship in section 7.2.2 only provide enough proof that the magnetite film formed on SA-210 carbon steel can be characterized as a single porous layer, but no depth or thickness information can be obtained for the resulted surface film. As was found from failure analysis of recovery boiler tubes, the majority of the inner surface of recovery boiler tube was covered by thin, protective magnetite film. However, oxide films with thickness of almost 500 μm were observed on the waterside tube surface directly adjacent to an external attachment weld. Ratio of anode/cathode areas in this type of tests is 1, but porous oxide film can still form under this conditions. The possible cause of this phenomenon is the high stress concentration effect on the inner surface of the boiler tubes in the vicinity of attachment welds. The stress concentration on the tube surface adjacent to external attachment weld during boiler shutdown or turn-on breaks the first formed protective film and creates naked metal surface which acts as a small anode, and the rest of the protective film acts as a large cathode. Therefore porous and non-protective oxide film forms due to the later-formed large cathode/anode area effect in the boiler. To verify if the stress concentration due to boiler shutdown or thermal strain during boiler operation will influence the formation of surface film, three special-designed tests were conducted in simulated boiler conditions.

An unstressed tensile sample was exposed to simulated boiler water condition (autoclave temperature ~ 300^{o}C, DO ~ 3ppm) in autoclave for 10 hours. A thin, compact, and seems protective magnetite film was observed on the tensile sample under optical microscope, as shown in Figure 7.7. It indicates that even under corrosion environment porous, non-protective film would not form if there is no significant effect of anode/cathode area ratio.

Another tensile sample was also exposed to same corrosive condition (autoclave temperature ~ 300^{o}C, DO ~ 3ppm) in autoclave for 10 hours, but with constant stretching at a strain rate of $2x10^{-6}$ S^{-1}, a thick, porous, and non-protective film with multi-SAC initiations was observed on the sample, as shown in Figure 7.8. The simulated result shows similar features to actual SAC initiations and porous, non-protective oxide film which were seen from real boiler tubes in service conditions, as shown in Figure 7.9. It confirms that the formation of surface film depends on not only water chemistry variables (temperature, DO level, etc.), but also anode/cathode area ratio effect created prior to or during surface film formation on material surface. It also indicates that stress concentration may help localized corrosion thus enable the oxide film to grow further. With application of stress, the oxide film cracks perpendicularly to the stress direction as well as to the metal/oxide interface.

The third test was designed based on the second test conditions. If the constant stretching in the second test was continued till the tensile sample was fractured (after ~35 hours), multiple cracks initiated on the smooth tensile samples were observed from the

external surface of sample, as shown in Figure 7.10. Surface pits were also found to form on this sample and the SAC crack initiation sites were mainly associated with those pits. Similar observations were reported by Congleton et al. [85] in their work on stress corrosion of iron-base alloys in high temperature water environments. Bloom and Newport [39] also reported that porous, non-protective film may eventually form pits on the surface due to film rupture/damage. Marsh [43] indeed showed that the morphology of oxide developed on carbon steel samples isolated from other surfaces appears as a thin compact film similar to the one reported by Bloom and Newport [39], whereas the film morphology in pits on the same sample was similar to the ones reported by Potter and Mann [30, 32].

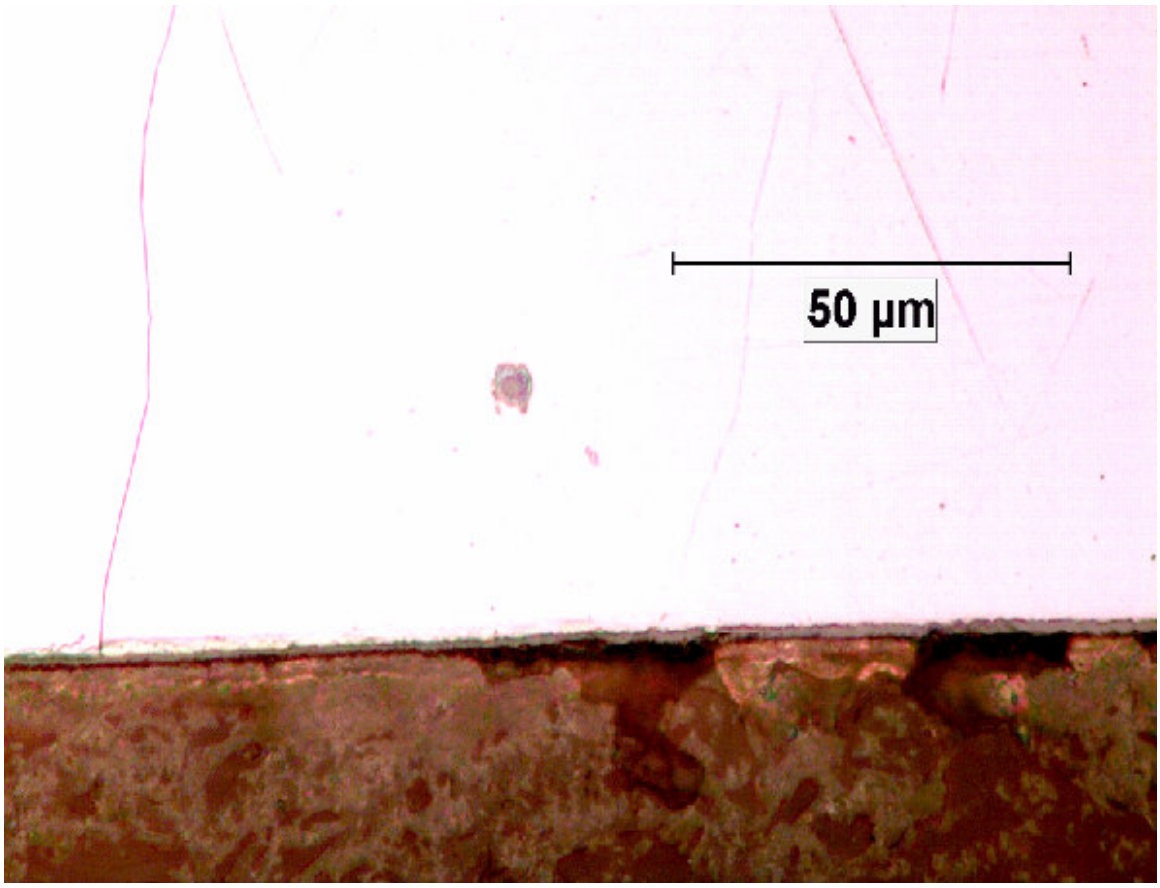

Figure 7. 7. Protective oxide film formed on unstressed tensile sample exposed to simulated boiler water (DO~3ppm, 300^{o}C) for 30 hours

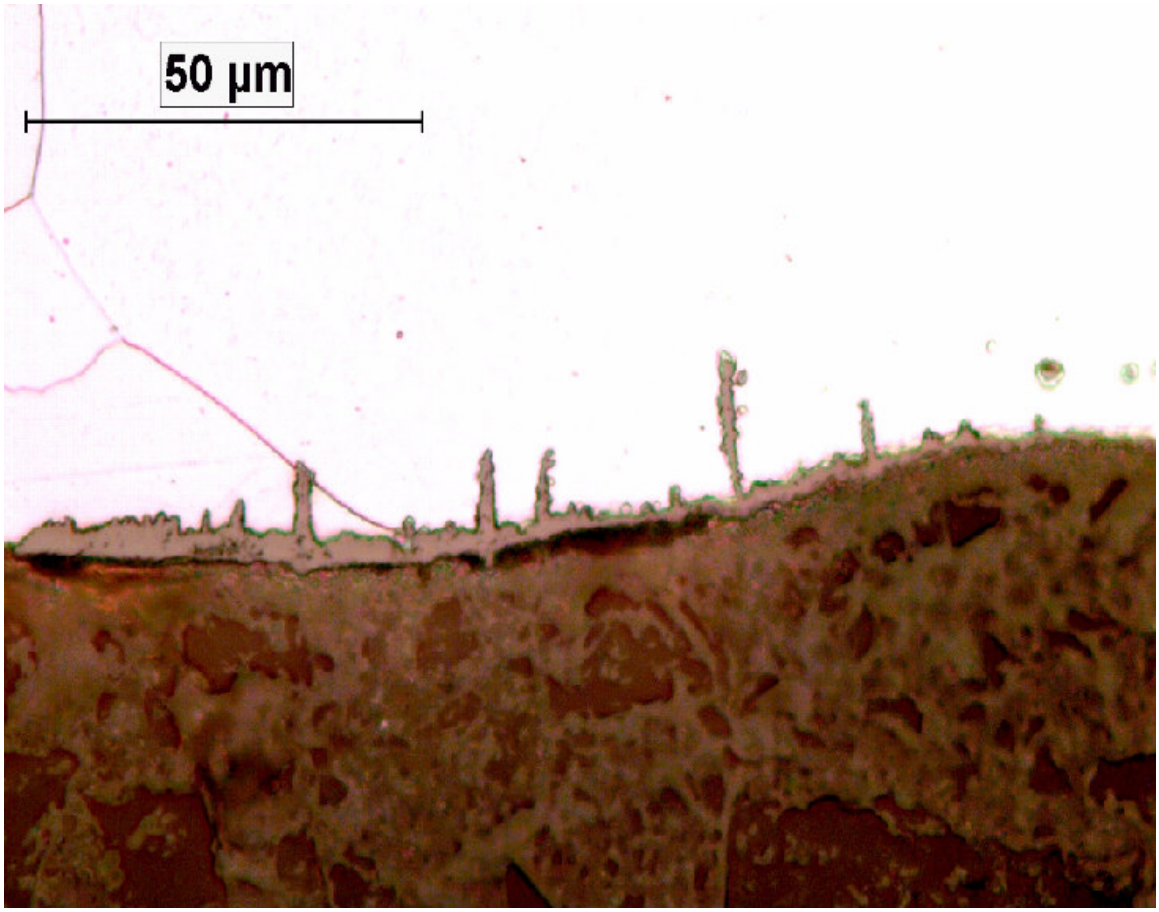

Figure 7. 8. SAC initiations and porous, non-protective oxide film formed on stressed tensile sample at a constant strain rate of $2x10^{-6}$ s^{-1} under simulated boiler water (DO~3ppm, 300^{o}C) for 30 hours

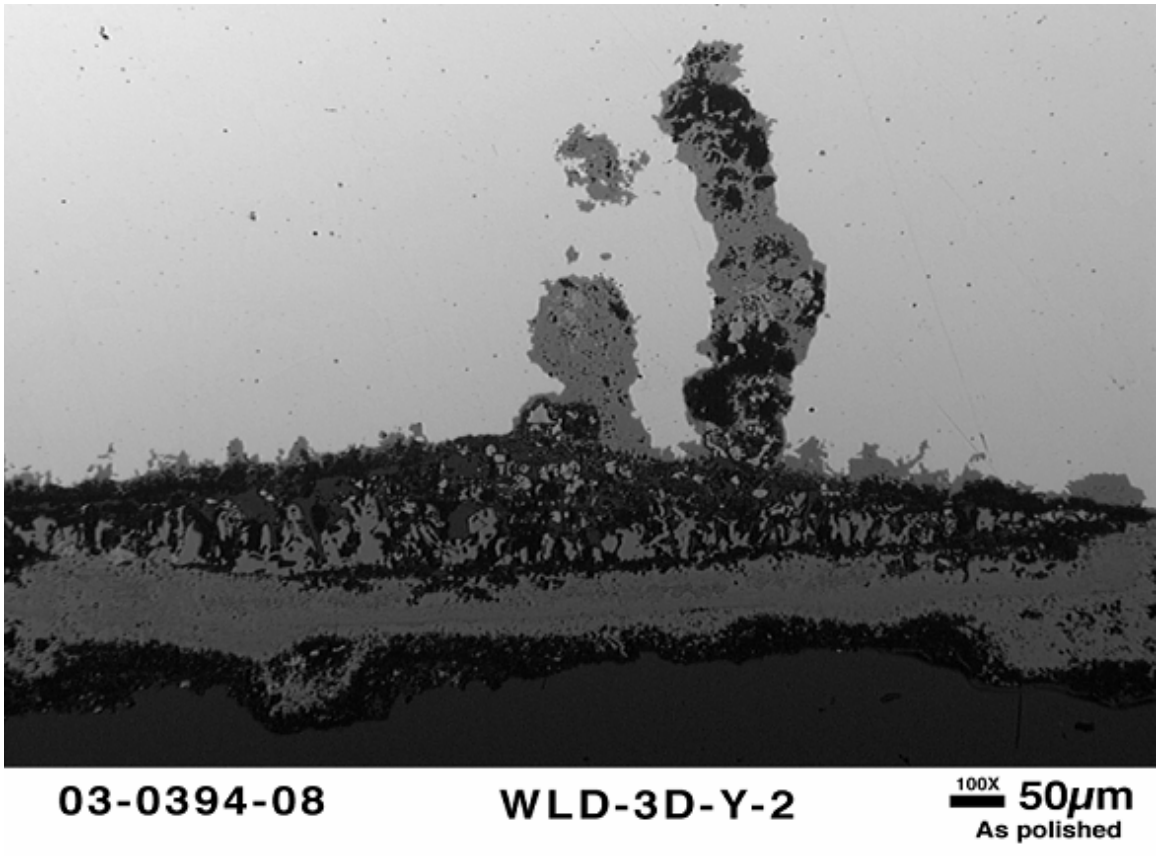

Figure 7. 9. SAC initiations and porous, non-protective oxide film formed on inner surface of boiler tube under service conditions

Figure 7. 10. Surface pits and associated SAC cracks on a SSRT sample tested at a constant strain rate of $2x10^{-6}$ s^{-1} in 3ppm oxygenated water at 300°C.

7.3. Mechanisms of SAC cracking

7.3.1. Mechanism of SAC Crack Initiation

The SAC initiation is not a product of any single variable. Temperature, dissolved oxygen (DO), film formation, anode/cathode area ratio, and stress localization are all required for SAC to initiate. They are correlated to each other in a way likely to be: SAC depends on stability of surface film; film formation depends on the level of DO, temperature of environment, and anode/cathode area ratio; temperature change during boiler operation will cause thermal stress, and stress and anode/cathode ratio help protective film grow into non-protective film; non-protective film plus stress localization during boiler shutdown lead to SAC initiation. It is also likely that those variables will work together to propagate SAC initiations further. Based on a systematic understanding of those variables the mechanisms of SAC crack initiation and propagation can be proposed, and SAC cracks can be simulated in lab by accelerating those variables accordingly.

Cracks formed in slow strain rate tests were transgranular with sharp crack tips. These stress corrosion cracks had more resemblance with the corrosion fatigue cracks typically found in utility boiler tubes. However, SAC cracks in industrial boilers are bulbous in morphology, with number of bulbs in some cases corresponding to the number

of shutdowns or chemical cleaning cycles that a tube had gone through. To simulate the effect of boiler shutdown conditions in on cracking, interrupted slow strain rate tests (ISSRT) were carried out. During boiler shutdown, water temperature is lowered to near room temperature and therefore stresses due to pressure and temperature are also lowered. However due to its design, tubes may still have some residual stress. If boiler operators are not careful, oxygen may enter the system during boiler shutdown periods. This cycle was simulated in laboratory by interrupting tests for given time period where the temperature is lowered and the stresses were reduced to some lower values. The loading curve of ISSRT test is shown in Figure 7.12. The boiler working conditions and a constant strain rate of $2x10^{-6}$ s^{-1} were applied to simulate boiler startup and normal operation stages (i.e., 0-15 hrs, 30-45 hrs; to simulate boiler shutdown the stress was lowered to 30% yield stress and oxygen was introduced into autoclave, (i.e., 15-30 hrs, 45-60 hrs). Tests were interrupted at different stages of these tests and the tensile samples were sectioned to check if crack morphology was different from the sharp cracks developed in normal slow strain rate or corrosion fatigue tests.

Based on the SAC crack initiation and growth results from slow strain rate tests, ISSRT, and magnetite film growth tests, a mechanism of SAC on carbon steel tubes and other water-touched surfaces in boilers is proposed. Various steps for this mechanism are shown schematically in Figure 7.11. On a new or thoroughly acid cleaned carbon steel boiler tube a compact and protective magnetite film may develop on the entire carbon steel surface under boiler operating conditions. During start up or shut down, the magnetite film can crack near weld attachments due to localized strain leading to local bare metal surface. Under these conditions, small areas of bare metal exposed due to the

magnetite film damage will act as anode whereas the surrounding tube surface with magnetite film will act as a large cathode. Under these conditions a non-protective porous magnetite with tetrahedral surface crystals will be formed in these areas, as shown in Figure 7.5 and Figure 7.8. The porous film may further lead to high local corrosion rates and easier corrosion fatigue or SAC crack initiation in these areas during startup or shut down. SAC cracks may propagate due to magnetite film (Fe_3O_4) fracture rather than by fracturing of the tube metal itself. Every time the film is damaged locally, the process can repeat itself when oxygenate boiler water comes in contact with the bare carbon steel surface to corrode it further and form new oxide film. During boiler shutdown if oxygen enters the boiler water system, this may produce typical SAC morphology for cracks. In the presence of oxygen the crack tips corrode preferentially and may lead to the formation of bulbous crack morphology. To verify this mechanism, tests were terminated at different stages to see crack initiation and propagation, as shown by different micrographs in Figure 7.12.

Results show that small pits initiate during first loading. Cracks propagate during second loading mostly from the initial pits. Crack tips were attacked in cases where oxygen was introduced in autoclave during shutdown. In cases where cracks were initiated but oxygen was not introduced during shutdown, cracks did not show any sign of crack blunting. The crack shapes of simulated SAC during different stages are exactly the same as we derived in our proposed SAC mechanism as shown in Figure 7.11 and Figure 7.12.

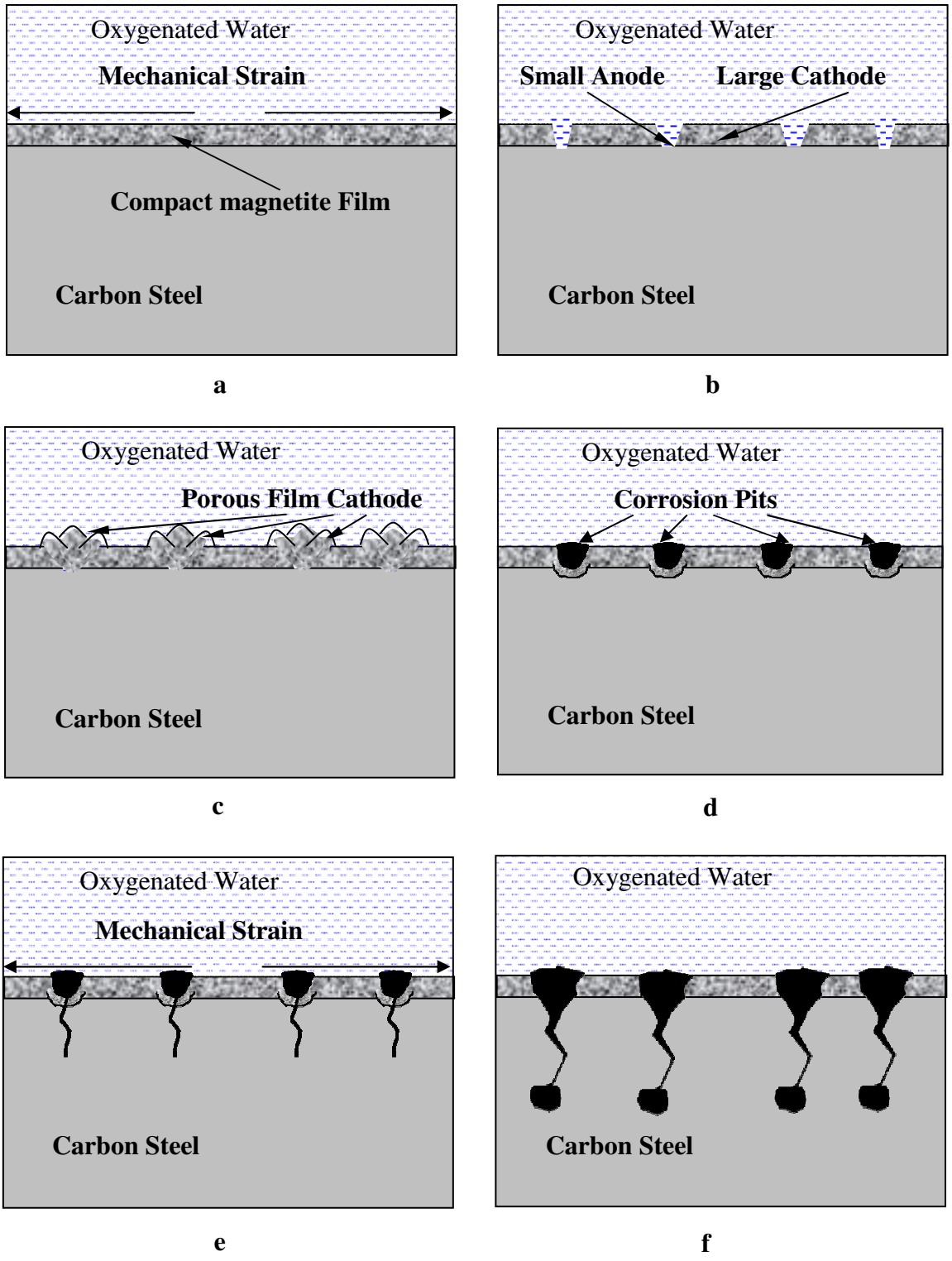

Figure 7. 11. (a-f) Schematic showing various steps in initiation and propagation of SAC cracks

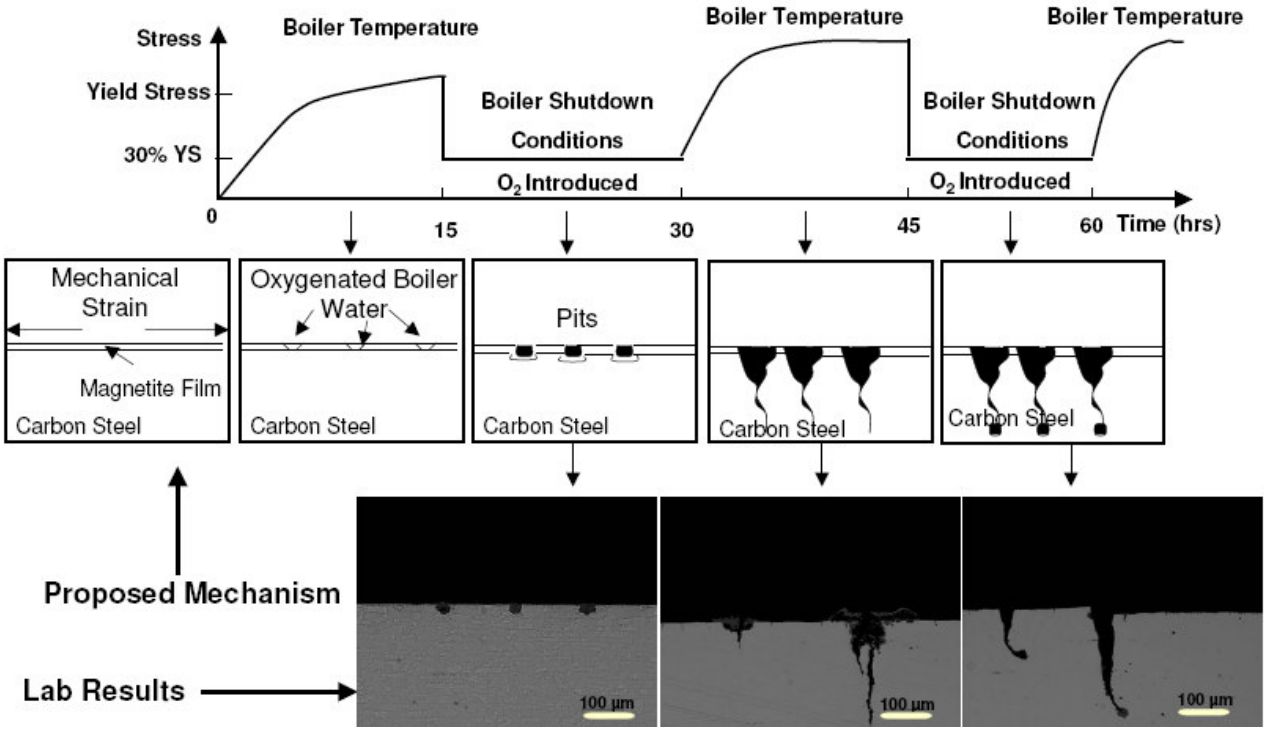

Figure 7. 12. Interrupted slow strain rate tests (ISSRT) to simulate boiler start up and shutdown conditions. Micrographs in this figure show crack morphology at certain time during these tests.

7.3.2. Mechanism of SAC Crack Propagation

Further interrupted tests were carried out to study the effect of boiler shutdown conditions on crack growth and morphology. Representative results are shown in Figure 7.13. Results indicate that relatively short interruptions (~ 15 hours) in SSRT tests, where the temperature was lowered to 80^{o}C and water was aerated for 10 minutes with oxygen, flowing at 1.0 L/min, produced active corrosion around the sharp crack tips. Numbers of bulbous growths correspond to number of interruptions in each test. Sharp stress corrosion cracks continued to propagate from the blunt crack tip on subsequent loading of test samples under simulated boiler conditions. Results from these tests show that the sharp corrosion fatigue cracks and the stress assisted corrosion (SAC) cracks with bulbous features may have the same growth mechanism but different morphology due to different water chemistry during boiler operation and shutdown. If interruption time was taken away from Figure 7.13.(b), the total net loading time to fracture samples are about the same (42.5 hrs and 42.6 hrs) as the net loading time shown in Figure 7.13.(a), which indicates that during interruptions or boiler shutdown crack tips may corrode but the cracks do not grow in length to any measurable extent. From the comparison of Figure 7.13.(b) and Figure 7.13.(c), we can also see that bulbous SAC cracks due to cyclic loading experienced by boiler tubes under service conditions can be successfully simulated in laboratory conditions.

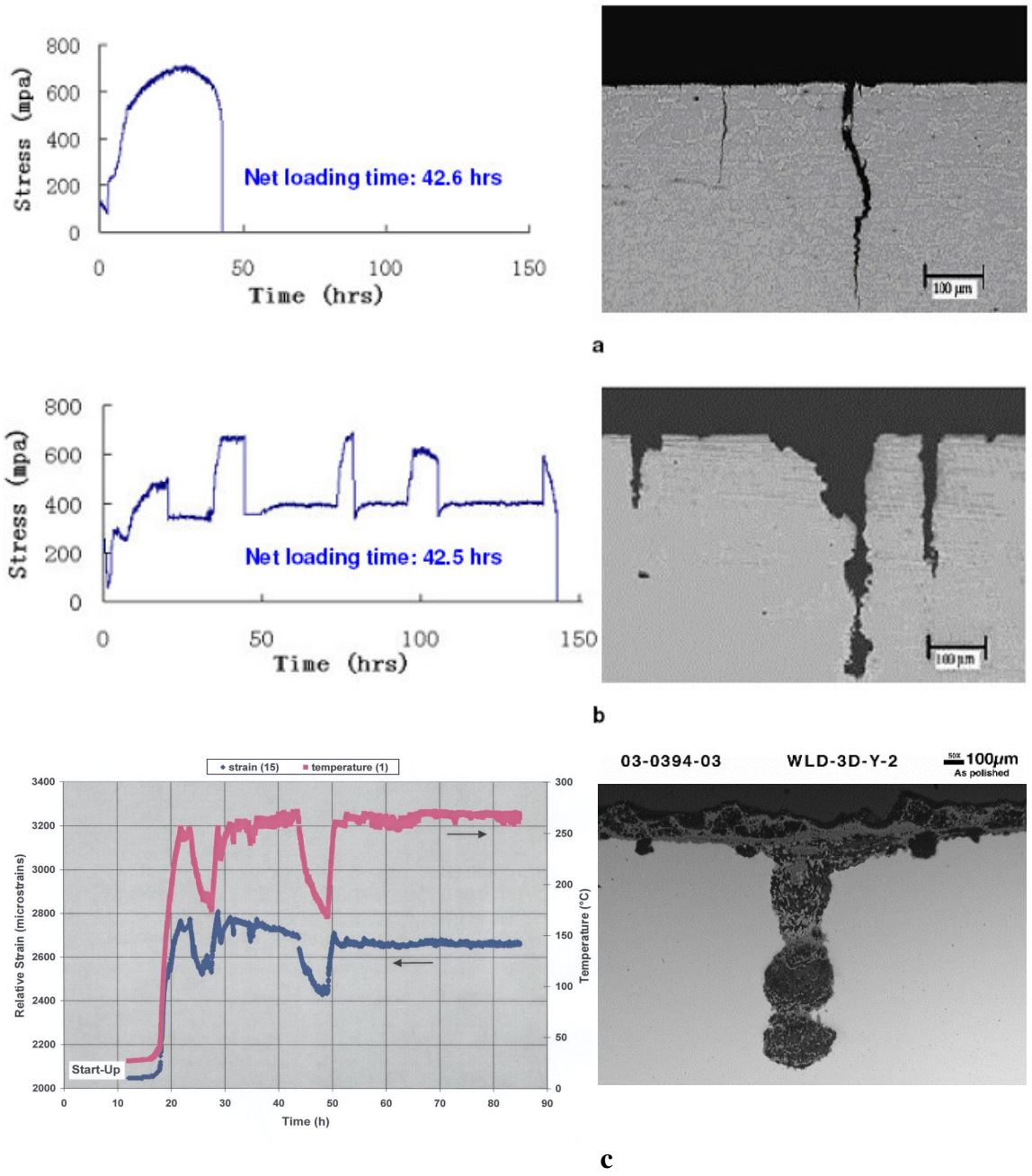

Figure 7. 13. Cracks from SSRT tests done in pure water at 300°C (a) Sharp crack from test without interruption. (b) Bulbous cracks from ISSRT test on SA-210 carbon steel under simulated boiler operation and shutdown conditions (c) Cyclic loading and bulbous SAC cracks on a water-wall tube removed from boiler

In order to check if the SAC crack growth can be arrested by reducing the dissolved oxygen to 5 ppb, ISSRT tests were conducted in lab conditions. A constant strain rate of $2x10^{-6}$ s^{-1} was applied on the tensile sample in oxygenate boiler water for 20 hours to initiate SAC cracks on the surface, followed by a interruption period where oxygen was introduced into test solution at 0.5 L/min for 30 hours to blunt the crack tips, then the dissolved oxygen level was lowered to 5ppb level and the sample was reloaded under constant extension rate. The resulting crack morphology of the fractured sample was shown in Figure 7.14. There was no sign of sharp crack growth initiating from the blunt crack tips formed during interruption period with dissolved oxygen in the water. These results indicated that the SAC crack growth can be arrested by controlling water chemistry to a low dissolved oxygen level. However, this effect may only be possible until the crack length is small enough where the stress intensity ahead of crack tip under full boiler loading is lower than the K_{IC} or K_{ISCC} (fracture toughness) of the material at operating temperatures in boiler water environment.

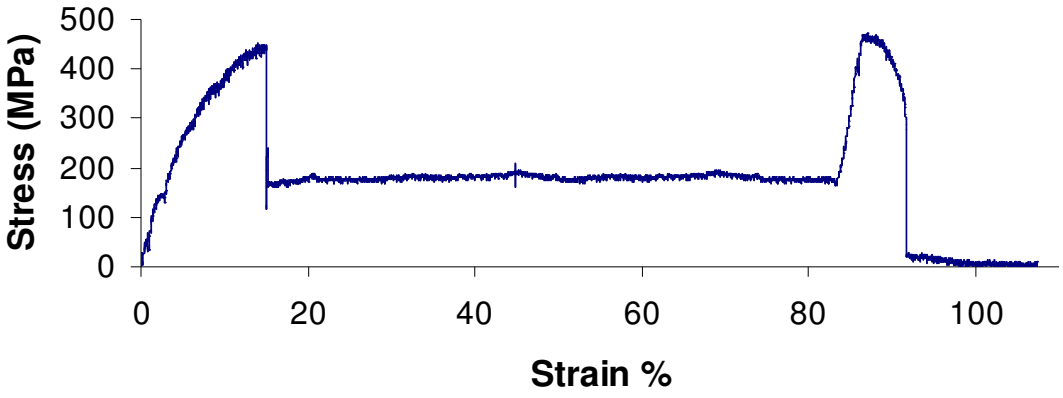

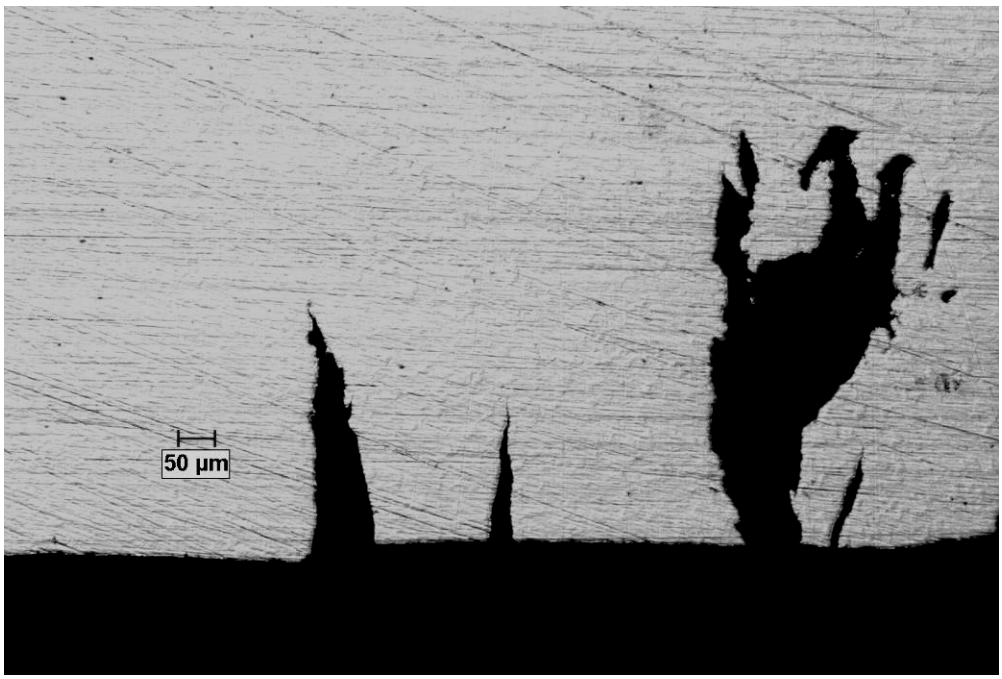

Figure 7. 14. Bulbous cracks from SSRT test at a constant strain rate of $2x10^{-6}$ s^{-1} with 1 interruption (introducing oxygen into simulated boiler water at a flow rate of 0.5 liter/min for 30 hrs + oxygen removal for 40 hrs)

7.4. Summery of SAC Mechanism

Magnetite film stability is the most important requirement for corrosion resistance of carbon steel in high temperature water. In normal boiler conditions, protection by magnetite film formation is achieved and this is verified by the good performance of most boiler systems and boiler tubes. When magnetite film is disrupted, either mechanically or chemically and in presence of excess oxygen, anodic activity at the disruption sites leads to accelerated loss of the carbon steel at these local areas. However, the magnetite film on the tube surface may not grow stress-free under constant temperature and pressure conditions.

With application of stress, the oxide film cracks perpendicularly to the stress direction as well as to the metal/oxide interface. During boiler operation, the tubes are subjected to tensile stresses, which may vary depending upon the residual and applied stresses in local areas. Therefore during shutdown the oxide film on metal surface will experience tensile stresses depending upon the magnitude of stress change in the base metal. Similarly, during startup, reverse stress cycle may be experienced by the base metal as well as oxide film. Westwood and Lee [91] have suggested that the operational stresses may be insufficient to cause damage in the magnetite film during normal boiler operation. However, failures are generally associated with external attachment welds, which may produce localized stresses sufficient to disrupt the magnetite film on the tube surface. In areas of high stresses like attachment welds, oxide film may get damaged

frequently by the cyclic loading experienced during boiler operation or during shutdown and new oxide will be developed locally. This may cause buildup of oxide in these areas. There is critical strain required for the magnetite film to fracture. However, the value of critical strain will depend upon the film properties which in-turn depends upon the environmental parameters, cyclic stress and temperature. When magnetite film is disrupted, either mechanically or chemically and in presence of excess oxygen, anodic activity at the disruption sites leads to accelerated loss of the carbon steel at these local areas.

Initial results from the recirculation-loop autoclave show that industrial boiler conditions can be simulated successfully in laboratory. It is believed that the mechanism of SAC is based on the damage of passive film rupture and transient anodic dissolution at a surface initiation site or crack tip. A mild steel sample oxidized in high temperature alkaline solutions and in electrical contact with a suitable area of magnetite (or noble metal like gold) in the same solution will, in general, produce a fine-grained porous film with a wide array of surface tetrahedral crystals at the film surface. For carbon steel in boiler water environments, relative anode/cathode area ratios have significant effect on the magnetite film morphology. Small ratios tend to produce a compact, protective film whereas large cathode to anode area ratio favors a porous non-protective film. Porous magnetite film thickness increases with time in boilers and may typically reach 10-15 μm. This is almost 10^4 times thicker than a typical "passive" film on iron. The porous non-protective film is weak mechanically thus may be easily ruptured by localized thermal strain during boiler shutdown, or chemical attacks (aeration with pH depression).

Through the break-down or destabilized porous magnetite film, the corrosion mediums can access the iron and keep corroding the iron and forming repassivity. Then pits formed on the surface of carbon steel. Those pits were shown to facilitate the SAC initiation in that the corrosion and damage accumulates around those pits and the stress concentration at the pit bottom results in the initiation of SAC under the thermal strain during another round of boiler operation. Tensile stress at the SAC crack tip during boiler shutdown period is required for pit formation; Pits formed on the surface of carbon steel facilitate the SAC initiation but are not necessary.

Pawel et al. [11, 45] have shown that areas of tubes with SAC cracks typically had thicker magnetite film then the other parts of the tube. This may either be due to the differences in the local heat transfer in areas with attachment welds or may be due to disruption of the protective magnetite film and subsequent local oxidation reaction producing thicker deposits. Schoch and Spahn [92] proposed a mechanism of crack initiation where the thick magnetite film may contain structural defects which may result in an initiation of fatigue failure of the thick magnetite film and thereby exposing underlying metal to further localized corrosion attack. This repeated action will locally consume metal creating oxide notch. Subsequent load cycles will cause progressive growth of this “chemico-mechanical” notch. They also proposed that in areas where the film is thinner, the damage does not initiate by film cracking but by a slip process in the substrate alloy [92]. Once the crack is effectively nucleated, stress concentration at the tip may favor rapid chemical/mechanical growth of localized failure.

Sharp corrosion fatigue cracks typically found in utility boilers and blunt SAC cracks in industrial boilers seem to have the same initiation and growth mechanism; however the shape differs due to the differences in the shutdown water chemistry control. Availability of oxygen during the shutdown may lead to crack blunting due to preferential corrosion and result into the bulbous shape of SAC cracks. Stress assisted corrosion in industrial boilers can be controlled by controlling O_2 to levels below 5 ppb and stress localization near attachment welds below the threshold values need to damage magnetite film in local areas. Other practical ways to prevent BTF may include design modification of boiler tubes to reduce stress concentration effect, quality control during manufacturing process of boiler tubes, and use of material with better mechanical properties and anti-corrosion performance. Mechanisms of SAC in boiler water environment can be identified and duplicated in a laboratory. This was done so that appropriate environmental (water treatment and chemical cleaning), operational (thermal stresses, attachment weld design/location), and material (mechanical properties, composition of base material and oxide films) options can be selected to reduce the severity and frequency of SAC. Further, identification of boilers with certain "risk factors" for SAC could lead to risk-based inspections which encompass frequency and scope for individual boilers.

CHAPTER 8: LIFE PREDICTION MODEL OF BOILERS

The present results show the effects of environmental variables (temperature, dissolved oxygen, stress amplitude, mean stress, loading frequency, strain rate, and grain size) on SAC cracking. The effect of each variable on SAC cracking respectively can be defined by a pair of mathematical equations which fit well into related experimental data. Each pair of mathematical equations shall be considered as valid not only in the range of conditions where the actual experiments were conducted, but also in conditions where the effects of other variables were taken into account based on the assumption that each variable influences SAC cracking independently. Therefore those individual quantified relationships can be correlated together mathematically to establish a comprehensive empirical model accounting for the role of all those variables. Three different conditions were defined to represent the empirical model: (1). no dramatic cyclic loading, (2). dramatic loading only, and (3). any combined conditions. Extra SSRTs were designed and conducted accordingly to validate the empirical model under these three conditions.

8.1. Effect of Temperature on SAC

From the results reputed in Chapter 4, the effect of temperature on SAC cracking can be expressed in a linear relationship (Figure 4.11),

$$V_1(x_1) = (2.65 \times 10^{-8}) \cdot x_1 - (2.52 \times 10^{-6}), \quad \textbf{Eq.8.1}$$

$$D_1(x_1) = 0.0534 \cdot x_1 - 6.362 \quad \textbf{Eq.8.2}$$

Where:

$$x_1 = Temperature, \quad in\ ^{o}C \quad ,$$
$$and$$
$$V_1(x_1) = Crack\ Velocity, in \quad mm/s,$$
$$D_1(x_1) = Crack\ Density, \quad in \quad \#of \quad cracks/mm$$

8.2. Effect of Dissolved Oxygen on SAC

From the results reputed in Chapter 4, the effect of dissolved oxygen on SAC cracking can be expressed in a power relationship (Figure 4.13 and Figure 4.14),

$$V_2(x_2) = (6.062 \times 10^{-7}) \cdot x_2^{2.135} \quad \textbf{Eq.8.3}$$

$$D_2(x_2) = 2.448 \cdot x_2^{0.9862} \quad \textbf{Eq.8.4}$$

Where:

$$x_2 = Dissolved\ Oxygen \quad (ppm),$$
$$and$$
$$V_2(x_2) = Crack\ Velocity(mm/s), \qquad D_2(x_2) = Crack\ Density(/mm)$$

8.3. Effect of Strain Rate on SAC Cracking

From the results reputed in Chapter 5, the effect of strain rate on SAC cracking can be expressed in a polynomial relationship (Figure 5.9),

$$V_3(x_3) = -1.15\times10^{6}\cdot x_3^2 + 7.49\cdot x_3 - 2.22\times10^{-6} \qquad \textbf{Eq.8.5(a)}$$

Or:

$$V_3(x_3) = -4.06\times10^{11}\cdot x_3^3 + 2.62\times10^{6}\cdot x_3^2 - 1.09\cdot x_3 + 3.46\times10^{-7}$$

(3^{rd}order polynomial fit) **Eq.8.5(b)**

And:

$$D_3(x_3) = 15.95 - 2.58\times10^{6}\cdot x_3 \qquad \textbf{Eq.8.6}$$

Where:

$$x_3 = Strain\ Rate \quad (1/s),$$
$$and$$
$$V_3(x_3) = Crack\ Velocity\,(mm/s), \qquad D_3(x_3) = Crack\ Density\,(/mm)$$

8.4. Effect of Grain Size on SAC cracking

From the results reputed in Chapter 6, the effect of strain rate on SAC cracking can be expressed in a polynomial relationship (Figure 6.9),

$$V_4(x_4) = 2.21\times10^{-7} \cdot x_4 + 1.51\times10^{-6} \quad \textbf{Eq.8.7}$$

$$D_4(x_4) = 0.0456 \cdot x_4 + 9.60 \quad \textbf{Eq.8.8}$$

Where:

$x_4 = Grain\ Size \quad (\mu m)$,

and

$V_4(x_4) = Crack\ Velocity\,(mm/s), \qquad D_4(x_4) = Crack\ Density\,(/mm)$

8.5. Effect of Cyclic Loading Conditions on SAC

8.5.1. Effect of Stress Amplitude on SAC

From the results reputed in Chapter 5, the effect of strain amplitude on SAC cracking can be expressed in a polynomial relationship (Figure 5.6),

$$V_5(x_5) = (1.58\times10^{-7}) \cdot \exp(0.0069 \cdot x_5) \quad \textbf{Eq.8.9}$$

$$D_5(x_5) = 2.38 \cdot \exp(0.00134 \cdot x_5) \quad \textbf{Eq.8.10}$$

Where:

$$x_5 = Stress\ Amplitude \quad (MPa),$$
$$and$$
$$V_5(x_5) = Crack\ Velocity(mm/s), \qquad D_5(x_5) = Crack\ Density(/mm)$$

8.5.2. Effect of Mean Stress on SAC Cracking

From the results reputed in Chapter 5, the effect of strain rate on SAC cracking can be expressed in a polynomial relationship (Figure 5.5),

$$V_6(x_6) = (5.56 \times 10^{-9}) \cdot \exp(0.0178 \cdot x_6) \qquad \textbf{Eq.8.11}$$

$$D_6(x_6) = 0.3421 \cdot \exp(0.0092 \cdot x_6) \qquad \textbf{Eq.8.12}$$

Where:

$$x_6 = Mean\ Stress \quad (Hz),$$
$$and$$
$$V_6(x_6) = Crack\ Velocity(mm/s), \qquad D_6(x_6) = Crack\ Density(/mm)$$

8.5.3. Effect of Stress Frequency on SAC Cracking

From the results reputed in Chapter 5, the effect of strain rate on SAC cracking can be expressed in a polynomial relationship (Figure 5.7),

$$V_7(x_7) = (1.52 \times 10^{-6}) \cdot \exp(-992.73 \cdot x_7) \qquad \textbf{Eq.8.13}$$

$$D_7(x_7) = 5.3944 \cdot \exp(-1217 \cdot x_7) \qquad \textbf{Eq.8.14}$$

Where:

$x_7 = Stress\ Frequency \quad (MPa)$,

and

$V_7(x_7) = Crack\ Velocity\,(mm/s), \qquad D_7(x_7) = Crack\ Density\,(/mm)$

8.6. Model of SAC Crack Growth Rate under Various Environments

Assuming that the variables like temperature, dissolved oxygen, stress amplitude, mean stress, loading frequency, strain rate, and grain size, are independent under test conditions, the crack velocity of SAC can be defined as:

$$F_V(x_1 \cdots, x_7) = C_V \cdot V_1(x_1) \cdot V_2(x_2) ..... \cdot V_7(x_7) \quad \textbf{(a)}$$

And the crack density of SAC can be defined as:

$$F_D(x_1 \cdots, x_7) = C_D \cdot D_1(x_1) \cdot D_2(x_2) ..... \cdot D_7(x_7) \quad \textbf{(b)}$$

These two equations can help to determine the related crack growth rate and propensity for crack initiation of SAC, for a given set of conditions. During a typical boiler operating operation, boiler tubes are known to experience three major types of cyclic loading:

Condition 1: No Dramatic Cyclic Loading

The first condition is defined to account for the cyclic loading due to the thermal fluctuation under normal boiler operation process. The stress amplitude is maintained as a constant of ~ 20MPa and the stress frequency is maintained as a constant of ~0.001 Hz. The mean stress is maintained as a constant of 520 MPa. Those values of stress variables

come from our lab tests driven by thermal fluctuation. The grain size of as received tensile sample is quantified as a constant of ~ 14.6 μm. Whereas, we allow changes in other environmental variables (temperature, dissolved oxygen, strain rate, and grain size).

Condition 2: Dramatic Cyclic Loading Only

The second condition is defined to account for boiler shutdown/turn-on, and process upset events which are known to bring dramatic cyclic loading to boiler tubes. Under this condition, we allow changes of all stress parameters (amplitude, mean stress, and frequency) to simulate dramatic cyclic loading conditions. Other variables are kept as constants. Test temperature is maintained as a constant of ~300^{o}C, dissolved oxygen is maintained as a constant of ~ 3ppm, strain rate is maintained as a constant of ~ $2x10^{-6}$ s^{-1}, and grain size of sample is maintained as a constant of ~ 14.6 μm.

Condition 3: Any Combined Loading Conditions

For the third condition, all seven variables identified and tested in this study will be varied.

8.6.1. Model of SAC Growth under Environmental Effects only (condition 1)

For the model considering only the small stress amplitude, higher frequency due to thermal fluctuation stress (*which was quantified as amplitude = 20 MPa, mean stress*

= *520 MPa, and frequency ~0.001 Hz*), SAC cracking can be defined as a function of temperature, dissolved oxygen, strain rate, and grain size:

$$C_V(x_1 \cdots, x_4) = C_{CV} \cdot V_1(x_1) \cdot V_2(x_2) \cdot V_3(x_3) \cdot V_4(x_4) \qquad \textbf{Eq. 8.15}$$

$$C_D(x_1 \cdots, x_4) = C_{CD} \cdot D_1(x_1) \cdot D_2(x_2) \cdot D_3(x_3) \cdot D_4(x_4) \qquad \textbf{Eq. 8.16}$$

Where:

$$x_1 = Temperature \quad (^oC)$$
$$x_2 = Dissolved \quad Oxygen \quad (ppm)$$
$$x_3 = Strain \quad Rate \quad (ppm)$$
$$x_4 = Grain \quad Size \quad (\mu m)$$
$$C_{CV} = Constant \quad (related\ to\ crack\ velocity)$$
$$C_{CD} = Constant \quad (related\ to\ crack\ density)$$

And:

$$V_1(x_1) = Crack\ Velocity \quad with\ x_1 \quad changing$$
$$V_2(x_2) = Crack\ Velocity \quad with\ x_2 \quad changing$$
$$V_3(x_3) = Crack\ Velocity \quad with\ x_3 \quad changing$$
$$V_4(x_4) = Crack\ Velocity \quad with\ x_4 \quad changing$$
$$D_1(x_1) = Crack\ Density \quad with\ x_1 \quad changing$$
$$D_2(x_2) = Crack\ Density \quad with\ x_2 \quad changing$$
$$D_3(x_3) = Crack\ Density \quad with\ x_3 \quad changing$$
$$D_4(x_4) = Crack\ Density \quad with\ x_4 \quad changing$$

And in equations 8.15 and 8.16, the only unknowns are C_{CV} and C_{CD}. Therefore the model of SAC growth under environmental effects can be determined by identifying the two coefficient constants (C_{CV} and C_{CD}), as follow:

Since:

$$C_V(x_1, x_2 = 3ppm, x_3 = 2e^{-6}1/s, x_4 = 14.6\mu m) = V_1(x_1)$$

$$\Rightarrow C_{CV} \cdot V_1(x_1) \cdot V_2(3) \cdot V_3(2e^{-6}) \cdot V_4(14.6) = V_1(x_1)$$
$$\Rightarrow C_{CV} \cdot V_2(3) \cdot V_3(2e^{-6}) \cdot V_4(14.6) = 1$$

$$C_V(x_1 = 300^oC, x_2, x_3 = 2e^{-6}1/s, x_4 = 14.6\mu m) = V_2(x_2)$$

$$\Rightarrow C_{CV} \cdot V_1(300) \cdot V_2(x_2) \cdot V_3(2e^{-6}) \cdot V_4(14.6) = V_2(x_2)$$

$$\Rightarrow C_{CV} \cdot V_1(300) \cdot V_3(2e^{-6}) \cdot V_4(14.6) = 1$$

$$C_V(x_1 = 300^oC, x_2 = 3ppm, x_3, x_4 = 14.6\mu m) = V_3(x_3)$$

$$\Rightarrow C_{CV} \cdot V_1(300) \cdot V_2(3) \cdot V_3(x_3) \cdot V_4(14.6) = V_3(x_3)$$

$$\Rightarrow C_{CV} \cdot V_1(300) \cdot V_2(3) \cdot V_4(14.6) = 1$$

$$C_V(x_1 = 300^oC, x_2 = 3ppm, x_3 = 2e^{-6}1/s, x_4) = V_4(x_4)$$

$$\Rightarrow C_{CV} \cdot V_1(300) \cdot V_2(3) \cdot V_3(2e^{-6}) \cdot V_4(x_4) = V_4(x_4)$$

$$\Rightarrow C_{CV} \cdot V_1(300) \cdot V_2(3) \cdot V_3(2e^{-6}) = 1$$

$V_1(300), V_2(3), V_3(2e^{-6}), V_4(14.6)$ can be calculated from those quantified mathematical equations respectively, and the SSRT under condition 1 provides a crack velocity of $5.39\times10^{-6}\ mm/s$, therefore we have:

$$C_V(x_1 = 300^oC, x_2 = 3\,ppm, x_3 = 2e^{-6}1/s, x_4 = 14.6\mu m) = 5.39\times10^{6}\ mm/s$$
$$\Rightarrow C_{CV}\cdot V_1(300)\cdot V_2(3)\cdot V_3(2e^{-6})\cdot V_4(14.6) = 5.39\times10^{-6}\ mm/s$$

And per our calculation from the quantified equations we know that:

$$V_1(300) = 5.43\times10^{-6}\ mm/s$$
$$V_2(3) = 6.31\times10^{-6}\ mm/s$$
$$V_3(2e^{-6}) = 5.39\times10^{-6}\ mm/s$$
$$V_4(14.6) = 4.73\times10^{-6}\ mm/s$$

$$\Rightarrow 0.99\cdot V_1(300) = 0.853\cdot V_2(3) = V_3(2e^{-6}) = 1.14\cdot V_4(14.6) = 5.39\times10^{-6}\ mm/s$$

So:

$$\frac{C_{CV}}{0.99\cdot0.85\cdot1\cdot1.14}\cdot(5.39\times10^{-6})^3 = 1 \qquad \textbf{Eq. 8.17}$$
$$\Rightarrow C_{CV} = 6.13\times10^{15}\ s^3/mm^3$$

Similarly for crack density we will have:

$$\Rightarrow C_{CD}\cdot D_2(3)\cdot D_3(2e^{-6})\cdot D_4(14.6) = 1$$

$$\Rightarrow C_{CD}\cdot D_1(300)\cdot D_3(2e^{-6})\cdot D_4(14.6) = 1$$

$$\Rightarrow C_{CD}\cdot D_1(300)\cdot D_2(3)\cdot D_4(14.6) = 1$$

$$\Rightarrow C_{CD}\cdot D_1(300)\cdot V_2(3)\cdot D_3(2e^{-6}) = 1$$

$D_1(300), D_2(3), D_3(2e^{-6}), D_4(14.6)$ can be calculated from those quantified mathematical equations respectively, and the SSRT under condition 1 provides a crack density of $10.26 \quad number/mm$, therefore we have:

$$C_D(x_1 = 300^o C, x_2, x_3 = 2e^{-6}1/s, x_4 = 14.6\mu m) = 10.26\, numner/mm$$
$$\Rightarrow C_{CD} \cdot V_1(300) \cdot V_2(3) \cdot V_3(2e^{-6}) \cdot V_4(14.6) = 10.26\, numner/mm$$

$$\Rightarrow$$

$$1.07 \cdot D_1(300) = 1.41 \cdot D_2(3) = 0.95 \cdot D_3(2e^{-6}) = D_4(14.6) = 10.26 \frac{number}{mm}$$
$$\Rightarrow C_{CD} = 1.33 \times 10^{-3}\, mm^3/number^3 \qquad \textbf{Eq.8.18}$$

Substitute equations.8.1-8.8, and equations 8.17-8.18 into equations 8.15 and Eq.8.16, then we have:

$$C_V(x_1 \cdots, x_4) = C_{CV} \cdot V_1(x_1) \cdot V_2(x_2) \cdot V_3(x_3) \cdot V_4(x_4)$$
$$= 6.13 \times 10^{15} \cdot (2.65 \times 10^{-8} \cdot x_1 - 2.52 \times 10^{-6}) \cdot (6.06 \times 10^{-7}) \cdot x_2^{2.135} \cdot$$
$$(-4.06 \times 10^{11} \cdot x_3^3 + 2.62 \times 10^6 \cdot x_3^2 - 1.09 \cdot x_3 + 3.46 \times 10^{-7}) \cdot$$
$$(2.21 \times 10^{-7} \cdot x_4 + 1.51 \times 10^{-6})$$

$$C_D(x_1, x_2, x_3, x_4) = C_{CD} \cdot D_1(x_1) \cdot D_2(x_2) \cdot D_3(x_3) \cdot D_4(x_4)$$
$$= 1.33 \times 10^{-3} \cdot (0.0534 \cdot x_1 - 6.362) \cdot 2.448 \cdot x_2^{0.9862} \cdot$$
$$(-2.58 \times 10^6 \cdot x_3 + 15.95) \cdot (0.0456 \cdot x_4 + 9.60)$$

$\Rightarrow$

$$C_V(x_1,x_2,x_3,x_4) = 3.72\times10^{9}\cdot(2.65\times10^{-8}\cdot x_1 - 2.52\times10^{-6})\cdot x_2^{2.135}\cdot (-4.06\times10^{11}\cdot x_3^3 + 2.62\times10^{6}\cdot x_3^2 - 1.09\cdot x_3 + 3.46\times10^{-7})\cdot (2.21\times10^{-7}\cdot x_4 + 1.51\times10^{-6}) \quad \textbf{Eq.8.19}$$

And

$$C_D(x_1,x_2,x_3,x_4) = C_{CD}\cdot D_1(x_1)\cdot D_2(x_2)\cdot D_3(x_3)\cdot D_4(x_4)$$
$$= 1.33\times10^{-3}\cdot(0.0534\cdot x_1 - 6.362)\cdot 2.448\cdot x_2^{0.9862}\cdot (-2.58\times10^{6}\cdot x_3 + 15.95)\cdot(0.0456\cdot x_4 + 9.60)$$

$\Rightarrow$

$$C_D(x_1,x_2,x_3,x_4) = 3.25\times10^{-3}\cdot(0.0534\cdot x_1 - 6.362)\cdot x_2^{0.9862}\cdot (-2.58\times10^{6}\cdot x_3 + 15.95)\cdot(0.0456\cdot x_4 + 9.60) \quad \textbf{Eq.8.20}$$

8.6.2. Model of SAC Cracking under Various Cyclic loading (condition 2)

For the model considering only dramatic cyclic loadings, with negligible changes of temperature, dissolved oxygen, strain rate, and grain size, the crack growth rate and crack density can be defined as below:

$$C_V^*(x_5, x_6, x_7) = C^*_{CV} \cdot V_5(x_5) \cdot V_6(x_6) \cdot V_7(x_7) \qquad \textbf{Eq. 8.21}$$

$$C_D^*(x_5, x_6, x_7) = C^*_{CD} \cdot D_5(x_5) \cdot D_6(x_6) \cdot D_7(x_7) \qquad \textbf{Eq. 8.22}$$

Where:

$$x_5 = Stress\ Amplitude \quad (MPa)$$
$$x_6 = Mean \quad Stress \quad (MPa)$$
$$x_7 = Stress \quad Frequency \quad (Hz)$$
$$C^*_{CV} = Constant \quad (related\ to\ crack\ velocity)$$
$$C^*_{CD} = Constant \quad (related\ to\ crack\ density)$$

And:

$$V_5(x_5) = Crack\ Velocity \quad with\ x_5 \quad changing$$
$$V_6(x_6) = Crack\ Velocity \quad with\ x_5 \quad changing$$
$$V_7(x_7) = Crack\ Velocity \quad with\ x_7 \quad changing$$
$$V_5(x_5) = Crack\ Density \quad with\ x_5 \quad changing$$
$$V_6(x_6) = Crack\ Density \quad with\ x_6 \quad changing$$
$$V_7(x_7) = Crack\ Density \quad with\ x_7 \quad changing$$

Since:

$$C_V^*(x_5, x_6 = 280MPa, x_7 = 0.001Hz) = V_5(x_5)$$

$$\Rightarrow C^*_{CV} \cdot V_5(x_5) \cdot V_6(280) \cdot V_7(0.001) = V_5(x_5)$$

$$\Rightarrow C^*_{CV} \cdot V_6(280) \cdot V_7(0.001) = 1$$

And:

$$C_V^*(x_5 = 300MPa, x_6, x_7 = 0.001Hz) = V_6(x_6)$$

$$\Rightarrow C^*_{CV} \cdot V_5(300) \cdot V_6(x_6) \cdot V_7(0.001) = V_6(x_6)$$

$$\Rightarrow C^*_{CV} \cdot V_5(300) \cdot V_7(0.001) = 1$$

$$C_V^*(x_5 = 300MPa, x_6 = 280MPa, x_7) = V_7(x_7)$$

$$\Rightarrow C^*_{CV} \cdot V_5(300) \cdot V_6(280) \cdot V_7(x_7) = V_7(x_7)$$

$$\Rightarrow C^*_{CV} \cdot V_5(300) \cdot V_6(280) = 1$$

There are no experimental results available for crack velocity under condition 2, so C_{CV}^* can be identified only if the following relationship is satisfied:

$$0.88 \cdot V_5(300) = 1.35 \cdot V_6(280) = 0.77 \cdot V_7(0.001) = 1.10 \times 10^{-6}\ mm/s$$

$$\Rightarrow \frac{C^*_{CV}}{0.91} \cdot 0.88 \cdot V_5(300) \cdot 1.35 \cdot V_6(x_6) \cdot 0.77 \cdot V_7(0.001) = 1.35 \cdot V_6(x_6)$$

$$\Rightarrow C^*_{CV} = \frac{0.756}{(1.1\times10^{-6})^2} = 7.56\times10^{11}\ s^2/mm^2$$

So:

$$\Rightarrow C^*_{CV} = 7.56\times10^{11}(s^2/mm^2) \qquad \textbf{Eq.8.23}$$

Similarly we will have:

$$C_D^*(x_5, x_6 = 280MPa, x_7 = 0.001Hz) = D_5(x_5)$$

$$\Rightarrow C^*_{CD} \cdot D_5(x_5) \cdot D_6(280) \cdot D_7(0.001) = D_5(x_5)$$

$$\Rightarrow C^*_{CD} \cdot D_6(280) \cdot D_7(0.001) = 1$$

$$C_D^*(x_5 = 300MPa, x_6, x_7 = 0.001Hz) = D_6(x_6)$$

$$\Rightarrow C^*_{CD} \cdot D_5(300) \cdot D_6(x_6) \cdot D_7(0.001) = D_6(x_6)$$

$$\Rightarrow C^*_{CD} \cdot D_5(300) \cdot D_7(0.001) = 1$$

$$C_D^*(x_5 = 300MPa, x_6 = 280MPa, x_7) = D_7(x_7)$$

$$\Rightarrow C^{*}_{CD} \cdot D_5(300) \cdot D_6(280) \cdot D_7(x_7) = D_7(x_7)$$

$$\Rightarrow C^{*}_{CD} \cdot D_5(300) \cdot D_6(280) = 1$$

There are no experimental results available for crack velocity under condition 2, so C_{CD}^{*} can be identified only if the following relationship is satisfied:

$$1.16 \cdot D_5(300) = 0.92 \cdot D_6(280) = 0.81 \cdot D_7(0.001) = 4.125 \frac{number}{mm}$$

$$1.16 \cdot C_{CD} \cdot 1.16 \cdot D_5(x_5) \cdot 0.92 \cdot D_6(280) \cdot 0.81 \cdot D_7(0.001) = 1.16 \cdot D_5(x_5)$$

$$\Rightarrow 1.16 \cdot C^{*}_{CD} \cdot (4.125)^2 = 1$$
$$\Rightarrow C^{*}_{CD} = 5.07 \times 10^{-2}\ mm^2 / number^2 \qquad \textbf{Eq.8.24}$$

Substituting Equations 8.9-8.14 and equations 8.23-8.24 into equations 8.21-8.22, then we have:

$$C_V^{*}(x_5, x_6, x_7) = C^{*}_{CV} \cdot V_5(x_5) \cdot V_6(x_6) \cdot V_7(x_7)$$

$$\Rightarrow$$

$$C_V^{*}(x_5, x_6, x_7) = C^{*}_{CV} \cdot 1.58 \times 10^{-7} \cdot \exp(0.0069 \cdot x_5) \cdot$$
$$5.56 \times 10^{-9} \cdot \exp(0.00178 \cdot x_6) \cdot 1.52 \times 10^{-6} \cdot \exp(-992.73 \cdot x_7)$$

$$\Rightarrow$$

$$C_V^*(x_5, x_6, x_7)$$
$$= C^*_{CV} \cdot 1.34 \times 10^{-21} \cdot \exp(0.0069 \cdot x_5 + 0.0178 \cdot x_6 - 992.73 \cdot x_7)$$

$$\Rightarrow$$

$$C_V^*(x_5, x_6, x_7) = 1.01 \times 10^{-9} \cdot \exp(0.0069 \cdot x_5 + 0.0178 \cdot x_6 - 992.73 \cdot x_7)$$

Eq.8.25

And:

$$C_D^*(x_5, x_6, x_7) = C^*_{CD} \cdot D_5(x_5) \cdot D_6(x_6) \cdot D_7(x_7)$$

Since:

$$C^*_{CD} = 5.07 \times 10^{-2}\ mm^2 / number^2$$

$$\Rightarrow$$

$$C_D^*(x_5, x_6, x_7)$$
$$= C^*_{CD} \cdot 2.38 \cdot \exp(0.00134 \cdot x_5) \cdot 0.3421 \cdot \exp(0.0092 \cdot x_6) \cdot 5.3944 \cdot$$
$$\exp(-1217 \cdot x_7)$$

$$\Rightarrow C_{CD}^*(x_5, x_6, x_7) = 0.223 \cdot \exp(0.00134 \cdot x_5 + 0.0092 \cdot x_6 - 1217 \cdot x_7)$$

Eq.8.26

8.6.3. Model of SAC Cracking under All Combined Variables (condition 3)

For the model which is capable of accounting for all affecting factors (ie., various cyclic loading conditions, temperature, dissolved oxygen, strain rate, and grain size of material), the crack growth rate and crack density can be defined as below:

$$F_V(x_1 \cdots, x_7) = C_V \cdot V_1(x_1) \cdot V_2(x_2) ..... \cdot V_7(x_7)$$

$$F_D(x_1 \cdots, x_7) = C_D \cdot D_1(x_1) \cdot D_2(x_2) ..... \cdot D_7(x_7)$$

And:

$$C_V(x_1 \cdots, x_4) = C_{CV} \cdot V_1(x_1) \cdot V_2(x_2) \cdot V_3(x_3) \cdot V_4(x_4)$$

$$C_D(x_1 \cdots, x_4) = C_{CD} \cdot D_1(x_1) \cdot D_2(x_2) \cdot D_3(x_3) \cdot D_4(x_4)$$

$$C_V^*(x_5, x_6, x_7) = C^*_{CV} \cdot V_5(x_5) \cdot V_6(x_6) \cdot V_7(x_7)$$

$$C_D^*(x_5, x_6, x_7) = C^*_{CD} \cdot D_5(x_5) \cdot D_6(x_6) \cdot D_7(x_7)$$

Now the model can be rewritten as:

$$F_V(x_1 \cdots, x_7) = C_{V,3} \cdot C_V(x_1 \cdots, x_4) \cdot C_V^*(x_5, x_6, x_7)$$

$$F_D(x_1 \cdots, x_7) = C_{D,3} \cdot C_D(x_1 \cdots, x_4) \cdot C_D^*(x_5, x_6, x_7)$$

$C_V(x_1 \cdots, x_4)$, $C_D(x_1 \cdots, x_4)$, $C_V^*(x_5, x_6, x_7)$, and $C_D^*(x_5, x_6, x_7)$ can be calculated from Eq.8.19, Eq.8.20, Eq.8.25, and Eq.8.26, and we have conducted SSRT under a certain set of conditions (**temperature = 300°C, dissolved oxygen = 3ppm, strain rate =2x10^{-6} s^{-1}, grain size = 14.6μm, amplitude = 300 MPa, mean stress = 280 MPa, and cyclic frequency ~0.00005 Hz**), to help identify the coefficient constants (C_V, 3 and C_D, 3) in the rewritten SAC model. The resulting crack velocity and crack density are:

$$F_V(300,3,2e^{-6},14.6,300,280,0.00005) = 1.10 \times 10^{-6}\ mm/s$$

$$F_D(300,3,2e^{-6},14.6,300,280,0.00005) = 4.17\ number/mm$$

Substitute the conditions of $\begin{cases} x_1 = 300^o C, \\ x_2 = 3\,ppm, \\ x_3 = 2\times10^{-6}\,s^{-1}, \\ x_4 = 14.6\mu m, \\ x_5 = 300MPa, \\ x_6 = 280MPa, \\ x_7 = 0.00005\,Hz \end{cases}$ into

Eq.8.19, Eq.8.20, Eq.8.25, and Eq.8.26, then we have:

$$F_V(300,3,2e^{-6},14.6,300,280,0.00005)$$
$$= C_{V,3}\cdot C_V(300,3,2e^{-6},14.6)\cdot C_V^{\ *}(20,520,0.00005) = 1.29\times10^{-6}\,mm/s$$
$$= C_{V,3}\cdot 5.39\times10^{-6}\cdot 1.10\cdot10^{-6} = 1.29\times10^{-6}\,mm/s$$
$$\Rightarrow$$
$$C_{V,3} = 2.2\times10^{5}\,s/mm$$

And,

$$F_D(300,3,2e^{-6},14.6,300,280,0.00005)$$
$$= C_{D,3}\cdot C_D(300,3,2e^{-6},14.6)\cdot C_D^{\ *}(20,520,0.00005) = 4.83\,number/mm$$
$$= C_{D,3}\cdot 10.26\cdot 4.12 = 5.21 number/mm$$
$$\Rightarrow$$
$$C_{D,3} = 0.1233 \quad mm/number$$

So:

$$C_V = 2.20\times10^{5}\,s/mm \qquad \textbf{Eq.8.27}$$

$$C_D = 0.1233 mm/number \qquad \textbf{Eq.8.28}$$

Thus the model equation of SAC cracking for various environmental and stress conditions can be given as:

$$F_V(x_1 \cdots, x_7) = 2.2\times10^5 \cdot C_V(x_1, x_2, x_3, x_4) \cdot C_V^{*}(x_5, x_6, x_7) \quad \textbf{Eq.8.29}$$

$$F_D(x_1 \cdots, x_7) = 0.1233 \cdot C_D(x_1, x_2, x_3, x_4) \cdot C_D^{*}(x_5, x_6, x_7) \quad \textbf{Eq.8.30}$$

Where:

$$\begin{aligned} &C_V(x_1, x_2, x_3, x_4) = \\ &3.72\times10^9 \cdot (2.65\times10^{-8} \cdot x_1 - 2.52\times10^{-6}) \cdot x_2^{2.135} \cdot \\ &(-4.06\times10^{11} \cdot x_3^3 + 2.62\times10^6 \cdot x_3^2 - 1.09 \cdot x_3 + 3.46\times10^{-7}) \cdot \\ &(2.21\times10^{-7} \cdot x_4 + 1.51\times10^{-6}) \end{aligned} \quad \textbf{Eq.8.19}$$

$$\begin{aligned} &C_D(x_1, x_2, x_3, x_4) = \\ &3.25\times10^{-3} \cdot (0.0534 \cdot x_1 - 6.362) \cdot x_2^{0.9862} \cdot \\ &(-2.58\times10^6 \cdot x_3 + 15.95) \cdot (0.0456 \cdot x_4 + 9.60) \end{aligned} \quad \textbf{Eq.8.20}$$

$$\begin{aligned} &C_V^{*}(x_5, x_6, x_7) = \\ &1.01\times10^{-9} \cdot \exp(0.0069 \cdot x_5 + 0.0178 \cdot x_6 - 992.73 \cdot x_7) \end{aligned} \quad \textbf{Eq.8.25}$$

$$\begin{aligned} &C_D^{*}(x_5, x_6, x_7) = \\ &0.223 \cdot \exp(0.00134 \cdot x_5 + 0.0092 \cdot x_6 - 1217 \cdot x_7) \end{aligned} \quad \textbf{Eq.8.26}$$

8.7. Experimental Verification of SAC Model under Cyclic Loading

As shown in Figures 8.1 to 8.6, the series of square data points (■) shown in the figures are the SAC crack initiation and propagation data extracted from SSRTs conducted in different cyclic loading conditions. The model of SAC cracking under cyclic loading effects can be established by curve fitting those data into **Eq.8.25 and Eq.8.26**, as marked in Figure8.1 to Figure 8.6, with solid blue line (-).

To compare the SAC model results for three cyclic loading variables with our experimental results, a SSRT experiment was carried out under condition 1, explained in section 8.6 for the model, with stress amplitude =20MPa, mean stress=520MPa, and stress frequency =0.001Hz. The crack velocity and crack density extracted from this test were plotted as the circular (●) point in Figure 8.1 to Figure 8.6. A good match can be seen from the comparison between the experimentally obtained (circular) data point resulted with the model predictions, shown as solid line and defined by **Eq.8.25 and Eq.8.26**. The crack velocity value $4.97\times10^{-6}\,mm/s$, and crack density value of 9.38 were derived from this model, which were close to the crack velocity of $5.39\times10^{-6}\,mm/s$, and the crack density value of 10.26 *#/mm* from the test. The relative error can then be calculated respectively as ~ 7.8% for crack velocity and ~ 8.5% for crack density.

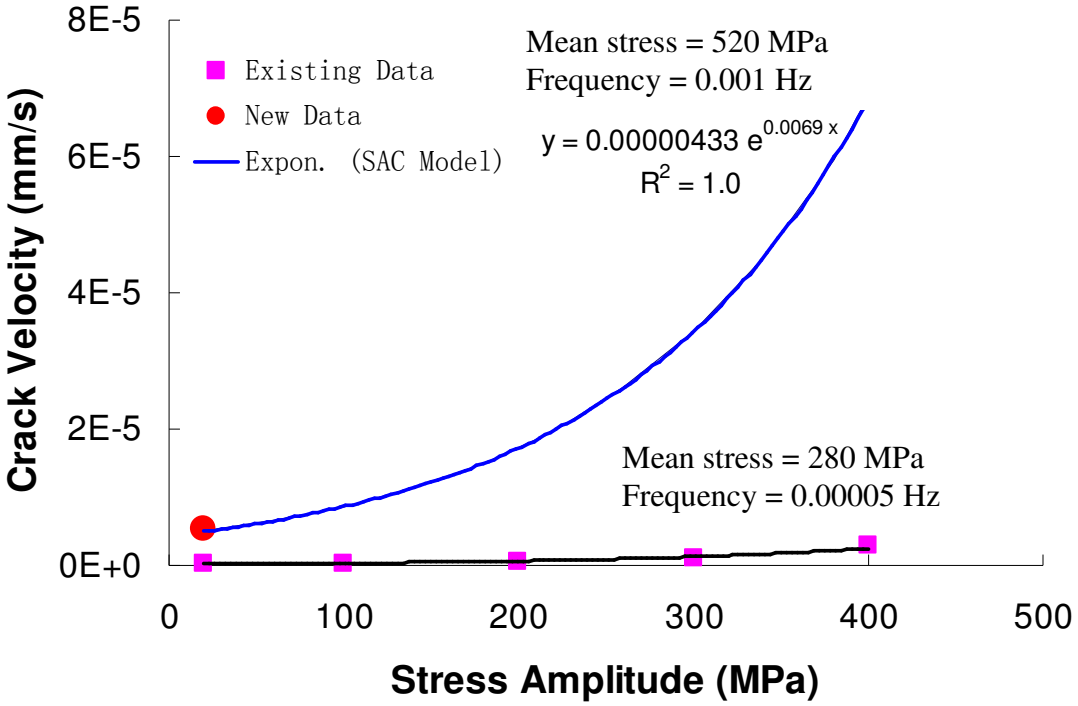

Figure 8. 1. Crack velocity vs stress amplitude prediction from model under condition 2 (constant variables: grain size ~ 14.6 µm, temperature ~300^{o}C, dissolved oxygen ~3ppm, strain rate ~2x10^{-6} s^{-1}), allow changes in stress conditions as shown in this figure.

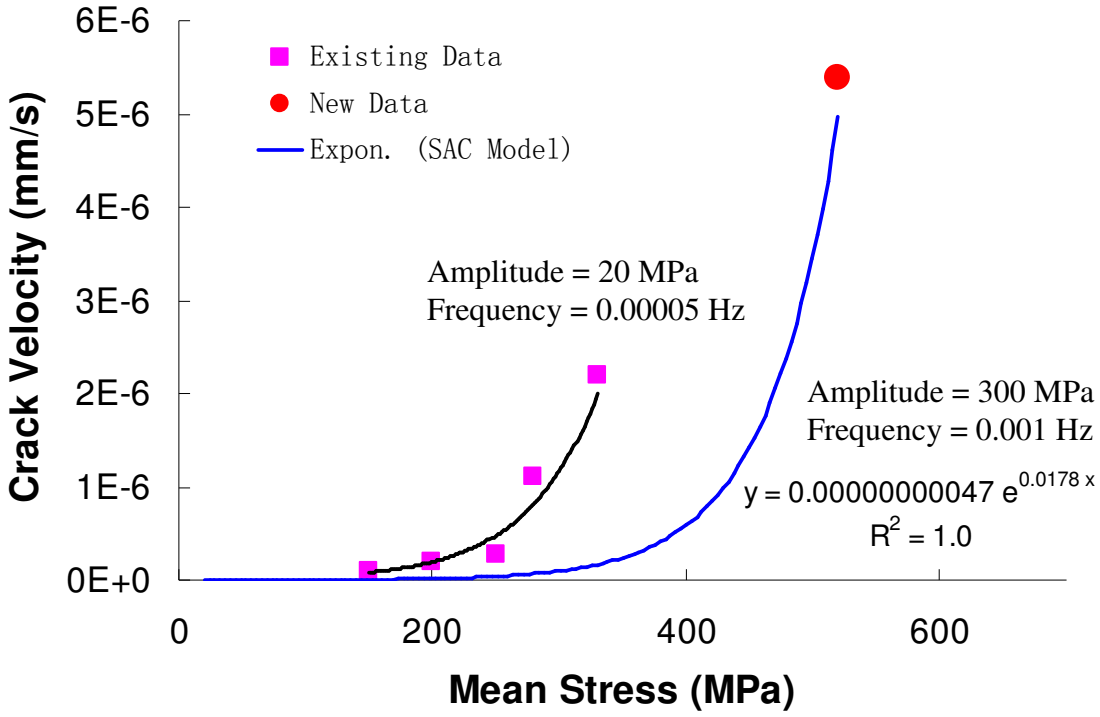

Figure 8. 2. Crack velocity vs mean stress prediction from model under condition 2 (constant variables: grain size ~ 14.6 µm, temperature ~300°C, dissolved oxygen ~3ppm, strain rate ~$2x10^{-6}$ s^{-1}), allow changes in stress conditions as shown in this figure.

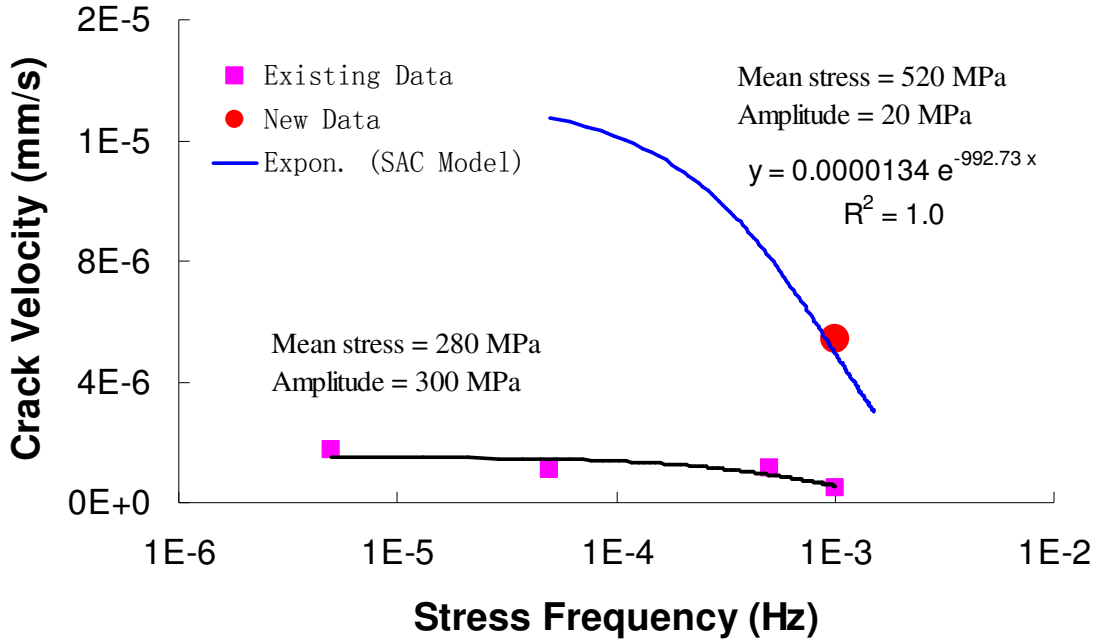

Figure 8. 3. Crack velocity vs stress frequency prediction from model under conditions 2 (constant variables: grain size ~ 14.6 µm, temperature ~300°C, dissolved oxygen ~3ppm, strain rate ~2x10^{-6} s^{-1}), allow changes in stress conditions as shown in this figure.

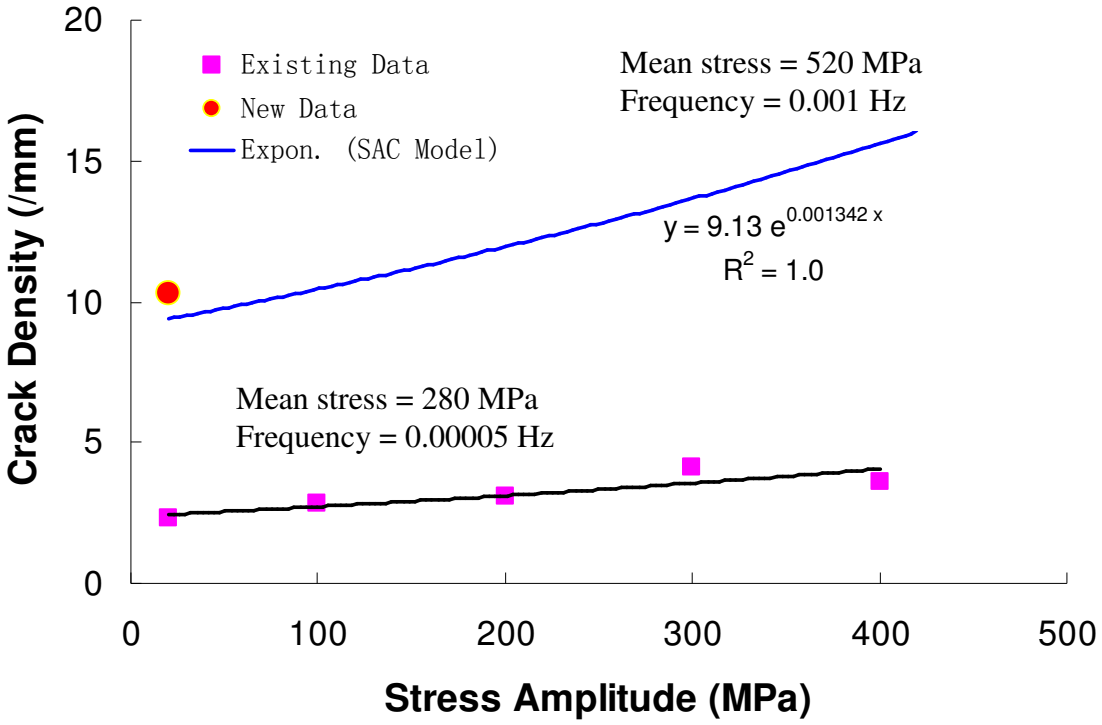

Figure 8. 4. Crack density vs stress amplitude prediction from model under condition 2 (constant variables: grain size ~ 14.6 µm, temperature ~300°C, dissolved oxygen ~3ppm, strain rate ~2x10^{-6} s^{-1}), allow changes in stress conditions as shown in this figure.

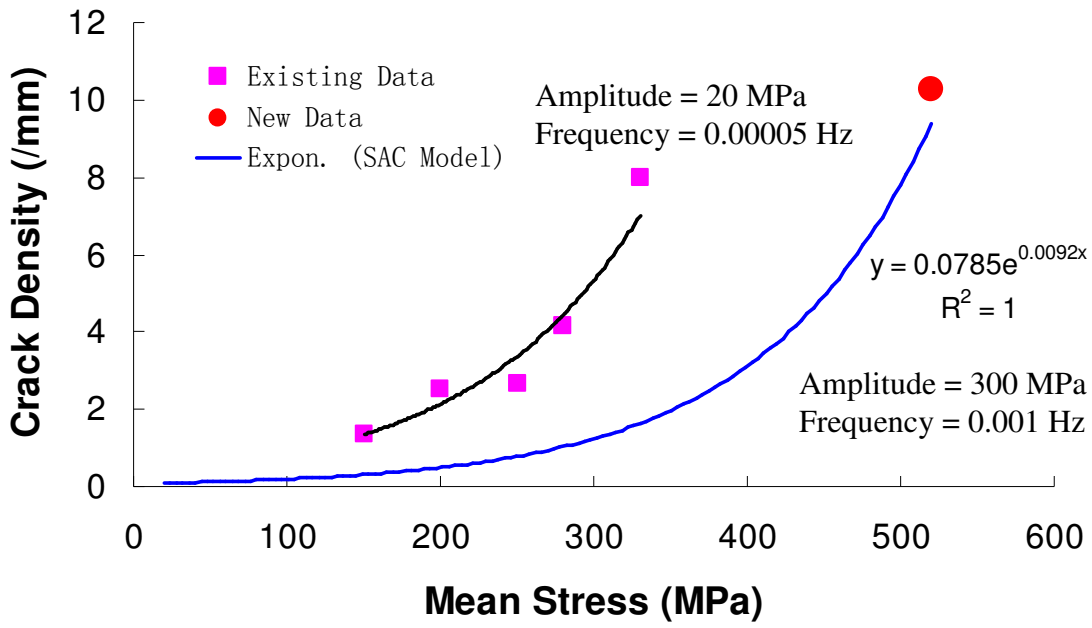

Figure 8. 5. Crack density vs mean stress prediction from model under condition 2 (constant variables: grain size ~ 14.6 µm, temperature ~300°C, dissolved oxygen ~3ppm, strain rate ~2x10^{-6} s^{-1}), allow changes in stress conditions as shown in this figure.

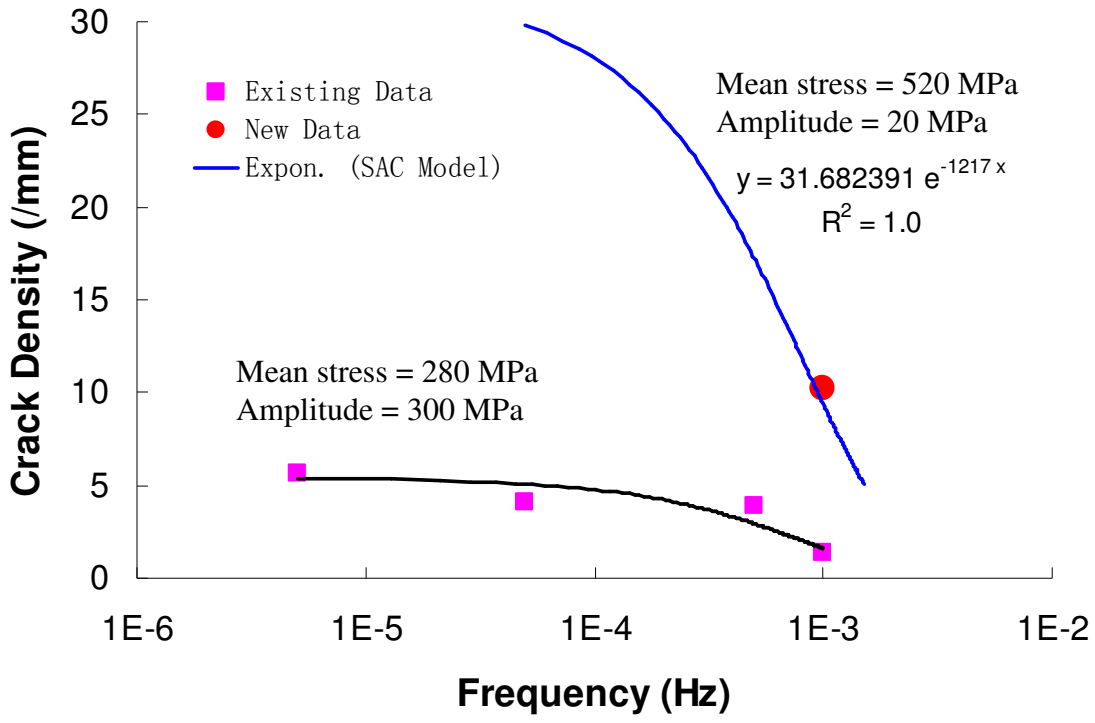

Figure 8. 6. Crack density vs stress frequency prediction from model under condition 2 (constant variables: grain size ~ 14.6 µm, temperature ~300°C, dissolved oxygen ~3ppm, strain rate ~2x10^{-6} s^{-1}), allow changes in stress conditions as shown in this figure.

8.8. Experimental Verification of SAC Model under All Combined Variables (Condition 3)

For the SAC model which is capable of accounting for all affecting factors (ie., stress amplitude, higher frequency due to thermal fluctuation stress, and temperature, dissolved oxygen, strain rate, and grain size of material), the crack growth rate and crack density were derived in section 8.6.3, as below:

$$F_V(x_1 \cdots, x_7) = 2.2\times10^5 \cdot CV(x_1, x_2, x_3, x_4) \cdot CV^*(x_5, x_6, x_7) \quad \textbf{Eq.8.29}$$

$$F_D(x_1 \cdots, x_7) = 0.1233 \cdot CD(x_1, x_2, x_3, x_4) \cdot CD^*(x_5, x_6, x_7) \quad \textbf{Eq.8.30}$$

Where:

$$\begin{aligned} &C_V(x_1, x_2, x_3, x_4) = \\ &3.72\times10^9 \cdot (2.65\times10^{-8} \cdot x_1 - 2.52\times10^{-6}) \cdot x_2^{2.135} \cdot \\ &(-4.06\times10^{11} \cdot x_3^3 + 2.62\times10^6 \cdot x_3^2 - 1.09 \cdot x_3 + 3.46\times10^{-7}) \cdot \\ &(2.21\times10^{-7} \cdot x_4 + 1.51\times10^{-6}) \end{aligned} \quad \textbf{Eq.8.19}$$

$$\begin{aligned} &C_D(x_1, x_2, x_3, x_4) = \\ &3.25\times10^{-3} \cdot (0.0534 \cdot x_1 - 6.362) \cdot x_2^{0.9862} \cdot \\ &(-2.58\times10^6 \cdot x_3 + 15.95) \cdot (0.0456 \cdot x_4 + 9.60) \end{aligned} \quad \textbf{Eq.8.20}$$

$$\begin{aligned} &C_V^*(x_5, x_6, x_7) = \\ &1.01\times10^{-9} \cdot \exp(0.0069 \cdot x_5 + 0.0178 \cdot x_6 - 992.73 \cdot x_7) \end{aligned} \quad \textbf{Eq.8.25}$$

$$\begin{aligned} &C_D^*(x_5, x_6, x_7) = \\ &0.223 \cdot \exp(0.00134 \cdot x_5 + 0.0092 \cdot x_6 - 1217 \cdot x_7) \end{aligned} \quad \textbf{Eq.8.26}$$

To verify the above SAC model established by **Eq. 8.29** and **Eq. 8.30**, another slow strain rate test was conducted in a condition under which all environmental variables were set up to be different from the baseline conditions where the SAC crack velocity and crack density data were known from previous experimental results. This specific condition was described as: test temperature ~ 280^{o}C, dissolved oxygen ~2.6ppm, grain size ~18 μm, strain rate ~3x10^{-6} s^{-1}, stress amplitude =40MPa, mean stress=500MPa, and stress frequency =0.0015Hz.

By substituting those values into **Eq. 8.29** and **Eq. 8.30**, the crack velocity and crack density can be calculated as: the crack velocity value of $3.65\times10^{-6}\,mm/s$, and crack density value of 2.85 *#/mm.* These two values were the predicted SAC behavior under condition (*). And the crack velocity of $4.16\times10^{-6}\,mm/s$, crack density of 3.375 *#/mm* were extracted from slow strain rate test under condition (*). The absolute relative error can then be calculated respectively as ~ 15.4% for crack velocity and ~ 12.3% for crack density.

The comparison between experiments and model prediction showed good agreement. However, the absolute relative error from SAC model under all combined conditions (condition 3) is slightly bigger than that from the SAC model under cyclic loading only (condition 2), which is ~ 7.8% for crack velocity and ~ 8.9% for crack density, as quoted from section 8.7. This SAC model is capable of better prediction, provided that more experimental data are available to reduce the inaccuracy of those quantified relationships between each environmental factor and SAC cracking.

8.9. Sample: Crack Length Prediction of Recovery Boiler Tube

Based on the SAC model defined in **Eq. 8.29** and **Eq. 8.30**, after the boiler tube have been working in various conditions for different amount of time, the maximum crack length a SAC crack can be determined by the following equation:

$$Cracklength = C_{V,condition\_1} \cdot t_{condition\_1} + C_{V,condition\_2} \cdot t_{condition\_2} + \cdots, + C_{V,condition\_i} \cdot t_{condition\_i}$$

Eq.8.31

The occurrences of various operating events experienced by a recovery boiler and the associated strain/temperature measurements of the tube OD surface at the heavy attachment location have been continuously monitored and recorded for 55 weeks, as shown in Table 5-1. In modern boiler systems, dissolved oxygen is handled by first mechanically removing most of the dissolved oxygen and then chemically scavenging the remainder. The level of dissolved oxygen (DO) of industrial boiler water during boiler operating can be reduced to the range of 5 ppb to 1 ppm. In order to get a conservative prediction, DO ~ 1 ppm is selected to represent the entire boiler operating processes. The input values of required variables and the resulted output values of the respective contribution of crack growth from each variable are listed in Table 8-1. The total accumulated crack growth during 55 weeks on a SA 210 boiler tube under conditions described in Table 8-1 is ~ 0.014 mm. Typically the wall thickness of an industrial boiler tube is know to be 6 mm to 10 mm [47, 48]. If 30% of tube thickness is assumed to be the critical crack size though the tube wall of industrial boiler [11], then this recovery boiler can be expected to work steadily under the ideal conditions defined in Table 8-1, for 136 years to 227 years without leaking problem though the tube wall.

However, during actual industrial boiler practices, the dissolved oxygen level in industrial boiler water can be brought to 4 ppm to 10 ppm, if the boiler water chemistry was not well controlled, or air entered the boiler cycle due to careless operation during boiler shutdown or emergency shutdown procedures. Therefore if a dissolved oxygen level ~ 10 ppm is selected to represent the boiler shutdown condition which deviated from the optimized condition defined by Table 8-1, a total accumulated crack growth of 0.25 mm over 55 weeks is expected on a SA 210 boiler tube. This condition is noted parenthetically in Table 8-1, its impact on SAC crack growth is also listed parenthetically there. Under such conditions, the recovery boiler made of SA 210 carbon steel is expected to work steadily for 8 years to 13 years before the occurrence of a possible boiler tube failure due to SAC cracking. The respective contribution to SAC crack growth from each boiler operating event can also be seen from Table 8-1. Although boiler shutdown/turn-on and boiler emergency shutdown procedure only occur a few times during 55 weeks and each occurrence only lasts few hours, they contributed more than 10% to the total accumulated SAC crack growth under ideal boiler operating practice, and up to 95% to the total accumulated SAC crack growth under conditions deviated from the ideal boiler operating practice. It indicates that the transient strain/stress events (boiler shutdown/turn-on, ESPs, chemical upsets) are of great importance and shall not be neglected in determining the total SAC crack growth in industrial boiler tubes, as well as in controlling boiler water chemistry. It shows that the usage of boiler tubing can be extended to more than 17 times of its existing life by merely controlling the dissolved oxygen level from 10 ppm to 1 ppm, which confirms out initial conclusion that water chemistry control is very cost effective.

Table 8- 1 Stress Events & Resulted Crack Growth Experienced by Recovery Boiler

Condition \ Events	Boiler Start-up Event	Boiler Shutdown Event	Emergency Shutdown Procedure	Process Upsets avg=60°C	Process Upsets avg=20°C	Norminal Boiler Operation
Temperature (°C)	290	290	290	290	290	290
Dissolved Oxygen (ppm)	1 (10)	1 (10)	1 (10)	1	1	1
Grain Size of SA210 (μm)	14.6	14.6	14.6	14.6	14.6	14.6
Mean Stress (MPa)	220	220	230	235	240	245
Amplitude (MPa)	300	300	160	80	40	10
Equivalent Frequency (Hz)	3.5E-05	3.5E-05	3.5E-05	4.6E-05	1.4E-04	0.001
Equivalent Strain Rate (s^{-1})	2.3E-6	2.3E-6	1.2E-6	3.7E-7	1.1E-7	2.2E-8
Occurrences in 55 weeks	1	1	2	8	33	-----
Event Duration (Hours)	3~4	3~4	6~8	5~6	2	~ 9000
Contributed Crack Growth From SAC Model (mm)	6.75E-4 (9.25E-2)	6.75E-4 (9.25E-2)	3.71E-4 (5.06E-2)	1.07E-4 (1.07E-4)	5.6E-3 (5.6E-3)	6.7E-03 (6.7E-3)
Contribution to Total SAC Crack Growth	5% (32.5%)	5% (32.5%)	3% (20%)	1% (~0)	39% (2%)	47% (3%)

8.10. Evaluation of Each Individual Factor

In order to evaluate the respective effect of each individual factor on SAC crack initiation and propagation, the percentage changes of crack density and crack velocity are plotted against the percentage changes of various factors (temperature, dissolved oxygen, strain rate, grain size, amplitude, mean stress, and frequency), as shown in Figure 8.7 and Figure 8.8. (the baseline conditions corresponding to 1 on X axis in Figure 8.7 and Figure 8.8 are: temperature ~ 300^{o}C, DO ~ 3 ppm, strain rate ~ 2x10^{-6} s^{-1}, grain size ~ 50 μm, amplitude ~ 300 MPa, mean stress ~ 400 MPa, frequency ~ 0.001 Hz. The associated crack velocity of ~ 1.16E-5 mm/s and crack density of 5.74 #/mm are also plotted as 1 on Y axis in Figure 8.7 and Figure 8.8.)

Reducing mean stress seems to be the most efficient way to reduce SAC crack initiation and propagation. When mean stress is controlled to 50% of the original mean stress, the crack velocity is reduced by 97%, and the crack density is reduced by 85%. Reducing temperature is also found to be very effective in reducing SAC. The crack velocity is reduced by 74% and the crack density is reduced by 83% when temperature is controlled to 50% of its original value. The SAC cracking is found to be totally eliminated if the test temperature is reduced by 60%. However, it is not practical to use temperature reduction to control SAC cracking because high temperature is an intrinsic characteristic of industrial boilers.

Reducing dissolved oxygen level by water chemistry control is another efficient way to reduce SAC cracking. At 50% of DO reduction, the SAC crack velocity is found to be reduced by 78%, and the crack density is reduced by 50%. The reduction of stress amplitude has strong influence on crack velocity but less effect on crack density. At 50% of amplitude reduction, the SAC crack velocity is found to be reduced by 65% and the SAC crack density is reduced by only 19%. The change strain rate somehow has a rather complicate effect on SAC cracking. At 50% of strain rate reduction, the SAC crack velocity is reduced by 73% while the SAC crack density is increased by 27%. However, when the strain rate is reduced to 10% of its original value, the SAC crack velocity is found to increase and the SAC crack density is found to decrease dramatically. The changes of grain size and frequency show less influence on SAC cracking than other variables. At 50% increment of frequency, the SAC crack velocity is reduced by 40% and the SAC crack density is reduced by 46%. At 50% reduction of grain size, the SAC crack velocity is reduced by 44% and the SAC crack density is reduced by 10% only.

The control on stress amplitude and frequency can only be done by limiting the occurrence of emergency shutdown procedure which is really difficult to apply in the actual practices. The control on dissolved oxygen can be done by chemical treatment, and the control on mean stress can be done by revising the structural design of the external attachment to minimize the localized stress and residual stress there. Therefore the most cost effective way to control SAC cracking is to mainly focus on reducing dissolved oxygen and localized stress, and to develop a material microstructure with small grain size as option to provide additional help on minimizing SAC cracking.

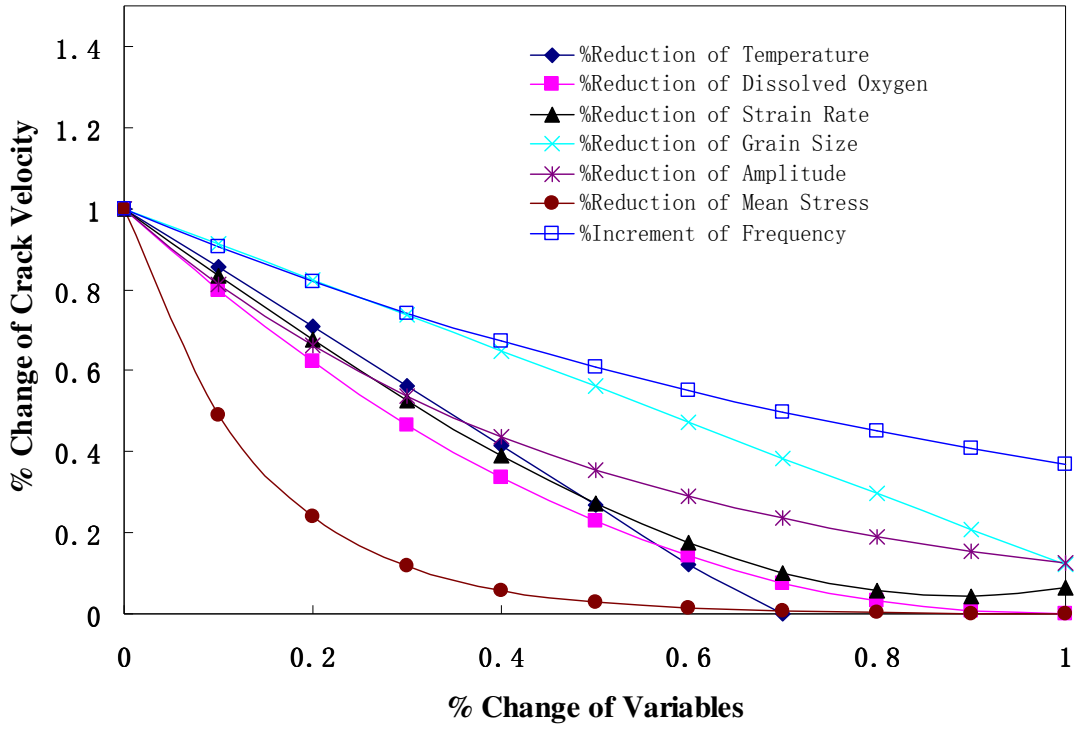

Figure 8. 7 Respective effect of each individual factor on SAC crack propagation

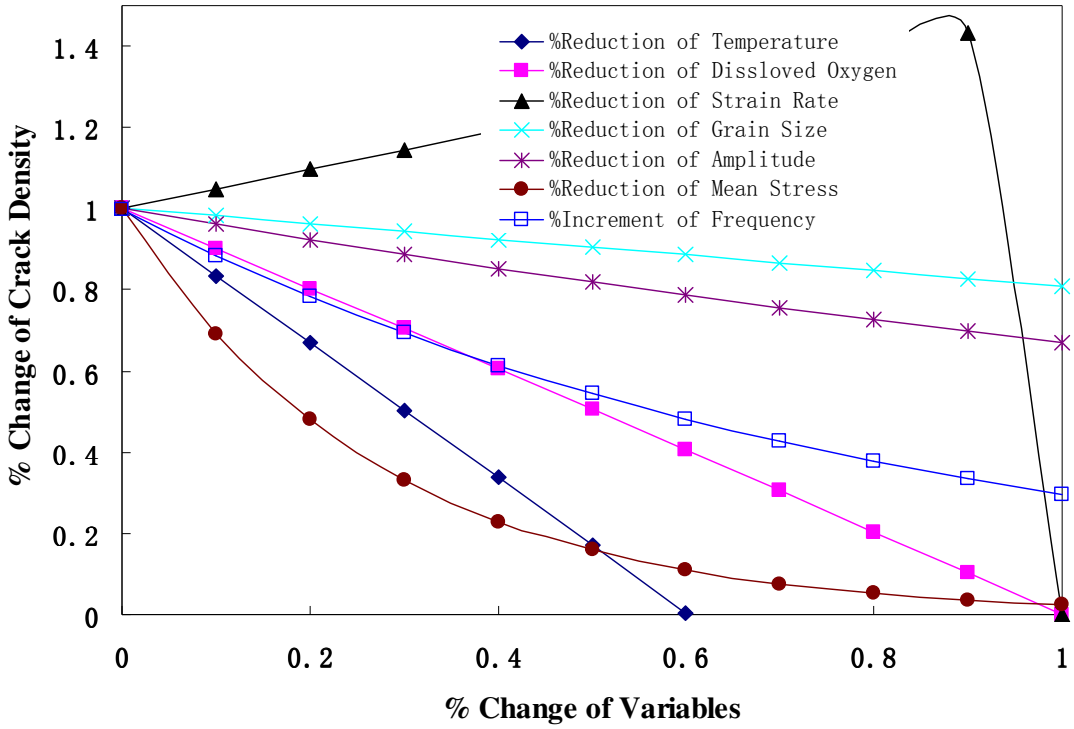

Figure 8. 8 Respective effect of each individual factor on SAC crack initiation

8.11. Life Prediction Model Considering Crack Coalescence Effects

We showed that it is possible to obtain reasonable agreement between observed and numerically simulated crack velocities for various factors applied to carbon steel SA-210 samples under simulated industrial boiler conditions. However, there remains a possible problem when applying this model to SSRTs in laboratory or severe service conditions. From the SSRTs conducted in this study and indeed in the development of SAC cracks on many structures in service, multiple bulbous cracks were observed over limited distance. In such situations, the merging or coalescence of multiple SAC cracks should be concerned, in sense of how crack coalescence will affect the crack growth rate, when multiple cracks merged into each other and became a much larger crack. This type of phenomenon is often revealed from service failure inspection of boiler tubes, indicating the number of SAC cracks have a significant effect on the remaining life of boiler tubes under a set of giving conditions.

Crack coalescence effect is a probabilistic part of life prediction. Parkins [47, 48, 85] have shown that the effective strain rate at crack tip is a function of the number of cracks found and applied strain rate. The evaluation of the crack tip strain rate was done by Congleton et al. [85], and the function of resulted crack velocity can be given as:

$$\dot{\varepsilon}_{CT} = \frac{75}{N}\dot{\varepsilon}_{app} + \frac{C_V}{5}\ln(\frac{1000}{N}) \qquad \textbf{Eq. 8.32}$$

$$C_{V,CT} = \frac{da}{dt} = \frac{Q_f}{\varepsilon_f} \cdot \dot{\varepsilon}_{CT} \cdot \frac{M}{z \bullet F_d} \qquad \textbf{Eq.8.33}$$

Where:

$\dot{\varepsilon}_{CT} = strain\ rate \quad at \quad crack \quad tip \quad (s^{-1})$
$\dot{\varepsilon}_{app} = applied \quad strainrate \quad (s^{-1})$
$C_V = crack \quad velocity \quad of \quad \sin gle - crack \quad (mm/s)$
$C_{V,CT} = crack \quad velocity \quad at \quad crack \quad tip \quad considering \quad crack \quad coalescence \quad effect \quad (mm/s)$
$Q_f = charge \quad density$
$\varepsilon_f = fracture \quad strain$
$Z = valency \quad of \quad solvated \quad species$
$F_d = Faraday's \quad constant$
$M = atomic \quad weith \quad of \quad metal$

Substitutes our model (Eq. 8.29 and Eq. 8.30) into the two equations above:

$$\dot{\varepsilon}_{CT} = \frac{75}{F_D \cdot L}\dot{\varepsilon}_{app} + \frac{F_V}{5}\ln(\frac{1000}{F_D \cdot L}) \qquad \textbf{Eq.8.34}$$

$$C_{V,CT} = \frac{da}{dt} = \frac{Q_f}{\varepsilon_f} \cdot \dot{\varepsilon}_{CT} \cdot \frac{M}{z \bullet F_d} \qquad \textbf{Eq.8.35}$$

Where:

$\dot{\varepsilon}_{CT} = strain\ rate \quad at \quad crack \quad tip \quad (s^{-1})$
$\dot{\varepsilon}_{app} = applied \quad strainrate \quad (s^{-1})$
$L = sample \quad length \quad (mm)$
$C_V = crack \quad velocity \quad of \quad \sin gle - crack \quad (mm/s)$
$C_{V,CT} = crack \quad velocity \quad at \quad crack \quad tip \quad considering \quad crack \quad coalescence \quad effect \quad (mm/s)$
$Q_f = charge \quad density$
$\varepsilon_f = fracture \quad strain \quad \%$
$Z = valency \quad of \quad solvated \quad species$
$F_d = Faraday's \quad constant$
$M = atomic \quad weith \quad of \quad metal$

Similarly, after the boiler has been working in various conditions for different amount of time, an estimation of the maximum crack growth of boiler tubing considering crack coalescence effect can be determined by the following equation (Eq. 8.36). The maximum crack length a SAC crack may have:

$$Cracklength = C_{V,CT,condition\_1} \cdot t_{condition\_1} + C_{V,CT,condition\_2} \cdot t_{condition\_2} + \cdots, + C_{V,CT,condition\_i} \cdot t_{condition\_i}$$

Eq.8.36

However, to be able to represent the crack coalescence effect of SAC more accurately, information regarding when cracks start to merge, what is the critical crack length for coalescence to occur, and how the distances between adjacent cracks will affect the merging, etc. need to be gathered from future experimental observations.

CHAPTER 9: GENERAL CONCLUSIONS

- Results from the SSRT tests indicate that a test temperature greater than ~110^{o}C and a level of dissolved O_2 higher than 5 ppb are necessary for crack initiation and growth in simulated boiler water environment.

- Without environmental effects, material ductility of carbon steel SA-210 increases when test temperature goes up. However, with dissolved O_2 in the water, the crack velocity and density increase with temperature (110^{o}C to 320^{o}C) in almost a linear way reducing the ductility at fracture due to SAC.

- Effect of temperature is more prominent with the influence of environment. Temperature effect on SAC tends to be detrimental in lab air conditions.

- Before and after SAC crack initiation, SAC in industrial boilers can be controlled by controlling dissolved O_2 to levels in water below 5 ppb before and after SAC crack initiation, or by minimizing the stress localization near attachment welds below threshold values needed to damage the magnetite film locally.

- Samples tested under cyclic stress conditions are more susceptible to environmentally induced crack initiation compared to equivalent monotonous

loading. Both high frequency low-amplitude and low frequency high- amplitude cyclic loading promote early crack initiation and growth.

- Crack susceptibility is found to be higher with higher mean stress, amplitude, and maximum stress, but lower with increasing cyclic frequency.

- Strain rates have significant affect on stress assisted corrosion of carbon steels in boiler water environments, especially under monotonous slow strain rates. The SAC crack initiation is dominant on the surface of carbon steel specimen under low strain rate loading in oxygenated boiler water environments.

- Heat-treatment of carbon steel with higher annealing temperature ($1100^{o}C$) and longer annealing time was needed to produce larger grain size and lower carbon levels at the surface layer of carbon steels. Boiler operating conditions ($300^{o}C$ – $350^{o}C$) may not enough to cause such micro-structural changes.

- Grain growth and decarburization make carbon steel more susceptible to SAC crack initiation and propagation under industrial boiler water environment when tested with SSRTs.

- Pearlite phase seems have more resistance to SAC crack growth than ferrite grain in pearlitic steels, SAC cracks tend to initiate from ferrite grain sites.

- Grain growth of carbon steel also affects fatigue properties of material under lab air conditions. Grain growth of carbon steel shows more influence on SAC crack initiation than propagation. However, the effects due to microstructural changes on mechanical properties in lab air environments do not explain the behavior seen in industrial water environments.

- SAC cracking susceptibility of carbon steel tubes can be reduced by quality control during manufacturing process and eliminating tube with large grained microstructure at its inner surface.

- SAC cracks are not caused by any single factor; the interaction between temperature and DO, or film formation, and stress conditions is another practical role. Sometimes temperature work together with loading can damage materials with high strength, such as super-alloys.

- For carbon steel in boiler water environments, relative anode/cathode area ratios have significant effect on the magnetite film morphology. Small ratios tend to produce a compact, protective film whereas large cathode to anode area ratio favors a porous non-protective film.

- Tensile stress at the SAC crack tip during boiler shutdown period is required for pit formation. Pits formed on the surface of carbon steel facilitate the SAC initiation but are not necessary.

- Sharp corrosion fatigue cracks typically found in utility boilers and blunt SAC cracks in industrial boilers seem to have the same initiation and growth mechanism; however the shape differs due to the differences in the shutdown water chemistry control. Availability of oxygen during the shutdown may lead to crack blunting due to preferential corrosion and result into the bulbous shape of SAC cracks.

- The life prediction model of SAC cracking can be established based on the quantified effects of each environmental factors on SAC crack initiation and propagation.

- The life prediction model of SAC cracking was evaluated by conducting slow strain rate tests under three types of simulated industrial boiler conditions. The SAC model was shown to be capable of obtaining reasonable agreement between observed and numerically simulated crack velocities for various factors applied to carbon steel SA-210 samples under simulated industrial boiler conditions.

- Higher accuracy of this SAC model may be gained by curve-fitting more experimental data and by taking crack coalescence effect into modeling efforts.

CHAPTER 10: IMPACT AND FUTURE WORK

This project used a team approach including industry contributors and research organizations to bring together the required experience, information, and financial and technical resources to accomplish the proposed tasks. The project was coordinated and managed by the Georgia Institute of Technology whereas an industrial advisory committee was formed for directing the project, with members from among the participating (in-kind) companies and experienced individuals who monitored progress and provided information and materials as appropriate. Technical execution of the project was accomplished primarily by Oak Ridge National Laboratory (ORNL) and Georgia Institute of Technology (GIT). Results from this project are relevant to the wide range of industry, including the chemical, petrochemical, and paper and pulp companies that operate boilers, the manufacturers of these boilers, the water treatment firms that are responsible for water quality; and the consultants and failure analysis experts that address boiler problems. In this study, the ASTM standards (E3, E7, E8, E112, E399, E647, E1820, and E1823) were followed in processes of specimen preparation, experimental measurement, and subsequent analysis. Results from this project are relevant to the wide range of industry, including the chemical, petrochemical, and pulp and paper companies that operate boilers, the manufacturers of these boilers, the water treatment firms that are responsible for water quality; and the consultants/experts of failure analysis that address boiler problems.

This research proposal focuses on how the environmental factors affect the initiation and propagation of SAC cracking. However, there is not single cause or simple solution to this type of waterside corrosion attack. The evidence indicates the importance of operating strain, residual strain, material properties, and environment. Future work needed is how the operating strain or residual strain affects on the initiation of SAC. In reality, boiler water is not stagnant during operation, so the effect of flow rate of boiler water on SAC should be another subject to complete the SAC study. In addition, metal material selection is very important aspects to prevent the initiation of SAC. How to identify an inexpensive alloy or metal with the best quality to prevent the SAC is another interesting research area. Further more, the mechanistic understanding of the magnetite disrupting during fatigue-type loading is not complete, more effort is needed in this area.

As for the life prediction model of boiler tubes, it does not take into account the conditions where large cyclic loading with mean stress less than zero (load cycles between compression and tensile modes), and also the curve-fitted equations all come from limited experimental results thus more experimental data will likely improve the accuracy of model as well. In cases where the crack density is high, multiple small cracks tend to merge into large SAC cracks as we noticed in this study. Thus crack coalescence will also influence the final life of boiler tubes. This will be probabilistic part of life prediction. Therefore, effect of crack coalescence on SAC need to be quantified and included into our empirical model.

REFERENCES

1) D.E. Carroll, D.E. Carroll, JR. *The ASME Code Simplified/Power Boilers*, 1997.

2) Terrell Croft, *Steam Boilers*, 1921.

3) G. E. Hider, A. M. Inst. C. E., M. I. Mech. E., *The Problem of Fluctuating Loads on Boilers*, 1931.

4) B. George, S. B. Haven, *The Design of Steam Boilers and Pressure Vessels*, 1915.

5) B. Dooley and W. McNaughton, *Boiler Tube Failures: Theory and Practices, Volume 1. Boiler Tube Fundamentals*, Palo Alto, CA, 1995

6) G. Smook, *Handbook for pulp and paper technologist 2nd Edition*. Angus wilde Publications, Vancouver, 1992.

7) R. P. Gangloff and M. B. Lves, "Environment-Induced Cracking of Metals", NACE-10, 1988.

8) R. B. Dooley and R. Pate, eds., Fourth International Conference on Cycle Chemistry in Fossil Boilers, held in Atlanta, GA, Sept., 1994, Final Report TR-104502, Electric Power Research Institute, Palo Alto, CA, Jan., 1995.

9) K. Ranjbar, "Failure analysis of boiler cold and hot reheater tubes", Engineering FailureAnalysis, 14, Issue 4, Pages 620-625, 2007 (June).

10) Fiss, E. C., American Power Conference, March, 1954.

11) P. M. Singh, D. Yang, and J. Mahmood, S. J. Pawel, "Stress Assisted Corrosion in Boiler Tubes—Failure Analysis", NACE Conference, Nashville, TN, 2007.

12) D. Yang, P. M. Singh, R. W. Neu, "Initiation and Propagation of Stress-Assisted Corrosion (SAC) Cracks in Carbon Steel Boiler Tubes", ASME-Journal of Engineering Materials and Technology, 129, pp. 559-566, 2007.

13) D. Yang, P. M. Singh, "Stress Assisted Corrosion in Boiler Tubes", 2007 International Chemical Recovery Conference, Canada, 2007.

14) D. Yang, P. M. Singh, R. W. Neu, "Role of Stress Conditions on Stress Assisted Corrosion Behavior of Carbon Steel Boiler Tubes", NACE Conference, Nashville, TN, 2007.

15) D. Yang, P. M. Singh, R. W. Neu, "Mechanism of Stress Assisted Corrosion Crack Initiation on Carbon Steels", TAPPI 2006 Conference, Atlanta, GA, USA, 2006.

16) D. Yang, P. M. Singh, and R. W. Neu, "Initiation and Propagation of Stress Assisted Corrosion (SAC) in Carbon Steel Boiler Tubes", Corrosion 2006, Paper No. 06241, San Diego, CA, USA, 2006.

17) D. Yang, P. M. Singh, and R. W. Neu, "Factors Affecting Stress Assisted Corrosion Cracking of Carbon Steels", proc. 9th International Fatigue Congress, Paper No. FT 383, Atlanta, GA, 2006.

18) D. Yang, P. M. Singh, and R. W. Neu, "Effect of Boiler Water Chemistry on Corrosion and Corrosion Fatigue of Carbon Steels," proc. 16th International Corrosion Congress, BJ, China, 2005.

19) D. J. Duquette, "Environmental Effects on General Fatigue Resistance and Crack Nucleation in Metals and Alloys", in Fatigue and Microstructure, American Society for Metals, Metals Park, Ohio, pp. 335-363, 1979.

20) R. B. Dooley, "A Vision for Reducing Boiler Tube Failures", Power Engineering, pp. 33-37, 1992 (March).

21) R. B. Dooley, "A Vision for Reducing Boiler Tube Failures: Part II", Power Engineering, pp. 41-42, 1992 (March).

22) T. A. Prater and L. F. Coffin, "The Use of Notched Compact-Type Specimens for Crack Initiation Design Rules in High-Temperature Water Environment", Corrosion Fatigue : Mechanics, Metallurgy, Electrochemistry, and Engineering, ASTM STP 801, T. W. Crooker and B. N. Leis, Eds., American Society for Testing and Materials, 1983.

23) R. B. Dooley, "A Vision for Reducing Boiler Tube Failures," Power Engineering, pp. 33-37, 1996(3).

24) J. Robertson, "The Mechanism of High Temperature Aqueous Corrosion of Steel," Corrosion Science, 29(11/12), pp. 1275-1291, 1989.

25) N. Nagata, "Environmentally Assisted Cracking of Structural Materials for Light Water Reactors," NRIM Special Report, No. 94-01, Tokyo, Japan, 1994.

26) J. D. Atkinson and J. E. Forrest, "Factors Influencing the Rate of Growth of Fatigue Cracks in RPV Steels Exposed to a Simulated PWR Primary Water Environment," Corrosion Science, 25(8/9), pp. 633-650, 1985.

27) X. Wu and Y. Katada, "Corrosion Fatigue Behavior of Low-Alloy Pressure Vessel Steels in High Temperature Water under Multi-Factor Conditions," Journal of Pressure Vessel Technology, 126(4), pp. 466-472, 2004.

28) E. M. Field, R. C. Stanley, A. M. Adams, and D. R. Holmes, "The Growth, Structure and Breakdown of Magnetite Films on Mild Steel," Proc. 2nd Int. Conf. Metallic Corrosion, New York, p. 829, 1963.

29) J. M. Olive, "A perspective of local analysis of corrosion-fatigue crack initiation and propagation," Rev. Met. Paris, N5, pp. 433-439, 2002 (May).

30) E. C. Potter and G. M. W. Mann, "Oxidation of Mild Steel in High-temperature Aqueous Systems," Proc., 1st International Congress on Metallic Corrosion, Butterworks, London, UK, p. 417, 1961.

31) B. N. Leis and J. A. Colwell, "Initiation of Stress-Corrosion Cracking on Gas Transmission Piping," Effects of the Environment on the Initiation of Crack Growth, ASTM STP 1298, W. A. Van Der Sluys, R. S. Piascik, and R. Z.awierucha, Eds., American Society for Testing and Materials, pp. 34-58, 1997.

32) E. C. Potter and G. M. W. Mann, "Mechanism of Magnetite Growth on Low-carbon Steel in Steam and Aqueous Solutions up to 550 Degrees C," Proc., 2nd International Congress on Metallic Corrosion, (New York) Butterworks, London, UK, p. 872, 1963.

33) K. M. Perkins, M.R. Bache, "Corrosion fatigue of a 12%Cr low pressure turbine blade steel in simulated service environments," International Journal of Fatigue 27, pp.1499–1508, 2005.

34) Higuchi, Makoto; Sakamoto, "Effects of temperature and dissolved oxygen on cyclic crack growth rate of carbon and low alloy steels in high temperature water". PVP (American Society of Mechanical Engineers), (Fatigue, Environmental Factors, and New Materials), 241-248, 1998.

35) O. Vosikovsky, W. R. Neill, and A. Carlyle, "The effect of seawater temperature on corrosion fatigue-crack growth in structural steels," Canadian Metallurgical Quarterly, 26(3), 25 1-7, 1987.

36) L. A. James and W. A. Van Der Sluys, "the effect of aqueous environments upon the initiation and propagation of fatigue cracks in low-alloy steels", Research Topical symposia, proceedings of corrosion 1996, pp.176-209, 1996.

37) G. Nakao, M. Higuchi; H. Kanasaki, K. Iida, Y. Asada, "Effects of Temperature and Dissolved Oxygen Contents on Fatigue Lifes of Carbon and Low Alloy Steels in LWR Water Environments," "Effects of the Environments on the Initiation of Crack

Growth", ASTM STP 1298, W.A. VanDer Sluys. R. S. Piascik, and R. Zawierucha, Eds,. American Society for Testing and Materials, 1997.

38) O. K. Chopra and W. J. Shack, "Evaluation of Effects of LWR Coolant Environments on Fatigue Life of Carbon and Low-Alloy Steels", "Effects of the Environments on the Initiation of Crack Growth", ASTM STP 1298, W.A. VanDer Sluys. R. S. Piascik, and R. Zawierucha, Eds,. American Society for Testing and Materials, 1997.

39) M. C. Bloom, G. N. Newport, and W. A. Fraser, "Steel Corrosion Mechanisms", Journal of the Electrochemical Society 1964, 111, Issue 12, pp. 1343-1347, 1964.

40) J. E. Castle and G. M. W. Mann, "Mechanism of Formation of a Porous Oxide Film on Steel", Corrosion Science 6, 6, pp 253-262, 1966.

41) S. R. Paterson, T. A. Kuntz, R. S. Moser, and H. Vailancourt, Boiler Tube Failures, Research Project 1890-1, Final Report CS-3945, Electric Power Research Institute, Palo Alto, CA, April, 1985.

42) Mitsubishi Heavy Industries, Ltd., Nagasaki Research and Development Center, "In-Situ Measurement of Metal Temperature and Pressure Water", presented at the Annual Meeting of the International Society for the Properties of Steam, Vancouver, Canada, 1988.

43) T. F. Marsh, "The Morphology of Magnetite Growth on Mild Steel in Alkaline Solutions at 316^{o}C", Journal of the Electrochemical Society, 113, 4, pp 313-318, 1966.

44) D. R. Holmes and G. M. W. Mann, "Critical Survey of Possible Factors Contributing to Internal Boiler Corrosion", Corrosion 21, 11, pp. 370-377, 1965 (November).

45) M. S. Odziemkowski (Univ of Waterloo); T. T. Schuhmacher; R. W. Gillham; E. J. Reardon, "Mechanism of oxide film formation on iron in simulating groundwater solutions: Raman spectroscopic studies", Source: Corrosion Science, v 40, n 2-3, pp 371-389, 1998 (Feb-Mar).

46) G. B. Sarma, S. J. Pawel, and P. M. Singh, 2006, "Modeling of Recovery Boiler Tube Wall Panels to Investigate the Effect of Attachment Welds on Stress-Assisted Corrosion," Corrosion 2006, Paper No. 06240, San Diego, CA, USA.

47) R. N. Parkins, "Factors Influencing Stress Corrosion Crack Growth Kinetics", department of Metallurgy and Engineering Materials, University of Newcastle upon Tyne, NE1 7RU, England.

48) R. N. Parkins,"Conceptual Understanding and Life Prediction for SCC of Pipelines", Proc. of Corrosion 1996, Research Topical Symposia, p1-p51, 1996.

49) J. M. Barsom, "Effect of cyclic stress from on the corrosion fatigue crack propagation below KISCC in a high yield strength steel", Corrosion Fatigue 1972; NACE-2:424.

50) J. M. Barsom, S. T. Rolfe, *Fracture and fatigue control in structures— applications of fracture mechanics*, Englewood Cliffs, NJ: Prentice Hall Inc; 1977.

51) K. Endo, K. Komai, "Effects of stress wave form and cycle frequency on low cycle corrosion fatigue". Corrosion Fatigue 1972; NACE-2:437–50.

52) K. Komai, "Failure Analysis and Prevention in SCC and Corrosion Fatigue Cases", International Journal of Fatigue 20, 145–154, 1998.

53) Z. Xia, D. Kujawski and F. Ellyin, "Effect of mean stress and ratcheting strain on fatigue life of steel", Int. J. Fatigue 18, No. 5, pp. 335-341, 1996.

54) Xianjie Yang, "Low cycle fatigue and cyclic stress ratcheting failure behavior of carbon steel 45 under uniaxial cyclic loading", International Journal of Fatigue, 27, pp.1124–1132, 2005.

55) M. D. Chapetti, H. Miyata, T. Tagawa, T. Miyata and M. Fujioka, "Fatigue crack propagation behaviour in ultra-fine grained low carbon steel", International Journal of Fatigue 27, pp. 235–243, 2005.

56) Yong Gao, Mukul Kumar, R. K. Nalla, and R. O. Ritchie, "High-Cycle Fatigue of Nickel-Based Superalloy ME3 at Ambient and Elevated Temperatures: Role of Grain-Boundary Engineering", Metallurgical and Materials Transactions A, 36A, 2005 (December).

57) W. V. Vaidya, "Fatigue Crack Propagation under a Microstructural Gradient in a Plain Carbon Steel", Scripta Metallurgica, 19, pp. 597-602, 1985.

58) P. B. Desch and J. J. Dillon, "Case Histories of Stress-Assisted Corrosion in Boilers," Corrosion 2004, Paper No. 04516, 2004.

59) W. R. Sylvester and G. Sidla, "Waterside stress-assisted corrosion cracking in boilers," Pulp & Paper Canada, 91(6), pp. 151-155, 1990.

60) W. B. A. Sharp, 2004, "An Overview of Stress-Assisted Corrosion in the Pulp and Paper Industry," Corrosion 2004, Las Vegas, NV, USA, Paper No. 04513.

61) W. B. A. Sharp, "The Strength of Recovery Boiler Tubes Containing Stress-Assisted Corrosion," proc. 11th International Symposium on Corrosion in the Pulp and Paper Industry, pp. 193-205, 2004.

62) P. M. Singh, J. J. Perdomo, J. Mahmood, and P. Conde, "Stress-Assisted Corrosion Simulation in the Laboratory," Power Plant Chemistry, 7(3), pp. 155-161, 2005.

63) M. J. Esmacher, N. N. Johnston, and M. A. Sargent, 2005, "Minimizing the Impact of Stress-Assisted Corrosion in Paper Mill Boilers", TAPPI Engineering, Pulping and Environmental Conference, Philadelphia, PA, United States, Aug. 28-31, 2005.

64) R. Hargrave, M. J. Esmacher, and N. Johnston, "Stress-Assisted Corrosion in Recovery Boilers," Corrosion 2004, Paper No. 04514, 2004.

65) D. Sidey, R. W. Coade, and R. W. Patterson, "Corrosion-Fatigue Boiler Tube Failures in Waterwalls and Economizer," Proc. Boiler Tube Failures in Fossil Power Plants, Atlanta, GA, 1987.

66) E. M. Labuda and R. D. Bartholomew, "Stress-Assisted Corrosion: Case Histories," Corrosion 2004, Paper No. 04520, 2004.

67) J. H. Bulloch, "Deaerator Feedwater Storage Vessel Weldment Cracking: Some Fractographic and Crack Extension Details", Int. J. Pres. Ves. & Piping 68, 1996.

68) P. M. Scott and D. R. Tice, "Stress Corrosion in Low Alloy Steels", Nuclear Engineering and Design 119, pp. 399-413, 1990.

69) M. D. Wright, "Stress Corrosion-cracking of Carbon and Low-alloy Steels in Nuclear Power Plant Pressure Vessels and Piping", Assessment methodologies for preventing failure: 410-2, 147-162, 2000.

70) J. Hickling and D. Blind, "Strain-induced Corrosion Cracking of Low-alloy Steels in LWR Systems-Case Histories and Identification of Conditions Leading to Susceptibility", Nuclear Engineering and Design 91, pp.305-330, 1986.

71) E. Lenz and N. Wieling, "Strain-induced Corrosion Cracking of Low-alloy Steels in LWR-systems-Interpretation of Susceptibility by Means of a Three Dimensional (T, strain, Dissolved Oxygen) Diagram", Nuclear Engineering and Design 91, pp.331-344, 1986.

72) EPRI Technical Report-102433-V1, *Boiler Tube Failure/Metallurgical Guide*, Prepared by Aptech Engineering Services, Inc., October 1993.

73) M.A. Hofer, D. Moran; Y. Shapiro, U. Meiri, A. Laor, Y. Epstein, M. Horowitz, K.E. Dennis, A.P. Goldberg, J.H. Bulloch, "Deaerator feedwater storage vessel weldment

cracking: some fractographic and crack extension details" The International Journal of Pressure Vessels and Piping, 68, Number 1, pp. 81-97(17), 1996 (August).

74) X. B. Lin, and R. A. Smith, "Finite Element Modeling of Fatigue Crack Growth of Surface Cracked Plates", Engineering Fracture Mechanics, 63, Issue 5, pp. 503-522, 1999 (July).

75) M. Stolarska, D. L. Chopp, N. Moes, and T. Belytschko, "Modeling Crack Growth by Level Sets in the Extended Finite Element Methods", Int. J. Numer. Meth. Engng, 51: pg. 943-960, 2001

76) D. C. Agrawal and R. Raj, Acta Metall., 37 (4), 1989.

77) B. F. Chen, J. Hwang, I. F. Chen, G. P. Yu, J. H. Huang, "A Tensile-film-cracking Model for Evaluating Interfacial Shear Strength of Elastic Film on Ductile Substrate", Surface and Coatings Technology, 126, pp. 91-95, 2000.

78) H. Kanasaki, A. Hirano, K. Iida, Y. Asada, "Corrosion Fatigue Behavior and Life Prediction Method under Changing Temperature Condition", ASTM STP 1298, 1997.

79) M. Higuchi, K. Iida, "Fatigue Strength Corrosion Factors for Carbon and Low-Alloy Steels in Oxygen-Containing High Temperature Water, Nuclear Engineering and Design, 129, pp. 293-306, 1991.

80) O. Jonas, "Molecular Modeling of Corrosive Environments in Cracks", Effects of the Environment on the Initiation of Crack Growth, ASTM STP 1298, 1997.

81) D. V. Ramsanooj and T. A. Shugar, "Modeling of Corrosion Fatigue in Metals in an Aggressive Environment", International Journal of Fatigue, 23, pp. 301-309, 2001.

82) S. B. Lambert, A. Plumtree, R. Sutherby, "Modeling of Environmental Crack Growth in Pipeline Steel", Corrosion 2000 Conference, Paper# 00364, NACE, Orlando, FL, USA, 2000.

83) D. Kujawski and S. Stoychev, "A Two Parameter Kmax and ΔK Model for Fatigue Crack Growth", 2006 Fatigue Conference, Atlanta, GA, USA, 2006.

84) A. Bhattacharya, P. M. Singh, "Stress corrosion cracking of welded 2205 duplex stainless steels in sulfide-containing caustic solution", Journal of Failure Analysis and Prevention, 7, Issue 5, 2007 (October).

85) J. Congleton, T. Shoji and R. N. Parkins, "The stress corrosion cracking of reactor pressure vessel steel in high temperature water", Corrosion Science, 25, (8-9), pp 633-650). 1985.

86) J. M. Hyzak and I. M. Bernstein, " The Role of Microstructure on the Strength and Toughness of Fully Pearlitic Steels", Metall. Trans. 7A, 1217-1224, 1976.

87) Askeland, R. Donald and Phule, P. Pradeep, T*he Science and Engineering of Materials*, Fifth Edition, pp.474.

88) N. Narasaiah, and K. K. Ray, "Role of Microstructure on Short Crack Propagation and Its Threshold", NACE Corrosion/2006 Conference, CA, USA, 2006.

89) D. Taylor, *Fatigue thresholds*, Butterworths and Co. (Publishers), London, 1989.

90) G. J. Fowler, A. S. Tetelman, "the Effect of Grain Boundary Ferrite on Fatigue Crack Propagation in Pearlitic Rail Steels", ASTM STP 664, 363-386, 1978.

91) H. J. Westwood, W. K. Lee, "Corrosion--Fatigue Cracking in Fossil-Fueled Boilers", J. Mater. Eng. 9, no. 2, pp. 163-173. 1987.

92) W. Schoch, and H. Spahn, "On the Role of Stress-Induced Corrosion and Corrosion Fatigue in Water-Wetted Boiler Components", Corrosion Fatigue: Chemistry, Mechanics, and Microstructure. Houston, TX, NACE, pp. 52-64, 1972.